Enhancing natural clinoptilolite for cesium and strontium removal, using activation, flotation and process intensification

Muhammad Yusuf

Submitted in accordance with the requirements for the degree of

Doctor of Philosophy

University of Leeds

School of Chemical and Process Engineering

May 2021

The candidate confirms that the work submitted is his own, except where work which has formed part of jointly-authored publications has been included. The contribution of the candidate and the other authors to this work has been explicitly indicated below. The candidate confirms that appropriate credit has been given within the thesis where reference has been made to the work of others.

Large portions of Chapter 3 appears in Paper 1, meanwhile significant parts of Chapter 4 are published as Paper 2 and the majority of Chapter 5 has been submitted as Paper 3.

Published Journal Papers

1. Prajitno, M.Y., Harbottle, D., Hondow, N., Zhang, H., Hunter, T.N., 2020. The effect of pre-activation and milling on improving natural clinoptilolite for ion exchange of cesium and strontium. *Journal of Environmental Chemical Engineering 8, 102991.* (Published)

2. Prajitno, M.Y., Tangparitkul, S., Zhang, H., Harbottle, D., Hunter, T.N., 2021. The effect of cationic surfactants on improving natural clinoptilolite for the flotation of cesium. *Journal of Hazardous Materials 402, 123567.* (Published)

3. Prajitno, M.Y., Taufiqurrakhman, M., Harbottle, D., Hunter, T.N., 2021. Kinetic Studies of Cs^{+} and Sr^{2+} Ion Exchange Using Clinoptilolite in Static Columns and an Agitated Tubular Reactor (ATR). *ChemEngineering 5, 9.* (Published)

The candidate was the main author and responsible for the experiments, analysis, figures, calculations and proof reading. The research was supervised by Associate Prof. Timothy N. Hunter and Associate Prof. David Harbottle. Experimental support was provided by Associate Prof. Nicole Hondow, Associate Prof. Huagui Zhang and Dr. Mohamad Taufiqurrakhman and all authors provided comments on the published papers.

Abstract

Clinoptilolite is a common zeolite adsorbent for heavy metals removal. Its ores are widely available, it can be simply utilised in exchange columns, while it has good ability to treat liquid radioactive wastes (LRW) such as cesium and strontium. It is also radiation tolerant, as its structure does not degrade or alter due to cesium and strontium radiation. However, only high grade clinoptilolite can be used in the nuclear industry, which will place significant challenges for ongoing effluent treatment operations worldwide, due to future critical supply issues. Therefore, this thesis investigates a number of industrially relevant techniques to enhance the quality of relatively low-grade clinoptilolite for application in the nuclear industry for cesium and strontium removal. In particular, studies focused on chemical pre-activation and milling, flotation and process intensification, as outlined herein.

Firstly, natural clinoptilolite, of relatively low-grade (as highlighted by impurities shown by electron microscopy) was investigated for its capability to remove cesium and strontium ions from fresh water and simulated seawater, by using a batch adsorption technique. Seawater is an important solvent to study, due to the reduction in metal adsorption performance from potassium interaction, and enhancements are critical for treating effluents from Fukushima, for example. To improve its capacity, the material was pre-activated with concentrated NaCl and HCl solutions. Additionally, it was milled to a number of < 300 μm size fractions, to expose exchange sites. The adsorption kinetics and equilibrium for natural and activated results were fitted with the theoretical models, where the adsorption capacity for both cesium and strontium were significantly improved by both pre-activation and milling. In simulated seawater solutions, all materials gave considerably reduced performance due to K^+ ion competition, with Sr^{2+} uptake decreased more extensively compared to Cs^+.

Secondly, flotation was investigated as a rapid separation technique to de-water fine, powdered clinoptilolite ion exchange resins by utilising cationic surfactant collectors, for the decontamination of radioactive cesium ions from nuclear waste effluent streams. Initial kinetics and equilibrium adsorption studies of cesium, suggested the large surface area to volume ratio of the fine clinoptilolite contributed to fast adsorption kinetics and high capacities. Measurements of particle sizes confirmed that adsorption of surfactant monolayers did not lead to significant aggregation of the clinoptilolite. Importantly for flotation, both the recovery efficiency and dewatering ratios were measured across various

surfactant concentrations. Optimum conditions were found with 0.5 mM of cetylpyridinium chloride (CPC) and addition of 30 µL of methyl isobutyl carbinol (MIBC) frother, giving a recovery of ~90% and a water reduction ratio > 4, highlighting the great viability of flotation.

Lastly, static elution column studies were performed with the natural clinoptilolite, to compare performance to the described batch tests, where process intensification was also performed using a novel agitated tubular reactor (ATR). Here, kinetic breakthrough curves were fitted using two models; Thomas and Modified Dose Response (MDR) models. During static column ion exchange, the maximum adsorption capacity (q_e) for ion concentrations of 200 ppm were ~171 mg/g and 16 mg/g for cesium and strontium respectively (correlating to 50% breakthrough times of 700 and 70 bed volumes). Reducing the concentration of strontium down to 100 ppm could lead to higher both q_e and bed volume, ~48 mg/g and 400 bed volumes, respectively. In contrast, reducing the residence time from 30 minutes to 15 minutes of 100 ppm strontium could decrease the q_e around 13-14 mg/g. By increasing the inner column diameter to 2 cm gave similar results to 1 cm column tests. Meanwhile, for process intensification of ATR, two-column lengths (25 and 34 cm) with 100 ppm strontium concentration and 15 minutes residence time were investigated. The 34 cm length significantly increased q_e and breakthrough times around 30%, in comparison to static columns, while process flowrates were increased ~three times for the same performance. Such considerable performance increases highlight the suitability of the ATR to deliver intensified ion exchange for a range of systems.

In conclusion, the enhancement of clinoptilolite using pre-activation and milling could considerably extend the range of natural clinoptilolite ores suitable for cesium and strontium treatment processing of relatively fresh water effluents, but improvements are required for treating cesium and strontium in saltwater in future work. Meanwhile, during flotation, it was observed that cesium contaminated clinoptilolite could be recovered up to ~90% with a water reduction ratio > 4. However, while highlighting its applicability, some aspects should be studied for future work, such as the optimum particle size of clinoptilolite, the solid/liquid ratio and influence of mixed metal ions (incorporating strontium). Also, the use of fine particles from pre-activated clinoptilolite could be investigated further during

flotation. In the static column and ATR studies, the ATR led to clear enhancements in the removal the strontium at a high rate. However, there are areas for improvement for future study, such as modifying the size of tubular reactor, its frequency or using pre-activated clinoptilolite.

Acknowledgements

First of all, great thanks to Allah, the most merciful and the most peaceful. Prayers and peace to be devoted to Prophet Muhammad, who has conveyed the teachings of truth to humankind.

The author would like to express his appreciation and gratitude to Associate Prof. Timothy Nie Hunter whom without his generous support and correct my direction whenever, I would lose the way toward achievement this work. Also, for Associate Prof. David Harbottle and Associate Prof. Olivier Cayre. Special thanks to Associate Prof. Huagui Zhang, Dr. Suparit Tangparitkul, Dr. Assim Fiaz, Alexander Saul, Associate Prof. Nicole Hondow and Dr. Mohamad Taufiqurrakhman for their guide and help during conducting this work.

Special thanks are extended to my scholarship, Indonesia Endowment Fund for Education (LPDP) for funding my PhD study along with laboratory research, living and family allowances as parts of the scholarship within 4 years and 4 months.

Warm words of gratitude to all lectures and staff in School of Chemical and Process Engineering whom help me either in giving advice or support to me. I thank all previous and current members of the Colloids and Polymer Engineering and Nuclear Research Groups who guided me in the lab and discussed my research in the group meetings. Heartfelt thanks to all my colleagues (especially Dr. Shafeeq Ahmed, Dr. Nafis Ul Haque, Dr. Ji Young Yoon, Dr. Mohammed Alshamsi, Dr. Maje Haruna, Dr. Shahid Pervaiz, Jennifer Enemmoh, Teh Dr. Sri Rahayu, and etc) for their continuous help and encouragement. With sincere also for my entire Indonesian community in Leeds and across the UK, especially for Geng Bawah Kampus, The family of Mbakdok Tika, Bang H. Arizka, Bang Aswin, Bang Haikal *Rahimahullah*, Haji Hafidz, Mas Anton, Dhe Brahma, K.H. Achmad Farid, Ustadz Dokter RS Bekti, Dhe Jumadi, Pak Hari Agung, Omtum Zain, Daeng Saad, Kang ARoh, JiSangkala, Uda Dodi, Dhe Vin, Ibu Fika, Budi KFC, Cak Thiro, Bos Bayu LP, Bos Ferry, Koor Yoga, Bang Alfen, The Goweser Leeds, Doktor Muda Harapan Bangsa, PPI and KIBAR Leeds and UK 2016-2020 members who always together in happiness and sadness.

I would like to uncounted thank to my parents Mr. Prajitno Pilih Prajogo and Mrs. Sunechi, my brother Mr. Muhammad Ibrahim and his wife Mrs. Rully Dwi Utami, my wife Anki Tias Yolanda, my son Ibrahim Kahfi Muhammad Prajitno and my daughter Humaira Az Zahra Bellevia Prajitno for their tireless giving me chance to achieve my hope, getting PhD degree in School of Chemical and Process

Engineering, University of Leeds. Last but not the least, I would like to thank for every reader who wants to take the benefits from my thesis.

Table of Contents

Table of Figures

Table of Tables

Nomenclature

Latin

a	: estimation of parameters in the non-linear regression MDR model
b	: the Langmuir constant related to the energy of adsorption, L/g
b	: estimation of parameters in the non-linear regression MDR model, L
C	: initial concentration, mM
C, C_e	: the equilibrium concentration of solute mg/L or ppm
C_0	: the initial concentration of solute, mg/L or ppm
h	: initial rate from Pseudo-Second order model, mg/g.min
K	: the equilibrium constant
k_1	: the observed rate constant of the Pseudo-First order model, g/mg.min
k_2	: the observed rate constant of the Pseudo-Second order model, g/mg.min
K_d, R_d	: coefficient distribution, mL/g
K_f	: constant for a given adsorbate, mg/g
K_{TH}	: the Thomas model constant, mL/mg.min
m	: the adsorbent mass, g
n	: constant for a given adsorbent
Q	: the effluent flow rate, mL/min,
q, q_t	: the amount of adsorbed solute at time t, mg/g
Q_c, q_m	: the maximum adsorption capacity, mg/g
q_e	: the amount of adsorbed solute at equilibrium, mg/g
R	: the universal gas constant, J/mol.K
T	: Temperature, K
t	: time, min
V	: the volume of solute, L
V_{eff}	: the effluent volume at time t, L

Greek

γ	: the surface tension for a specific surfactant initial concentration, N/m
γ_0	: the surface tension of the pure solvent, N/m
Γ_{max}	: the maximum surface coverage of surfactant, mol/m^2
ΔG	: Gibbs free energy, kJ
ΔH	: enthalpy, kJ
ΔS	: entropy, kJ/K

Abbreviations

AAS	: Atomic Absorption Spectrophotometer
ATR	: Agitated Tubular Reactor
BET	: Brunauer–Emmett–Teller
CMC	: the critical micelle concentration
CPC	: cetylpyridinium chloride
CTAB or HTAB	: etyltrimethylammonium bromide
EDAB or EHDA-Br or EHDa-Br	: ethylhexadecyldimethylammonium bromide
EDL	: electrostatic double layer
EDX	: Energy Dispersive X-ray
HAADF	: High Angle Annular Dark Field
HEU	: Heulandite
IAEA	: The International Atomic Energy Agency
ILW	: Intermediate Level Waste
LHS	: Left-Hand Side
LLW	: Low Level Waste
LRW	: Liquid Radioactive Waste
MDR	: Modified Dose Response
MIBC	: methyl isobutyl carbinol
MTZ	: Mass Transfer Zone
PFO	: Pseudo-First Order
PI	: the process intensification
PSO	: Pseudo-Second Order
RHS	: Right-Hand Side
SEM	: Scanning Electron Microscopy
SIXEP	: The Site Ion Exchange Effluent Plant
STEM	: Scanning Transmission Electron Microscopy
Surfactant	: surface active agent

TM	: Thomas Model
TPC	: three-phase contact
UK	: United Kingdom
XRD	: X-Ray powder Diffraction

Chapter 1 Introduction

Chapter 1 gives a brief introduction to the use of clinoptilolite to remove radioactive cesium and strontium ions (the focus of this study) and the various techniques that have been used for their removal from liquid effluents. Subsequently, research novelty, research aims, and objectives are also highlighted in this chapter. Finally, an outline of the topics to be discussed in following sections of the thesis are also provided.

1.1. Research background, novelty and opportunities

Nuclear fission is the process of decomposing a heavy nucleus into fission products and several neutrons (1). In nuclear power plant generation, the heavy nucleus Uranium-235 (^{235}U) are bombarded with slow neutrons in fission reactions, resulting in an energy of around ~200 MeV (1 eV = $1x10^{-19}$ J) and fission products with different half-lives (1, 2). Among these fission products, Cesium-137 and Strontium-90 are types of radioactive waste which belong to the highest yield fission products (6.337% and 4.505%, respectively) (1, 3, 4). Both radioisotopes are classified as the Intermediate Level Wastes (ILW) due to half-lives (around 30 years) and their low heat generation (1, 3-8). Also, it is essential to treat these radioisotopes because of their high solubility in an aqueous environments, which can cause cancer or acute death to humans and aquatic life (8-14). Therefore, immobilisation is required to keep the public and environment safe from the hazard potential that may arise from this waste.

There are several techniques to manage cesium and strontium release from nuclear effluents, such as: precipitation, flotation, vitrification, ion exchange column and many more (1, 5, 6, 15-17). To date, much of this research has focused on removal using ion exchange, especially using clinoptilolite as ion exchange and adsorbent material (15, 18-32). Clinoptilolite (or ‘clino’ as it is often called in short) has been relied on for radioactive waste disposal, because its ores can easily be found around the world, and high-grade material does not require a complicated treatment process in order to make it ready to use to treat liquid radioactive wastes (LRW). It also has good material resistance to high radioactive exposure (18, 23, 28).

However, there are a number of limitations to using clinoptilolite, including its poor efficiency in high salinity, such as seawater, which has been reported by Wajima (33). Additionally, within the nuclear industry, clinoptilolite is commonly used to remove radioactive cesium and strontium, because it has high cation-exchange capacities and selectivity for both elements, especially for cesium. (18, 20, 21, 24, 25, 27-31, 34-36). However, the only clinoptilolite that can be used in the nuclear industry, is the highest-grade material. For example, on nuclear sites such as Sellafield (the UK's largest nuclear reprocessing site) their clinoptilolite is only obtained from a single deposit in California, which has good selectivity for both ^{137}Cs and ^{90}Sr, and contains a low level of impurities (32, 37-39). Therefore, potential future supply issues are a critical concern to the industry. Indeed, even though deposits of clinoptilolite are numerous around the world, performance characteristics are very variable, and most material is not of a grade sufficient for nuclear use, due to contaminant impurities. Thus, it is important to study the possibility of using natural low-grade clinoptilolite, which is not commonly used in the nuclear industry, to determine its potential as an alternative in the case of work supply disruption.

The challenge of using relatively low-grade clinoptilolite for cesium and strontium removal undertaken in this thesis, is to investigate how well different, relatively straight forward, methods work to increase its capability to a meet similar quality to the type currently uses at Sellafield. Initially, the use of chemical pre-activation and milling are investigated. As reported by Motsa *et al*, it has been found that adding acid and salts to clinoptilolite during pre-treatment can increase lead adsorption capacity (40). Therefore, similar pre-activation methods could be one of the new ways to increase cesium and strontium removal. Also, in fact, several studies have discussed using milled/crushed clinoptilolite on heavy metal ion removal (21, 29, 30), but these did not focus on different particle size effects in this regard. The study of different particle size effects is important, because it will not only show how the different sizes may affect cesium and strontium removal performance, but can also be used to determine the best ion exchange technique (either in continuous columns or batch contact tanks) for removing cesium and strontium. Moreover, the study of clinoptilolite in a saline environment, based on lessons from the Fukushima accident in 2011, also offers a great opportunity, as this remains a currently under-researched area (33, 41). This is because it became evident that the seawater used in the cooling water cycle at Fukashima prevented the use of clinoptilolite or any natural zeolites. Therefore, there is a great need to study the effects of activation and milling on

increasing the adsorption in saline environments, and a comprehensive study on the specific effects of ions competition during adsorption (23, 33, 42).

The second topic investigated in this thesis is flotation. Flotation may be an excellent candidate to dewater fine powdered clinoptilolite, allowing smaller particles to be used in a batch reactor system. As stated (with regards to milling) finer particles with higher surface area to volume ratio should improve flotation efficiency, allowing lower grade material to be used (43-45). Also, flotation is an option due to the high capability for solid ion exchange, high dewatering factor and smaller residence times compared to gravitational sedimentation (46, 47). Moreover, in the nuclear industry, the flotation technique is used increasingly for separating solids, which contain radioisotopes such as cobalt, as part of rapid nuclear dewatering processes (30, 48-56). Even though some evidence suggests that flotation can be used for nuclear effluent treatment, there remains a lack of knowledge regarding how clinoptilolite can been used in the nuclear industry, especially regarding the influence of adsorbed cesium or strontium. Many knowledge gaps can still be observed, such as the potential for surfactant collector adsorption to remobilise and remove contaminated radioisotopes; the effect of ion contamination which can reduce recovery during flotation removal; and the optimum parameters between the recovery and good dewatering ratio. Research on using clinoptilolite with the flotation technique is critical, because it can provide a potentially viable option for a rapid nuclear dewatering process.

The last novelty in this study is the use of natural, relatively low-grade clinoptilolite for the cesium and strontium using ion exchange column and agitated tubular reactor (ATR). Column ion exchange has been commonly used for this remediation in the nuclear industry around the world, such as at Sellafield, UK (32, 57-60). Also, in ion exchange columns, no further treatment such as milling is required, because reducing the particle size can increase the pressure drop which can, in turn, reduce the adsorption of nuclear waste (32, 37). Dyer *et al*. (32) also reported that clinoptilolite has been found successfully to remediate nuclear liquid wastes, such as cesium and strontium (32). However, the clinoptilolite that has been used fulfilled the UK's nuclear regulatory standard, with a very small amount of impurities. For that reason, the use of relatively low-grade clinoptilolite for removing cesium and strontium by using ion exchange column technique is an important area to study.

Another way to utilise lower grade clinoptilolite is to use an intensified ion exchange system. In particular, systems that generate higher mass transfer rates,

such as Rotating Bed Reactors, have proven to lead to enhanced ion exchange in removing contaminants from liquids, including dyes, fertilisers and heavy metals (61-65). However, RBRs have a limitation on performing in high percentage of removal species, as they are dependent on rotation speed and small residence time which resulting multiple passes in order to meet the high percentage (65). As an alternative, another way to enhance the percentage of removal species is by designing flow reactors that can generate shear independently (to improve mixing), which agitated tubular reactors (ATR) are the example. ATR are intensified reactor plug-flow reactor where high rate lateral shear is generated with inner agitator bar, decoupling mixing dynamics from the bulk flow (61, 66). The application of ATR remains limited and novel, as there has been no research related to nuclear liquid treatment. However, the enhanced lateral shear should provide better mixing, thereby allowing increased flow rates to be accessed, which possibly can be used for rapid ion exchange column process, which has been explained on simulation by He *et al* (67, 68). The gaps which can be studied include the design of continuous adsorption process and the calculation and analysis after the process. This study is vital due to the visibility of enhancing the nuclear effluent separation process by ion – exchange column technique. So later on, from this study, the ATR can be an alternative solution for rapid nuclear effluent separation process.

1.2. Research aims and objectives

Aim: This study explores the capability of using natural, relatively low-grade clinoptilolite to remove cesium and strontium in nuclear applications. Different ion exchange techniques will be investigated to produce an alternative, high efficiency solution in the case of a future supply shortage of high-grade material. The project's aim will be achieved by addressing the following objectives.

Objectives:

(1) To study the adsorption of cesium and strontium on natural relatively low-grade clinoptilolite in clean water and saline environments.

(2) To optimise clinoptilolite performance using chemical activation and milling to improve the adsorption of cesium and strontium.

(3) To study the use of flotation for the rapid dewatering of contaminated powdered clinoptilolite.

(4) To study continuous elution column and intensified agitation techniques in order to enhance cesium and strontium removal in an industrial relevant process.

1.3. Thesis outline

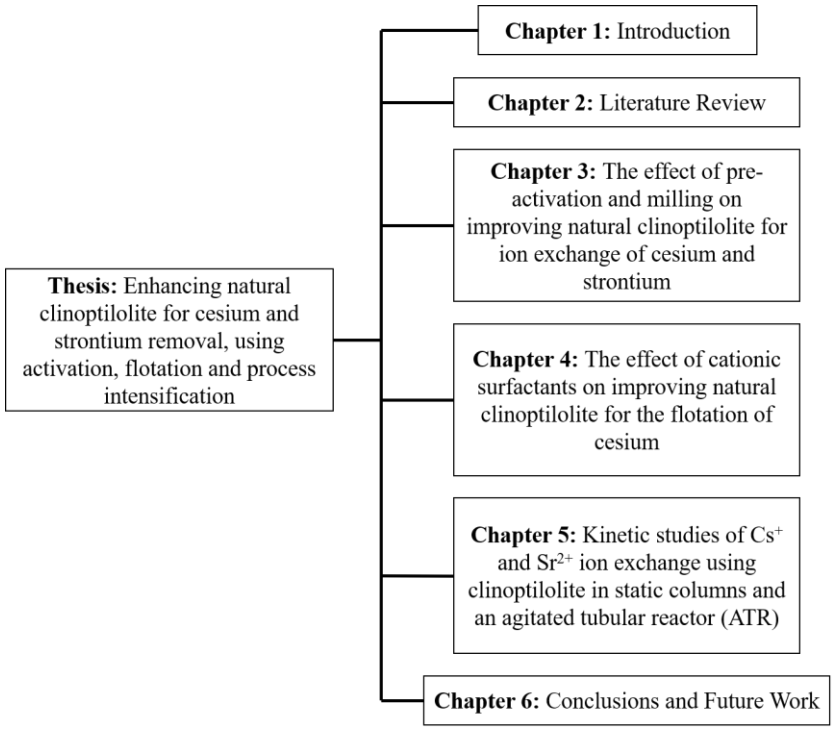

Figure 1.1: Flow diagram of thesis outline

Based on Fig. 1.1, the main contributions of the thesis are highlighted. Chapter 1 will cover the research background, novelty, and opportunity; research aims and objectives; and thesis outline. The fundamental and science of the thesis experiments and analysis will be explained in Chapter 2. The effect of pre-activation and milling were used to study the improvement in natural low-grade clinoptilolite during cesium and strontium adsorption, which will be explained in Chapter 3. The particle characterisation of natural low-grade clinoptilolite was studied in this chapter. In addition, acid and salt were used for pre-activation; meanwhile, the ball milled technique was used for particle size reduction. Enhancements were evaluated and compared to the natural low-grade clinoptilolite. This chapter also studied the effect of ion competition in cesium and strontium removal. The ions were among the highest concentrations in seawater,

which are potassium, sodium and calcium. Overall, this work highlights that the pre-activation and milling of clinoptilolite can be used significantly to enhance the grade of the ore for nuclear effluent treatment in low-salinity conditions.

Meanwhile, in Chapter 4, the rapid dewatering of fine contaminated clinoptilolite powder with cesium is studied, using froth flotation. Cesium contamination was studied due to the fact that clinoptilolite offers the best way to remove cesium compared to strontium, according to Chapter 3. Two cationic surfactants with different concentrations were used in order to find the optimum condition for flotation recovery along with a good water reduction ratio. In this chapter, the surface tension method was also used to study the potential adsorption of surfactants onto contaminated powdered clinoptilolite.

In Chapter 5, natural relatively low-grade clinoptilolite was used in static ion exchange columns and an agitated tubular reactor (ATR). The types of ion, effect of concentration, volume of adsorbent and residence time were studied in this chapter. Meanwhile, in the ATR, different volumes of adsorbent were studied and compared with the static columns to highlight efficiency gains in using an intensified process technology.

The thesis' conclusions and suggestions regarding future work are presented in Chapter 6. This chapter covers the aims and objectives of this research, which is to develop a better understanding of the effect of optimised clinoptilolite with regard to removing cesium and strontium using various techniques, especially the adsorption, flotation, column and continuous agitation techniques. This research shows that optimised clinoptilolite has the potential to lead to a positive improvement in cesium and strontium removal. The opportunities for future work in this area are also summarised in this chapter.

Chapter 2 Literature Review

In this literature review is discussed five sections; including cesium-137 and strontium-90 in the Section 2.1; clinoptilolite as an ion exchange material for heavy metal removal especially for cesium and strontium in the Section 2.2; adsorption process in the Section 2.3; flotation for rapid waste separation in the Section 2.4; and Measuring ion exchange performance in operational continual-flow elution columns in the Section 2.5; and the summary of literature review in the Section 2.6. These sections are constructed into flow diagram in Figure 2.1.

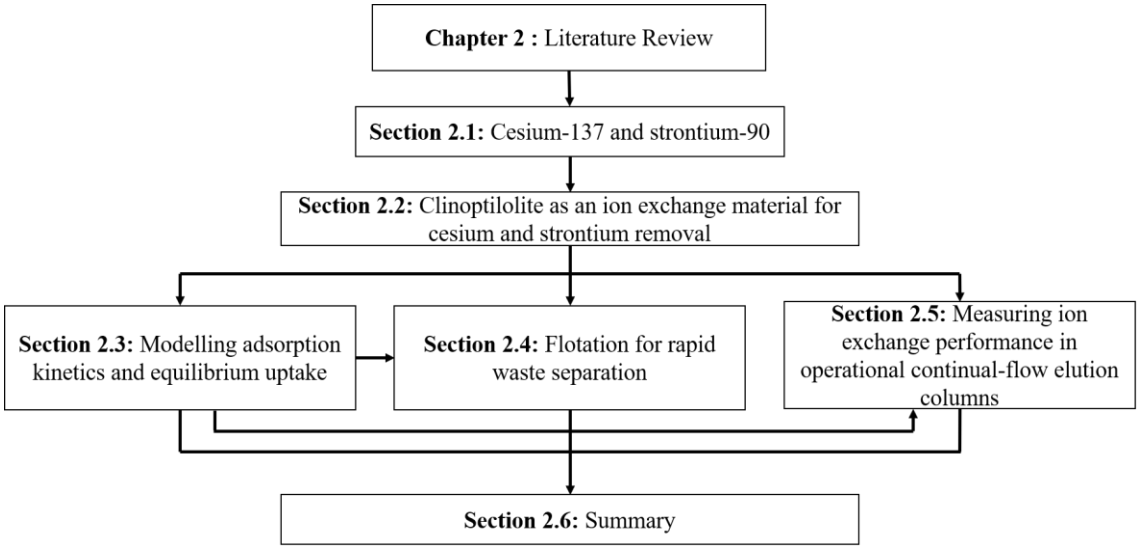

Figure 2.1: Flow diagram of literature review

According to Figure 2.1, the Cesium-137 and strontium-90 section covers the background on radioactive cesium-137 and strontium-90 ions. Also, the subsection gives a brief description on how to remove these radioisotopes, with a focus on the adsorption technique. The Clinoptilolite section presents details on the use of clinoptilolite in treating heavy metals, and specifically for its use with cesium and strontium removal. The Adsorption section describes the general mechanism of the adsorption and ion exchange processes, adsorption kinetics and equilibrium and the effect of ion competition during the adsorption process. Meanwhile, the flotation section includes background details of the flotation process, including surfactants and the effect of surfactant particle interaction in the flotation process. Finally, Measuring ion exchange performance in operational continual-flow elution columns section discusses the general use of vertical elution ion exchange column processes for cesium and strontium removal and

the potential alterative using intensified methods, such as an agitated tubular reactor (ATR).

2.1. Cesium-137 and strontium-90

Any radioactive materials that are wastes from nuclear power plants (NPP) and other nuclear activities such as research or even medicine are called radioactive wastes.

Radioactive wastes are extremely hazardous, with a wide variation to reduce their energy by half (half-life) from tens up to thousands of years. Therefore, regulations are required to protect humans from getting any radiation effects. The International Atomic Energy Agency (IAEA) has categorised radioactive wastes into different classes, depending on their activity, half-life and also the requirement of containment heat dissipation (3). However, this classification could be different, depending on the categorisation purpose. For example, in countries such as the United Kingdom (UK), wastes are generally classified into three categories (High Level Waste (HLW), Intermediate Level Waste (ILW) and Low Level Waste (LLW)), where the difference is only on the potential ability of heat generation on their radionuclides (2, 5, 69). The classification is regularly updated in order to create more safety management to the waste. The latest classifications from IAEA are mentioned at Figure 2.2.

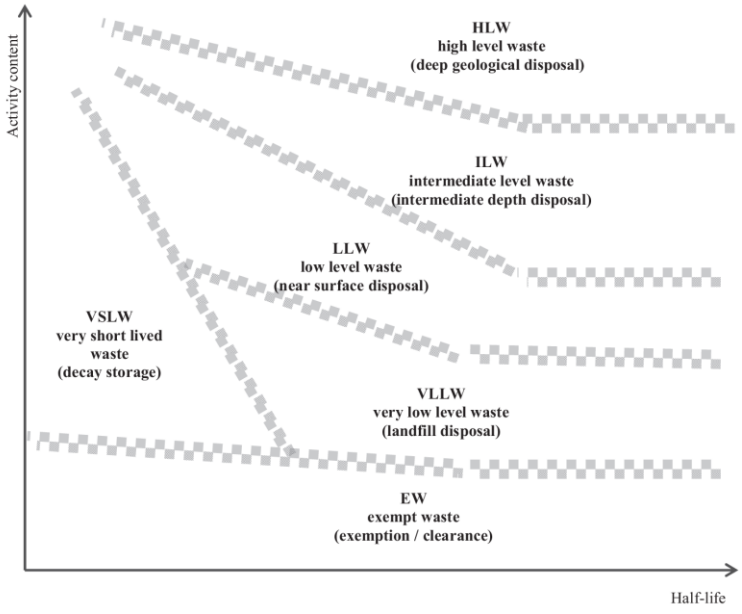

Figure 2.2: Conceptual illustration of the waste classification scheme (3)

Generally, radioactive cesium-137 and strontium-90 bearing wastes are classified as intermediate level wastes (ILW) (3, 70) which is shown in Figure 2.2. Radioactive cesium and strontium salts are very soluble in water phase and thus potentially are released into the soils, rivers and oceans (1). Therefore, treatments are required to remove them from effluent streams, resulting in solid wastes which is usually stored at near-surface sites or deep geological repositories, with a varying depth between tens to hundreds of meters (3, 5, 71). The disposal routes should be designed for minimal intrusion of human activities to prevent ongoing exposure (3, 5, 71).

Cesium-137 (^{137}Cs) is a beta-emitting radioisotope form of cesium, which is obtained from fission products from the fission reaction of uranium-235 and other fissionable isotopes in nuclear activities. It is one of the highest yield ratio of medium-lived fission products product in nuclear reactors (around 6.337 %) with an activity of 3.215 TBq/gr and half-life around 30.17 years . When it decays, it has two daughters as illustrated in Figure 2.3.a. In addition, strontium-90 (^{90}Sr) is beta emitter with variance half-life of from 28 years up to 29.1 years (1). Similarly to cesium-137, strontium-90 mainly forms from the fission of uranium-235 and other fissionable isotopes. It also belongs to one of the most yield ratio of medium-lived fission product, with around 4.505 %, while the activity is 5.21 TBq/gr (1).

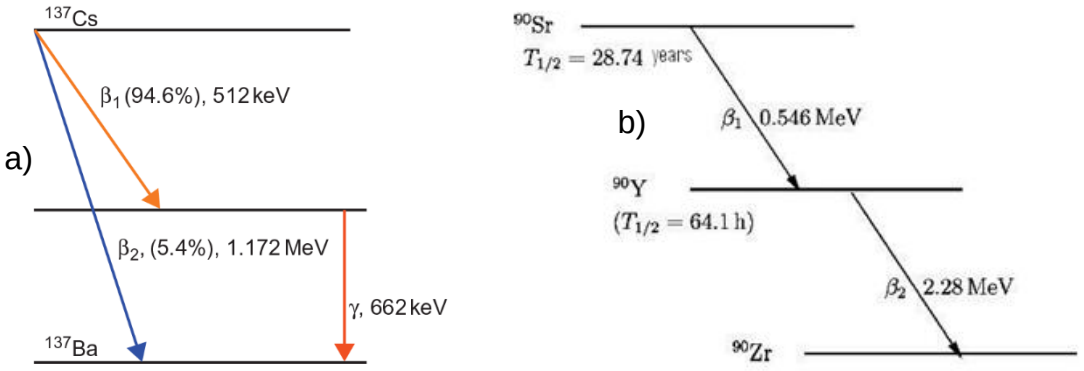

Figure 2.3: Decay scheme and energy emitted of: a.) ^{137}Cs and b.) ^{90}Sr (1)

Figure 2.3.a. explains how cesium-137 (^{137}Cs) decays into several radioisotope elements and emits energy. It shows that almost 95% of it decays to form barium-137m (^{137m}Ba) and the rest is formed as barium-137 (^{137}Ba) which is more stable as a radioisotope. Barium-137 has a half-life of 154 seconds and is used for gamma emitter, because it emits gamma spectra with energy 0.6617 MeV. (1, 3, 10). Meanwhile, strontium-90 decays to ^{90}Y then ^{90}Zr with following decay scheme in Figure 2.3.b.

Radioactive cesium and strontium are considered as one of the most problematic of short and medium lived fission products, due to their highly mobile nature within the environment, connected to their high solubility in water (1). The high solubility of cesium in water, is due to the production of cesium hydroxide as the primary corrosion product, which is a highly water-soluble compound. In addition, strontium-90 is high water soluble and also easily transported with rain and groundwater into soils. Once these have been uptaken by plants or consumed by humans, between 30% and 40% is absorbed into blood and deposited in bone or in soft tissue, wherein even small amounts can cause cancer and in large amounts can cause severe acute sickness or even death (1, 5, 30).

Even though radioactive cesium and strontium are considered to be hgihly dangerous and hazardous, at right dosage, both radioactive isotopes can be used in some applications, such as moisture-density gauges in the construction industry, levelling gauges in piping and tanks industry, thickness gauges and well-logging in the drilling industry. These radioactive can also be used in medicine for treating cancer during radiotherapy treatment (1).

Because of these characteristics, there is a significant academic and industrial driver to undertake research in managing and removing these two radioisotopes from industrial wastes and environmental flows.

2.1.1. Cesium-137 and strontium-90 removal from effluent streams

The idea of radioactive waste management, is to control radioactive waste production and release for the purpose of protecting human life and the environment from radioactive effects now and into the far future (1, 3, 10). In order to maintain human and environment health, the generation of radioactive waste should be controlled, in general, as following Figure 2.4 (1).

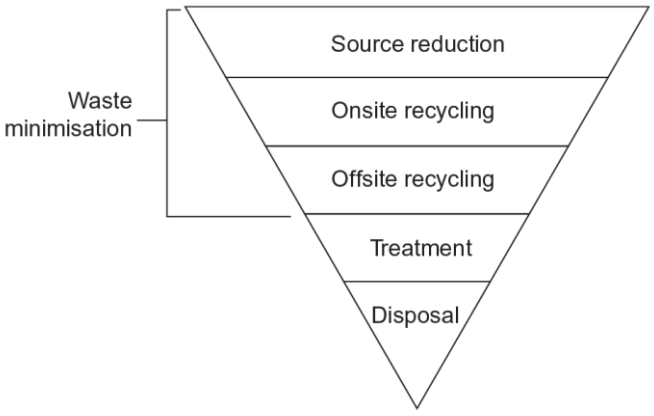

Figure 2.4: Control of radioactive waste generation (1)

Based on Figure 2.4, the main idea is to concentrate and manage radioactive waste rather than release it into the environment. This control should include pre-treatment, treatment, conditioning, storage and disposal. Every step should be followed with appropriate safety requirements and adequate regulation by country and federation. Time management should be taken into account in practice, to prevent human exposure (1).

There are some aspects that need to be considered during radioactive waste treatment, such as physical, chemical and radiological properties (1). Due to their high radiological hazard and water solubility, cesium-137 and strontium-90 are considered to be the primary mobile radioisotopes that are removed from any liquid effluents which come into contact with radioactive fuels (e.g. cooling circuit waters, pond waters and effluents from fuel reprocessing).

There are many techniques that can be used for removing these radioisotopes from the effluent depending on raw materials availability, simplification method, cost and removal efficiency (1, 2, 10, 72, 73). For many studies, research is conducted on stable chemical isotopes rather than radioisotopes, because of the small differences in chemical properties to the radioisotopes, saving the cost by removing strict regulation (15, 21, 49, 74). However, to get a better understanding about radiation behaviour, sometimes radiotracers are also used (21, 74, 75). Some techniques that can be used for removing radioactive cesium and strontium from waste effluent are presented in Table 2.1, and will be discussed throughout this literature review.

In brief, the techniques for removing cesium and strontium from waste effluents may be generally differentiated into batch adsorption, ion exchange column, precipitation and evaporation. Each technique described in Table 2.1. has a specific purpose and use. For example, for fast and simple operation, batch adsorption is the best choice (15). However, this technique cannot be operated in a continuous system; therefore, the ion exchange elution columns are more often used in many industrial systems (1, 76). For highly saline conditions, or for when multiple heavy metals are needed to be removed, precipitation reactions offer an alternative (1, 43, 54, 76-80). Lastly, evaporation is a simple operation that results in very high decontamination factors, however, it can generate corrosion issues reducing reactor lifetimes, and is very energy intensive (1, 76). Evaporation will not be considered in any detail within this thesis.

Table 2.1: Some techniques are available for radioactive cesium and strontium removal

	Batch adsorption	Ion exchange column	Precipitation	Evaporation
Introduction	The liquid radioactive incorporates with the adsorbent in the mixing reactor. The adsorbent can be from inorganic materials such as zeolite, kaolinite and clinoptilolite (18, 23, 29, 81-83); can be from conjugate material (84, 85) and from membrane (86, 87).	The radioactive effluent are injected continuously through ion exchange column to contact the adsorbent depth in the bottom side of the column (32, 57-59). The adsorbent usually from inorganic material such as zeolite and clinoptilolite (32, 59).	The radioactive effluent is precipitated using insoluble compounds such as hydroxides, carbonate, phosphates and ferrocyanides. Normally followed with gravitational separation or filtration dewatering, but often now studies remove via flotation (43, 54, 77-80).	The radioactive effluent is removed in the vapour phase (1, 76, 88, 89)
Advantages	Fast, efficient reaction and simple operation (15)	Continuous process and simple operation (1, 76)	Appropriate for saline conditions (1, 43, 54, 76-80)	Simple operation (1, 76, 88, 89)
Disadvantages	One process only where the adsorbent requires further treatment to be stored (1, 15).	The process usually takes slow and adsorbent size is crucial where small size could affect higher gravitational force while reducing the removal quality (21, 32, 76).	Gravitational sedimentation of flocculated precipitates is relatively slow where large vessels are required (54, 79)	The process takes long time and could raise potential problems such as corrosion and foaming (1, 76). Also, very energy intensive.

2.2. Clinoptilolite as an ion exchange material for heavy metal removal

As mentioned in Table 2.1, clinoptilolite is one of the most common adsorbents for cesium and strontium removal. Natural clinoptilolite can be found in many ore deposits, such as rocks and within sediments such in soil, lava, or even in shallow lakes (90-94). In essence, clinoptilolite is a common form of heulandite (HEU) type zeolite, with a distinctive framework and topology and Si/Al ratio >4.0. The complex chemical formula is different depending on the origin of clinoptilolite. However, its formula commonly should generally contain the constituent ratios, as described in the below formula (95).

$$(K_2, Na_2, Ca)_3[(Al_6Si_{30})O_{72}].24H_2O$$

This is arranged in a framework consisting of ten- and eight-tetrahedral rings that form pores within channels in the centres of the rings capable of ion exchange, which generally have a diameter within the interval 3 - 8 Angstroms (96, 97). Cations such as K^+, Na^+ and Ca^{2+} are located in in the interstices within the crystal structure, and are present to balance the charge, due to aluminium induced charge imbalance (97). The ratio of these cations also determines the type of clinoptilolite (e.g., K-clinoptilolite; Na-clinoptilolite and Ca-clinoptilolite types). During the sorption process, cations from the environment such as cesium and strontium will induce the interstices or replace the existing cations in the interstices. The cesium and strontium adsorption generally occurs at the surface, rather than internal channels (98). This process will take place until there is no place of interstices can be placed or replaced by the cations from environments (99). The schematic process of sorption process on clinoptilolite is described in Figure 2.5.

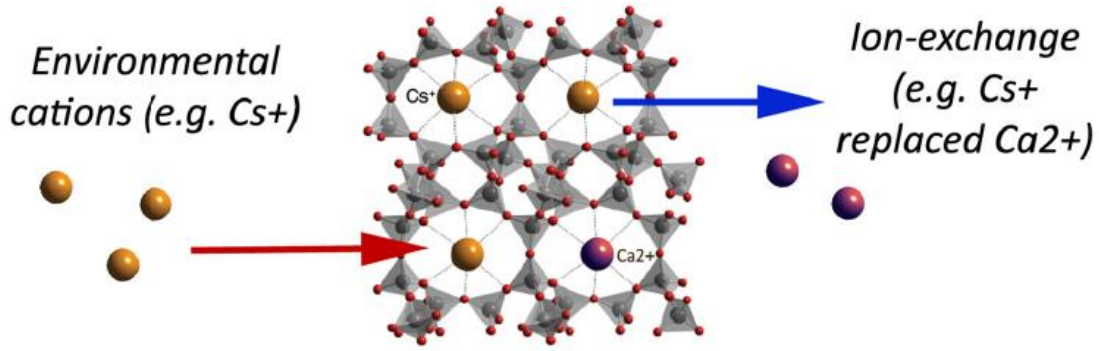

Figure 2.5: The schematic process of cesium sorption on clinoptilolite (99)

Meanwhile, to study the characteristic of natural clinoptilolite, scanning electron microscopy (SEM), X-ray powder diffraction (XRD), surface charge and particle size distribution analyses are commonly used (30, 31, 97, 100). From SEM imaging, the characteristics of natural mined clinoptilolite powders consist of irregular shaped particles, as shown in Figure 2.6 (30, 31, 97, 100). Meanwhile, from XRD result, which is showed in Figure 2.7., shows that the pattern of the natural clinoptilolite sample has an obvious crystalline structure and the pattern is identified similar to peaks for heulandite (HEU) pattern at 9.86° , 11.17° and 22.34°(30, 97). In addition, clinoptilolite used as an ion exchange resin normally has a particle size distribution within 100 – 300 µm and zeta potential within -30 down to -40 MeV (20, 25, 27, 30).

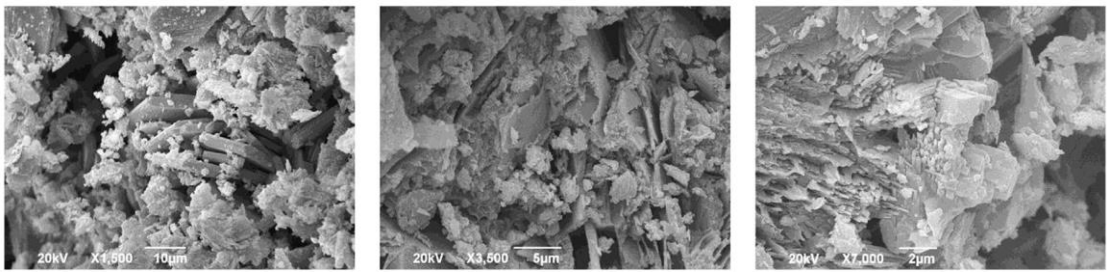

Figure 2.6: SEM of raw samples of natural clinoptilolite (97)

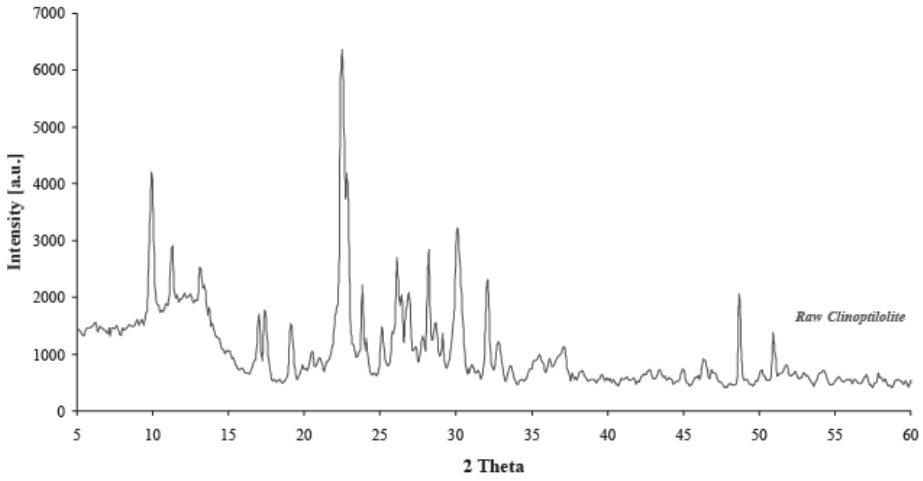

Figure 2.7: XRD pattern of raw (natural) clinoptilolite (97)

The use of clinoptilolite as an ion exchange resin, is not only common within nuclear industry, but it is also applied in a range of non-nuclear applications. For example, natural clinoptilolite can be found in ammonia removal from the water, where has widely been used as an additive to animal feed for removing ammonia in animal manure (99). Also, it can be found in heavy metal waste treatment industries, for removing many species, such as arsenic,

cadmium, copper, iron, lead and zinc removal from waste water (40, 101-107). The reason for the wide use of clinoptilolite in non-nuclear applications, is because it has a negatively charged lattice which can balanced by cations from heavy metals in solution (101, 103, 106). It is abundantly available in many deposits around the world, while it can attain high adsorption capacity, and is a simple treatment and low cost treatment (40, 99, 101, 104, 106). However, while specific clinoptilolite deposits may have high adsorption capacity, there is large natural variation, and thus researchers in many areas are focused on understanding methods to improve its capacity, such as improving particle surface area properties, use of chemical pre-treatments or production of synthetic variants (40, 101, 103, 107-110).

For example, one promising improvement technique is to pre-exchange with chemicals such as salts (MnO_2, NaCl) or acids (20, 21, 23, 40, 107). This pre-treatment usually called 'activation' (as it leads to activation of a higher percentage of ion exchange sites by exchanging with contaminants). The effect of activation to the metal ions, as described by Motsa *et al.*, is highlighted in Figure 2.8 for the removal of lead ions using clinoptilolite (40).

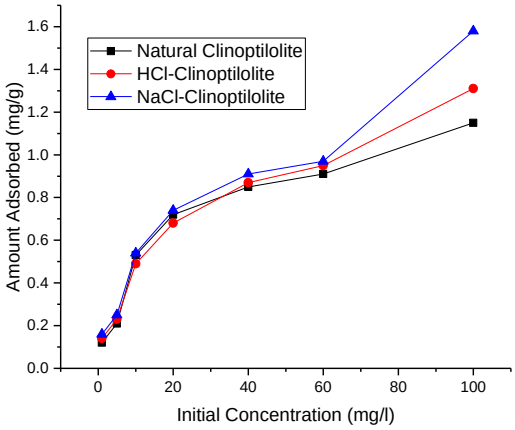

Figure 2.8: Pb uptake by various activated clinoptilolite in adsorption technique (40)

Based on Figure 2.8, the activated clinoptilolite shows better performance compared to natural clinoptilolite. The reason is because salt ions such as Na^+ are monovalent (and so easily exchanged) but also belong to the most weakly bound ions in clinoptilolite compared to other alkali and alkaline earth metal ions. Thus, exchange with other heavy metals is enhanced (111). Meanwhile, with an acid treatment, acid could increase both specific surface area and microporosity, also improving the amount adsorbed of metal ions (112). Both salt and acid can remove the impurities that block pores, by replacing the impurity ions (22, 113,

114). Therefore, the effective surface area is increased which enhances the adsorption capacity.

2.1.1 Clinoptilolite as an ion exchange material for cesium and strontium removal

In the nuclear industry, clinoptilolite can be found as a current ion exchange resin of choice in a number of waste processing facilties worldwide, such as for radioactive cesium and strontium removal from fuel storage pond waters at Sellafield, UK (Europes largest nuclear waste treatment facility) where around 4000 m^3 water/day are treated in the Site Ion Exchange Plant (SIXEP) (2, 37, 115). It has also been reported in the National Reactor Station, Idaho, USA where around 4 x 5.3 ft^3 columns 12000 gal water/ft^3 were treated using clinoptilolite (1, 5, 115). Moreover, spent clinoptilolite is incorporated easily into a cement matrix which can reduce the volume and immobilize the effluent from leakage and spillage (1). This has been reported by the Moscow Scientific-Industrial Association RADON, Moscow, Rusia where clinoptilolite contains LRW up to 10^{-3} Ci/L was incorporated with cement mortar up to 1 m^3/h (116).

There has been a large number of studies into the use of clinoptilolite for removing cesium-137 (Cs-137) and strontium-90 (Sr-90) from liquid nuclear effluents, with a few key papers summarised in Table 2.2.

Table 2.2: The use of clinoptilolite in removing Cs^+ and Sr^{2+}

No.	Initial concentration (ppm)	Adsorption Capacity (mg/g)	Refs.
1.	Cs^+: 5-1000 Sr^{2+}: 5-1000	49.02 9.8	(18)
2.	Cs^+: 7.9-3946.5	170.35	(29)
3.	Cs^+: 0.132-13290.5	3	(15, 21)
4.	Cs^+: 50-3500 Sr^{2+}: 50-3500	185.18 70.42	(31)
5.	Sr^{2+}: 50-400	20.58	(100)
6.	Sr^{2+}: 10-2500	65.63	(117)

Adsorption capacity is the maximum capacity of the adsorbent to host ions from effluent during the exchange process, where its calculation is explained in more detail within the adsorption equilibrium discussion (Section 2.3) (15, 20, 21, 118, 119). The adsorption capacity of clinoptilolite for cesium and strontium is

quite variable, as highlighted in Table 2.2. This variation could be due to many aspects which can't be identified individually; such as the selection of an appropriate solid/liquid ratio, where lower solid/liquid ratio may increase the adsorption capacity (15, 18, 21, 29, 117). It also found that pre-activation by adding chemical to the natural clinoptilolite could also affect the adsorption capacity (31, 100, 120). In addition, reducing the particle size of clinoptilolite used in exchange could also induce a high adsorption capacity through the greater surface area to volume ratio (31, 117), while natural variation in clinoptilolite properties is also a factor (as discussed).

Also from Table 2.2, it is noted that the concentration range of ions previously studied is varied, and depends on the actual waste concentrations encountered in the nuclear industry (1, 32, 37, 121). In general, the actual radioactive waste concentration of cesium and strontium is considered to be very low, and often less than 5-10 ppm (1, 32, 37, 121). Meanwhile, investigating high concentrations of ions is often used only during experiments in order to determine the maximum adsorption capacity of the adsorbent.

It is also critically noted from Table 2.2 that cesium has a significantly higher adsorption capacity than strontium, which is caused by its strong relative affinity to zeolite ion exchange sites and the valency effect. The hydrated ionic radii and ion concentration play a significant role in this affinity (18, 20). Smaller radii will move more freely into and out of the clinoptilolite channels (18, 25), while in general. the adsorption of monovalent ions such as cesium (Cs^{+}) is much more energetically favourable than divalent ions including strontium (Sr^{2+}) (20, 23).

One significant of clinoptilolite for nuclear applications is that solution pH does not strongly affect the Cs^{+} adsorption capacity, where it has been found that at pH 2 – 12, adsorption remained almost constant (18, 20). Similar to Cs^{+}, Sr^{2+} is also quite stable between pH 2 – 10, in terms of its adsorption capacity. However, it has been found that Sr^{2+} increased significantly after pH 10 which might be caused by the adsorption of Sr^{2+} and $Sr(OH)^{+}$ on OH^{-} surface groups and also by less competition from H^{+} ions for adsorption sites (18).

The ability of adsorbent to adsorb adsorbates also depends on the intermolecular forces of the adsorbate itself, especially in large sludge production, where many monovalent cations are obtained. Particularly, ions that are found to be hard to be adsorbed have a larger ionic radii, and are less competitive compared heavy metal monovalent cations (which conversely have smaller hydrated ionic radii, see Table 2.3). For example, strontium is less competitive compared to potassium (K^{+}), sodium (Na^{2+}) and calcium (Ca^{2+}) ions during

strontium adsorption, which leads to a rapid reduction in high saline waters such as sea water, as shown in Figure 2.9 (38). This is because K^+, Na^+ and Ca^{2+} ions will block the strontium adsorption. As explained by Woods and Gunter (25, 122), the affinity of adsorbent toward ions depended on their hydrated ionic radii (Table 2.3). Smaller hydrated ionic radii could move more freely in or and out of the adsorbent channels during adsorption process (18, 25, 123).

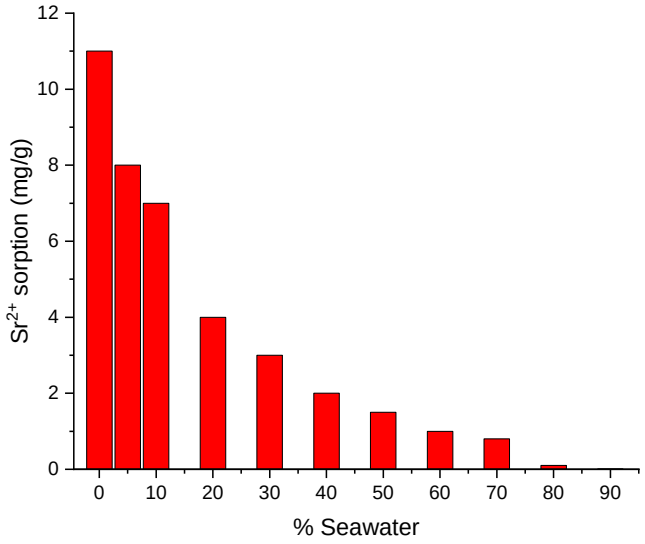

Figure 2.9: The influence of seawater concentrations on sorption of strontium on clinoptilolite (38)

Table 2.3: The hydrated radii in difference ions for selected ions (122)

Ion	Hydrated Radii (Å)
Na^+	3.58
K^+	3.31
Cs^+	3.29
Ca^{2+}	4.12
Sr^{2+}	4.12

2.3. Modelling adsorption kinetics and equilibrium uptake

As discussed, ion exchange along with other methods of adsorption are common techniques being used for the treatment of radioactive wastes. To determine the reaction process, thermodynamics is usually used, balancing Gibbs free energy (ΔG), enthalpy (ΔH) and entropy (ΔS). Inglezakis and Zorpas

(124) classified the reaction process into three types which are physisorption, ion exchange and chemisorption. The classification is classified based on the activation energy in Table 2.4 (124).

Table 2.4: Process classification (124)

Type	Activation energy range (kJ/mol)
Physisorption	<40
Ion exchange	24-40
Chemisorption	>40
Ion exchange in zeolites	0.2-80

First is where interaction between ions, atoms or molecules adsorbed (called the adsorbate) with the substance (adsorbent) is purely physical, where the interaction is a result of van der Waals forces or electrostatic interactions which this process is called physisorption (5). Second is chemical adsorption, where the adsorbate is chemically bonded to the surface of adsorbent (5, 20, 125). The last is ion exchange, where an adsorbate ion is exchanged with an adsorbent ion (124), and normally has activation energies closer to physisorption, however, strong ion exchange interaction may lead to energies closer to chemisorption.

Thermodynamic reactions for cesium and strontium removal by clinoptilolite type species in different systems have been found to be endothermic in nature (24, 29, 31, 100, 126), where the adsorption capacity is increased by increasing the temperature, as well as exothermic in other systems (21, 27, 127), where the adsorption capacity is decreased by increasing the temperature. Examples of endothermic and exothermic reactions for cesium and strontium removal are presented in Figure 2.10 (21, 31).

a)

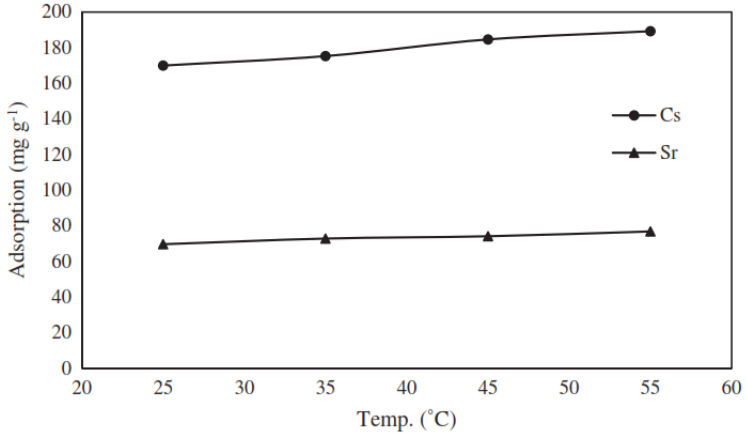

b)

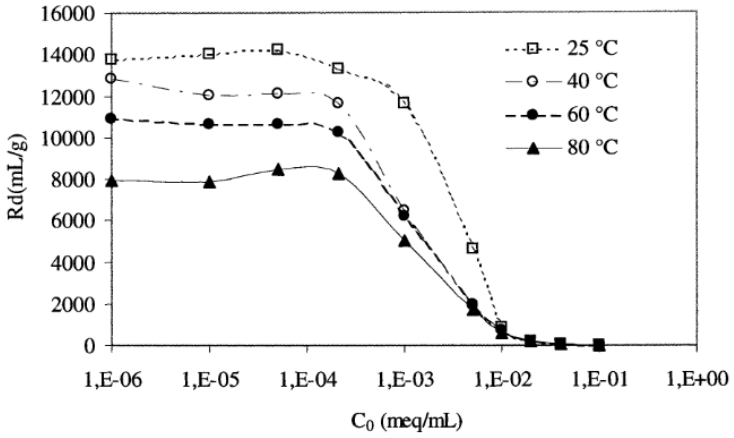

Figure 2.10: The example of: a) endothermic reaction of cesium and strontium by potassium nickel hexacyanoferrate (KNiFC) – clinoptilolite activation (31) and b) exothermic reaction of cesium removal from natural clinoptilolite (21)

Thermodynamic adsorption energies can be calculated by plotting the distribution coefficient (K_d or R_d) versus reciprocal temperature (1/T) from Eq. (2.1) (31).

$$\ln K_d = -(\Delta H/RT) + (\Delta S/R) \qquad \textbf{(2.1)}$$

where R is gas constant (8.315 J/mol.K) and T is temperature (K). The enthalpy and entropy values can be obtained from the slope and intercept of the linear plot, respectively such as in Figure 2.11 (31).

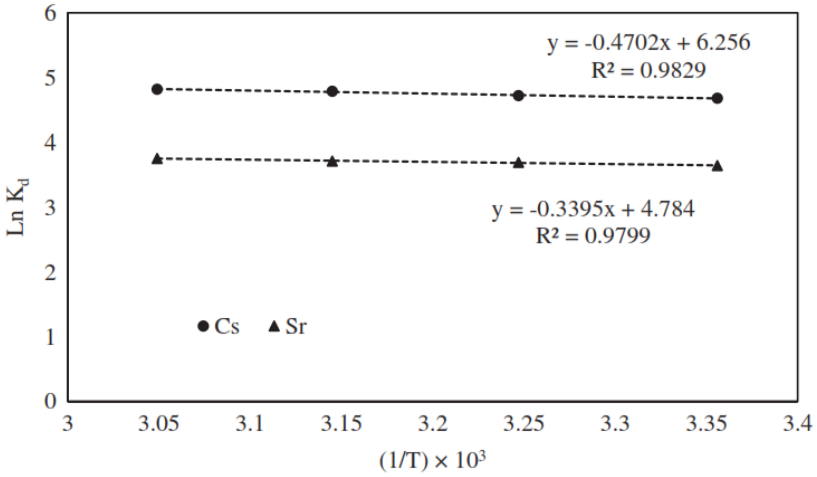

Figure 2.11: The linear plot of ln Kd vs (1/T) for cesium and strontium removal by potassium nickel hexacyanoferrate (KNiFC) – clinoptilolite activation (31)

Then the Gibbs free energy of adsorption can be obtained from Eq. (2.2) (5).

$$\mathbf{\Delta G = \Delta H - T\Delta S} \quad \textbf{(2.2)}$$

From Fig. 2.11, it shows that the enthalpy (ΔH) is in positive, which means the process was endothermic; otherwise, the negative values refer to exothermic reaction (31). Meanwhile, the positive or negative values of entropy (ΔS) relate to the kinetic reaction of the randomness at solid-liquid interface increased during adsorption, where positive values could increase the rate, while negative value will decrease the kinetic rate of randomness reaction (31, 128-130). Amanipour and Faghihian (31) showed that cesium had higher entropy values than strontium, which correlated to the higher adsorption of cesium than strontium. The value of Gibbs free energy (ΔG) determines whether the reaction is spontaneous or not. A negative Gibbs free energy indicates that the adsorption process is spontaneous, otherwise the reaction is nonspontaneous (31, 128-130). Based on Fig. 2.11, the Gibbs free energy decreases along with increasing temperature. It infers that the spontaneous adsorption process directly proportional to the increment of temperature (31). However, it shows that the increasing temperature does not affect so much to the adsorption capacity; therefore, clinoptilolite is used due to its thermal stability.

If the thermodynamics of adsorption is considered in reaction terms, the kinetics of adsorption is required for a full understanding of the adsorption process, when dealing with changes in chemical properties in terms of time and rates of changes (27, 30, 114). It is interesting, because studies into the understanding of adsorption kinetics leads to knowledge on a range of practical problems such as catalysis, corrosion and removal of ions from effluents (100, 131, 132). In addition, general kinetics of adsorption are also highly variable, where some kinetics studies of cesium and strontium by clinoptilolite have been found for times ranging from 8 minutes up to 1 day (18, 28, 30, 100) to reach equilibrium, as shown in Figure 2.12. According to Fig. 2.12, the equilibrium is achieved when the amount of adsorbed solute (q_e or Q_e) reaches a plateau with time. The amount of adsorbed solute can be determined from Eq. (2.3).

$$\boldsymbol{q_e = \frac{(C_0 - C_e)}{m} V} \quad \textbf{(2.3)}$$

where q_e is the amount of adsorbed solute (mg/g), C_0 is the initial concentration of solute (mg/L), C_e is the equilibrium concentration of solute, m is the adsorbent mass and V is the volume of solute.

Various equilibrium times, ranging up to 24 hours have also been found with other ions using clinoptilolite (101, 103, 105-107, 133-137).

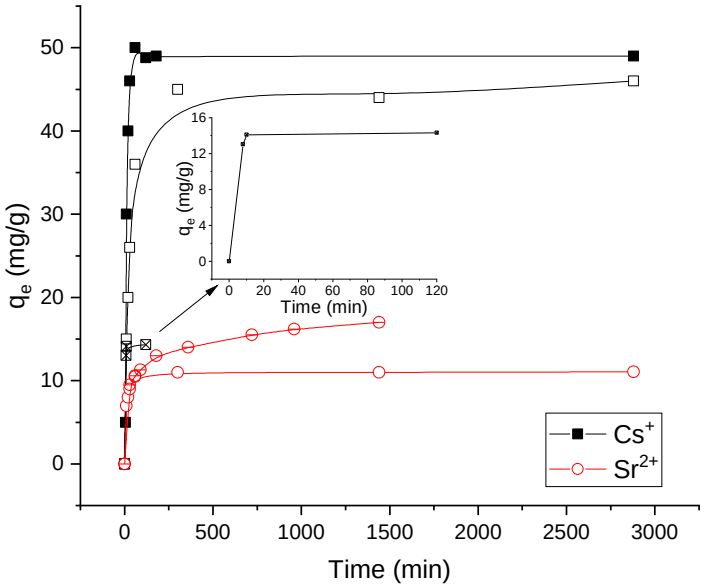

Figure 2.12: The adsorption kinetics of cesium and strontium removal by clinoptilolite from literatures For black rectangular De Haro-Del Rio *et al* (30); empty fill for cesium and strontium is from Smičiklas *et al* (18); Meanwhile for strontium, empty fill with cross-line is from Rajec and Domianová (28); and empty fill with diagonal line is from Huang *et al* (100).

Fig. 2.12 shows that the cesium adsorption reaches equilibrium in various times from 8 minutes up to 6 hours (18, 28, 30), where Rajec and Domianová (28) reported that the cesium could reach equilibrium within 8 minutes. Meanwhile, the strontium adsorption has been reported to reach equilibrium in between 6 hours up to a day, where Huang *et al* (100) reported that equilibrium was reached after a day. Various adsorption kinetics of cesium and strontium have also been found with other adsorbents apart from clinoptilolite (20, 23, 38, 59, 82-85, 123, 127, 138-143). In addition, El-Kamash reported that the concentration of ion was not varied enough to see the effects of equilibrium time, which is shown Figure 2.13 (59). According to Fig. 2.13, the concentration only affects the adsorption capacity, however, one would expect concentration to affect uptake kinetics when varied by a greater degree.

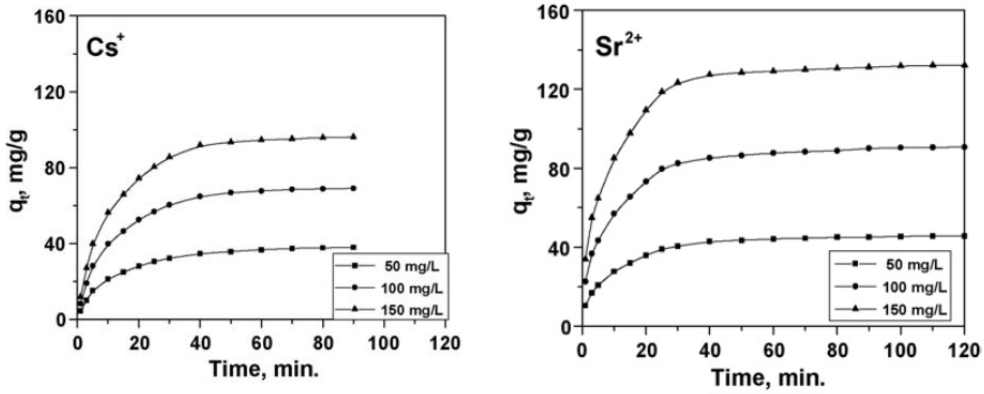

Figure 2.13: The different concentration of cesium and strontium in adsorption kinetics (59)

To understand the kinetics of adsorption process, various kinetic models have been applied. However, there are two models that are most commonly used for studying the mechanisms of practical adsorption processes. The first is Pseudo First Order (PFO) which was introduced by Lagregen (144). PFO is one of the most widely used for the adsorption of solutes from a liquid solution. PFO can be determined as Eq. (2.4) below (131, 144, 145) :

$$\frac{\mathbf{d_q}}{\mathbf{d_t}} = \mathbf{k_1}(\mathbf{q_e} - \mathbf{q}) \qquad \textbf{(2.4)}$$

where q and q_e are the grams of solute sorbed per gram of sorbent at any time and at equilibrium, k_1 is the observed rate constant of the Pseudo-First order model and t is time. By integrating Eq. (2.4) for the boundary conditions t = 0 to t = t and q = 0 to q = q gives Eq. (2.5) below:

$$\mathbf{ln}\frac{(\mathbf{q_e}-\mathbf{q})}{\mathbf{q_e}} = -\mathbf{k_1 t} \qquad \textbf{(2.5)}$$

The second major model considered is the Pseudo Second Order (PSO) rate model. The PSO model can be expressed in Eq. (2.6) (131, 146, 147):

$$\frac{\mathbf{d_q}}{\mathbf{d_t}} = \mathbf{k_2}(\mathbf{q_e} - \mathbf{q})^2 \qquad \textbf{(2.6)}$$

By integrating Eq. (2.6) for the boundary conditions t = 0 to t = t and q = 0 to q = q gives Eq. (2.7):

$$\frac{\mathbf{1}}{(\mathbf{q_e}-\mathbf{q})} = \frac{\mathbf{1}}{\mathbf{q_e}} + \mathbf{k_2 t} \qquad \textbf{(2.7)}$$

By rearrange the order of Eq. (2.7) to obtain linear form, Eq. (2.6) can be derived in Eq. (2.8):

$$\frac{\mathbf{t}}{\mathbf{q}} = \frac{\mathbf{1}}{\mathbf{k_2 q_e}^2} + \frac{\mathbf{1}}{\mathbf{q_e}}\mathbf{t} \quad \textbf{(2.8)}$$

where k_2 is additionally the observed rate constant of the Pseudo-Second order model. Note, normally the initial adsorption rate is also used for comparison, *h* (mg/g.min), where h could be determined in Eq. (2.9).

$$\boldsymbol{h} = \mathbf{k_2 q_e}^2 \quad \textbf{(2.9)}$$

To understand which model is fitted with the kinetics of adsorption process, the linearized fit from Pseudo-First order and Pseudo-Second order is plotted which the example is shown in Figure 2.14 (100). From Fig.2.14a, the rate constant of PFO is obtained from slope of fit. Meanwhile, From Fig. 2.14b, the amount of adsorbed solute at equilibrium (q_e) is obtained by reciprocal of slope of fit. Then, the PSO constant rate is determined from reciprocal of intercept multiply by the square of q_e. In addition, the initial rate (*h*) is determined from reciprocal of intercept. The R^2 from both models will be compared which the closest R^2 will describe the phenomenon during sorption process.

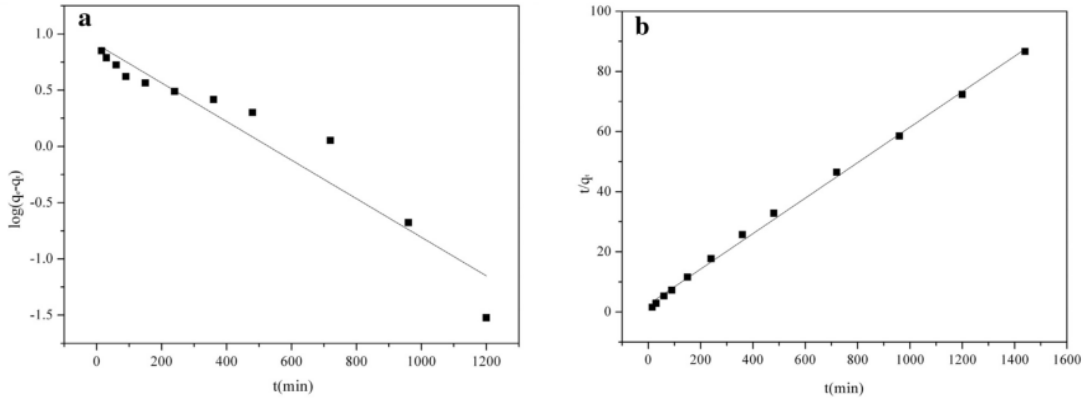

Figure 2.14: The linearized fit of: a) Pseudo-First order and b) Pseudo-Second order during strontium removal using clinoptilolite composite (100)

The PSO is considered as the initial adsorbate concentration is lower than the surface coverage and capacity of adsorbent, while the PFO is considered as the initial adsorbate concentration is higher than the surface coverage and capacity of adsorbent (131, 148). While, most of cesium and strontium removal studies have shown that Pseudo-Second order (PSO) has better fit with higher R^2 than Pseudo-First order (PSO) (24, 27, 29-31, 34, 100, 117, 126) .

Another critical aspect of adsorption to quantify is the isotherm equilibrium. It gives the relation between the amount of adsorbed ions by a unit mass of adsorbate and the amount of remaining ion in solution under equilibrium

conditions. The equilibrium isotherm gradient is described in Figure 2.15 (18). The amount of adsorbed solute (q_e) increases gradually with increasing of equilibrium concentration of solute (C_e). The equilibrium isotherm is achieved when the adsorption capacity is invariant with the equilibrium concentration (reaching an adsorption plateau) q_e is considered to be the maximum adsorption capacity (18, 20, 118).

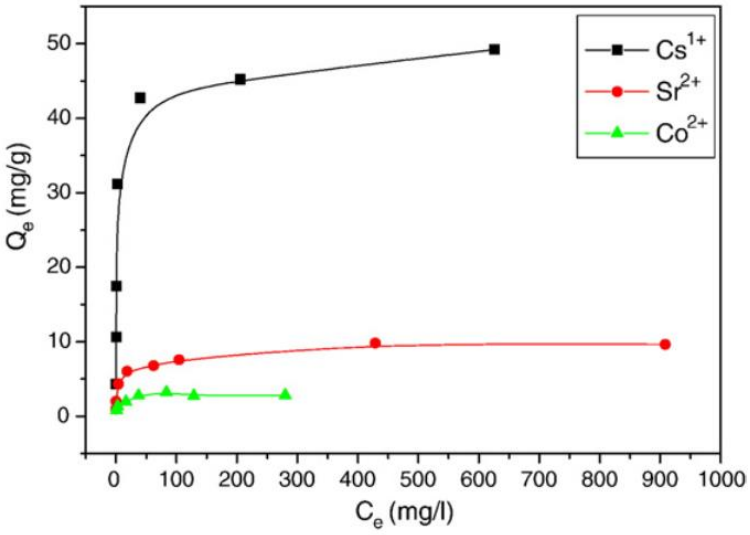

Figure 2.15: The adsorption equilibrium of cesium, strontium and cobalt by clinoptilolite (18)

During the adsorption process, not all adsorbate ions are adsorbed by adsorbent. To understand this behaviour, the distribution coefficient (K_d) can be applied for justification. The distribution coefficient is the amount of solute adsorbed in reference to the initial solution concentration, which corresponds to the mobility of ion solute to adsorbent. K_d (mL/g) and can be determined in Eq. (2.10)

$$K_d = \frac{(C_0 - C_e)}{Ce} \frac{V}{m} \qquad (2.10)$$

In general, the distribution coefficient will decrease as the equilibrium concentration of solute increases, as illustrated in Figure 2.16 (149).

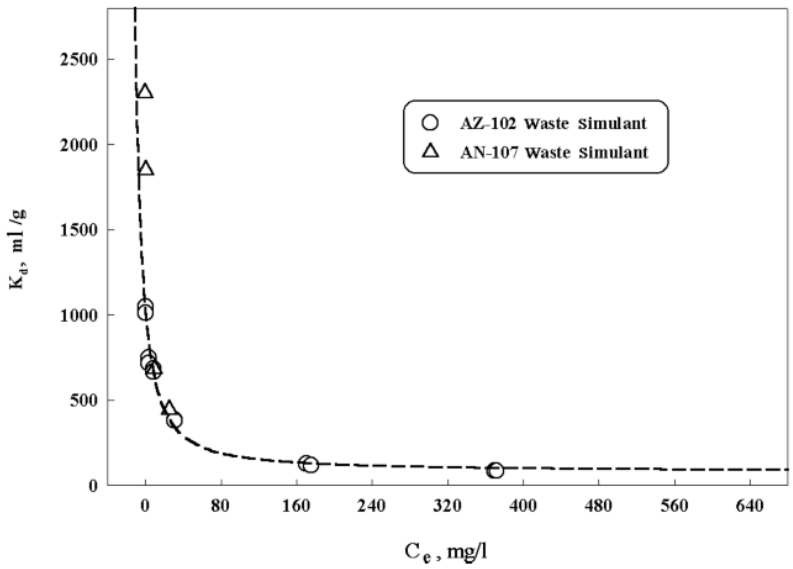

Figure 2.16: The distribution coefficient (K_d) of cesium from different waste simulants using ion exchange resin (149)

From Fig. 2.16, the decrease of K_d results in slower mobility of solute to the adsorbent. It could be due to some aspects such as: the adsorbent capacity reaches a maximum where the ion solute has already occupied all the sites; and the solute concentration is higher than the adsorbent surface coverage, where the ion solute then has to occupy less favourable sites (149, 150).

A number of models have been developed to represent the various type of adsorption processes, where Langmuir and Freundlich models are the most frequent utilised for ion adsorption (15, 20, 21, 118, 119). The Langmuir model assumes the solid surfaces have uniform sites, and no interaction between sorbed ions takes place, thus all adsorbed species can interact only with adsorption sites (40, 118). This model is developed for the systems in which sorption leads to deposition of a single layer of solute ions on the sorbent surface and it assumes that the energy of sorption for each molecule is the same and independent of surface coverage. Also, the overall sorption kinetics are negligible when compared with the initial rate of sorption (18, 118). The isotherm can be expressed in the linear form, as follows in Eq. 2.11:

$$\frac{\mathbf{C_e}}{\mathbf{q_e}} = \frac{\mathbf{1}}{\mathbf{Q_c b}} + \frac{\mathbf{1}}{\mathbf{Q_c}} . \mathbf{C_e} \qquad \textbf{(2.11)}$$

where q_e (mg/g) and C_e (mg/L) denote the equilibrium concentration of sorbate in the solid and the liquid phase, Q_c (mg/g) is the maximum adsorption capacity, and b (L/g) is the Langmuir constant related to the energy of adsorption (18). A straight line can be obtained by plotting $\frac{C_e}{Q_e}$ against C_e.

Meanwhile, Freundlich model assumes an energetically heterogeneous set of sorption sites with the sorption energy varying exponentially (118). It is the most widely used non-linear model to describe the dependence of sorption adsorbate concentration. The general expression of this isotherm model is given by:

$$\mathbf{q_e = K_f C_e^{\frac{1}{n}}} \quad \textbf{(2.12)}$$

The linear form from Eq. (2.12) can be expressed as follows:

$$\mathbf{\log q_e = \log K_f + \frac{1}{n} \log C_e} \quad \textbf{(2.13)}$$

where q_e (mg/g) and C_e (mg/L) denote the equilibrium concentration of sorbate in the solid and the liquid phase, K_f and n are constants for a given adsorbate (mg/g) and adsorbent.

To understand which model is normally best fitted to the adsorption equilibrium, examples of linearised fits from Langmuir and Freundlich models are plotted in Figure 2.17 (100). From Fig. 2.17a, the maximum adsorption capacity (Q_c) could be obtained from the slope of the fits and the Langmuir constant (b) is determined from the reciprocal of multiplication from intercept with the maximum adsorption capacity. Meanwhile, from Fig. 2.17b, the adsorption affinity (K_f) adsorbate is obtained from the intercept and the Freundlich constant for adsorbent (n) is reciprocal of slope. The determined R^2 values between these models are usually be used to explain which model best fits the data, where in the case example below indicates the Langmuir model best fits to strontium removal using clinoptilolite composite (100).

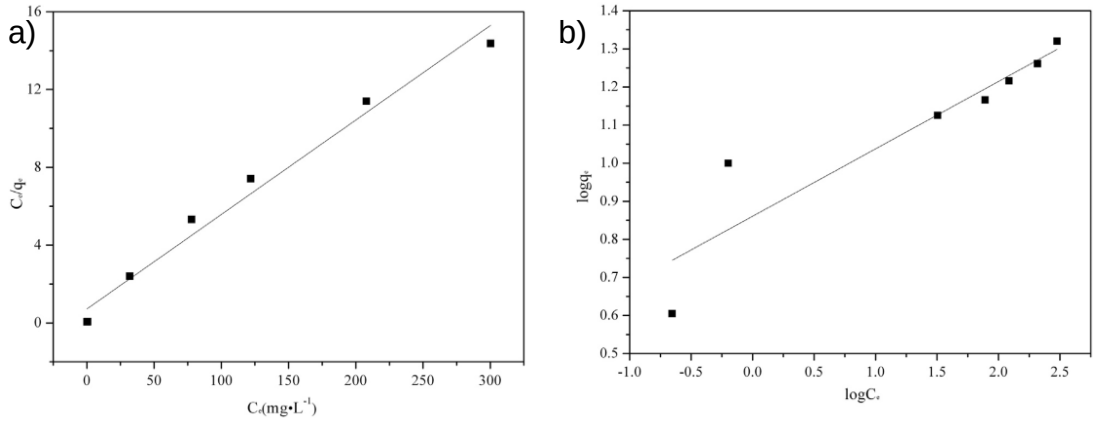

Figure 2.17: The linearized fit of: a) Langmuir and b) Freundlich models during strontium removal using clinoptilolite composite (100)

To date, there has been no comprehensive study to quantitatively link clinoptilolite contamination to cesium and strontium exchange reduction, which may aid in understanding mechanisms for pre-activation and particle size reduction to enhance both the kinetics and equilibrium up-take of these two key radio ions in low-grade ores. Also, adsorption reduction in simulated seawater solutions is important, as clinoptilolite and similar zeolites are known to be significantly affected by high saline effluents (23, 33, 38, 41), which has been a critical issue in the processing of emergency cooling waters at Fukushima, for example (151-153).

2.4. Flotation for rapid waste separation

In general, resin systems are operated in simple vertical elution ion exchange columns. However, ion exchange columns use large particles that are materially inefficient (due to the surface area to volume ratio). If smaller, higher surface area particles are used, and there are increased pressure loss issues with a related reduction in the available flowrates (21, 32).

Nevertheless, finely milled particles can enhance the uptake of cesium and strontium, in line with increases in the specific surface area of the adsorbent (31, 117), so investigating alternative processes whereby fine particles can be used is highly industrially beneficial. For example, fine particles can be used in batch adsorption tank mixers to enhance the removal of cesium and strontium from nuclear waste effluent but, while efficient from a material perspective, the secondary separation of the fine particles is a critical concern. Usually, gravitational clarifiers and separators are used for such purposes, but these are slow processes that possess a relatively poor dewatering ability, leading to voluminous sludge. Therefore, to overcome these issues, flotation is suggested in this study as an alternative process for separating the fine and highly efficient powdered ion exchanger, with significantly greater dewatering factors and shorter residence times than is possible when using gravitational sedimentation(46, 47). Flotation technique is basically used to remove heavy metal ions or separate the minerals from waste effluent, which could beneficially increase the wanted or unwanted minerals. Depending on the objective of the flotation itself, this could also lead to the volume of the waste effluent being reduced significantly (77, 154-156).

There are a lot of fields that use the flotation technique as an engineering solution, such as mineral processing (lead-zinc, copper and nickel ore and also

precious metals, such as silver and gold, which are associated in small amounts with other minerals) (157, 158), waste water treatment (such as lead, copper, cadmium, zinc) (157, 159, 160), paper recycling (154, 157) and events in nuclear treatment (30, 48-54). In terms of its application in nuclear-related fields, ion flotation and combined co-precipitation methods have been used to remove radioisotopes of cesium, strontium and cobalt, while fine particle flotation has been used for the separation of soils and as part of nuclear wastewater treatment processes (30, 48-54). It has also been demonstrated recently to be a viable technique for the separation of cesium-contaminated colloidal clay (55, 56).

From a rapid dewatering perspective, the flotation process is based on generating hydrophobic metal ion contaminated particles in effluent, by using surface active agents (surfactants) as collectors and then floating them by incorporating air bubbles (48, 77, 155, 156, 161-165). In order to achieve a successful flotation process, the selection of a surfactant is required in order to maximize the hydrophobicity of the waste particles that carry metal ions and so enable it to be floated (56, 163, 165-167). The surfactant itself usually consists of two parts with opposite polarity. Its head of surfactant is polar and the tail is non polar. The tail itself is chain of hydrocarbon (154, 156, 163, 165). As the head of surfactant is polar, the head will interact with the ion of particle and force the tail to be hydrophobic into the effluent (48, 77, 154-156, 161-165). Therefore, surfactants also called as collectors in this area, due to the ability to collect particles from the effluent (56, 154, 163).

At the same time, the interaction of surfactants and particles may change the surface tension, and increase the agglomeration and attachment at the interface (165, 168). The surface tension itself is essential to study in flotation systems, because it can indicate if particles becomes hydrophobic due to the interaction between surfactant, as the surfactant is then depleted from solution (165). The hydrophobic tails of free surfactants, will interact with the air bubbles when the air is being injected into the system (56). The interaction of hydrocarbon chains with the air bubbles resulting foams (56). Foam is a dispersion of gas bubbles in a smaller volume of liquid stabilised by surfactants, and is typically composed of polyhedral gas bubbles with liquid films residing between the bubbles (169). By adding the gas (air) injection through the solution, it will increase the interfacial area of the air-water, in which case the particles can be concentrated with the collector as a froth phase (53, 170).

Foams should be controlled by setting the collector concentration below the critical micelle concentration (CMC). CMC is basically defined as the specific concentration of surfactant where it starts to stop the adsorption in the air-water interface by showing the decreasing surface tension and then starting to form a plateau whenever the surfactant concentration increases (171). When the concentration of the collector is higher or equal to the CMC, bulk precipitates that are non-surface active are formed and reduce the efficiency of the flotation process (53). In this case, the bilayer of surfactant was fully formed and saturated as foam forms without any interaction with the ions solute (156). It is noted that increasing the surfactant concentration could increase the foam volume, although it will reduce the liquid fraction in the liquid phase. To obtain rapid flotation, the air bubble numbers should be increased by reducing the air/water interfacial tension (156, 163). The reagent that is usually used for this scenario is called the frother. The most common frother is MIBC (methyl isobutyl carbinol) (56, 154, 163).

2.4.1. Surfactant adsorption and mechanism for the flotation process

Surface active reagents (surfactants) are long-chain molecules that contain both hydrophilic (interacts with the water phase) and hydrophobic (repels against the water phase) moieties, which normally consist of a polar head group and non-polar tail (154, 163, 171). When surfactants interact with non-surface active ions of interest (in this case cesium and strontium), these ions will be co-adsorbed with the surfactant either electrically or chemically (170). These interactions will change the hydrophobicity of the surfactant with the ions in the air-water interface (48, 77, 154, 155, 163, 170, 172).

In general, cationic surfactants have been reported to be the best collector types, due to the negative charge of most minerals, including zeolites (30, 56, 114, 173, 174). This type of surfactant can be adsorbed by particle surfaces' electrostatically better than other types of surfactants (156), leading to an increase in particle hydrophobicity at optimal concentrations, thereby enhancing floatability. The general mechanism is described in Figure 2.18. (156).

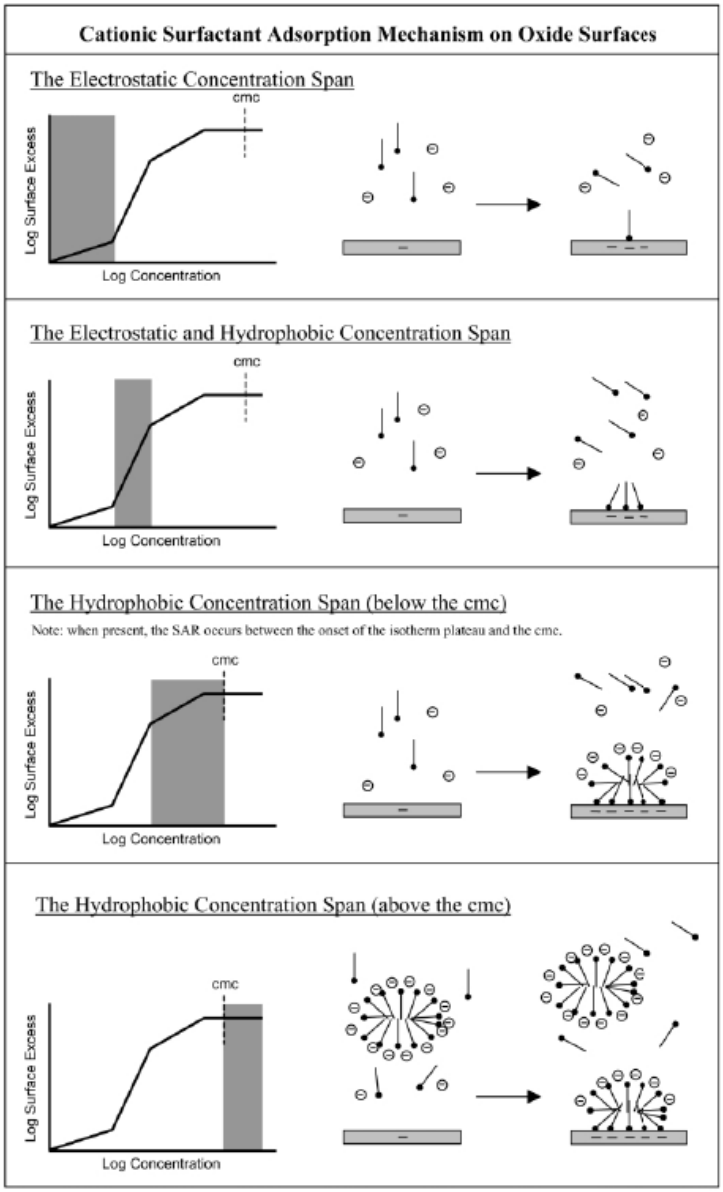

Figure 2.18: Mechanism of cationic surfactant adsorption (156)

In Figure 2.18, the mechanism of cationic surfactant adsorption consists of four steps; the electrostatic concentration span, the electrostatic and hydrophobic concentration span, and the hydrophobic concentration span (below and above the CMC). The different regions on the log surface excess and log concentration are similar to the adsorption isotherm model, which starts from region I to region IV.

In region I, where the surfactant concentration is usually very low, the first span surfactant molecules are electrostatically adsorbed on the particle surface sites. Often, the head of a cationic surfactant, which contains positive charge groups, will interact with the surface site of the particle that contains a negative

charge. In this region, the surfactant is usually fully adsorbed by the particle. In region II, where both electrostatic and hydrophobic concentration effects occur, increasing the concentration of cationic surfactants will contribute larger numbers of surfactant molecules to the system which will increase the hydrophobicity of the adsorbate. The tail of the surfactant, which is hydrophobic, will act as a new nucleation point for further adsorption by hydrophobic interaction; however, in this span, electrostatic interaction also occurs. This region represents the maximum adsorption, where the overall surface charge is neutralised (156). Once the surfactants are adsorbed on all available sites of the particle with the head facing towards the surface (while the tail protrudes into the solution), this condition is called a “hemimicelle” or “admicelle” (175). In region III, there is no electrostatic interaction that occurs due to the minimisation of the charge sizes from the surfactant adsorption. Also, once an admicellar configuration is formed, hydrophobic patches are formed on the surface (156). Once the admicellar is fully formed, there will be no more adsorption and create bilayer of the admicellar, which occurs in region IV after the CMC. In this region, the increasing concentration may increase the number of bilayers formed by the admicellar (156).

There are a number of examples of cationic surfactants on the market, such as etyltrimethylammonium bromide (CTAB or HTAB), etyltrimethylammonium chloride (CTAC), ethylhexadecyldimethylammonium bromide (EDAB or EHDA-Br) and cetylpyridinium chloride (CPC) (156, 167, 172, 176-178). In this discussion, EHDA-Br and CPC are highlighted in the following paragraphs, due to their proven ability to collect heavy metal contaminated clay and zeolite particles (56, 174). Ethylhexadecyldimethylammonium bromide (EDAB or EHDA-Br) and cetylpyridinium chloride (CPC) are cationic surfactants with the molecular formula $C_{20}H_{44}BrN$ and $C_{21}H_{38}ClN$, respectively. The chemical structures from both surfactants are described in Figure 2.19 (179).

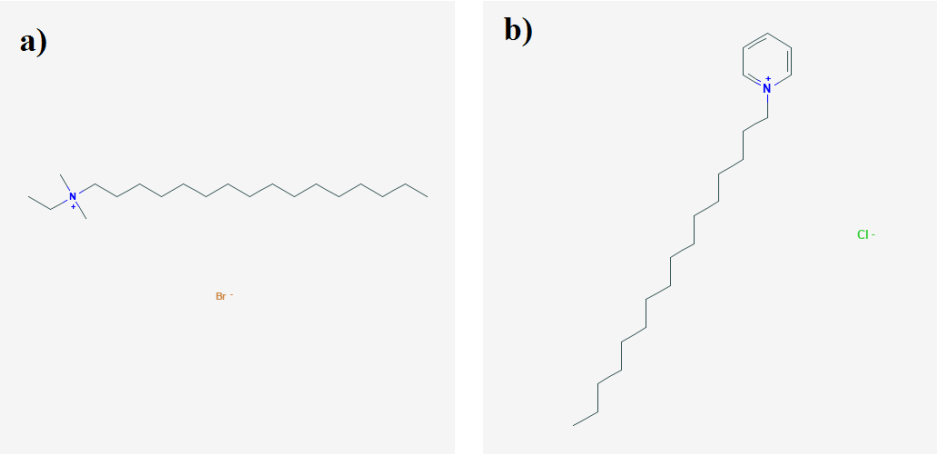

Figure 2.19: Chemical structure depiction from: a) EHDA-Br and b) CPC (179)

EHDA-Br is a quaternary ammonium salt, where the ammonium salt has four alkyl groups, usually contains 12-18 carbon atom chains, and has the N^+ ion as positive charge after being mixed into water solution (176, 180, 181). This surfactant's performance is usually fairly independent of solution pH. EHDA-Br is reported to have beneficial effects for heavy metal removal such as cadmium, nickel and zinc from acid solution (176, 177, 180-182). In nuclear applications, it has also been used for cesium contaminated soil recovery (56). Meanwhile, CPC also belongs to a quaternary ammonium cation, where the nitrogen ion has four alkyl groups and the N^+ ion as positive charge. Similar to EHDA-Br, CPC's activity is also independent of pH (183), while CPC has a reported ability to collect metal ion contaminated zeolite particles (174, 183). It has also been used for the flotation of cesium contaminated clays (78).

2.4.2. Surfactant and particle interactions in flotation

Froth is a three-phase structure comprising air bubbles, solids and water (169). In nuclear waste treatment, froth flotation may be an important advanced treatment for collecting solid waste for rapid dewatering purposes. Theoretically, the bubble–particle mechanism occurs in a three-phase contact (TPC) formation, comprising the liquid/gas and liquid/solid interfaces (184-189). Nguyen *et al* (184, 190) separated the steps of the bubble-particle interaction attachment mechanism into three parts, as shown in Figure 2.20.

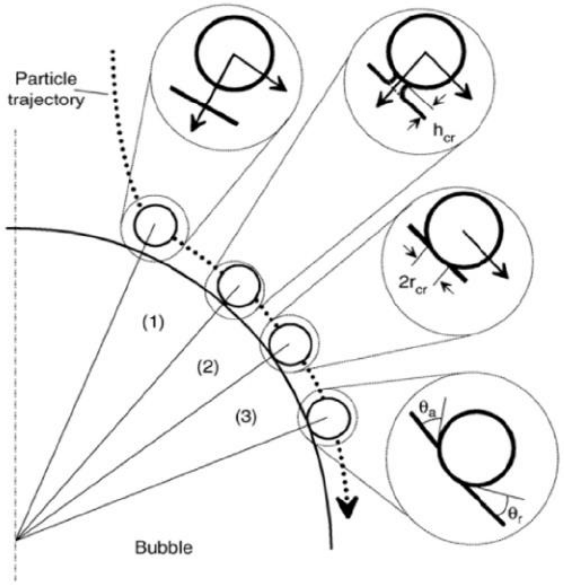

Figure 2.20: A schematic of the three steps of bubble–particle interaction (184, 186, 190)

In Fig. 2.20, the three steps of attachment are illustrated by the number in parentheses. The first step is to drain the wetting film to a critical thickness. In this step, the particles will be forced by the surface forces to align with the bubble in a radial direction in order to make the bubble-particle attachment possible. The surface force includes van der Waals, electrostatic double layer (EDL) and hydrophobic forces (191). In this case, the surfactants could lead the particle to become increasingly hydrophobic, leading to more complete adhesion to the bubble (183, 191). The induction time, which is the time of drainage wetting film to some critical thickness, was introduced by Sven-Nilsson (185, 189, 190) to quantify the interaction in a tangential direction, perpendicular to the bubble-particle line. The second step is the film rupture and the formation of a contact line. When the particle is touching the pulp of the bubble, the liquid film is formed, and due to the induction time, this film will thin and rupture after reaching a critical thickness. Once this occurs, a contact line is formed in the form of a three-phase contact (TPC). Then the contact line will expand, which is the last step until the stable wetting perimeter occurs (184-186). Albijanic *et al* (191) explained that increasing the concentration of the surfactant may increase the number of successful bubble-particle attachments and decrease the attachment time, but when the surfactant reaches the CMC, the number and time of the bubble-particle attachment is reversed (owing to the formation of a double surfactant layer, rendering the particle hydrophilic.

In flotation, the froth stability depends on the chemical structure of an additional species - the frother. The frother is usually based on a non-polar water repellent group, where methyl isobutyl carbinol (MIBC) is probably the most common frother used in the mineral processing industry (169). In general, the maximum particle size of recoverable minerals decreases with the increasing branching of the hydrocarbon backbone of alcohol frothers (192, 193), while the particle selectivity and bubble growth in the froth phase are all influenced by both the frother type and concentration, as well as the particle type (169).

Altering the gas flow could also accelerate the foam production. At a very low gas flow rate, a uniform sized bubble is produced, which is driven by buoyancy and rises through the system (194). However, while the bubble sizes are uniform, the production rates are low. Once the gas flow increases, the bubbles become less uniform due to bubble coalescence and breakage. However, this change, from a low to a high gas flow rate, could also increase the interfacial area and turbulence at the interface which leads to more effective particle contact in the froth phase. At the same time, it can reduce the foam stability (195).

According to Walcarius *et al* (183), the mechanism of surfactant adsorption onto heavy metal ion-contaminated zeolite particles is driven by electrostatic interactions exclusively to the external surfaces of the particles. However, increasing the concentration of the surfactant may lead to hydrophobicity-driven secondary adsorption. Additionally, increasing the surfactant concentration further could lead to the over adsorption of the surfactant onto the particles and replacement of the contaminated metal ions, which are already adsorbed on the zeolite particles. Once the condition is above the CMC, the bilayer of the surfactant reduces the adsorption of heavy metal onto the active site. The overall combination of surfactants, heavy metal ions and contaminants on the zeolite surface is shown schematically in Figure 2.21.

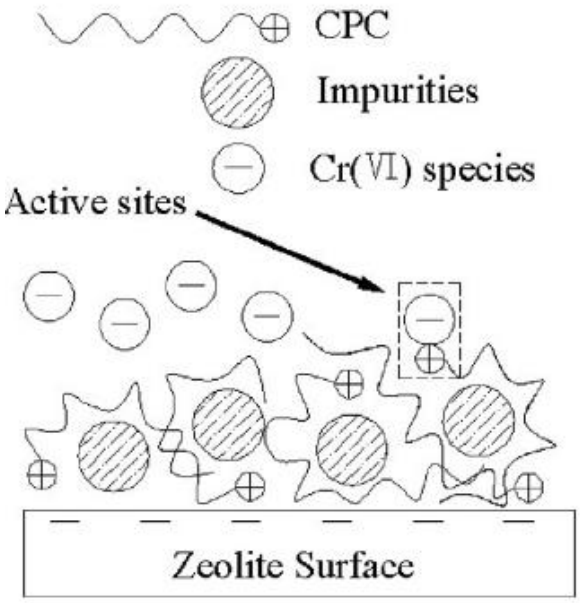

Figure 2.21: Co-precipitation mechanism on CPC-OHZ surface (174)

For the context of flotation for waste dewatering purposes (as opposed to mineral selectivity), both the percentage of the waste in the froth as well as the water reduction ratio can be measured, as shown in Figure 2.22 (196). The water reduction ratio or volume reduction (196) is the ratio between the initial volume of the suspension and final volume remaining after the flotation process. By using Eq. (2.14), the water reduction ratio can be obtained.

$$\boldsymbol{water\ reduction\ ratio} = \frac{\boldsymbol{V_0}}{\boldsymbol{V_0 - V_e}} \qquad \textbf{(2.14)}$$

where V_0 (mL) is the initial volume of the suspension and V_e (mL) is the volume of liquid remaining in the flotation cell after completion. Meanwhile, the flotation recovery is calculated by using Eq. (2.15), where, m_o is initial mass of contaminated particle (g) and m_e is the mass of recovered contaminated particle (g).

$$\% = \frac{(\boldsymbol{m_0 - m_e})}{\boldsymbol{m_0}} \times \boldsymbol{100}\% \qquad \textbf{(2.15)}$$

From Fig. 2.22, the addition of sodium lauryl sulphate (SLS) surfactant collector increased the recovery of contaminated cobalt complexes ($CoEDTA^{2-}$) onto MgAl-Layered double hydroxides (LDHs) anionic clays. However, in general, the water reduction decreases as the flotation percentage increases with collector concentration. At low concentrations of collector, the recovery is low, because of insufficient adsorption onto the contaminated clay to enhance the particle contact angles to promote a high degree of recovery. As collector concentration increases

to around monolayer coverage, the recovery significantly increases. However, increasing the surfactant concentration from low to the CMC may also create an overly wet froth phase, which can entrain both the solid and liquid rather than separate them (197-199) (thus water reduction ratio decreases). The decrease of recovery at very high concentrations of collector is because of the bilayer formation, which causes a reduction in the particle contact angle, as mentioned previously. It shows also that the presence of simple ethanol alcohol as a frother (in place of branched MIBC) leads to both lower recovery and a sharper reduction in the water reduction ratio (164, 191, 196). This is because of solid-liquid entrainment from the synergetic interaction of the surfactant and frother at the air-water interface (164, 197, 198, 200-202). However, the addition of branched frothers also has a limitation, since adding excessive amounts of frother to the air-liquid interface could reduce the amount of adsorption between the surfactant and the contaminated particles, resulting in reduced recovery. The authors in Fig. 2.22 conclude that an optimum concentration between surfactant concentration and MIBC is required in order to obtain the higher recovery of contaminated particles, while the water reduction ratio does not fall too much.

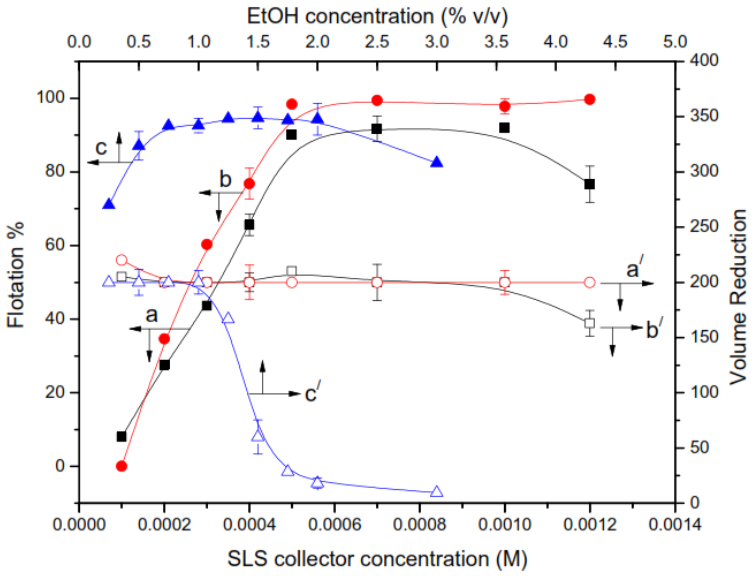

Figure 2.22: The flotation of contaminated $CoEDTA^{2-}$ complexes onto MgAl-Layered double hydroxides (LDHs) anionic clay by using SLS as the collector (a: one time addition; and b: two times addition) and ethanol as the frother (c) (196)

Moreover, the role of particles in stabilising the froth has been reviewed by Hunter *et al* (165). It has been mentioned that particle size, the residence time of the particles, the composition of the particles and the ability to rupture or stabilise liquid films could affect the froth stability (188, 203, 204). Bigger particle sizes could lead to detachment due to gravitational bubble-particle interactions,

meaning that often there is a maximum floatable particle size (188, 204). For most nuclear applications, however, it is anticipated that most sludges and ion exchange resins to be floated would be fine particles (to enhance their surface area to volume ratio, as discussed) and thus the rupture of bubbles by large particles is not deemed significant. Additionally, in nuclear dewatering systems, ruptured foam post-separation is not an issue, as the collected foam will be driven directly to another medium for forward treatment (such as solidification and encapsulation).

Lastly, it is important to emphasise that, in general, given the evidence that flotation can be used as a successful technique for nuclear effluent treatment from previous research (30, 48-56), it is perhaps surprising there has been no previous specific studies on its use to separate radioisotope contaminated clinoptilolite or other zeolites. It is noted that previous work by Walcarius *et al.* (183) on the flotation of lead-adsorbed faujasite zeolite highlights its potential in similar systems, and a critical focus of this thesis is to understand how flotation could be used to separate cesium adsorbed clinoptilolite for nuclear dewatering applications.

2.5. Measuring ion exchange performance in operational continual-flow elution columns

One of the most common types of adsorption operations that provides a reliable and cost-effective method for radioactive effluent treatment is continual flow column ion exchange. In a UK nuclear context, for example in 1984, a column process was used by British Nuclear Fuel Limited (BNFL) for alkaline remediation from nuclear fuel storage pond waters by using clinoptilolite as adsorbent. This column ion exchange was established in the site ion exchange effluent plant (SIXEP) in the Sellafield site, UK (32) which still operates to this day. Here, large granular adsorbent is placed inside vertical reactor tanks. Then, the solute that will be remediated, is filled continuously eluted through the columns with a certain flow rate to generate a required column residence time (29). In the nuclear and heavy metals remediation industries, column ion exchange has been used for recovering various ions such as cesium, strontium, lead and uranium (32, 57, 59, 205, 206). In addition, column ion exchange has been also widely used in various non-nuclear applications, such as removing copper, cadmium and methylene blue (60, 207-213). Critically, unlike the potential to use flotation separation, vertical columns operate with large granular

particles (>250 µm) and thus, while cost-effective, are inefficient from a material perspective. Another critical goal of the thesis work is to understand whether the principles of process intensification can be used to optimise column ion exchange, using an intensified reactor.

2.5.1. The column ion exchange process

A general column process involves the ion exchange resin becoming progressively exhausted with exchanged ions over time in an adsorption band. As this process belongs to a continuous system, this adsorption band is called the transfer zone (MTZ) or primary sorption zone (PSZ) with a fixed total bed adsorption (60). This mechanism is illustrated in Figure 2.23.

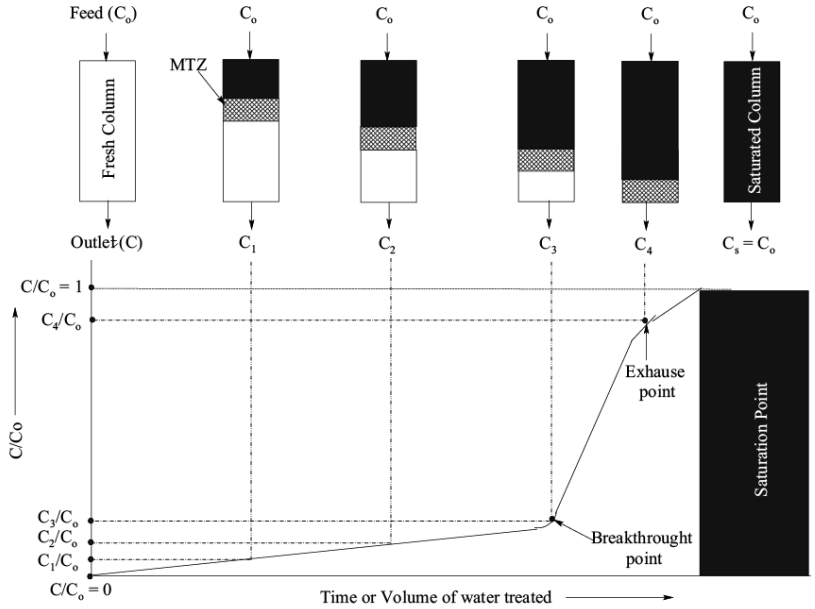

Figure 2.23: The mechanism of breakthrough in elution columns by movement of the mass transfer zone (60)

In Fig. 2.23., C_0 and C represent the concentration of remediated or treated ions at the inlet and outlet, respectively. When the feed effluent contacts with adsorbent, the C/C_0 is equal to 0. In this condition, MTZ is not moving and initial sorption takes place. The zero value refers to the maximum sorption that occurs in the particular system. Then, by the time C/C_0 increases up to the value of 1, where the column becomes fully saturated, the MTZ is wholly gone. The ideal breakthrough and exhaust points are shown in Figure 2.24.

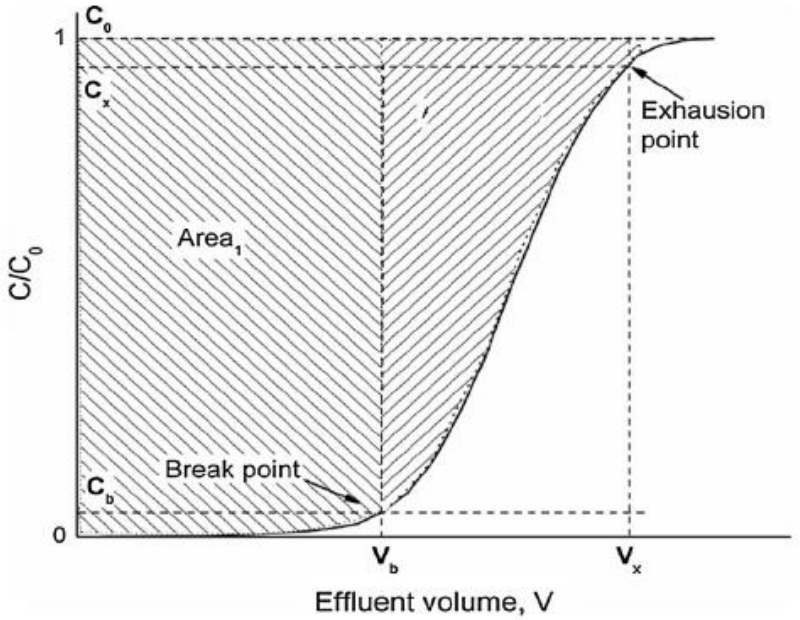

Figure 2.24: Ideal breakthrough/exhaustion curve for column ion exchange(60)

The sorption band starts from the top surface of the adsorbent with the effluent. By increasing the volume of the feed into the column, the sorption band continually moves down to the bottom of the adsorbent as it becomes exhausted with ions exchanged. Once exchanged ions from effluent occupy most adsorption sites the adsorbent, the C/C_0 start increasing slightly in slope, which is described as the breakthrough point. Once ions from the effluent fully occupy the adsorbent sites, the C/C_0 will increase drastically up towards the feed concentration. When the outlet concentration is the same as the feed concentration, it is at the exhaustion point.

There are a lot of factors that affect the breakthrough performance of ion exchange resins; such as the flowrate, the inlet concentration and types of ion of effluent (32, 57, 59, 60, 206, 214). It is found generally, for example, that increasing the flowrate will shift the breakthrough curve to the left (i.e. the resin becomes less efficient). This shift, where the breakthrough becomes faster, is due to the decreasing of the contact time between the effluent ions and the adsorbent. In this case, increasing the effluent flowrate will reduce the adsorption process (32, 59, 60, 206). However, as reported by McCabe *et al* (215), modifying the flowrate but maintaining a similar residence time (i.e. by increasing column height) will not alter the breakthrough point significantly. Therefore, in most systems, there is a balance between the operational sizes of columns and their flowrate requirements.

Meanwhile, increasing the concentration of contaminant ions in the effluent will also decrease the breakthrough point, for a given flowrate. As expected, a larger number of ions per volume of effluent will lead to a higher driving force for adsorption, and the ion exchange adsorption sites becoming fully occupied at lower total process volumes (57, 59, 60, 214). It has also found that the types of ion effluent could affect the breakthrough, as shown with cesium and strontium adsorption on brick kiln waste in Figure 2.25 (205). This figure shows that cesium has better breakthrough compared to the strontium, which is consistent with their batch adsorption behaviour discussed in Section 2.3, due to differences in their valency and hydrated ionic radii (20, 57, 59, 173, 214, 216), where smaller hydrated ionic radii will occupy more sites in adsorbent channels (18, 25, 123). As also mentioned earlier, the figure also shows the flowrate affects the breakthrough, where a smaller flowrate makes the breakthrough longer.

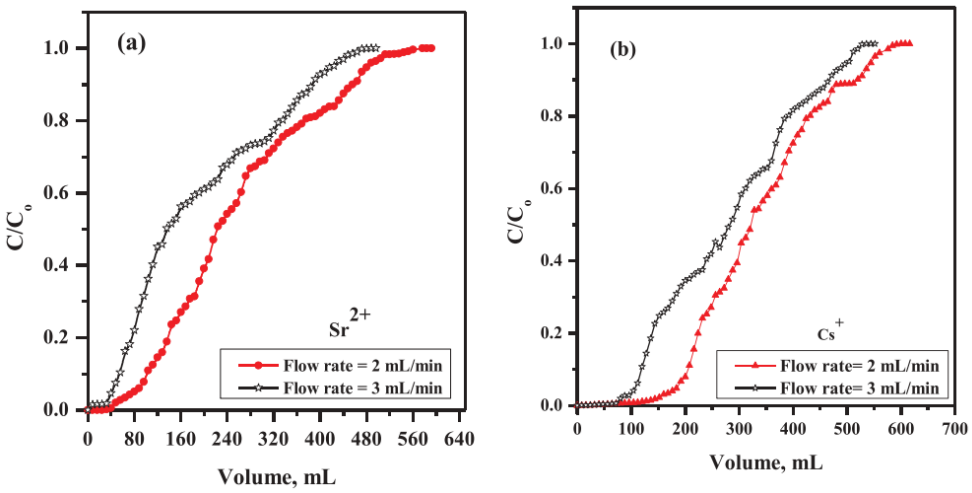

Figure 2.25: The breakthrough of 100 ppm concentration of: a) strontium and b) cesium at different flowrates , 4 cm bed depth and using brick kiln waste as adsorbent (205)

To study the adsorption kinetics from column processes, there are various models that can be used as fitting, such as: Thomas model (TM), Bed depth service time model (BDST), Adam and Bohart model (ABM), Model dose response (MDR) and many more (29, 32, 58-60, 209, 211, 217). Each model has different assumptions in order to fit to the breakthrough curve. The Thomas model (TM) is the probably most general and widely used for column studies (60, 208, 213, 217, 218). In addition, Ararem *et al* (57, 214) used this model for fitting the adsorption of cesium and strontium removal in their column study and was deemed relevant for the effluent studies presented in this thesis. The Thomas model is based on an assumption that the adsorbate is adsorbed onto the surface

of adsorbent directly (219). The column adsorption is expressed as Eq. (2.16) below:

$$\frac{\mathbf{C_e}}{\mathbf{C_0}} = \frac{\mathbf{1}}{\mathbf{1+exp\left[\frac{K_{TH}}{Q}(q_e m - C_0 V_{eff})\right]}} \quad \textbf{(2.16)}$$

where C_e is the outlet concentration at time t (mg/L), C_0 is the feed concentration (mg/L), K_{TH} is the Thomas model constant (mL/mg.min), q_e is the equilibrium capacity of adsorption (mg/g), m is the mass of adsorbent (g), Q is the effluent flow rate (mL/min), and V_{eff} is the effluent volume at time t (L). In order to determine K_{TH} and q_e, the model can linearised as follows in Equation 2.17, where plotting $ln(C_0/C_e - 1)$ versus V_{eff}, gives a gradient of $\left(\frac{k_{TH}}{Q} C_0\right)$ and intercept of $\frac{k_{TH}}{Q}(q_e m)$.

$$\mathbf{\ln\left(\frac{C_0}{C_e} - 1\right) = \frac{K_{TH}}{Q}(q_e m) - \left(\frac{k_{TH}}{Q} C_0\right) V_{eff}} \quad \textbf{(2.17)}$$

Yan *et al* (220), looked at a modification of the Thomas model to minimized some of the associated error due to experimental uncertainties. This new model derived from Yan *et al* is now generally described as the modified dose response (MDR) model. The MDR model can be expressed as Eq. (2.18) below:

$$\frac{\mathbf{C_e}}{\mathbf{C_0}} = \mathbf{1} - \frac{\mathbf{1}}{\mathbf{1+\left(\frac{V_{eff}}{b}\right)^a}} \quad \textbf{(2.18)}$$

Here, *a* and *b* are fitting parameters in the non-linear regression model, where *b* has the unit of L. Here, *a,* the power law exponent and *b* (L) are constant values. The linearised model is shown in Equation 2.19, where plotting $ln(C_0/C_e - 1)$ versus $ln(V_{eff})$ gives a gradient of *a,* while *b* can be determined from the intercept.

$$\mathbf{\ln\left(\frac{C_0}{C_e} - 1\right) = a \ln(b) - a \ln\left(V_{eff}\right)} \quad \textbf{(2.19)}$$

The MDR model has been found to be more accurate in fitting breakthrough curves than the Thomas model (206, 220-222), where a fitting example is shown in Figure 2.26 where immobilized biomass was used as adsorbent to remove Nickel (220). It is shown from Fig. 2.26 that the MDR model has a better fit compared to the Thomas model, due to additional degrees of freedom, as it is based on a lower number of physical parameters. However, importantly, both models allow estimation of the equilibrium adsorption capacity (q_e), where, for the MDR model, q_e can be calculated from Equation (2.20) (220). Therefore, column breakthrough performance can be directly related to batch adsorption performance (as given in Section 2.3).

$$q_e = \frac{bC_0}{m} \quad \textbf{(2.20)}$$

To date, despite the wide use of clinoptilolite, there has been no comprehensive study comparing column operation to batch adsorption, in order to fully understand the influence of contaminants on performance in nuclear applications. Also, investigations into the use of relatively low-grade clinoptilolite for cesium and strontium adsorption is critical, as there are current supply shortages of high-grade zeolite for nuclear applications. Understanding methods to improve the efficiency of low-grade ores will significantly reduce the potential for future supply issues. It is this that is a focus point of this thesis research. In particular also, as examined in the proceeding section, the use of an intensified reactor design will be utilised to help increase the efficiency of ion exchange columns, overcoming both operational issues with elution columns and poor material properties of low-grade ores.

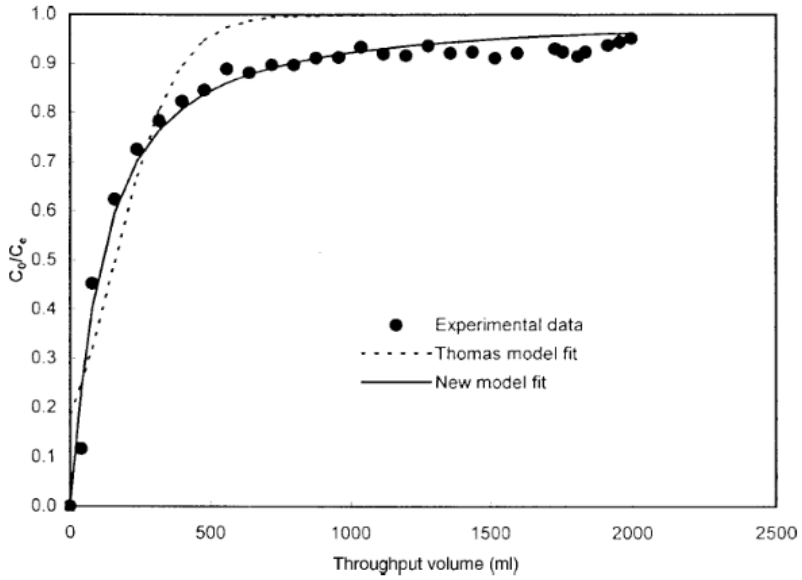

Figure 2.26: The re-fitting curve of Thomas and MDR (New model) models onto Nickel breakthrough using immobilized biomass as an adsorbent (220)

2.5.2. Intensifying ion exchange column operation using an Agitated tubular reactor (ATR)

Process intensification (PI) is defined as a process which can provide a sustained, safer and significant improvement in chemical manufacturing and processing, while decreasing the volume of equipment, energy consumption, waste formation, production cost (223). A number of different technologies can

be used as part of PI of effluent treatment. The most common current technology for intensifying ion exchange column processes are rotating bed reactors (RBR), which can be used for removing contaminants from liquids, including dyes, fertilisers and heavy metals (61-65). However, RBR still have significant limitations, especially when it is used for high percentage removal species, because of the dependency on rotation speed and small residence time (65). Thus, as an alternative, this thesis investigates a similar intensifies reactor called the agitated tubular reactor (ATR) as an alternative solution to the RBR issue for ion exchange. ATR are an intensified reactor plug-flow reactor where independently high rate lateral shear is generated with inner agitator bar, decoupling mixing dynamics from the bulk flow (61, 66). ATR can be used in many applications such as precipitation, separation, particle coating, milling, etc (224). However, because the technology is still new, the research using this technology are few (66, 68, 224, 225). In addition, there is still no intensive study using ATR for nuclear liquid treatment.

A potential method of using an agitated tubular reactor (ATR) in effluent separation processes is basically similar to batch adsorption operation. Here, solid particles as adsorbents will contact liquid effluent. However, the difference is the effluent can be used in a continuous system, where their suspension is generated from the lateral shear. Even though the principle is quite similar to the batch adsorption process, it likely closer to column process than batch adsorption process due to the continuity. A scheme of this process is shown in Figure 2.27.

In Fig. 2.27.a, an ATR schematic is shown, highlighting its movement based on free agitation from internal agitator where solid particles are placed (Fig. 2.27b) from the shaken reactor body. Then, the fluid is fed into the inside of an external tube (Fig. 2.27c) and interacted with the solid particle while the external tube is being shaken. The agitation will help the product (effluent) flows to the outlet and the particle inside of internal agitator contact with the effluent freely and completely. In addition, this mixing could be effective in order to keep the mixtures suspended and well dispersed through the continuous flow of the product (224).

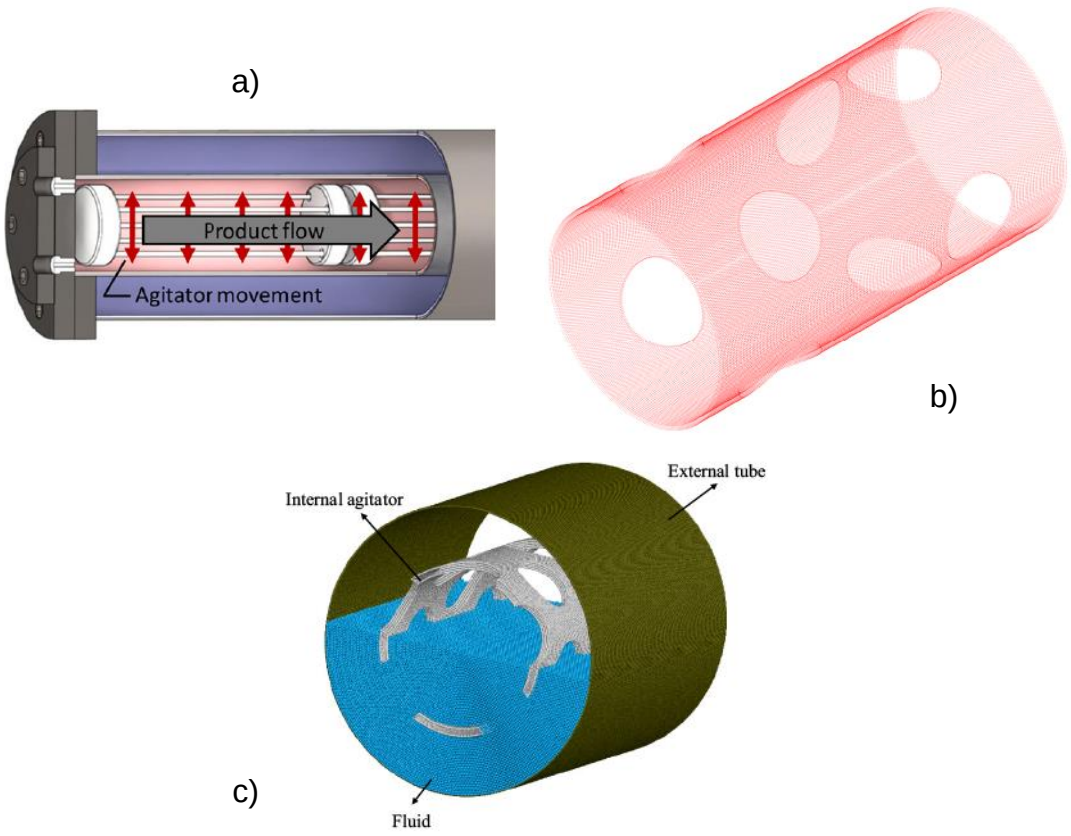

Figure 2.27: The schematic of ATR process. a) the tubular reactor of ATR (66); b) the internal mixing element and where the solid particle is placed (225); c) the simulated process in ATR system (68)

Previous numerical simulations have been undertaken to describe the fluid dynamics of the ATR process (68, 225). In this simulation, the fluid velocity magnitude in different phases along with the agitator motion and the position of agitator are illustrated in Figure 2.28.

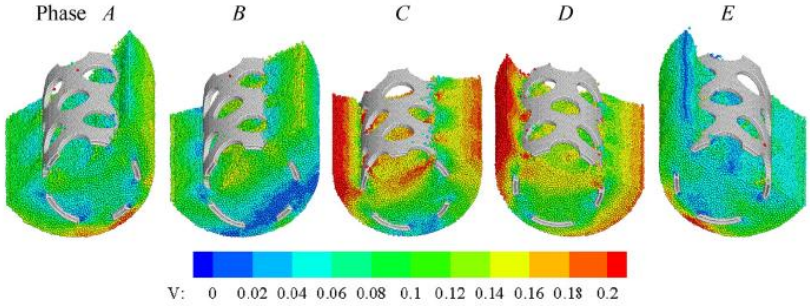

Figure 2.28: The velocity profile in a half-filled ATR system at different phases, in which phase A = 0.581π, B = 0.906π, C = 1.150π, D = 1.393π and E = 1.637π. Fluid particles are coloured by velocity magnitude in the reference frame of the tube (68).

From Fig. 2.28, it shows that the local variations from different phases still occur due to the existence of the internal agitator. In Phase A, it shows that the local maximum of the fluid particles is found to be focused in the area between the internal agitator tube and the reactor, which is similar to phase E (68). However, it will be changed when the internal agitator's motion and position are also changed. This phenomenon mainly due to the small velocity between the internal agitator and the external reactor tube at the contact region, at the same time, the particle is being squeezed and compressed by the agitator tube (68, 225). The local maximum of the fluid particles position can be represented as the maximum phases of ion exchange occurs, where the particles are fully contacted with the product. The local maximum of the fluid particles velocity can be found also in the near to surface holes of internal agitator tube. The surface holes also help the product well mixed with the particles, so the adsorption process could be more effective. In adsorption processes, the particle size of the adsorbent is selected to be higher than the surface hole in order to prevent adsorbent removal through the outlet, and to keep the effluent flowing through inside of the internal agitator tube.

Based on above principle, it is hypothesised that process intensification (PI) of effluent treatment is possible using an agitated tubular reactor (ATR), where an opportunity exists to investigate the rapid ion removal, comparing to column ion exchange. Currently, to date, no studies into the use of the ATR for intensified effluent treatment have being conducted. Increasing the rate of column ion exchange is essential, because it can cut production cost and process time, and overcome some of the innate inefficiencies of elution columns.

2.6. Summary

Natural clinoptilolite is a heulandite type zeolite, and contains a negative surface charge that is commonly used for removing heavy metal ions (such as cesium and strontium) from effluent, using ion exchange. However, there still a strong industrial need to improve the adsorption performance of its natural ore, for example by pre-activating with acid and salts or by milling, to allow lower grade material to be used for industrial applications. It is also important to study the effect of ion competition during batch adsorption process. This competition, such as with seawater ions, may critically reduce performance. It is of particular interest to see how both pre-activation and milling may affect clinoptilolite performance

for cesium and strontium removal in nuclear effluent treatment, and how ion competition in saline conditions affects it.

However, batch adsorption processes raise another problem, the post-treatment removal of clinoptilolite that has been contaminated with cesium and strontium ions, as a solid waste. In order to tackle this issue, a flotation method could be a viable solution for rapid dewatering and waste separation. Flotation could help to transfer the used clinoptilolite into a waste repository to be safely stored and the batch reactor could be used again. The flotation study proposed in this thesis will cover the selection of surfactants and then investigate the optimisation of these surfactants for efficient flotation efficiency and high dewatering ratios. Additionally, the optimisation of collectors, such as MIBC, is also importance for study, to understand its influence on the percent of clinoptilolite recovery and dewatering ratio.

As batch adsorption is non continuous, column ion exchange is a commonly used alternative solution for continuous processing. It is then also important to study the performance natural low-grade clinoptilolite, which would not qualify for the nuclear industry, in continuous column processes, where a direct comparison to batch adsorption can be achieved using kinetic models. However, there significant disadvantages of using continuous elution column ion exchange, as it is a slow flow rate process (due to pressure drop issues) and efficiency is adsorbent particle size dependent. Therefore, a process intensification (PI) methodology is suggested here, in order to increase the process speed and adsorption quality. In particular, an Agitated Tubular Reactor (ATR) will be studied as an alternative to continuous column operations, where there has been no previous reported study in the use of this technique for ion exchange, especially for cesium and strontium removal, despite its advantages in other chemical processes.

Chapter 3 The effect of pre-activation and milling on improving natural clinoptilolite for ion exchange of cesium and strontium

3.1 Synopsis

The contents of this chapter may contain repetition from either Chapter 1 and 2 in order to strengthen the messages from this chapter.

Natural clinoptilolite, of relatively low-grade, was investigated for its capability to remove cesium and strontium ions from water and simulated seawater. To improve its capacity, the material was pre-activated with concentrated NaCl and HCl solutions. Additionally, it was milled to a number of < 300 µm size fractions, to expose exchange sites. Electron microscopy was used to characterise the naturally occurring impurities, where regions of high iron and potassium content was shown to correlate to lower levels of cesium adsorption. Adsorption kinetics for natural and activated resins with 5, 300 and 1500 ppm salt solutions were fitted with the Pseudo-Second Order (PSO) rate model. Activation led to clear increases in initial adsorption rate for both Cs^+ and Sr^{2+}, but only enhanced the overall rate constant for Cs^+, due to the weaker interaction of the Sr^{2+}. Equilibrium isotherms were compared with Langmuir and Freundlich monolayer models, where the adsorption capacity (Q_c) for Cs^+ was 67 mg/g which increased by over 100% with NaCl activation to 140 mg/g. Values for Sr^{2+} were significantly lower at 35 mg/g, with a considerably smaller enhancement with activation to 52 mg/g. Milling of the natural clinoptilolite was found to increase Cs^+ uptake to similar levels as activation, in a linear correlation with specific surface area; although, improvements for Sr^{2+} were again lower, due to its weaker interaction with surface sites. In simulated seawater solutions, all materials gave considerably reduced performance due to K^+ ion competition, with Sr^{2+} uptake decreased more extensively compared to Cs^+. Overall, this work highlights that pre-activation and milling of clinoptilolite can be used to significantly enhance the grade of the ore for nuclear effluent treatment in low-salinity conditions.

3.2 Introduction

Natural clinoptilolite, which is considered as non nuclear-grade and has impurities, is used as an alternative solution when supply issues of nuclear-grade

ores exist. In the United Kingdom (UK), clinoptilolite is used as an ion exchange resin for ^{137}Cs and ^{90}Sr removal from nuclear fuel cooling ponds, such as at the Sellafield site in Cumbria (32, 37-39, 226) and contains a low level of impurities (32, 37-39).

Activation and milling have been used to enhance the ion uptake performance (20, 21, 23, 40, 107, 108). Of particular importance for nuclear effluent treatment, which has not been previously studied in detail, is the effect of pre-activation on increasing the uptake of strontium in clinoptilolite, as generally, strontium adsorption capacities are much lower than for cesium (18). Additionally, it is important to consider the role of pre-activation on adsorption kinetics, as well as equilibrium behaviour. Another technique that may potentially be used to increase natural ion capacity, is to expose additional exchange sites through increasing the surface area to volume ratio by milling (227, 228).

To further understand the extent to which pre-activation and milling can optimise ion exchange materials, this thesis details investigations using relatively low-grade natural clinoptilolite ore, pre-activated with concentrated sodium salt and acid solutions. While clinoptilolite is a well-researched ion exchange material for a variety of heavy metals, as highlighted, it is vital for applications in nuclear effluent treatment and other related industries, to study the use of natural ores with relatively high levels of impurities, in order to assess the potential for future supply issues. In particular, the use of cheap ion pre-treatments combined with the use of finer milled fractions may provide important engineering solutions to critically expand usable sources for effluent treatments.

To date, there has been no comprehensive study to quantitatively link clinoptilolite contamination to cesium and strontium exchange reduction, which may aid in understanding mechanisms for pre-activation to enhance both the kinetics and equilibrium up-take of these two key radio ions in low-grade ores. Therefore, for this study, characterisation of the zeolite using elemental mapping from scanning transmission electron microscopy is firstly completed, to indicate naturally occurring contaminants, and their potential impact on adsorption. The influence of activation on both the removal of cesium and strontium are measured, where rate kinetics and equilibrium adsorption behaviour are quantified for various systems. In addition, the performance of various milled sieve fractions is also compared against the un-milled ore. Adsorption reduction in simulated seawater solutions is lastly examined, as clinoptilolite and similar zeolites are known to be significantly affected by high saline effluents (23, 33, 38,

41), which has been a critical issue in the processing of emergency cooling waters at Fukushima, for example (151-153). Previous studies have highlighted that a number of ions may reduce the exchange process between media and radioactive waste, especially larger monovalent ions such as potassium (K^+) (23, 33, 42), and it is of interest to examine whether activation mitigates or extenuates these effects.

3.3 Experimental

3.3.1 Materials

The natural clinoptilolite used was supplied from Holistic Valley as a ~300 µm powder. Cesium chloride (CsCl) and strontium chloride ($SrCl_2$) were Analytical Grade with purity ≥ 99.0% and supplied by Sigma-Aldrich and Fisher Scientific, respectively. Meanwhile for the pre-activation, sodium chloride (NaCl) Analytical Grade with purity ≥ 99.0% from Fisher Scientific and Hydrochloride Acid (HCl) ACS reagent 37% from Fluka were used. For ion competition, potassium chloride (KCl), sodium chloride (NaCl) and calcium chloride ($CaCl_2$) analytical grade with purity ≥ 99.0% were supplied by Fisher Scientific.

It is noted that the sourced clinoptilolite is a relatively low-grade product used as a health supplement. While the grade was not pre-tested specifically, it assumed it was not of a sufficient grade to be used currently for specific nuclear effluent treatment. However, it is representative of readily available natural ore. Prior to the experiments, the clinoptilolite was rinsed several times with distilled water at neutral pH, with the supernatant being removed in order to get a homogeneous particle size with reduced fines, and to remove any naturally present ions. After every rinse, the supernatant was measured using a conductivity meter until an equilibrium value was reached. The rinsed clinoptilolite was then dried at 100 ºC for 24 hours in a laboratory oven (18).

3.3.2 Particle characterisation

The crystal structure of the clinoptilolite was characterised using X-ray diffraction (XRD) with a Bruker D8. Results were analysed using X'Pert HighScore to identify the elemental structure. The zeta potential of clinoptilolite was measured using a Colloidal Dynamics Zeta Probe, in order to determine the change in surface charge between natural and pre-activated clinoptilolite, and through adsorption of different concentrations of cesium and strontium salts.

A Hitachi TM3030 Bench Top scanning electron microscope (SEM) was used to image and analyse the clinoptilolite at low magnification. Further, High Angle Annular Dark Field (HAADF) Scanning Transmission Electron Microscopy (STEM) and Energy Dispersive X-ray (EDX) spectroscopy was used to analyse elements present in the natural clinoptilolite. HAADF-STEM was conducted on an FEI Titan^3 Themis G2 operating at 300 kV fitted with 4 EDX silicon drift detectors, and a Gatan One-View CCD. EDX spectroscopy and mapping was undertaken using the Bruker Esprit v1.9 software. STEM samples were prepared by dispersing the powder in methanol, with a drop placed on a holey carbon coated copper grid. STEM-EDX additionally characterised the location of adsorbed cesium, through measurement of samples mixed with 5000 ppm of cesium chloride for 24 h (using an identical procedure to that outlined in the proceeding section). At least five areas from one cesium adsorbed natural clinoptilolite sample were analysed using STEM-EDX. Samples were then rinsed a number of times to remove excess salt and dried before measurement. Additionally, in order to study the cationic exchange capacity in different pH conditions, 20 g/L dispersions of clinoptilolite were stirred at 300 rpm for 3 hours. The pH changes were measured using a pH meter. 0.1 M of HNO_3 and KOH were used to adjust the pH.

3.3.3 Salt and acid pre-activation

Clinoptilolite was pre-activated using concentrated sodium chloride salt (denoted ‘NaCl-clinopilolite’) and hydrochloric acid (denoted ‘HCl-clinopilolite’). For NaCl-clinopilolite, 100 g/L solid – liquid ratio of rinsed clinoptilolite was mixed with 1 M NaCl solution at room temperature for 24 h in a rotary carousel. The mixture was then centrifuged, filtered and the suspension rinsed with 300 mL of Milli-Q water, with the washing process repeated several times until conductivity reached an equilibrium value. Figure A1 in the Appendix A presents the conductivity of acid and salt activated samples after a number of washes. The conductivity is observed to reach a baseline, correlating to the natural material, after four washes, which was taken as a minimum for all activation tests. The final suspension was then mixed with 25 mL of methanol for 1 h, before being filtered and dried at 50 ºC for 3 h (20). The same overall process was repeated for acid activation, with the use of 1 M HCl in place of the sodium salt (40, 108, 229). By replacing the impurities that block the pores channel with either salt or acid ions, activation can enhance the adsorption capacity and increase the effective surface area (22, 113, 114).

3.3.4 Batch adsorption experiments

All the batch adsorption experiments were conducted in polypropylene conical centrifuge tubes in order to prevent Si contamination from glassware and also potential Cs^+ adsorption onto glassware, as evidenced in an earlier study by Chorover *et al* (82). Cesium (Cs^+) and strontium (Sr^{2+}) ion solutions were measured separately to analyse each individually during adsorption experiments.

To measure adsorption kinetics, cesium chloride (CsCl) and strontium chloride ($SrCl_2$) stock solutions (1 M) were diluted with Milli-Q water at neutral pH (which tends to ~6.5, and close to buffered pH values encountered in industry (32)) to a nominal initial concentration of 5 ppm, which is similar to the concentration range used in previous research (18, 20), and of relevance for nuclear effluent treatment (20, 23). Then, 0.4 g of clinoptilolite was dispersed in 20 mL samples of the CsCl/$SrCl_2$ solutions, giving a solid/liquid ratio fixed at 20 g/L for different shaking times (21). Suspensions were placed on an orbital shaker at 150 rpm (at room temperature) for 30 min, 1 h, 2 h, 4 h, 6 h, 12 h, 24 h and 48 h respectively (18). The dispersions were then centrifuged using a Megafuge 16R for 10 min at 7000 rpm, and the separated supernatants were decanted using a 20 mL syringe with 0.3 µm filter. Natural clinoptilolite dispersions containing higher initial salt levels of 300 ppm and 1500 ppm were also prepared and kinetic concentration differences measured, to understand the effect of initial ion level on dynamic adsorption.

The amount of Cs^+ and Sr^{2+} adsorbed by both natural and activated clinoptilolites at each specific time was determined as q_t (mg/g) and removal percent, using the methodologies described in the Eqs. (3.1) and (3.2).

Here, C_o (ppm) is the initial concentration of salt ion, C_e (ppm) is final equilibrium concentration, m (g) is the mass of adsorbent and V (L) is the volume of the suspension.

$$\boldsymbol{q_t = \frac{(C_0 - C_e)}{m} V} \qquad \textbf{(3.1)}$$

The percent adsorption of Cs^+ and Sr^{2+} was determined using Equation 3.2, where, C_o (ppm) and C_e (ppm) are as defined above.

$$\% = \frac{(C_0 - C_e)}{C_0} \times \mathbf{100}\% \qquad \textbf{(3.2)}$$

Adsorption kinetic fits were determined using Pseudo-First Order (PFO) and Pseudo-Second Order (PSO) rate models to derive the adsorption rate

constant (k_1 and k_2) and initial rate of adsorption (h) (see Eqs. 2.4 - 2.9 in Section 2.3) (18, 30, 131, 146, 148, 230-232).

To determine the equilibrium adsorption behaviour, both Cs^+ and Sr^{2+} from 1 M stock solutions were diluted with Milli-Q water at neutral pH in order to get various initial concentrations from 5 ppm up to 4000 ppm, and again mixed with natural and activated clinoptilolite with a solid/liquid ratio fixed at 20 g/L. All suspensions were then placed on an orbital shaker for 48 h, and supernatants separated as described above. Equilibrium data was fitted with both Langmuir and Freundlich isotherm monolayer adsorption models (see Eqs. 2.11 and 2.12 in Section 2.3).

All supernatants were measured and analysed using an Atomic Absorption Spectrophotometer (AAS) Varian 240fs machine, in which the cesium data were collected using a cesium lamp with wavelength and optimum working range of 459. 3 nm and 5 - 4000 ppm respectively. For strontium, dilutions were required for every Sr^{2+} solution in which the initial concentration was higher than 10 ppm, in order to ensure levels were within the concentration threshold of the AAS. A strontium lamp was used with wavelength and optimum working range set at 460.7 nm and 0.02 - 10 ppm respectively.

3.3.5 Effect of ion competition on adsorption

To consider the potential impact on cesium and strontium removal in saline conditions, ion competition between K^+, Na^+ and Ca^{2+} ions (as mixed chloride solutions) was analysed, to represent the most significant portion of seawater ions (233). Cs^+ and Sr^{2+} were firstly fixed at 5 ppm while K^+, Na^+ and Ca^{2+} were fixed at 380 ppm, 10556 ppm and 400 ppm, respectively (as a seawater simulant). Additionally, tests were undertaken with Cs^+ and Sr^{2+} fixed at 5 ppm, while K^+, Na^+ and Ca^{2+} were varied from 5 ppm up to 4000 ppm (with a ratio of 1:1:1) in order to study Cs^+ and Sr^{2+} adsorption in different saline conditions. Sample preparation and analysis with AAS were completed as described above.

3.3.6 Particle milling and surface area analysis

The effect of particle milling was investigated to study the influence of surface area on the adsorption of cesium and strontium. Clinoptilolite was milled using a Planetary ball milled (PM) 100 ball mill. 3 cm inner diameter and ~750 g of stainless steel planetary balls with 10:1 of weight ratio between balls and powder were placed into mill with the natural clinoptilolite (109, 234). The machine was then set at 550 rpm for 20 mins. These were determined as the

optimum parameters, from initial development tests at various rpm and milling times. The initial development tests can be seen in Figure 3.1. The milled particles were then sieved in different fraction sizes from 103 µm down to less than 53 µm, using a Sieve Shaker AS 200 Control (Retsch GmbH) for 10 min. Once the process was completed, the clinoptilolite was separated using a course brush in order to observe its uniformity. These processes were repeated three times to ensure a low level of fines.

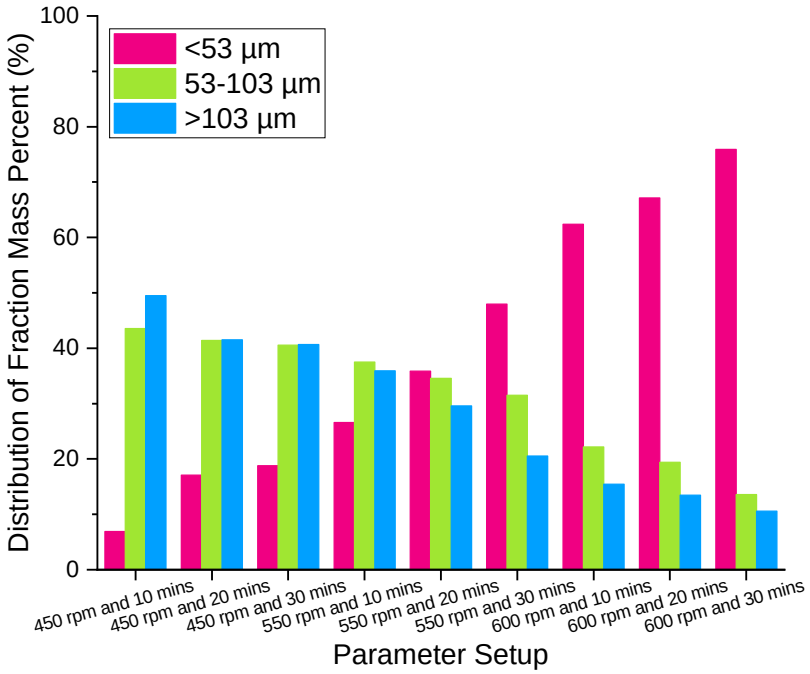

Figure 3.1: The mass percent of each distribution size after milling in different parameter setups.

To prove the dispersion homogeneity, all samples were analysed using a Malvern Mastersizer 2000E laser diffractometer, and the particle size distributions of different sieve fractions is shown Figure 3.2. In addition, XRD results have been shown in Appendix Figure A2, which display the post-milled XRD analysis, confirming that all fractions still match with the natural clinoptilolite.

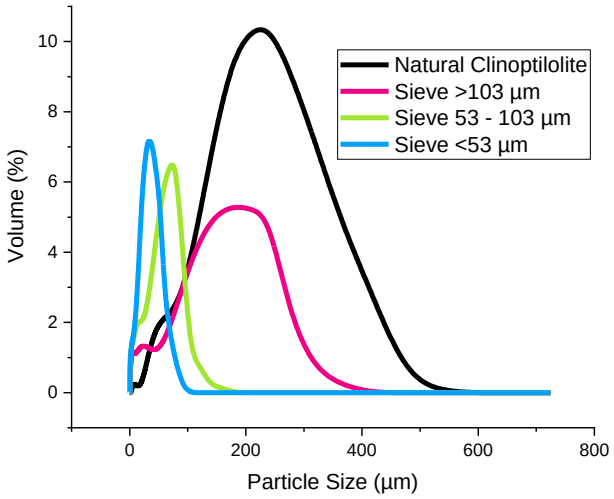

Figure 3.2: Particle size distributions of natural clinoptilolite for different sieve fractions comminuted using a ball mill.

This figure indicates that the particle size distribution of natural clinoptilolite is within 180 - 300 µm size range. Additionally, the median d_{50} size of natural clinoptilolite, sieve >103 µm, sieve 53 – 103 µm and sieve <53 µm are 246.04 µm, 120.56 µm, 55.65 µm and 23.15 µm, respectively, with relatively good separation between the fractions. Some fine particle were found in >103 µm sieve fractions, likely because of particle entrapment effects. Even though the sieve was brushed three times, some fine particle potentially could still have been trapped in between large particles. Decreasing the d_{50} from milling should increase the adsorption of ions, because of the greater surface area to volume ratio of each fraction (109, 235, 236).

Each of the sieved particle fractions were measured using the Micromeritics Tristar 3000 to determine the *Brunauer–Emmett–Teller* (BET) surface area. Before active measurements, each sample was degassed using a Micromeritics FlowPrep 060 gradually under N_2 at variable temperatures. The temperature was set at 80°C for 30 min, then increased to 120°C for another 30 min, before finally being degassed at 300°C for 5 h. For the active measurements, the dead volume was initially measured with the He gas as before being removed under vacuum. N_2 gas was then injected and adsorption isotherms recorded, where the amount of adsorbed gas per mass of particle sample is correlated to the total surface area and mean pore diameter of the particles, assuming monolayer coverage. The adsorption/desorption isotherm of all fractions of clinoptilolite are shown in Appendix A, Figure A3.

The measured surface area and mean pore diameter of the natural clinoptilolite was 10.812 m^2/g and 2.02 nm, while the sieve fractions gave 30.949 m^2/g and 2.33 nm (sieve >103 µm), 42.719 m^2/g and 2.67 nm (sieve 53 – 103 µm) and 43.606 m^2/g and 2.71 nm (sieve <53 µm). The surface areas of the acid and salt activated materials were similarly measured, giving 46.521 m^2/g and 2.89 nm; and 47.111 m^2/g and 2.91 nm for the HCl and NaCl activated respectively. It is noted that an equivalent spherical area for a non-porous particle of 250 µm would be only ~0.01 m^2/g. The surface area and mean pore diameter during this experiment also follow other clinoptilolite surface area works that were around 10–150 m^2/g, where the mean pore diameter have been generally found to to be around 2–5 nm (21, 110, 237-240). Hence, the actual specific surface area values (being almost 3 orders of magnitude greater) highlight the influence of the interstitial exchange sites on significantly increasing the material ionic porosity, a critical feature in the ion exchange performance of zeolites. The increase in BET surface area on activation, also indicates the role of initial charge loading on accessing these porous sites and gives initial confidence in the success of the activation processes. Measured surface areas are also broadly consistent with previous work on activated zeolites (110). The activation could remove the impurities that block the channels, therefore the effective surface area is increased (22, 113, 114).

3.4 Result and discussion

3.4.1 Characterisation of clinoptilolite

Images from the high angle annular dark field (HAADF) scanning transmission electron microscopy (STEM) used to analyse the natural clinoptilolite with adsorbed cesium are shown in Figure 3.3, with associated elemental mapping. Appendix A, Figure A4 displays representative images from SEM analysis at 100x and 1000x magnification, for the natural and activated clinoptilolites. The morphology of the samples are irregular crystals, consistent with crushed natural minerals. There were no changes evident from the pre-activation routine (see Fig. A4, Appendix A).

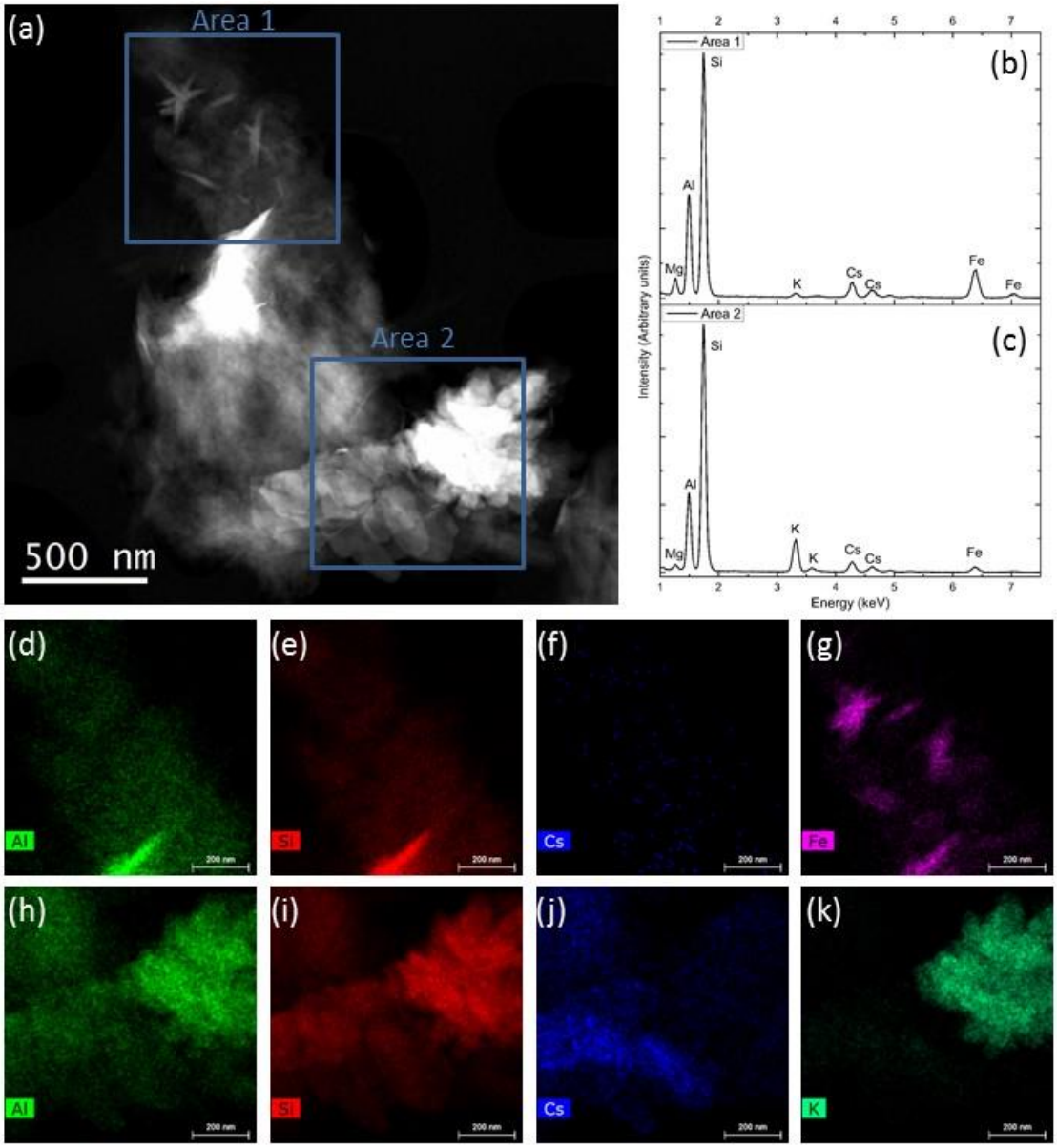

Figure 3.3: Electron microscopy analysis of natural clinoptilolite after equilibrium adsorption of 5000 ppm cesium chloride. (a) HAADF STEM image of part of the sample, with areas indicated for further analysis. EDX spectra from these two regions are shown in (b) and (c), with the spatial distribution of elements shown for Area 1 in (d) Al, (e) Si, (f) Cs and (g) Fe, and for Area 2 in (h) Al, (i) Si, (j) Cs and (k) K. The author would like to acknowledge Dr. Nicole Hondow and team for conducting the sample analysis using High Angle Annular Dark Field (HAADF) Scanning Transmission Electron Microscopy (STEM) and Energy Dispersive X-ray (EDX) spectroscopy

The energy dispersive X-ray (EDX) spectroscopy analysis shown in Fig. 3.3, was used to understand both the extent of naturally present surface contamination and its influence on cesium adsorption. In addition to the expected aluminium and silicon peaks (as clinoptilolite is an aluminosilicate zeolite) cesium

from adsorption was also detected, as well as several other elements (Fig. 3.3b-c). EDX spectra from different areas suggested relatively high concentrations of elements such as iron and potassium. Area 1 (Fig. 3.3d-g) highlighted the presence of iron based contaminants, which also appeared to reduce cesium adsorption, from the low density cesium element map of this area (Fig. 3.3f). Area 2 suggested additionally, large regions of potassium ions are also present in the natural mineral. This area also had high levels of cesium adsorption, but notably less so in the region of high potassium density. Given that potassium is a strongly competing ion, this is perhaps not surprising, and such adsorbed ionic impurities could considerably contribute to low adsorption uptake of cesium and strontium (31). Additionally, mineral impurities (such as those potentially leading to the presence of the iron) may also affect the clinoptilolite performance (18, 23). The presence of iron in clinoptilolite is similar to other work using natural clinoptilolite (241). The presence of potassium and iron as contaminants is also shown in Figure 3.4 (from another sample area). In this figure, sodium and calcium, which are parts of chemical structure of natural clinoptilolite (according to Sub Chapter 2.2 in Chapter 2) are also shown more clearly. Similar to the Al and Si, they display relatively homogenous levels across the sample, highlighting they are part of the zeolite matrix. The potassium and iron, on the other hand show areas of high and low levels, inferring heterogeneous contaminations.

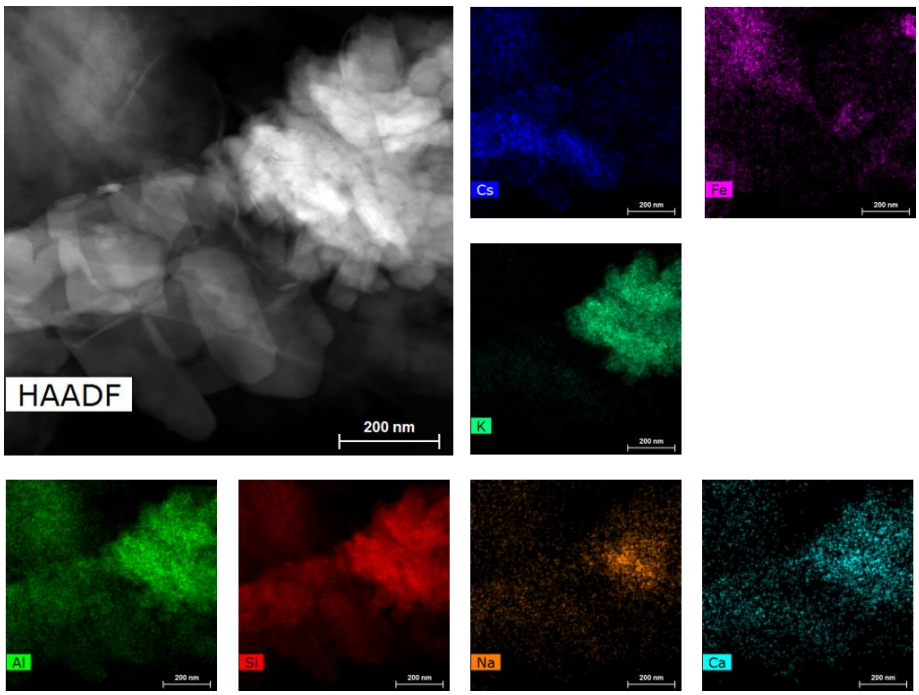

Figure 3.4: Electron microscopy analysis of natural clinoptilolite after equilibrium adsorption of 5000 ppm cesium chloride from another investigated area. The author would like to acknowledge Dr. Nicole Hondow and team for conducting the sample analysis using High Angle Annular Dark Field (HAADF) Scanning Transmission Electron Microscopy (STEM) and Energy Dispersive X-ray (EDX) spectroscopy.

In order to study the importance of the observed impurities, and also the influence of the sodium and acid activation, XRD patterns of the powder samples were measured and compared to the X'Pert HighScore database, as shown in Appendix A, Figure A5. The natural clinoptilolite, as well as both the sodium and acid activated materials, were all matched to calcium type clinoptilolite, with no evidence for a significant presence of other minerals. Such a result would infer that the elemental impurities evident in the STEM-EDX (Fig. 3.2) are largely from adsorbed surface ionic contaminants, rather than bulk mineral differences. The pre-activation currently does not change the structure of clinoptilolite significantly, but only affects the concentration of exchangeable ions which can increase the surface reactivity (40, 238).

The influence of pre-activation on the zeta potential of clinoptilolite is presented in Figure 3.5, where the potential of the natural clinoptilolite is compared to NaCl-Clinoptilolite, HCl-Clinoptilolite and milling samples. The clinoptilolite is naturally highly negatively charged, which reduces with the activation treatments. These changes indicate that activation not only results in ion exchange with existing charge groups, but adsorption of sodium and

hydrogen ions into interstitial or surface sites with no ions naturally present (thus reducing the net surface negative charge). Such changes are also consistent with the increase in measured specific surface areas on activation. Additionally, the sodium and hydrogen ions will be electrostatically attracted to the negatively charge surface of the clinoptilolite, leading to further adsorption. Meanwhile, the zeta potential of milling is found to be relatively similar to natural clinoptilolite. For highly expandable clays, electrostatic surface interactions can lead to a distinct two layer adsorption model, where firstly, inter-layer ion exchange sites control interaction, before secondly, surface interactions dominate (55). While clinoptilolite and zeolites more generally, do not normally exhibit explicit two site adsorption behaviour, previous studies using other ions, such as lead, have found both monolayer adsorption and heterogeneous surface conditions exist (103).

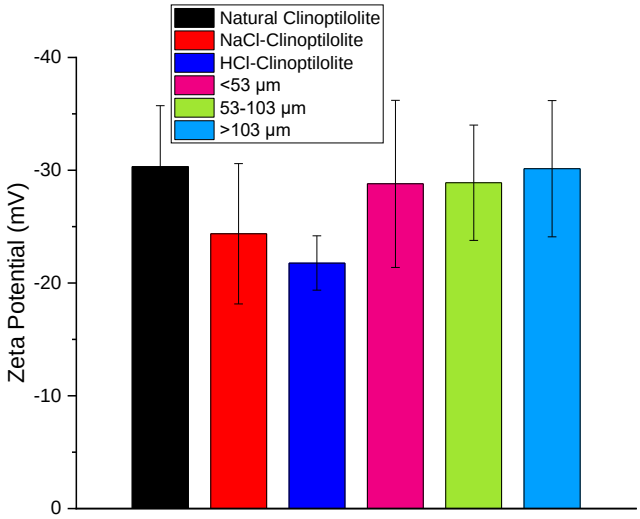

Figure 3.5: Zeta potential of natural and pre-activated clinoptilolite (HCl-Clinoptilolite and NaCl-Clinoptilolite) and milling at neutral pH

The influence of electrostatic attraction is also evident from the changes to natural clinoptilolite zeta potential in solutions of increasing cesium and strontium, as shown in Figure 3.6. Both cesium and strontium adsorption leads to a monotonic decrease in the magnitude of the measured zeta potentials (less negative values) and approach steady-state values, which likely corresponds to the ion adsorption capacity. Again, such changes to zeta potential values indicate that not only ion exchange, but electrostatic surface adsorption of ions occur. Whether such multiple adsorption site interactions occur through largely homogeneous or heterogeneous exchanges during surface adsorption can be

determined from Langmuir and Freundlich fittings (see Sub Section 3.4.3). However, the monotonic change in zeta potential would also infer there is no direct evidence for a separated dual-site adsorption mechanism, but rather potentially ion exchange and electrostatic surface adsorption occurs collectively. Additionally, the similar magnitudes for the potential changes for both strontium and cesium adsorption would indicate much lower number density of strontium (as it is divalent). To confirm this, a charge balance was also completed by calculating the equivalent of both ions per litre of solution, in order to understand how the electrostatics vary between cesium and strontium for equivalent charges. To determine the equivalent, Equation 3.3 has been used, where *valence* is the valency of the ion and *Ar* is the atomic weight of the ion.

$$\boldsymbol{mEq/L = \frac{C_0 \times valence}{Ar}} \qquad \textbf{(3.3)}$$

The result of equivalent for both ions is shown in Figure 3.7. This figure shows that the strontium equivalent charge per litre is higher than cesium, because of higher valency of strontium than cesium. Critically though, when comparing to zeta potentials, it highlights that on an equivalent charge basis, the zeta potential changes much more slowly with strontium adsorption, in comparison to cesium. This result infers that lower relative levels of strontium ions are absorbing onto the clinoptilolite than cesium for the same equivalent charge.

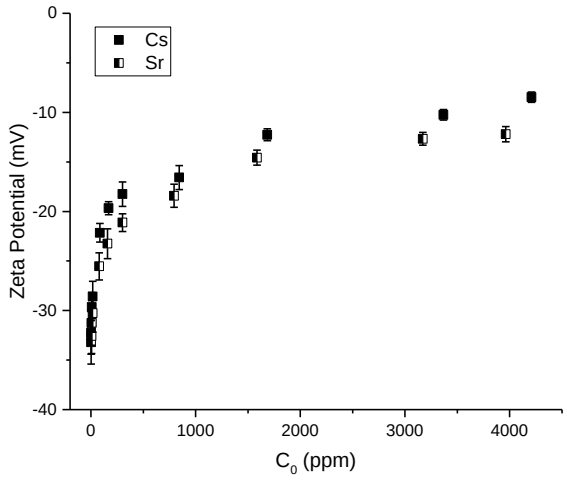

Figure 3.6: Zeta potential of natural clinoptilolite at neutral pH with different concentrations of Cs^{+} and Sr^{2+} ions

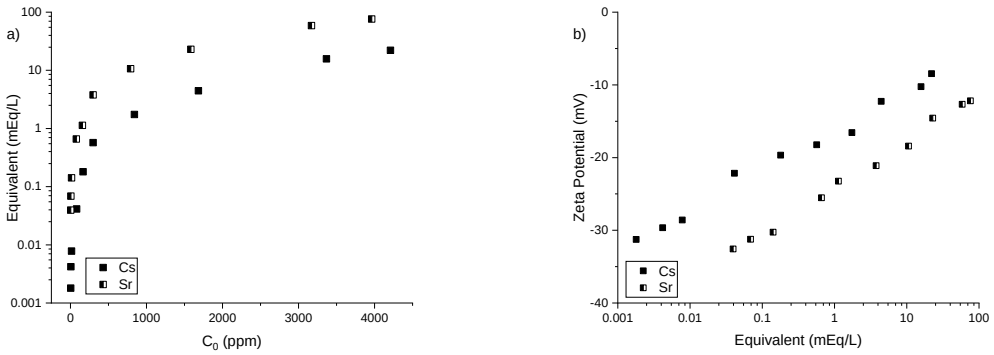

Figure 3.7: The equivalent/litre at neutral pH with different equilibrium concentrations and b) zeta potential vs the equivalent/litre of Cs^+ and Sr^{2+} ions.

3.4.2 Adsorption kinetics modelling

The adsorption kinetics of Cs^+ and Sr^{2+} on natural and pre-activated clinoptilolite (NaCl-Clinoptilolite and HCl-Clinoptilolite) are compared for 5 ppm salt solutions in Figure 3.8 a) and b), where adsorption is shown in terms of q_t (the adsorption ratio, in mg/g) and the percentage removal of the initial 5 ppm ion dose. Additionally, the Cs^+ and Sr^{2+} adsorption kinetics for the natural clinoptilolite at two further initial ion concentrations of 300 ppm and 1500 ppm are shown in Figure 3.9. For all cases at 5 ppm presented in Fig. 3.8, cesium and strontium ions are observed to reach equilibrium within around 360 min (6 h), which is consistent with previous studies on similar systems (18, 20, 30, 136, 145, 242, 243). For the natural clinoptilolite at higher salt levels, equilibrium adsorption occurs at a slightly greater time of 500 min (or ~8 h).

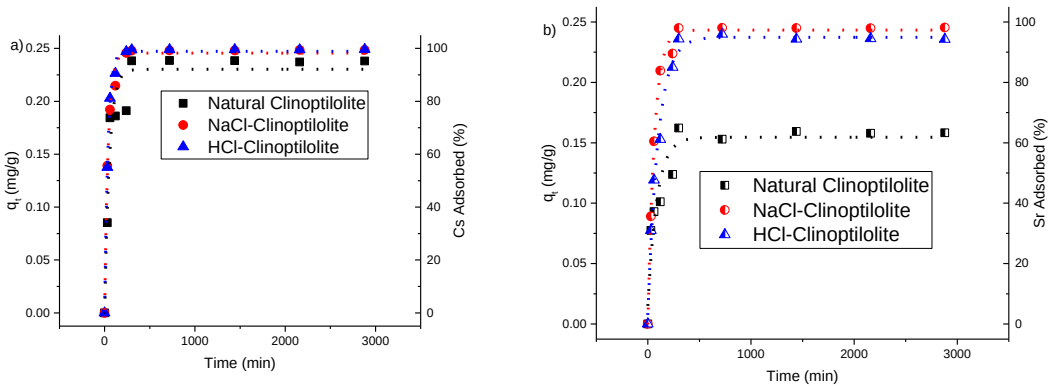

Figure 3.8: Uptake of 5 ppm cesium and strontium chloride solutions after different adsorption times, from 15 min to 48 h, onto natural and pre-activated clinoptilolite (HCl-Clinoptilolite and NaCl-Clinoptilolite); a) Cs^{+} and b) Sr^{2+}. Left vertical axes represent adsorption per mass of ion exchange, while right vertical represent total removal percentages.

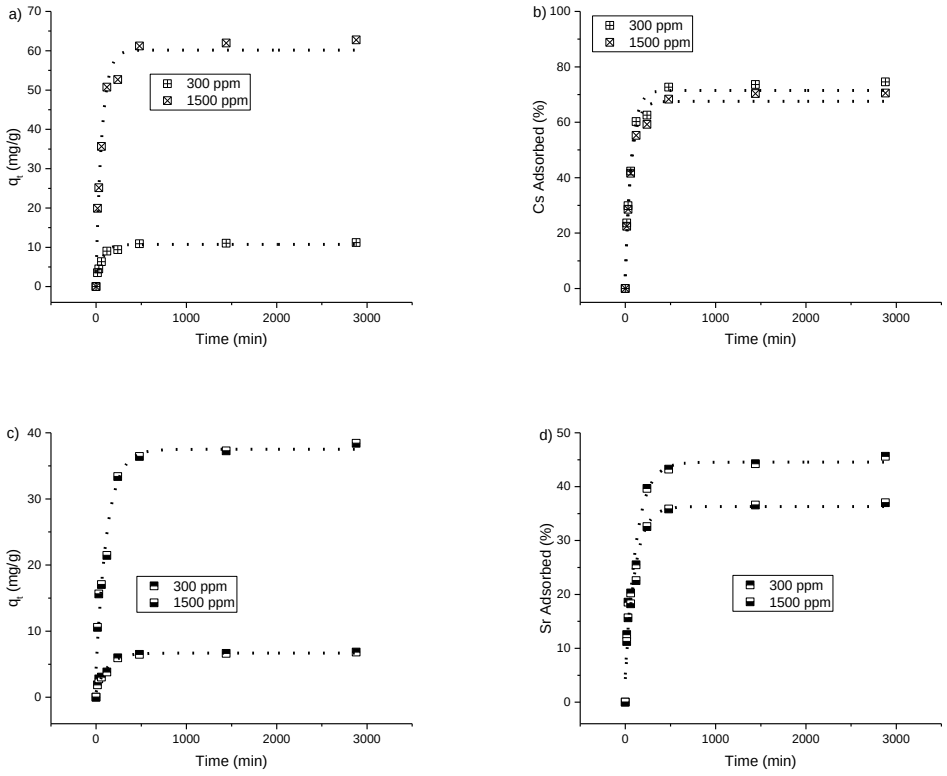

Figure 3.9: a) Natural clinoptilolite uptake of 300 and 1500 ppm Cs^{+} for different adsorption times from 15 minutes to 48 hours; b) $^{+}$ adsorbed percent of 300 and 1500 ppm Cs^{+} for the same times. c) Clinoptilolite uptake of 300 and 1500 ppm Sr^{2+} for different adsorption times from 15 minutes to 48 hours; d) adsorbed percent of 300 and 1500 ppm Sr^{2+} for the same times.

It is noted that in the case of cesium at 5 ppm, the influence of pre-activations does not appear to be significant, in terms of improving adsorption amount (see Fig. 3.8a). However, this result is likely from the relatively low concentration of cesium used and high removal percentages in all cases, even for the natural non-activated material. It would be expected that for higher cesium dosages, enhancement from activation would become more evident (as discussed in reference to Figure 3.10a following). Nevertheless, pre-activation does appear to considerably improve adsorbed amounts of strontium (Fig. 3.8b) with both NaCl and HCl activation similarly enhancing removal from ~60% to almost 100% in the 5 ppm dose (139).

Pseudo-First Order (PFO) and Pseudo-Second Order (PSO) rate analysis (as described within the Chapter 2 Section 2.3, Eqs. 2.4-2.9) were used to generate equilibrium rate constants and initial adsorption rate values from natural clinoptilolite kinetic adsorption data at 5, 300 and 1500 ppm, as well as the activated clinoptilolites at 5 ppm. The equilibrium rate constant (k_2, g/mg.min) and the initial adsorption rate (h, mg/g.min) derived from the PSO model for all systems are shown in Table 3.1. The PFO and PSO plots used to fit model values are shown in the Appendix A (Figure A6 and A7) where the R^2 values from PSO values from all experiment were close to 1 and significantly higher than R^2 values from the PFO model. The preference for PSO rate modelling, indicates that the rate-limiting step is the surface chemisorption (PSO), where the removal from a solution is due to physicochemical interactions between the two phases (solid and liquid) (27, 30, 34, 131).

Based on results shown in Table 3.1 for 5 ppm salt concentrations, the pseudo-second order constants (k_2) for Cs^+ are slightly larger through activation with sodium or acid (indicative of the enhanced kinetic interactions) although Sr^{2+} rate constants are not significantly altered (perhaps as ion-surface interaction is weaker in all cases). However, the initial adsorption rate (h) is enhanced considerably for both Cs^+ and Sr^{2+} with clinoptilolite activation. Additionally overall, initial adsorption rate values (mg/g.min) are about twice as large for Cs^+ than with Sr^{2+}, in all cases. The change in k_2 with concentration is also consistent in comparison to other research work, where the pseudo-second order constant (k_2) tends to be lower when the concentration is increased (18, 29, 30, 59). Therefore, the 1500 ppm concentration has a lower k_2 value than 300 ppm and 5 ppm ion concentrations for both ions.

For natural clinoptilolite at the higher initial ion concentrations of 300 and 1500 ppm, there is a distinct drop in the PSO rate constants for both cesium and strontium ions, owing to the increased influence of ion competition on the interaction with adsorption sites, which correlates to the longer times required to reach equilibrium adsorption (see Fig. 3.9). This behaviour means that adsorption kinetics are more optimal for low initial concentrations of ions, which is consistent with previous work (18, 30). Conversely, the initial adsorption rates (*h*) increase in a close to linear trend with concentration, owing to the higher initial number density of ions, again in agreement with previous research (18, 31, 126, 230).

Table 3.1: Pseudo-second order rate constants (k_2), initial adsorption rates (h) and adsorbed solute amounts at equilibrium (q_e) from dynamic uptake tests of Cs^+ and Sr^{2+} solutions.Data shown for natural clinoptiloilite at 5 ppm, 300 ppm and 1500 ppm, as well as sodium and acid activated clinoptilolite at 5 ppm.

Cs^+				
Material	k_2	h	$q_{e,cal}$	$q_{e,exp}$
	(g/mg.min)	(mg/g.min)	(mg/g)	(mg/g)
Natural clinoptilolite (5 ppm)	0.163	0.009	0.241	0.238
Natural clinoptilolite (300 ppm)	0.003	0.353	11.532	11.185
Natural clinoptilolite (1500 ppm)	0.001	1.980	61.377	59.365
NaCl activated clinoptilolite (5 ppm)	0.383	0.024	0.250	0.248
HCl activated clinoptilolite (5 ppm)	0.472	0.029	0.250	0.249
300 ppm (18)	0.57	1.177	45.53	45.12
23.7 ppm (29)	0.1432		1.86	
400 ppm (30)	0.0015		54.05	51.23
100 ppm (59)	0.0015	8.88	76.69	69.00
Sr^{2+}				
Material	k_2	h	$q_{e,cal}$	$q_{e,exp}$

	(g/mg.min)	(mg/g.min)	(mg/g)	(mg/g)
Natural clinoptilolite (5 ppm)	0.183	0.005	0.161	0.158
Natural clinoptilolite (300 ppm)	0.003	0.142	7.143	6.843
Natural clinoptilolite (1500 ppm)	0.001	0.796	30.615	29.348
NaCl activated clinoptilolite (5 ppm)	0.186	0.011	0.248	0.245
HCl activated clinoptilolite (5 ppm)	0.127	0.007	0.240	0.236
300 ppm (18)	1.47	1.177	45.53	45.12
100 ppm (59)	0.002	18.3	94.97	90.7

3.4.3 Equilibrium adsorption profiles

The relationship between the equilibrium concentration (C_e) versus final adsorbed amounts of Cs^+ and Sr^{2+} (mg/g clino and adsorbed percentage) are shown in Figure 3.10 a) and b), respectively. The uptake (q_e) of both ions is increased along with the final concentration (C_e) monotonically as expected for a monolayer coverage (18, 20, 30, 31, 59, 244). The percentage of initial ions removed as the equilibrium concentration is increased actually decreases quite considerably with C_e, as all available ion exchange sites become occupied at relatively low concentrations for both cesium and strontium ion solutions.

It is evident from Fig. 3.10 that Cs^+ displays much stronger adsorption behaviour compared to Sr^{2+}, with a factor of 2 to 3 in relative adsorbed amount for a given concentration. Such differences compare well to previous literature on cesium and strontium uptake in clinoptilolites and other zeolites (15, 18, 25, 30, 119, 126). The reason for the enhanced affinity of the cesium, is the general low energy state of adsorption for large monovalent ions in zeolite ion exchange sites. The effect of ion valency is significant, where the divalent strontium will be at a higher free energy state than the monovalent cesium (20, 173, 216). Additionally, on a mass basis (as given) divalent ions have to exchange with two monovalent ions for electron neutrality, and thus total loadings will be lower.

It is also evident that activated clinoptilolite gives pointedly better performance compared to the natural material for both cesium and strontium

systems. While differences were not as evident for the 5 ppm kinetic trials (shown in Fig. 3.8), as the removal percentage was higher in all cases, enhancements in ion exchange capacity are increased with C_e. By initial activation with small monovalent salts such sodium (or acid groups), which are weakly bound compared to other alkali and earth metals, exchange with larger ions including both cesium and strontium are highly energetically favourable (40, 111, 112). There is a relatively small difference between salt and acid activated systems, although sodium activation performed best for both cesium and strontium removal overall.

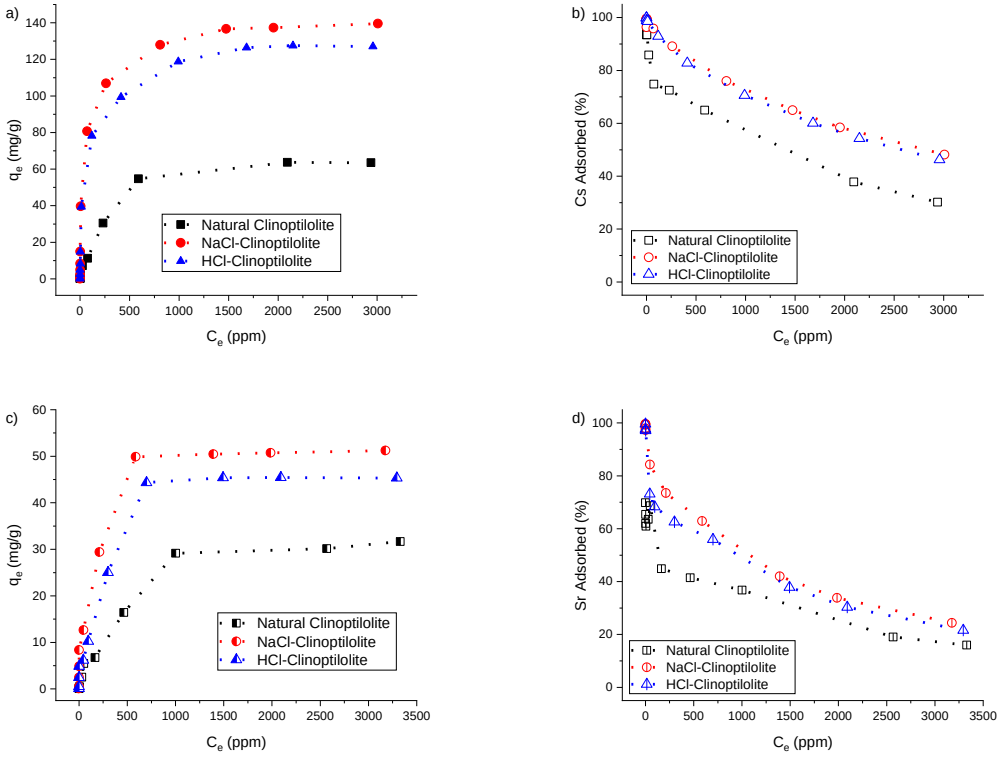

Figure 3.10: Equilibrium uptake per mass of ion exchange resin (mg/g) (left, closed symbols) and adsorption percent (right, open symbols) versus cesium and strontium salt concentration onto natural and pre-activated clinoptilolite; a) Cs^+ and b) Sr^{2+}. Connecting dashed lines are to guide the eye.

While all reported adsorption tests were completed at neutral pH (correlating with pH values encountered during radionuclide removal in industry (32)), the influence of pH on the cation exchange capacity was correlated by observing changes in pH from H^+ uptake for dispersions at different initial pHs. Given in the Figure 3.11 shows the percentage removal of H^+ for systems at initial pHs from 3 – 9. All systems, apart from pH 9 resulted in removal percentages >

99%, highlighting similar strong cation exchange behaviour over a broad pH range, whereas removal was reduced to < 80% for the pH 9 system, and was negligible for higher pH systems. Overall performance is consistent with expectations of a significant reduction in performance for high pH conditions, due to partial degradation of the clinoptilolite (32).

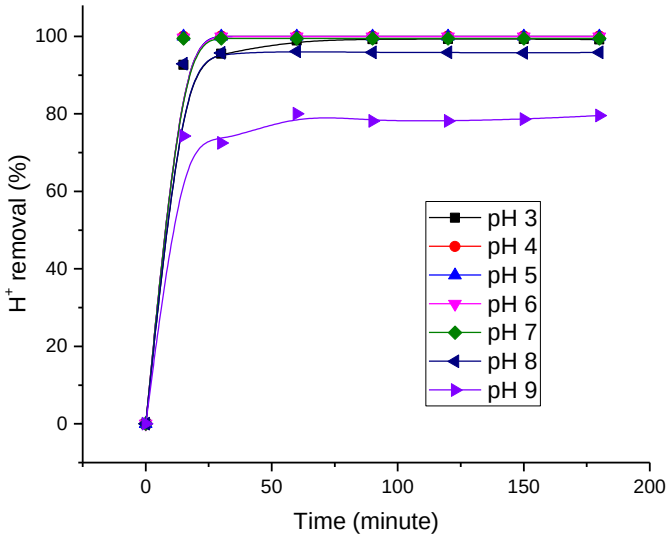

Figure 3.11: The percentage removal of H+ calculated from the increase in pH, for systems at different initial pH after 3 hours

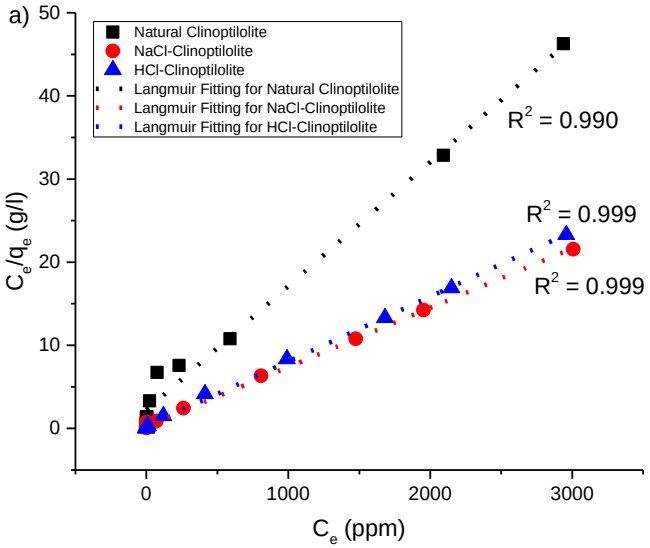

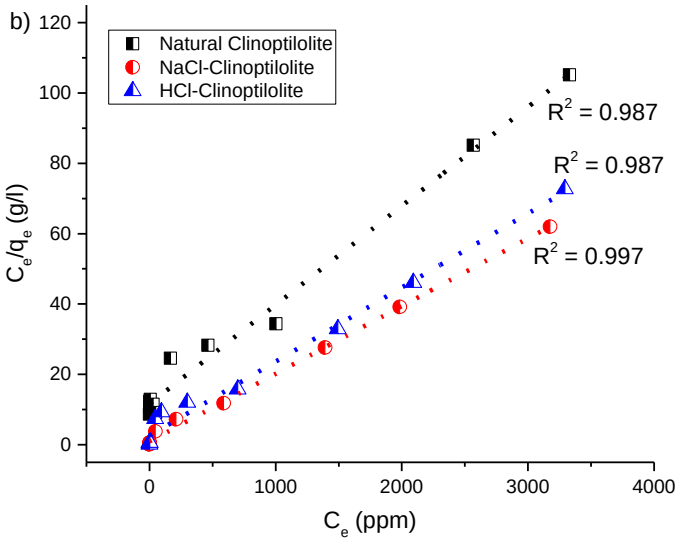

Figure 3.12: Langmuir isotherms of equilibrium salt adsorption for a) Cs^{+} and b) Sr^{2+} onto natural and pre-activated clinoptilolite. Dashed lines represent linear fits.

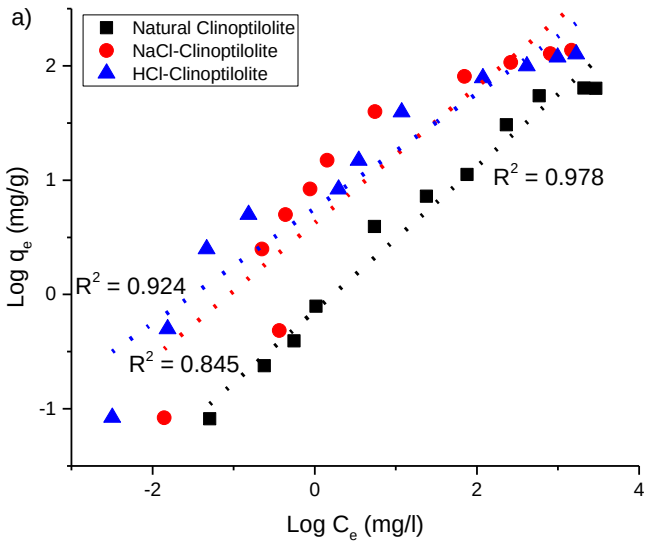

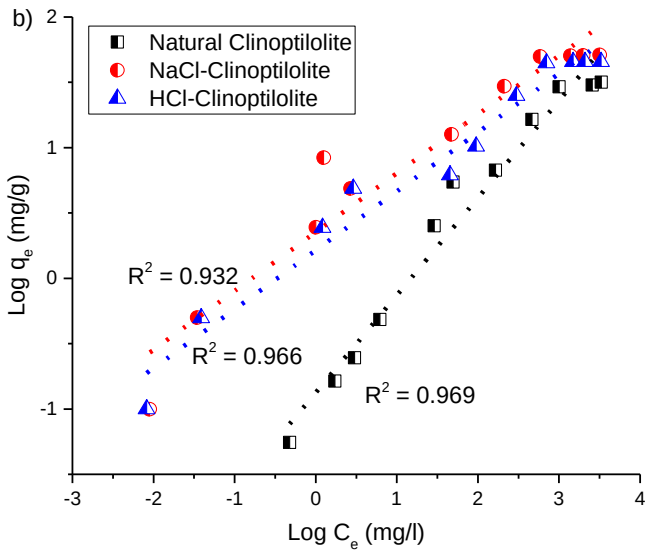

Figure 3.13: Freundlich isotherms of equilibrium salt adsorption for a) Cs^{+} and b) Sr^{2+} onto natural and pre-activated clinoptilolite. Dashed lines represent linear fits.

Langmuir and Freundlich theoretical models were applied to the equilibrium adsorption data for both the natural and activated clinoptilolite. The Langmuir model is based on the assumption that each active site of the homogenous surface is occupied by only one molecule, where the energy of adsorption is constant and independent of surface coverage (15, 18, 21, 31, 105, 132). Meanwhile, the Freundlich model considers that adsorption takes place on a heterogeneous surface with non-uniform distribution of adsorption energy, which decreases logarithmically with increasing coverage (15, 21, 59, 103, 107, 127, 245). The results of the Langmuir model fits are presented in Figure 3.12, in the linear form (where C_e/q_e is plotted against C_e) for a) cesium and b) strontium adsorption. Similarly, the Freundlich fits are presented in Figure 3.13 ($logq_e$ versus *logCe*). Additionally, resulting adsorption coefficients from Cs^{+} and Sr^{2+} data are given in Tables 3.2 and 3.3, for Langmuir and Freundlich models respectively.

Table 3.2: Langmuir isotherm fit parameters for equilibrium Cs^+ and Sr^{2+} adsorption on natural clinoptilolite , as well as salt and acid activated clinoptilolite.

Cs^+			
Material	Q_c *(mg/g)*	*b* (dm^3/g)	R^2
Natural clinoptilolite	67.046	0.007	0.990
NaCl activated clinoptilolite	140.533	0.030	0.999
HCl activated clinoptilolite	128.167	0.025	0.999
Sr^{2+}			
Material	Q_c *(mg/g)*	*b* (dm^3/g)	R^2
Natural clinoptilolite	35.557	0.002	0.987
NaCl activated clinoptilolite	51.975	0.021	0.997
HCl activated clinoptilolite	47.489	0.008	0.987

Table 3.3: Freundlich isotherm fit parameters for equilibrium Cs^+ and Sr^{2+} adsorption on natural clinoptilolite, as well as salt and acid activated clinoptilolite

Cs^+			
Material	K_f *(mg/g)*	*n*	R^2
Natural clinoptilolite	0.143	1.585	0.978
NaCl activated clinoptilolite	0.615	1.863	0.845
HCl activated clinoptilolite	0.730	2.125	0.924
Sr^{2+}			
Material	K_f *(mg/g)*	*n*	R^2
Natural clinoptilolite	0.075	1.342	0.969
NaCl activated clinoptilolite	0.354	2.222	0.932
HCl activated clinoptilolite	0.451	2.218	0.966

From Table 3.3, the adsorption capacity (Q_c) is more than double for cesium adsorption between natural clinoptilolite and NaCl-Clinoptilolite (from ~67 to 140 mg/g). Values for strontium are considerably smaller and show a reduced

enhancement with activation (from ~35 to ~52 mg/g). Additionally, activation energies were calculated for cesium and strontium adsorption on the natural and pre-activated materials using the derived Langmuir constants for the affinity of adsorption (as detailed in the Appendix A, Table A1 and Eq. A1) where energies were higher for Sr^{2+} adsorption, as expected, with significant reductions to both Cs^{+} and Sr^{2+} values upon activation. Generally, these results are well within performance requirements for ongoing nuclear effluent treatment, and suggest simple sodium salt pre-activation will enable many lower grade natural clinoptilolite ores to be used in nuclear process plants, greatly expanding the potential supply sites for future procurement.

The Freundlich adsorption affinity constants (K_f, from Table 3.3) are relatively low in all systems, although again consistent with previous research on cesium removal from clinoptilolite (27). Proportionally though, activation leads to an even larger increase in performance than for the adsorption capacity (increasing K_f by almost a factor of five in all cases). The low concentration performance assessment from Freundlich fits must be made with some caution however, as R^2 values are lower than for the Langmuir model (although still > 0.9 in most cases). Such differences are similar to trends previously observed, and indicates monolayer coverage of the adsorbent occurs with similar chemical interaction forces across the ion concentration range (18, 183, 246).

The effect of particle milling on the performance of clinoptilolite was observed by measuring the percentage removal of cesium and strontium salt solutions at initial concentrations of 300 and 1500 ppm. The results are presented in Figure 3.14, for the natural un-milled material, as well as the salt and acid activated material (also un-milled) in comparison to natural milled particles at three sieve fractions i) < 53 μm, ii) 53-103 μm and iii) > 103 μm mesh.

It is clear that milling strongly enhances the uptake of cesium, with percentage removal increasing for both initial salt concentrations to around the capacity of the activated materials. Uptake also follows the change in size, with higher removal for smaller sieve fractions, and is in agreement with the understanding that increasing the specific surface area leads to a corresponding increase in adsorption sites, promoting enhanced ion exchange with the cations (109, 235, 236). To quantify the effect of surface area to a greater degree, the adsorption data for the milled fractions was reanalysed, giving the adsorbed percentage for the same initial salt concentrations of 300 and 1500 ppm, in terms of the calculated specific surface areas, for each fraction, as given in Figure 3.15.

Data for the salt activated clinoptilolite is also presented in terms of its associated specific surface area.

It is evident from Figure 3.15a that, as expected, there is a similar linear increase in adsorbed amount of cesium with the surface area of the clinoptilolite, at both concentrations. Interestingly also, this relationship appears to hold for the activated clinoptilolite, which has a slightly larger surface area than the smallest milled fraction with corresponding increase in adsorption for the 1500 ppm solution (for the 300 ppm solution, both the smallest sieve fraction and activated sample achieve 100% removal). This trend highlights that for cesium, both milling and pre-activation may lead to significant increases in adsorption sites with similar enhancements to material performance.

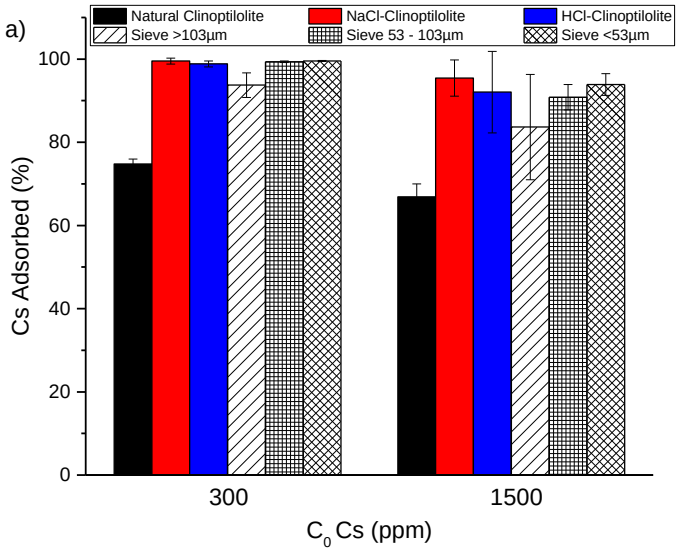

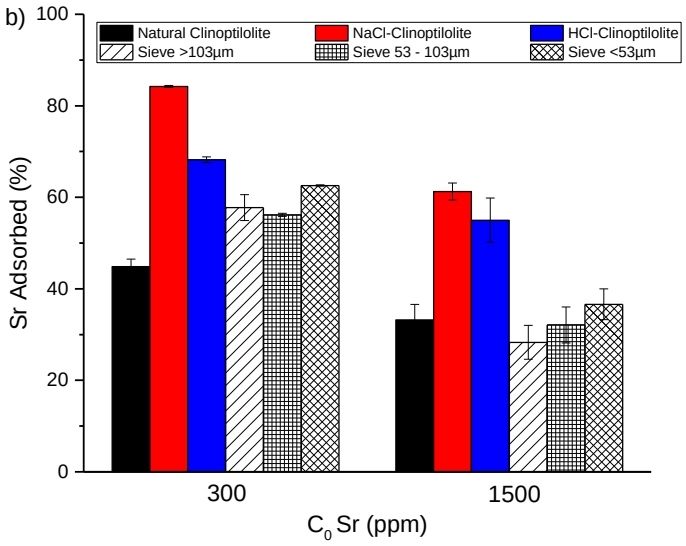

Figure 3.14:Total adsorption percent for different clinoptilolite treatments (acid and salt activation, as well as three milled fractions) at two different initial salt concentrations, in comparison to the natural mineral; a) Cs^{+} and b) Sr^{2+}.

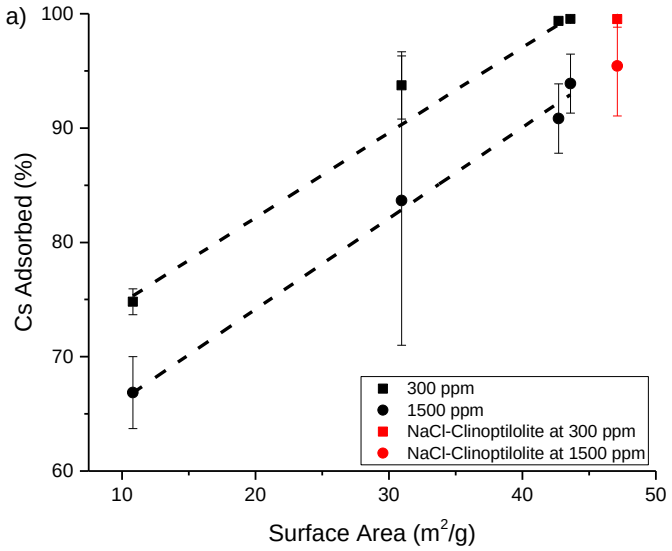

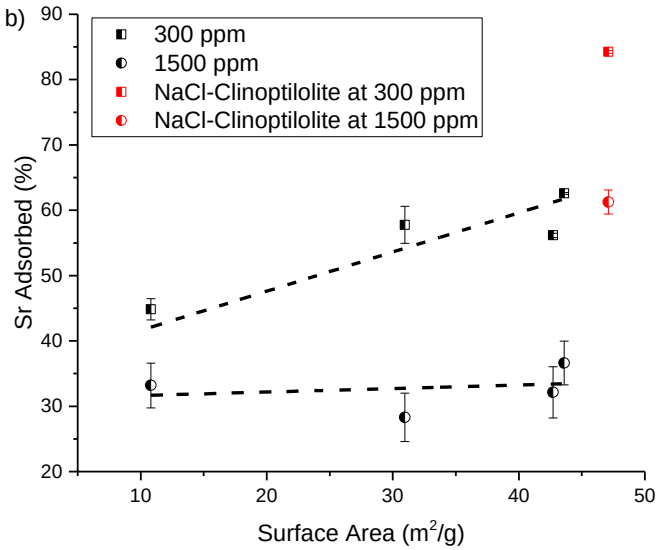

Figure 3.15: Adsorption percent versus specific surface area for the different mill fractions, as well as salt activated clinoptilolite at two different initial salt concentrations; a) Cs^{+} and b) Sr^{2+}. Dashed lines represent linear fits to the milled fractions

For strontium adsorption (Figure 3.15b), the increase in adsorption with surface area of the milled fractions is much less pronounced. Indeed, for the 1500 ppm concentration (which is well beyond concentrations relating to the maximum equilibrium adsorption) almost no increase in capacity is observed until the very highest milled surface area. It is clear also that the effect of pre-activation on adsorption is greater than milling, for equivalent specific surface areas. As clinoptilolite has interstitial ion exchange sites, making it ionically porous to some degree, decreasing particle size through milling will lead to an increase in the number of these exposed interstitial sites, as well as the external surface area (19). However, for strontium, the influence of contamination present in the non-activated samples dominates interaction behaviour, and it is clear that milling the material, while increasing the active surface area, does not remove the influence of these contaminants. For example, it appears that the potassium and iron minerals observed with EDX (Figs. 3.3 and 3.4) may be prevalent throughout the clinoptilolite, and while they will not influence the adsorption of cesium to a high degree (as cesium has higher relative affinity) they appear to continue to disrupt the adsorption of strontium. Thus, the number of available adsorption sites remains low (19, 247) and the effect of pre-activation is much more pronounced (as it will lead to the removal of the ionic contaminants, such as the potassium). Therefore, in order to increase the Sr^{2+} adsorption performance, it would be

suggested to couple particle milling with salt or acid activation. It is further noted, that the milled clinoptilolite would be too small for a vertical column ion exchange, as decreasing the particle size will lead to high pressure loss and reduce column performance (59, 248, 249). Nevertheless, it would be extremely useful for batch adsorption in a rapid contact mixing tank, where the waste could then be easily dewatered using flotation, for example (49, 55, 56, 163, 166, 183, 250).

3.4.4 Effect of ion competition on adsorption

The effect of simulated seawater (containing K^+ at 380 ppm, Na^+ at 10556 ppm and Ca^{2+} at 400 ppm) on the adsorption of Cs^+ and Sr^{2+} with natural and pre-activated clinoptilolite is presented in Figure 3.16. Here, ion removal performance is shown in terms of the distribution coefficient (K_d) as defined in Eq. 2.10.

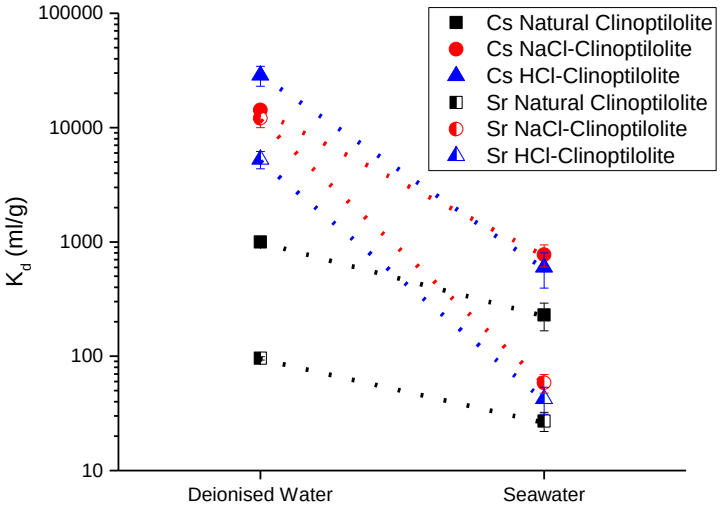

Figure 3.16: The distribution coefficent (K_d) for 5 ppm Cs^+ and Sr^{2+} solutions in deionised water and in a simulated seawater, with represenative concentrations of K^+ (380 ppm), Na^+ (10556 ppm) and Ca^{2+} (400 ppm). Data shown for natural and pre-activated clinoptilolite.

The influence of salinity on reducing the adsorption of Cs^+ and Sr^{2+} is important for ongoing processing of nuclear effluents from seawater cooling, such as occurring currently at Fukushima. It is evident from Fig. 3.16 that the K_d of cesium and strontium from all systems reduces significantly in seawater conditions. Given the relatively low affinity of Na^+ and Ca^{2+} to clinoptilolite (37), it is assumed the major reason for the reduced performance is ion competition from the K^+ ions (18, 119). As potassium is assumed to have a higher affinity than

strontium (37), its influence on strontium adsorption in seawater is comparatively greater (with Sr^{2+} distribution coefficients for activated clinoptilolite reducing by two orders of magnitude, in comparison to one order for Cs^{+}).

To further investigate the reduction of Cs^{+} and Sr^{2+} adsorption due to ion competition, distribution coefficients were measured for natural and activated clinoptilolite materials, in solutions of increasing competing ion concentration from 5 up to 4000 ppm (using mixtures of K^{+}, Na^{+} and Ca^{2+} ions in a 1:1:1 ratio) with Cs^{+} and Sr^{2+} held at 5 ppm. Results, given in terms of the concentration of competing ions, are shown in Figure 3.17. Similar to Fig. 3.16, clear reductions to the distribution coefficient K_d are observed for both cesium and strontium systems, in a power law relationship with competing ion concentration. Indeed, direct measurement of K^{+}, Na^{+} and Ca^{2+} uptake from the saline solution could also be measured simultaneously with the AAS technique, and are reported in the Figure 18. It is observed that ionic affinity follows the expected trend at all solution concentrations of $Cs^{+} > K^{+} > Sr^{2+} > Na^{+} > Ca^{2+}$, and while the general affinity for cesium to clinoptilolite is still above that of potassium (37), the much larger concentration of the latter will dominate surface interactions as the saline solution concentration increases. Interestingly, the exponent gradients for all activated clinoptilolite with cesium and strontium are similar, as interactions are dominated by the competing potassium ions, due to the low 5 ppm level of Cs^{+} and Sr^{2+}. Exponents are also higher for the activated clinoptilolite than the natural material, as activation with either sodium or acid will similarly enhance adsorption of potassium, due to its high affinity, and therefore it is apparent that activation by itself cannot reduce salinity effects in clinoptilolite. Evidence of K^{+} dominancy in comparison to Na^{+} and Ca^{2+} have also been found in previous research studies (33, 38, 251, 252).

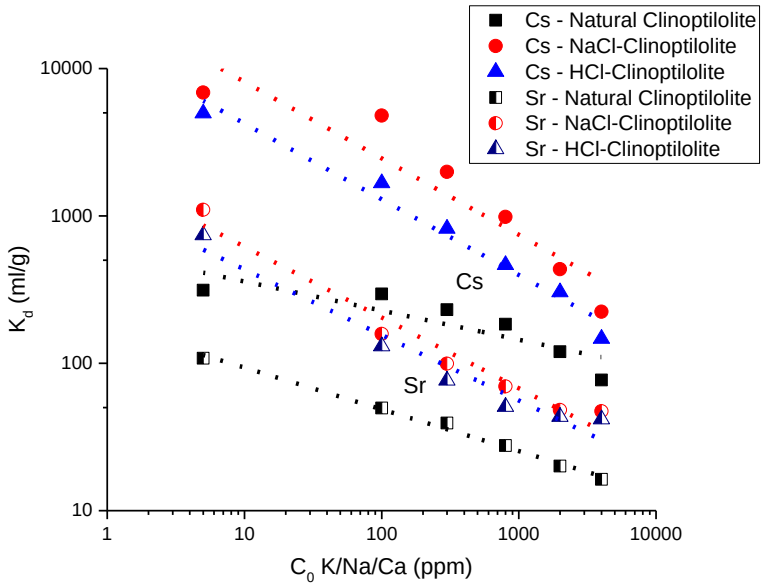

Figure 3.17: The distribution coefficent (K_d) for 5 ppm of Cs^+ and Sr^{2+} solutions in different concentrations of K^+, Na^+, Ca^{2+} (1:1:1 ratio of each) from 5 to 4000 ppm. Data shown for natural and pre-activated clinoptilolite. Dashed lines represent log-log fits.

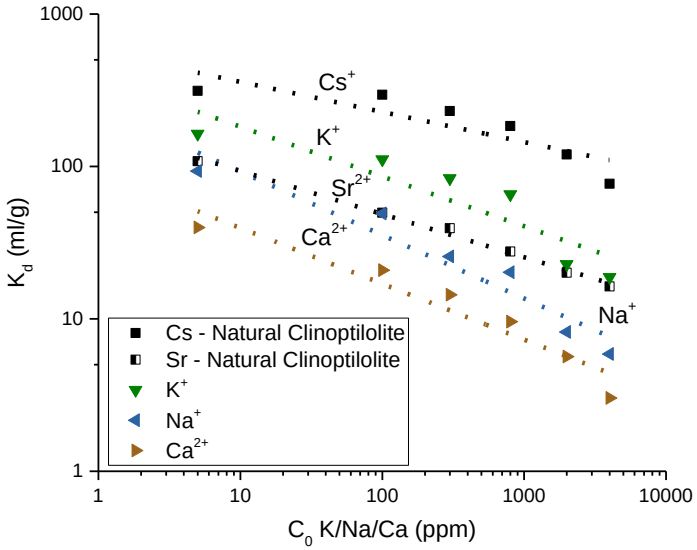

Figure 3.18: The distribution coefficient (K_d) for 5 ppm of Cs^+ and Sr^{2+} as well as variable concentrations of K^+, Na^+, Ca^{2+} (1:1:1 ratio of each) from 5 to 4000 ppm with natural clinoptilolite. Dashed lines represent log-log fits

3.5 Summary

This study investigated the use of acid and sodium chloride activation, as well as particle milling, to increase the performance of relatively low-grade clinoptilolite for removing cesium and strontium ions from nuclear effluents. The natural ore was characterised using STEM-EDX and XRD, where regions of high potassium ion contamination and iron based impurities were evident that correlated to areas of lower cesium and strontium uptake. Changes to clinoptilolite zeta potentials with cesium and strontium adsorption indicated heterogeneous surface interactions occurring, driven both by ion exchange from interstitial sites and electrostatic surface attraction, although there was no evidence of separate two-site adsorption mechanisms.

Adsorption kinetics of natural and pre-activated materials in 5 ppm Cs^+ and Sr^{2+} salts were fitted using a Pseudo-Second Order model with the average linear regression (R^2) ~ 0.99 in all cases. While activation increased the initial adsorption rate of both cesium and strontium, the overall rate constant (k_2) was only enhanced in cesium systems, due to the general low affinity of the strontium. Equilibrium isotherms were compared with Langmuir and Freundlich monolayer models, with the former providing closer fits. The Langmuir adsorption capacity (Q_c) for cesium was increased by over 100% in sodium activated clinoptilolite (from ~67 to 140 mg/g), while values for strontium were considerably smaller with a lower enhancement with activation of ~50% (from ~35 to ~52 mg/g).

Additionally, the effect of milling was observed to give a similar increase in performance to activation for cesium removal, with a strong linear dependency between adsorbed amount and overall specific surface area, where a combination of these two techniques will likely to lead to a much greater ion exchange capacity. The influence of contaminants on strontium removal in milled fractions was notably more significant, which reduced relative adsorption in comparison to associated surface area increases on un-activated samples. The influence of ion competition on adsorption was also investigated, using solution mixtures of Na^+, Ca^{2+} and K^+, to represent seawater type solutions. The distribution coefficients (k_d) of both cesium and strontium were significantly reduced, with the magnitude of reduction directly proportional to the concentration of competing ions (from power-law fits) while pre-activation actually led to a more critical drop-off in uptake. Collectively, these results highlight that pre-activation and milling could be used to considerably extend the range of natural clinoptilolite ores suitable for nuclear treatment processing of relatively

fresh water effluents, but for high saline waters, modern synthetic products will still be required.

Chapter 4 The effect of cationic surfactants on improving natural clinoptilolite for the flotation of cesium

4.1 Synopsis

It is noted that some of contents may similar to previous chapters to help understanding the chapter study.

Flotation using cationic surfactants has been investigated as a rapid separation technique to dewater clinoptilolite ion exchange resins, for the decontamination of radioactive cesium ions (Cs^+) from nuclear waste effluent. Initial kinetic and equilibrium adsorption studies of cesium, suggested the large surface area to volume ratio of the fine zeolite contributed to fast adsorption kinetics and high capacities (q_c = 158.3 mg/g). Adsorption of ethylhexadecyldimethylammonium bromide (EHDa-Br) and cetylpyridinium chloride (CPC) surfactant collectors onto both clean and 5 ppm Cs^+ contaminated clinoptilolite was then measured, where distribution coefficients (K_d) as high as 10,000 mL/g were evident with moderate concentrations CPC. Measurements of particle sizes confirmed that adsorption of surfactant monolayers did not lead to significant aggregation of the clinoptilolite, while < 8% of the 5 ppm contaminated cesium was remobilised. Importantly for flotation, both the recovery efficiency and dewatering ratios were measured across various surfactant concentrations. Optimum conditions were found with 0.5 mM of CPC and addition of 30 µL of MIBC frother, giving a recovery of ~90% and a water reduction ratio > 4, highlighting the great viability of flotation to separate and concentrate the contaminated powder in the froth phase.

4.2 Introduction

This chapter investigates how fine, powdered ion exchange resins may be used in large batch processes as adsorbents, and recovered using froth flotation, as an alternative to their use in ion exchange columns.

It is noted that powdered mineral adsorbers can be recovered using gravitational sedimentation, when combined with co-precipitation methods to aid separation rates (43-45) such as in cesium removal (54, 253). Unfortunately,

solid-liquid dewatering rates of these types of sludges is slow, resulting in voluminous secondary wastes that are difficult to treat themselves. Therefore, to overcome these issues, flotation is investigated in this chapter as an alternative process to separate fine and highly efficient powdered ion exchange material, with greater dewatering factors and considerably smaller residence times than is possible from gravitational sedimentation (46, 47, 253).

Flotation is commonly used in a number of applications, either for removing heavy metal ions, to separate minerals from gangue material or simply as a rapid technique to dewater suspensions, where the concentrated sludge fraction is removed along with the froth (77, 154-156, 162). Particle or aggregate flotation is based on the removal of solids through adsorption onto foam interfaces, by using surface active agents (surfactants) as collectors to modify particle contact angles (48, 77, 155, 156, 161-165). In order to achieve a successful flotation process, the selection of a suitable collector is required in order to maximize the hydrophobicity of the particles to ensure strong adsorption to bubble interfaces (56, 163, 165-167). Often, a separate frother additive is also used, such as methyl isobutyl carbinol (MIBC), to obtain rapid flotation with fine bubbles (56, 154, 163).

There are many industrial sectors that use flotation as an engineering solution, such as minerals processing, wastewater treatment and paper recycling, while it is a technique of increasing interest for nuclear effluent treatment (30, 46, 77, 154-156, 160, 162, 163, 166, 167, 254-257). In terms of its application in nuclear related fields, ion flotation and combined co-precipitation methods have been used to remove radioisotopes of cesium, strontium and cobalt, while fine particle flotation has been used for the separation of soils and as part of nuclear wastewater treatment processes (30, 48-54). It has also been demonstrated recently as a viable technique for the separation of cesium contaminated colloidal clays (55, 56).

Given the evidence that flotation can be used as a successful technique for nuclear effluent treatment from previous research, it is perhaps surprising there has been no previous specific studies into its use to separate contaminated clinoptilolite, although previous work by Walcarius *et al.* (183) into the flotation of lead-adsorbed faujasite highlights its potential in similar systems. However, there are some significant questions that remain into the potential viability of this process. Perhaps most importantly, is the potential for adsorption of surfactant collectors to remobilise and remove contaminated radioisotopes that have been adsorbed, and additionally, whether the effect of ion contamination reduces the

interaction of the collectors and thus flotation removal. Also, for flotation to be considered for rapid dewatering, the process needs to be optimised to not only maximise recovery, but also reduce water carry-over in the froth phase, to ensure good dewatering ratios.

Therefore, in this study, the flotation performance of cesium contaminated, fine clinoptilolite is investigated. The type of material processed, is based upon post-adsorption ion exchange powder, utilised for the removal of radioisotopes from nuclear effluents in batch contact tanks. Two cationic surfactants (Ethylhexadecyldimethylammonium bromide and Cetylpyridinium chloride) are used as collectors, where their adsorption density and structure is measured on both clean and contaminated material. The flotation recovery of the contaminated clinoptilolite is optimised by varying both collector concentration and through the addition of MIBC frother, where importantly, both flotation removal and dewatering ratio are measured.

4.3 Experimental

4.3.1 Materials

Natural clinoptilolite was supplied from Fluorochem as a nominal ~ 7 µm powder (product code S25114). The natural clinoptilolite used in this chapter was different to that used in Chapter 3. Because of the limitation of research time, fine pre-milled clinoptilolite was used, which was assumed to have a high specific surface area. Cesium chloride (CsCl) Analytical Grade with purity ≥ 99.0% was purchased from Sigma-Aldrich. For surfactant adsorption and flotation studies, two cationic surfactants were selected; Ethylhexadecyldimethylammonium bromide (EHDA-Br) and Cetylpyridinium chloride (CPC) supplied by Merck Millipore and Sigma-Aldrich, respectively. EHDA-Br has previously been used for the flotation of cesium contaminated clays (56), while CPC is an ammonium based cationic surfactant of the same chain length with a pyridine head group, and has been used previously to float metal ions (49, 78, 183). Methyl isobutyl carbinol (MIBC) with purity ≥ 99.0% (Sigma-Aldrich) was used as a frother, as common in flotation studies (56, 154, 163).

4.3.2 Particle characterisation

The zeta potential of 1 wt% of clinoptilolite was measured using a Zeta Probe (Colloidal Dynamics) in order to determine the change in surface charge

of natural clinoptilolite through adsorption of different concentrations of cesium salt. The zeta potential of natural clinoptilolite was found to be -13.575 mV ± 0.881 mV.Fig. B1 within the Appendix B shows the zeolite particle zeta potential versus initial concentration of cesium ions, where it is evident that although the potential becomes lower in magnitude with Cs^+ adsorption, it remains negative under all concentrations. This result infers cationic surfactants will interact strongly with the surface across a wide range of cesium contaminations.

To analyse the powder structure, a TM3030 (Hitachi Ltd.) bench top scanning electron microscope (SEM) was used to image the clinoptilolite powder, as shown in the Appendix B (Fig. B2) at two scales. The powder presents itself as irregular shaped crystals, consistent with crushed zeolite minerals from other studies (18, 20, 21, 24, 28, 31, 34, 36, 106, 246). Sizing from SEMs suggested all particles were < 30 µm, in agreement with supplier specifications. The Brunauer–Emmett–Teller (BET) particle surface area was determined with a Tristar 3000 (Micrometrics) using the same procedure as outlined in previous research. The resultant surface area was measured as 44.7 m^2/g, which is consistent to that of < 53 µm milled clinoptilolite particles previously characterised in Chapter 3. Unlike in Chapter 3, the EDX analysis was not conducted because the cesium deposition in the clinoptilolite was assumed to be similar to the previous chapter.

4.3.3 Cesium adsorption on clinoptilolite

To measure adsorption kinetics, cesium chloride (CsCl) stock solution (1 M) was diluted with Milli-Q water at neutral pH (which tends to a pH of ~6.5) to a nominal initial concentration of 5 ppm, in line with previous studies on cesium adsorption (55, 242). The 5 ppm solution was then filled into a polypropylene conical centrifuge tube. Polypropylene tubes were used in order to prevent Si contamination from glassware and also potential of Cs^+ adsorption onto the tubes, as evidenced in an earlier study (82). Then, natural clinoptilolite was dispersed into the solution at a fixed 20 g/L solid/liquid ratio. All suspensions were then placed on an orbital shaker at 150 rpm (at room temperature) for different times from 30 min until 48 hours. The suspensions were then centrifuged using a Heraeus Megafuge 16R (Thermo-Scientific) for 10 min at 7000 rpm, and the separated supernatants were decanted using a 20 mL syringe with 0.3 µm filter. Cesium concentrations from extracted supernatants were measured using a 240FS Atomic Absorption Spectrophotometer (AAS) (Varian-Agilent) utilising a

cesium lamp set with a wavelength of 459.3 nm (suitable for concentrations from 5 – 4000 ppm).

The amount of Cs^+ adsorbed by clinoptilolite at different specific times was determined from AAS measurements in terms of the relative kinetic adsorption amount, q_t (mg/g) and removal percent, using the methodologies described within the Chapter 3, Sub Section 3.3.4 (Eqs. 3.1-3.2). Adsorption kinetic fits were determined using the Pseudo Second Order (PSO) rate model to derive the adsorption rate constant (k_2) and the initial rate of adsorption (h) (see Chapter 2, Section 2.3, Eq. 2.9).

For the equilibrium adsorption study, 1 M CsCl stock solution was diluted with Milli-Q water at neutral pH in order to get various initial concentrations from 5 ppm up to 4000 ppm with a solid/liquid ratio fixed at 20 g/L. All suspensions were then placed on an orbital shaker for 48 hours, with supernatants being extracted and analysed by AAS as described above. Equilibrium data was fitted with both Langmuir and Freundlich isotherm monolayer adsorption models (see Chapter 2, Section 2.3, Eqs. 2.11-2.12).

4.3.4 Surfactant adsorption at the air-liquid and solid-liquid surface

The two cationic surfactants were prepared in different concentrations from 0.01 mM to 20 mM. To obtain desired concentrations, 1 M of EHDA-Br and CPC solutions were diluted with Milli-Q water at neutral pH. The solutions were then analysed using a Theta Optical Tensiometer (Biolin Scientific) in order to measure the air-water surface tension via droplet profiling. The instrument was housed in a temperature-controlled chamber (20 °C +/- 0.5 °C) and a constant droplet size (~10 µL) was used for all experiments. Surface tension versus surfactant concentration data were also fitted to the Langmuir monolayer model, for concentrations below the critical micelle concentration, given in Eq. 4.1.

$$\boldsymbol{\gamma = \gamma_0 + RT\Gamma_{max}\ln\left(\frac{1}{1+KC}\right)} \qquad \textbf{(4.1)}$$

Here, γ (N/m) is the fitted surface tension for a specific surfactant initial concentration, C (M), γ_0 is the surface tension of the pure solvent, R is the universal gas constant (8.315 J/mol.K), T is system temperature (293.15 K), while Γ_{max} is the maximum surface coverage of surfactant (mol/m^2) and K is the equilibrium constant (M^{-1}) (258, 259). Model fits were obtained numerically by minimising the error between theoretical calculated values of surface tension and measured readings using MS Excel Solver™, with Γ_{max} and K the independent

variable parameters. The goodness of fit was determined using the R^2 ('RSQ') function.

Surface tension tests were also used to measure the amount of cationic surfactant adsorbed onto both natural and pre-contaminated clinoptilolite (which had been initially mixed with 5 ppm of Cs^+ for 24 hours before separation, washing and drying by using Eqs. 2.10 and B1). After mixing different concentrations of both surfactants with 20 g/L clinoptilolite suspensions for 24 hours, the clear supernatants were extracted and filtered to remove any particles, as described above in Sub Section 4.3.3. The surface tension of these supernatant solutions was then measured and compared to the Langmuir fits of the pure surfactants to determine the concentrations after adsorption (via back-calculation), and thus importantly, the amounts adsorbed. Additionally, a control supernatant solution from surfactant-free dispersions was examined to determine the contribution of any fine nanoparticles (< 200 nm) that may possibly have been left in the supernatant solution. The measured surface tension was ~72.8 mN/m, and thus close to the expected value for pure water-air, confirming minimal influence on measured values (260, 261).

Additionally, the influence of surfactant adsorption on particle stability was assessed by measuring the particle size distribution of 5 ppm Cs-contaminated clinoptilolite (at 20 g/L) with different concentrations of both cationic surfactants (from 0.01 mM to 20 mM). The suspensions were mixed on an orbital shaker at 15 rpm (at room temperature) for 24 hours, before being placed in Grant XUBA3 ultrasonic bath for 5 minutes in order to fully disperse. Suspensions were then analysed using a Mastersizer 2000E laser diffractometer (Malvern Panalytical Ltd).

4.3.5 Flotation experiments

Flotation experiments were performed by adding 3 g of dried 5 ppm Cs-contaminated clinoptilolite into a laboratory-scale flotation cell (column diameter and height: 65 mm and 97 mm) as utilised in a previous study by the authors (55, 56). Foam was generated from direct injection of air through a sintered glass plate with micron-sized pores (see Appendix B, Fig. B3). Different concentrations of the cationic surfactants, from 0.01 to 20 mM, were added into the cell, with the solid/liquid ratio fixed at 20 g/L (which corresponds to a ~0.9 vol.% pulp concentration or 2 wt.%). The agitation of the suspension was provided by an overhead stirrer, with a 0.75 inch, 4-blade, 45° pitched impeller rotating at 300 rpm for 5 minutes. The air flowrate was fixed at 0.2 L/min. To measure the

material separated in the froth, the overhead stirrer was reduced to 100 rpm for 10 minutes and 50 µL of MIBC frother was added to the suspension (which is a similar amount to that previously reported for the flotation of Cs-contaminated clays (55, 56)) while the air flowrate was increased to 0.7 L/min. The change from low to high gas flow rate was performed to increase the interfacial area and turbulence at the interface, generating effective contact of the particles in the froth (195). The froth containing recovered Cs^+ contaminated clinoptilolite was collected into a 400 mL beaker, before being dried at 100 °C and weighed in order to study the recovery (see Equation 2.15 in Sub Chapter 2.4.2). The process was conducted in batch system, in which the flotation cell dimension, air flowrate, the rotating stirrer speed and stirring time are similar to previous work for the flotation of Cs-contaminated clay (55, 56). The volume of the remaining liquid fraction was measured, in order to calculate water reduction ratio, as given in Equation 2.14 in Sub Chapter 2.4.2.

Additionally, in order to study the effect of varying frother concentration, the same process was repeated with a fixed concentration of cationic surfactant and variable added frother volume up to 50 µL. The effect of variable cesium contamination was also studied, using clinoptilolite prepared by repeating the same procedure from Sub Section 4.3.4, where initial cesium concentration was varied from 5 – 1000 ppm. Then, flotation extraction was repeated using a fixed concentration of CPC type surfactant and the addition of the optimal frother volume.

4.4 Results and discussion

4.4.1 Cesium adsorption onto clinoptilolite

Initial batch ion adsorption experiments were conducted to understand both the equilibrium adsorption of cesium on the clinoptilolite and its adsorption kinetics. The equilibrium adsorption data is given in Fig. 4.1, presented in terms of the equilibrium Cs^+ concentration, along with associated Freundlich and Langmuir monolayer fits (for details for fitting, see Appendix B, Fig. B4 and Table B1).

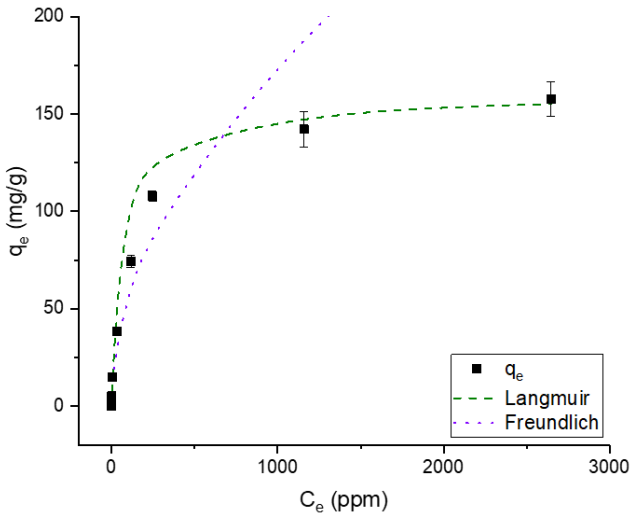

Figure 4.1: Equilibrium clinoptilolite adsorption of cesium at various concentrations with Langmuir (dashed line) and Freundlich (dotted line) model fits.

The performance of the clinoptilolite at removing cesium compares very favourably to other research on similar materials (18, 20, 24, 30, 31, 105). In fact, cesium adsorption capacity is about twice that of unmodified clinoptilolite sourced from a different supplier that was used by in Chapter 3, Sub Section 3.4.3, highlighting likely low levels of ion-contamination in the zeolite (which was shown to reduce adsorption with the other material). Secondly, its strong performance is also likely due to its small particle size (< 30 µm) giving a large surface area to volume ratio (and thus a relative increase in surface exchange sites), where it has also been shown previously in Chapter 3, Sub Section 3.4.3 that milling low-grade clinoptilolite to smaller sizes with a similar surface area considerably increased its capacity . It is noted that as clinoptilolite is generally used as bead material in ion exchange columns, the usable size range is much larger (with associated lower surface to volume ratio). Therefore, if flotation can be used as a viable rapid separation method for such fine particles, it represents a much more efficient processing route, from a material perspective.

In order to study how the adsorption takes place, theoretical Langmuir and Freundlich model fits were applied to the data (see Appendix B, Fig. B4). The Langmuir model is based on a homogenous surface where only one molecule occupies each active site. Alternatively, the Freundlich model considers that adsorption takes place on a heterogonous surface with non-uniform distribution of adsorption energy. Based on these figures, the equilibrium data was fitted most

appropriately with the Langmuir model (higher R^2 value, see Appendix B, Table B1) indicating that adsorption occurs as a monolayer with similar adsorption energies, which is again similar to results found in other work on zeolites (18, 31, 126)

The kinetics for an initial Cs^+ concentration of 5 ppm is shown in the Appendix B (Fig. B5) with adsorption given in terms of both relative adsorbed amount, q_t (mg/g) and percentage of initial concentration adsorbed over time. Data was fitted using the linear pseudo second order (PSO) rate model (see Appendix B, Fig. A5). It is observed that adsorption reaches an equilibrium plateau within 360 mins (6 h) which is consistent with previous studies on similar systems. Based on Appendix B, Fig. B6, the R^2 of the PSO fit was 0.99, where the adsorption rate constant determined is shown in Appendix B, Table B2. The kinetics data is consistent to previous research on ion exchange resins, where adsorption was also fitted accurately using a PSO model (30). Data also suggests that the smaller particle size of the powdered zeolite used in this study leads to fast kinetics from the PSO rate constant (k_2 equalled 0.516 g/mg.min, as given in Appendix B, Table B2) which is higher than natural clinoptilolite values generally found in previous research (e.g. 0.0015 (30) and 0.163 g/mg.min from Chapter 3, Sub Section 3.4.2) and also consistent with acid activated clinoptilolite of a similar surface area (0.472 g/mg.min) from Chapter 3, Sub Section 3.4.2. The PSO fit also indicates that the reaction is more inclined towards chemisorption at exchange sites, where the forces involved are valence forces of the same kind as those operating in the formation of chemical compounds (18, 146, 230, 262).

4.4.2 Surfactant adsorption at the solid-liquid and air-liquid surface

The particle size distribution of Cs-contaminated clinoptilolite with different surfactant concentrations of EHDa-Br and CPC, was measured to highlight any potential issues of surfactant adsorption on dispersion stability, as presented Fig. 4.2.

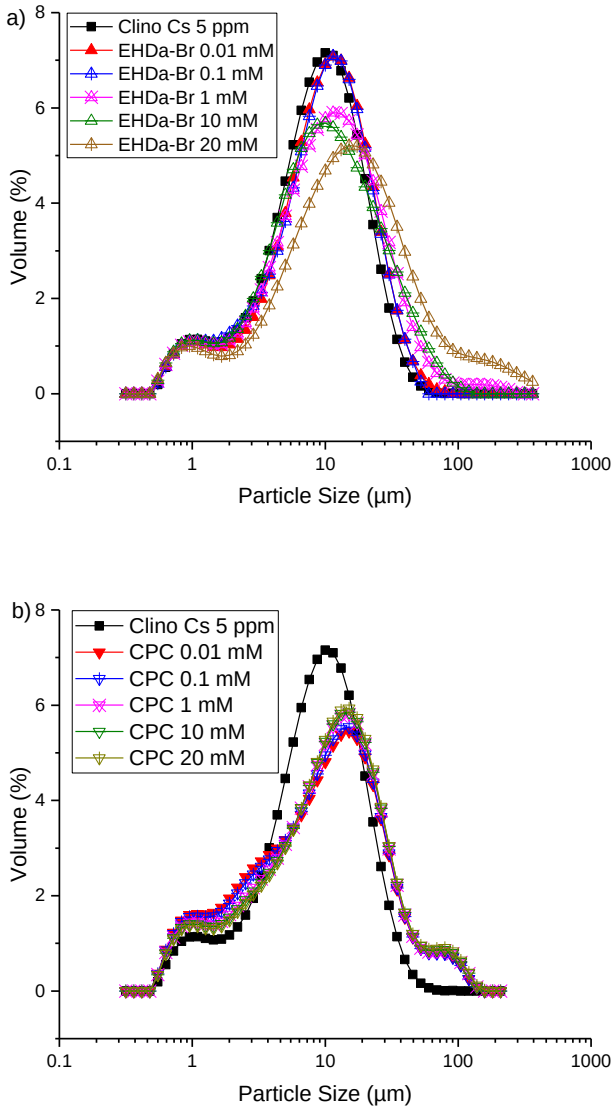

Figure 4.2: Clinoptilolite particle size distribution with different surfactant concentrations of a) EHDA-Br and b) CPC.

It is evident that neither surfactant causes a major shift in particle size, although both produce a small, consistent, increase as concentration is varied. The median size (d_{50}) of natural clinoptilolite is 8.5 µm. Meanwhile, d_{50} of 5 ppm Cs^+ contaminated clinoptilolite is 8.9 µm, which increases to 10.0 µm in 20 mM EHDa-Br. Similarly, the d_{50} of Cs-contaminated clinoptilolite is 10.5 µm in 20 mM CPC surfactant. Despite the minor differences in d_{50}, there is a more significant increase in polydispersity of the systems, and an additional shoulder at larger particle sizes, which is likely associated with clinoptilolite agglomeration. As the cationic hydrophilic head group of the surfactant adsorbs onto the anionic particle surface, it should lead to the particles having greater hydrophobicity at monolayer

coverage (from the hydrophobic tail group) and thus a greater surface energy in the water environment, reducing stability. While changes to particle surface energy from surfactant adsorption do not appear great enough to cause large-scale flocculation, it does not necessarily indicate that it is not sufficient for flotation. Indeed, it is known that particles can stabilise foam/froth interfaces with contact angles in the order of 60 – 70° (56, 165) where partially hydrophobic particles in this range are largely stable in water (263). Therefore, large increases in size would perhaps not be expected, but the changes observed do infer substantial surfactant adsorption does occur (100, 104, 131).

The equilibrium air-water surface tension of EHDA-Br and CPC surfactants is shown in Fig. 4.3, a) and b) respectively. Also given are associated Langmuir fits (using Equation 4.1) that considers monolayer adsorption of surfactant at the air-water interface to a given maximum coverage (Γ_{max}) associated with the critical micelle concentration (CMC) (168, 258, 259, 264, 265). The CMC for both surfactants was found experimentally to be similar, at ~0.85 mM which is close to values reported in literature (EHDA-Br = 0.8 mM and CPC = 0.84 mM) (156). Additionally, the fitted Γ_{max} values were 3.85 × 10^{-6} mol/m^2 for CPC and 4.48 × 10^{-6} mol/m^2 EHDA-Br, which are also consistent with previous studies on CPC and other similar cationic surfactants (266, 267). Furthermore, the R^2 values for the Langmuir fits were > 0.97 with both surfactants, giving confidence that they represented reliable models.

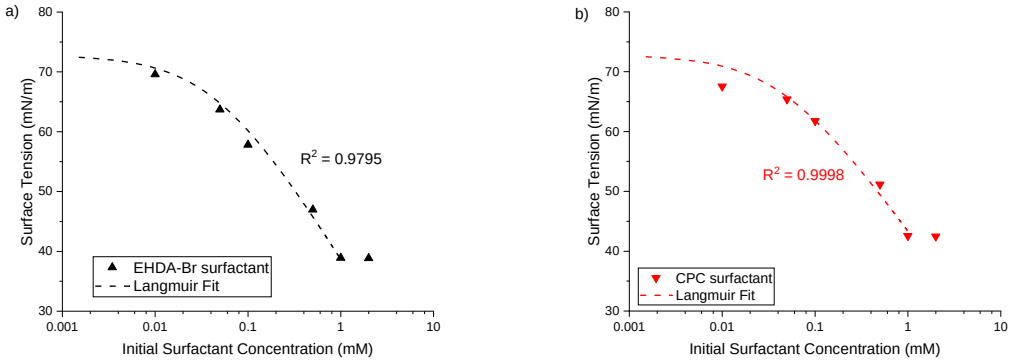

Figure 4.3: Air-water surface tension versus surfactant concentration ; a) EHDA-Br and b) CPC. Dashed lines represent Langmuir surfactant monolayer fits (Eq. 4.1).

The surface tension of mixed surfactant-clinoptilolite systems is shown in Fig. 4.4, with respects to the pure surfactants, for clean clinoptilolite and material contaminated with 5 ppm Cs^+. A cesium concentration of 5 ppm was used

because the actual radioactive waste concentration of cesium is considered to be very low, and often less than 5-10 ppm (1, 32, 37, 121). Again, it is noted that the surface tension data for these mixtures represents that of the clear supernatants of centrifuged pre-mixed suspensions, and thus indicates the concentration of non-adsorbed surfactant remaining in the system (268). It is evident that the surface tension of clinoptilolite mixed systems is significantly higher at low to moderate additions of either surfactant than the pure solutions, suggesting adsorption onto the clinoptilolite has substantially depleted the free-surfactant from the system, resulting in higher measured values. It also appears that the CPC performs better on Cs-contaminated clinoptilolite, as the surface tension response is almost identical to the uncontaminated system, while values for the EHDA-Br surfactant are measurably lower with cesium contamination. In addition, if the cesium contaminated is increased, the surface tension will potentially increase, because the presence of the metal ions may reduce the hydrophobicity of the surfactant and affect its adsorption, as explained in Olesen *et al*. (269).

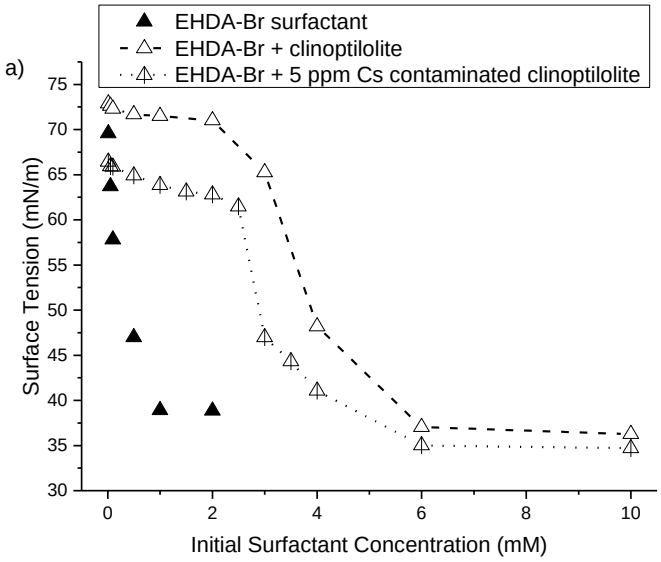

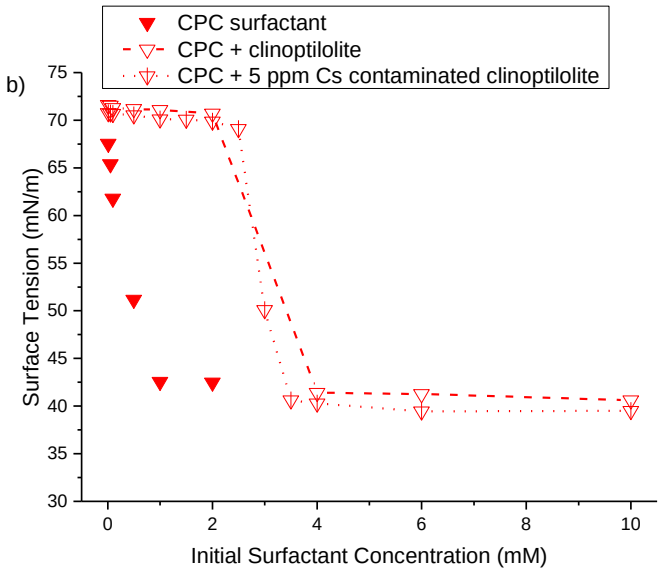

Figure 4.4: Surface tension of pure EHDA-Br and CPC surfactants , as well as that of the depleted liquid after adsorption onto natural clinoptilolite and 5 ppm Cs^+ contaminated clinoptilolite, from different initial surfactant concentrations; a) EHDA-Br and b) CPC. Connecting dashed and dotted lines are to guide the eye.

Surface tension values for the mixed surfactant-clinoptilolite systems (from Fig. 4.4) were converted to surfactant concentration using the Langmuir fits of the pure systems (Fig. 4.3). Then, the amount of surfactant adsorbed was calculated from the difference to the initial concentration added. Results are presented for both EHDa-Br and CPC in Fig. 4.5, a) and b) respectively, in terms of the distribution of coefficient (K_d) and the percent of surfactant adsorbed (%) from natural clinoptilolite and Cs-contaminated material, based on the equilibrium concentrations of surfactant. These values were calculated using the Eq. 2.10 and Eq. B1 in Appendix B (23, 252)

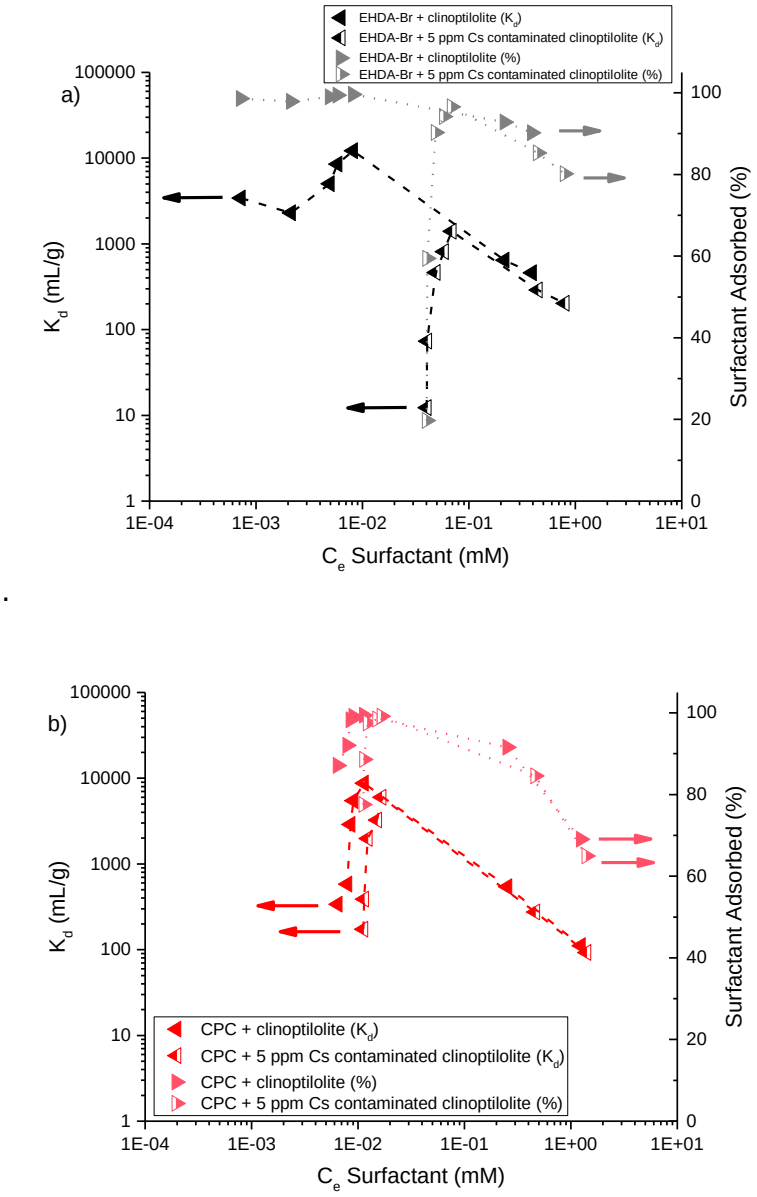

Figure 4.5: Surfactant adsorption onto natural clinoptilolite and 5 ppm Cs^+ contaminated clinoptilolite from different initial surfactant concentrations, shown in terms of the distribution coefficient, K_d (mL/g) (LHS) and adsorbed percent (RHS) versus equilibrium concentration; a) EHDA-Br and b) CPC. Connecting dashed and dotted lines are to guide the eye.

From Fig. 4.5, both natural and contaminated clinoptilolite are seen to adsorb significant amounts of either surfactant, as K_d increases by two orders of magnitude with initial surfactant concentration. At intermediate concentrations above the peak in K_d, there is a gradual reduction in the percentage for surfactant adsorbed (which is accentuated in K_d, due the relatively high solids ratio of 20 g/L). Above an equilibrium surfactant concentration of ~0.1 times the CMC, the adsorbed percent more rapidly decreases, suggesting a plateau in the adsorbed

amount, although delineation between concentration regimes is not clear. It is noted that these equilibrium surfactant values are low, due to the high percentage of initial surfactant adsorbing for low to moderate concentrations.

The gradual reduction in adsorption percent above the peak K_d values is likely firstly because of increased competition for surface sites, as the number of surfactant molecules increases. It is common for small molecules and ions that the fraction of adsorbed species will reduce with concentration, even as the total adsorbed amount increases. Indeed, the adsorption behaviour of these surfactant species is complex, due to the formation of a bilayer (or admicelle) at the solid surface (156, 165) which produces an eventual plateau in adsorbed amount. Once a monolayer of surfactant has formed, hydrophobic interactions between monomers start increasing, leading to further adsorption occurring with the surfactant head-groups facing both toward the substrate and the solution. Once the admicelle structure has fully formed (which usually occurs below the CMC) there will be no additional interaction between the surfactant and clinoptilolite, as both the surface bilayer and solution micelles will be cationic (156, 165, 270). It is also evident quantitatively that the adsorption of EHDA-Br is much more reduced with Cs-contaminated clinoptilolite, whereas very little difference is observed with CPC. It is known from Appendix A, Fig. A10 that Cs^+ adsorption will reduce the magnitude of the surface charge, while Cs^+ ions will also occupy potential surfactant adsorption sites. As there is no significant reduction of adsorption with CPC for the same level of cesium contamination, it would suggest that the reduction in surface charge is more detrimental to EHDA-Br adsorption than CPC.

Additionally, it is important to understand whether adsorption of surfactant onto the contaminated zeolite causes some of the Cs^+ ions to be removed from exchange sites (which is possible if there is a sufficient difference in adsorption energies). Any remobilisation of Cs^+ ions may mitigate the use of surfactant enhanced flotation as a rapid separation technique. To study this effect, the amount of mobile Cs^+ was measured in the supernatants of mixed suspensions of surfactant with 5 ppm Cs-contaminated clinoptilolite (noting from Appendix Fig. B4, that initial removal of this concentration is > 99%). Fig. 4.6 presents these results for both surfactants, in terms of the total measured remobilised Cs^+ amount (in ppm) and percentage of the initial 5 ppm dose, using Appendix A, Eq. A2. The amount of Cs^+ remobilised into the supernatant does increase for both surfactants up to the adsorption plateau around the CMC. Due to the stronger interaction of the CPC (shown in Fig. 4.5) the amount of Cs^+ ions remobilised is

also correspondingly slightly greater than for EHDA-Br. However, given that the maximum removed Cs^+ was < 8% with both surfactants, it is clear co-adsorption is energetically preferred, and such losses are not thought to be detrimental to the industrial viability of the process.

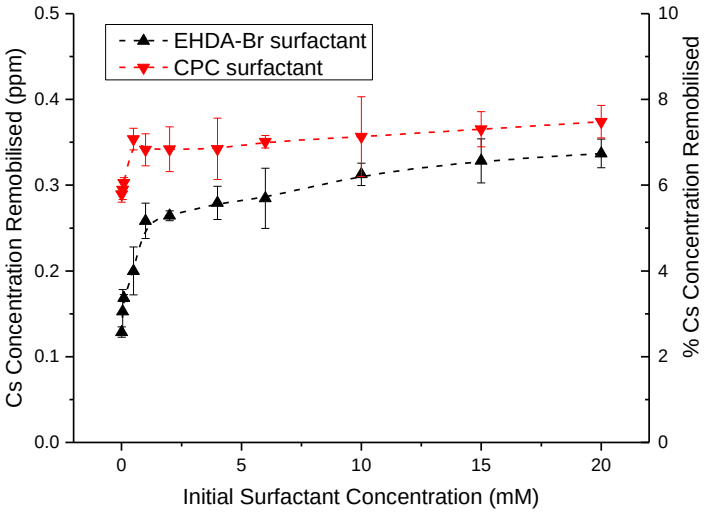

Figure 4.6: The remobilised concentration of Cs^+ removed from clinoptilolite through adsorption of surfactant for different initial concentrations, shown as removed ppm from an initial 5 ppm Cs^+ solution (LHS) and percent removal (RHS). Dashed lines are to guide the eye

4.4.3 Flotation experiments

Fig. 4.7 presents both the recovery and water reduction ratio for the flotation of 5 ppm Cs^+ contaminated clinoptilolite, as surfactant concentration is varied for a) EHDA-Br and b) CPC. Recovery was calculated according to Appendix A, Eq. A3 (48) and the water reduction ratio with Eq. 4.2 (196). Systems with and without the addition of 50 µL MIBC frother are both included. At low concentrations of either surfactant, there is insufficient adsorption onto the contaminated clinoptilolite to enhance particle contact angles to promote a high degree of recovery. As surfactant concentrations increase to around monolayer coverage, the recovery increases in both cases. Also, both surfactants recover greater levels of contaminated clinoptilolite with the addition of frother, due to the presence of MIBC increasing the number and stability of bubbles in the froth (164, 191, 196). By increasing the air flowrate, the number of bubble-particle interactions is enhanced, while MIBC keeps the bubbles sufficiently stable for a required period before they detach and rupture (182, 195, 271). Nevertheless, increasing the air flowrate further could increase turbulence levels and decrease

the rupture time (195). In this system, the rupture of the bubble-particle aggregates from buoyancy driven differences is not significant as the particles are relatively small, and so should not be removed under gravity (165, 198).

The water reduction ratio data shown in Fig. 4.7 highlights an inverse relationship to the clinoptilolite recovery in both cases. At low surfactant concentrations, the high apparent water reduction ratio is an artefact of the low total volume of froth recovered (with therefore low associated water content). At high surfactant concentrations however, there is a clear trade-off between the recovery of clinoptilolite and the need for the froth to contain a low fraction of water to enable sufficient dewatering of the contaminated suspensions (78, 196, 253).

The reason for the low water reduction ratios at high surfactant concentration is due to water entrainment in the froth. Above the CMCs, adsorption of the surfactant at the air-water interface will be maximised, creating an overly wet froth phase that will act to entrain both clinoptilolite and water, rather than acting to separate the solid-liquid phases (197-199). In addition, above the CMC (at ~1 mM) the addition of MIBC frother does not considerably alter either contaminated clinoptilolite recovery or water reduction ratio, because of the dominating interactions of the surfactant collector on froth dynamics (56, 156, 163, 183, 191). Therefore, based on Fig. 4.7, an optimal system was found at 0.5 mM CPC surfactant with the addition of 50 µL MIBC (Figure 4.7b). For these conditions, the Cs-contaminated clinoptilolite recovery in the froth phase was ~90%, while the water reduction ratio in the froth was still acceptable at > 4.

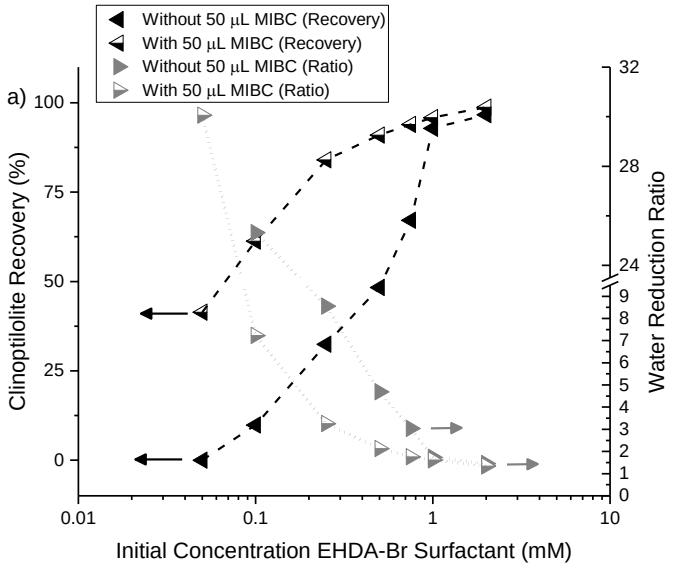

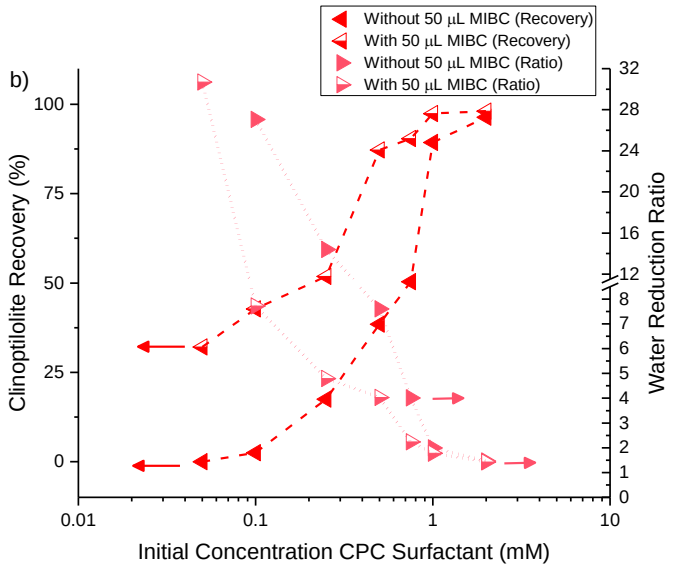

Figure 4.7: The effect of MIBC frother on the flotation recovery of clinoptilolite (LHS) and associated water reduction ratio (RHS) with different initial surfactant concentrations; a) EHDA-Br and b) CPC. Connecting dashed lines are to guide the eye for clinoptilolite recovery and dotted lines are to guide the eye for water reduction ratio

It is noted that dewatering ratios of 3 – 4 are certainly also possible in gravitational sedimentation of similar concentration dispersions, depending on the level of system aggregation (272, 273). However, the residence time in gravitational thickeners for such consolidation would be tens of minutes, rather than the seconds in a flotation cell. Therefore, one of the critical benefits of flotation in this system is the rapidity of the process. Additionally, given the initial suspension concentration of 20 g/L, a maximum possible dewatering ratio of ~ 15 - 20 may be expected, which would equate to a solids level of approximately 40 wt% (and so approaching or beyond the transition to a consolidated solid gel). Thus, while dewatering levels may be further optimised, ratios of ~4 are still considered relatively high. Indeed, future improvements may be gained simply by passing the concentrate froth through a second flotation cycle, which is readily achievable because of the rapid nature of flotation separation. In addition, while flotation for mineral separation is often conducted at higher pulp densities, concentrations are of the same order as used in the flotation of water treatment sludges, while also similar to previous recoveries of clay adsorbents (55, 56).

Using CPC surfactant at the optimum 0.5 mM concentration, the influence of varying MIBC dose was then investigated, as it has previously been demonstrated to critically alter the flotation of cesium contaminated clays (56).

The results are shown in Fig. 4.8, again in terms of both clinoptilolite recovery and water reduction ratio.

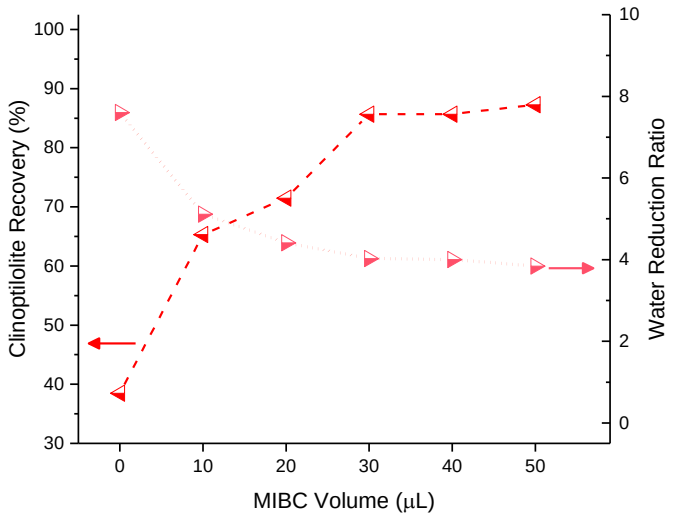

Figure 4.8: The effect of different added MIBC volumes on flotation recovery of clinoptilolite (LHS) and associated water reduction ratio (RHS) with fixed 0.5 mM CPC concentration. Connecting dashed line is to guide the eye for clinoptilolite recovery and dotted line is to guide the eye for water reduction.

Enhancement in clinoptilolite recovery is observed as MIBC dose increases towards 30 µL, whereupon it reaches a plateau for the volumes studied, indicating a limiting concentration for MIBC interaction with the froth. Considering the high surface tension data for the 5 ppm Cs-contaminated clinoptilolite with 0.5 mM CPC (Fig. 4.4) there is unlikely to be a large amount of unbound surfactant in this system. Thus, while it is known that surfactant mixtures may interact synergistically with MIBC at the air-water interface (164, 200-202), in this case, the concentration of free CPC surfactant in solution is low (which would correspondingly explain the poor material recovery with no MIBC added). Therefore, the development of a plateau in recovery at intermediate MIBC concentrations is likely purely from the interaction mechanism of MIBC at the air-water interface, where it is known to stabilise foam films primarily through changes to interfacial elasticity rather than surface tension (202, 274). Indeed, Bournival *et al.* (275) have previously demonstrated a plateau response at intermediate concentrations of MIBC in the direct coalescence of bubbles measured by high speed video, due to an increase in the dampening constant related to bubble oscillations.

Lastly, the effect of cesium contamination on clinoptilolite flotation was studied, given the potential variance in natural contamination levels (32, 55, 56) and the reduction in zeta potential with cesium adsorption (Appendix B, Fig. B1). Here, 0.5 mM CPC surfactant and 30 µL MIBC were selected as these parameters gave the optimum result in terms of both clinoptilolite recovery and water reduction ratio. The effect of increasing cesium contamination on clinoptilolite during flotation is displayed in Fig. 4.9.

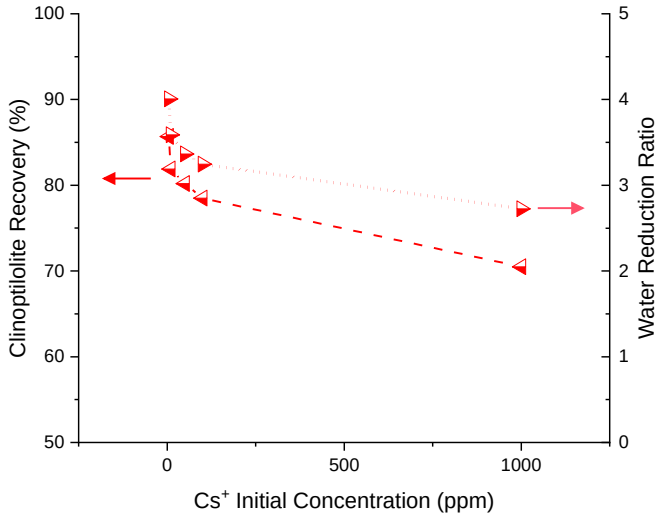

Figure 4.9: The effect of different levels of adsorbed Cs^+ contamination on the flotation recovery of clinoptilolite (LHS) and associated water reduction ratio (RHS) with fixed concentration of CPC (0.5 mM) and MIBC (30 µl added). Connecting dashed line is to guide the eye for clinoptilolite recovery and dotted line is to guide the eye for water reduction.

From this figure, it is clear that increasing the cesium concentration decreases both the recovery and water reduction ratio (with greatest recovery for non-contaminated material) although performance is still reasonable for cesium contamination levels < 100 ppm (which would be considered an upper limit for nuclear applications (32)). While heavy metal ions are often added as mineral flotation activators with anionic surfactant collectors (276), in this case, both Cs^+ and the cationic CPC compete for the negative clinoptilolite surface sites (as noted in comparison to Appendix B, Fig. B1 and Fig. 4.6). It is likely that the observed decrease in flotation is due to primarily the clinoptilolite zeta potential changes (Appendix B, Fig. B1), where increasing the cesium concentration leads to a less negative potential. If the zeta potential becomes less negative, the adsorption of cationic surfactants to the particle surface will also correspondingly decrease. Furthermore, any reduced surfactant adsorption at the solid-liquid

interface will lead to higher concentrations of free surfactant in solution and thus potentially more synergistic interactions with the MIBC increasing the foaming interactions (163, 183). Any increase in foamability will lead to more entrainment of water in the froth, decreasing the water reduction ratio. Additionally, as the foam production is higher, the association of surfactant with contaminated clinoptilolite will be reduced, as the formation of the surfactant bilayer will occur at lower added concentrations.

Nevertheless, there are potential methods to improve the flotation of the heavily contaminated clinoptilolite that are currently being investigated. Firstly, the particle size of the powder (d_{50} of 8 – 10 µm) may be slightly below optimal sizes for flotation, where it is often found that particles in the range of 50 – 100 µm maximise recovery (277, 278) although this range is certainly not universal (279). What certainly is common is that very fine particles tend to be collected to a greater degree through entrainment in the liquid films (rather than by adsorption onto bubbles) which would lead to high recoveries, but low associated dewatering ratios, as found. Additionally, an understanding of the flotation kinetics would greatly aid in defining the most efficient column residence time for flotation using multiple passes. For the completed experiments, the flotation cell was run over 10 mins, which was sufficient to achieve the maximum potential separation in a single column. Normally however, flotation kinetics follow a first order rate model, where recovery at longer times considerably reduces (279). This reduction is largely due to partitioning of surfactant collector and frother into the separated froth, which depletes their concentrations from the active flotation cell, reducing the foam quality and stability. Therefore, it may be more industrially effective to separate the highly contaminated systems using several flotation cells in series with low residence times.

4.5 Summary

This study examined the use of cationic surfactants to enhance the flotation of cesium contaminated powdered clinoptilolite, as an alternative to gravitational separation or the use of large resins in elution columns. Initial kinetic and equilibrium adsorption studies of cesium uptake, suggested the fine zeolite particle size (and associated large surface area to volume ratio) contributed to fast adsorption kinetics and high capacities (q_c = 158.261 mg/g) when compared to much previous literature on non-modified clinoptilolite. The co-adsorption of EHDa-Br and CPC surfactants onto both clean and 5 ppm Cs^+ contaminated

clinoptilolite was then measured, using surface tension measurements modelled with a Langmuir isotherm. Distribution coefficients (K_d) as high as 10,000 mL/g were evident with moderate concentrations of surfactant (below those leading to bilayer formation) where CPC outperformed EHDa-Br on Cs-contaminated samples. Measurements of particle size confirmed that adsorption of surfactant monolayers did not lead to significant flocculation of the particles, suggesting good stability for flotation separation. Importantly also, less than 8% of pre-adsorbed cesium was removed through subsequent adsorption of surfactant, highlighting that co-adsorption was energetically favourable, which is critical for flotation to be accepted as a feasible recovery technique.

In flotation tests, increasing surfactant concentration from both surfactants continually improved the recovery of 5 ppm Cs^+ contaminated clinoptilolite, while conversely impacting on performance by reducing the water reduction ratio (assumed to be due to higher levels of liquid entrainment). Moreover, the incorporation of MIBC frother considerably enhanced recovery further, for volume additions up to 30 – 50 µL. Overall, it was found that CPC surfactant at an 0.5 mM initial concentration and 50 µL MIBC gave optimum conditions for both recovery (at ~90%) while maintaining an adequate water reduction ratio (~4) leading to significant dewatering and consolidation of the zeolite in the froth phase. The effect of varying initial contaminated cesium concentration on clinoptilolite was also studied, where a clear reduction in recovery was observed for levels > 80 ppm (although this concentration is well above those relevant for most nuclear applications (20)). Overall, this investigation showed that by using cationic surfactants, flotation is a viable and industrially scalable technique for the separation of fine clinoptilolite that are used for the removal of cesium ions in nuclear applications. Additionally, it may also have far reaching applications to improve the material efficiency of many types of zeolites relevant to the clean-up of industrial effluents, from sectors such as mining, textiles and consumer fine chemicals.

Chapter 5 Kinetic studies of Cs^+ and Sr^{2+} ion exchange using clinoptilolite in static columns and an agitated tubular reactor (ATR)

5.1 Synopsis

This chapter contains similar contents to previous chapters in order to help the reader synthesise the message.

Natural clinoptilolite was studied to assess its performance at removing cesium and strontium ions, using both static column ion exchange and an agitated tube reactor (ATR) for process intensification. Kinetic breakthrough curves were fitted using the Thomas and Modified Dose Response (MDR) models. With the static column ion exchange, it was found that the maximum adsorption capacity (q_e) for ion concentrations of 200 ppm were ~171 mg/g and 16 mg/g for cesium and strontium respectively (correlating to 50% breakthrough times of 700 and 70 bed volumes) highlighting the poor material ability to exchange strontium. Reducing the concentration of strontium down to 100 ppm, however, led to a higher q_e of ~48 mg/g (and a 50% breakthrough time of 400 bed volumes). Meanwhile, halving the column residence time to 15 minutes decreased the q_e for 100 ppm strontium solutions down to 13-14 mg/g. All kinetic breakthrough data correlated well with maximum adsorption capacities from previous batch studies, where in particular, the influence of concentration on the slow uptake kinetics of strontium was evidenced. Additional experiments with a double diameter column (of 2 cm) gave similar results to 1 cm column tests, inferring consistent scale-up performance. For the ATR studies, the poorest performing system (being a 15 min residence time and 100 ppm strontium) was selected for direct comparison. Here, two column lengths were investigated (of 25 and 34 cm) with the clinoptilolite embedded directly into the agitator bar. The 34 cm length column significantly outperformed the static vertical columns, where the adsorption capacity and breakthrough time were enhanced by ~30%, assumed to be due to heighted kinetics from shear mixing. Critically also, the increase in performance was achieved with a relative process flow rate over twice that of the static columns.

5.2 Introduction

In nuclear waste effluent treatment, while batch systems offer greater process flexibility (15, 29), they are much less operationally efficient overall, and require large mixing units. Therefore, most nuclear treatment systems operate static ion exchange columns (29, 60), where the effluent is continuously injected through a fixed bed depth of adsorbent; such as with the Site Ion Exchange Plant (SIXEP) at Sellafield in the UK (one of Europe's largest legacy nuclear sites) (32, 57-60). However, there are several critical limitations to ion exchange column operation, which result in low throughput. In particular, large particle sizes (> 250 μm) are required to reduce frictional pressure drop issues. Therefore, as ion exchange in zeolites primarily occurs through surface sites, resins are not materially efficient, due to the low surface area to volume ratio. Indeed, previous work by the current authors has shown clear enhancements to cesium and strontium uptake, as clinoptilolite is milled to increase the relative surface area (280). Columns must also be run at very low liquid velocities to further limit frictional pressure drop, and importantly in addition, mitigate the slow adsorption kinetics associated diffusive ion exchange interactions (21, 32, 280). Overall, these process limitations significantly increase the footprint of industrial ion exchange operations, as a number of units have to be run in parallel to achieve required output rates.

Thus, there is significant industrial interest in enhancing ion exchange operational efficiencies, where importantly for this study, methods of process intensification offer particular advantages. In general, process intensification (PI) is focused on novel operational unit designs that can provide step-changes in process efficiency, while considerably decreasing equipment foot-prints, energy consumption and/or waste formation (223), often achieved through unit modularisation and process combination. While originally focused on fine chemicals production, there is increasing research into the PI of multiphase solids handling operations, driven largely by successes in the pharmaceuticals industry (224).

The use of PI in effluent treatment processes specifically, is comparatively less developed, although it is an area with a lot of potential to drive solutions through technology transfer. In many respects, flotation can be considered one of the original PI techniques for effluent treatment. While primarily adapted for minerals separation (165, 281), it has gained increasing use as a rapid solid-liquid separation technique for wastewater sludges and mineral wastes, dramatically reducing unit footprints and enhancing throughout rates when compared to

traditional gravity separators. Indeed, there has been a number of studies published into its use to separate nuclear wastes and adsorbents used for effluent treatment (49, 54, 56, 75, 79, 172, 281, 282). PI methods are also being used in conjunction with the development of related nanotechnologies for effluent treatment (283); such as with rapid magnetic separation methods to capture and recycle magnetic nano-adsorbents (284, 285).

In particular for granular/resin ion exchange, there has been interest in using intensified flow reactors to overcome constraints associated with diffusion limited adsorption kinetics (61-64, 223). One of the most prevalent examples in literature are rotating bed reactors (RBRs), which were originally designed for gas-liquid separation operations, where high centrifugal gravity fields lead to enhanced mass transfer characteristics. More recently, they have also been utilised for the removal of contaminants from liquids, including dyes, fertilisers and heavy metals (61-65). However, the disadvantage of RBRs is that they have relatively small residence times, which are dependent on the rotation speed, and thus for high percentage removal of species, effluent requires multiple passes. Therefore, flow reactors which can generate additional shear (to improve mixing) independently of process throughput or residence time would be highly beneficial. One such example design, is agitated tubular reactors (ATRs), which are intensified plug-flow reactors, where high rate lateral shear is generated with inner agitator bar, decoupling mixing dynamics from the bulk flow (61, 66). A number of authors have characterised mixing dynamics and performance of ATRs (66, 225, 283), such as in simulations by He *et al* (67, 68), who found volumetric mass transfer more efficient with enhanced energy dissipation, in comparison to batch processes. However, while these initial characterisation studies highlight potential advantages of ATR systems, to date, there has been no comprehensive study on utilising ATRs as intensified ion exchange units.

Therefore, in this study, the performance of a zeolite ion exchange resin is assessed in both static vertical columns, as well an intensified ATR, to remove strontium and cesium ions. Here, clinoptilolite is selected as the ion exchange media, owing to its common use in nuclear effluent treatment (32, 57-60, 280). In vertical elution column tests, kinetic breakthrough is measured for various ion concentrations, residence times and column diameters, in order to compare adsorption data to previous batch studies of the same systems (280), allowing optimisation of column operation. For the ATR studies, an industrially relevant pilot-scale device was selected, where the influence of different column lengths is investigated by embedding resin into the agitator bar. Critically, kinetic

breakthrough performance is matched to static column results, both through enhancements to the equilibrium adsorption of the clinoptilolite, as well as the relative process flowrates achieved from either system.

5.3 Experimental

5.3.1 Materials

Natural clinoptilolite was supplied from Holistic Valley as a ± 300 µm powder (280). Cesium chloride (CsCl) and strontium chloride ($SrCl_2$) were Analytical Grade with purity ≥ 99.0%, supplied by Sigma Aldrich and Fisher Scientific, respectively.

Prior to column studies, treatment was required to gain a homogeneous particle size with low level of polydispersity (specifically to ensure a low level of fines) and remove any naturally present ions, which has previously been shown to impact on its performance (280). Firstly, the clinoptilolite was rinsed several times with distilled water at neutral pH, where the supernatant on every rinse was removed and measured using a conductivity meter until values reached an equilibrium low level. The rinsed clinoptilolite was then dried at 100 ºC (18) and sieved using an AS 200 shaker (Retsch GmbH) with a 250 µm mesh for 30 minutes. Once the process was completed, the clinoptilolite was separated using a course brush in order to observe its uniformity. These processes were repeated three times in order to ensure a low level of fines. The sieved clinoptilolite was analysed using a Mastersizer 2000E laser diffractometer (Malvern Panalytical Ltd). The average particle size distribution is shown within the Appendix C, Fig. C1, where the mean particle size was measured as ~312 µm

5.3.2 Static column ion exchange experiments

Column ion exchange studies were carried out in a fritted chromatography glass column with a 10 mm inner diameter and 300 mm height (59), as illustrated in Fig. 5.1a), while the real picture was shown in Appendix C, Fig. C2a. The clinoptilolite was fixed at a 6 cm bed depth, which has been shown in previous research by El-Kamash (59) to be sufficient for good performance. Additionally, liquid flowrates through the column were adjusted to initially give a residence time of 30 minutes (2 bed volumes [BV] per hour), which was initially assumed to be a reasonable residence time for high performance from previously determined adsorption kinetics of strontium (280). Further studies were also completed with

a faster flowrate to give a residence time of 15 minutes (4 BV per hour) and thus an expected lower overall performance. Additionally, scale-up experiments were conducted in a similar fritted glass column with a 2 cm diameter and a residence time of 15 minutes. Scale-up tests were conducted with two different bed heights, one where the volume of clinoptilolite was conserved (using a 1.5 cm bed height) and secondarily with the same 6 cm bed height to the smaller column.

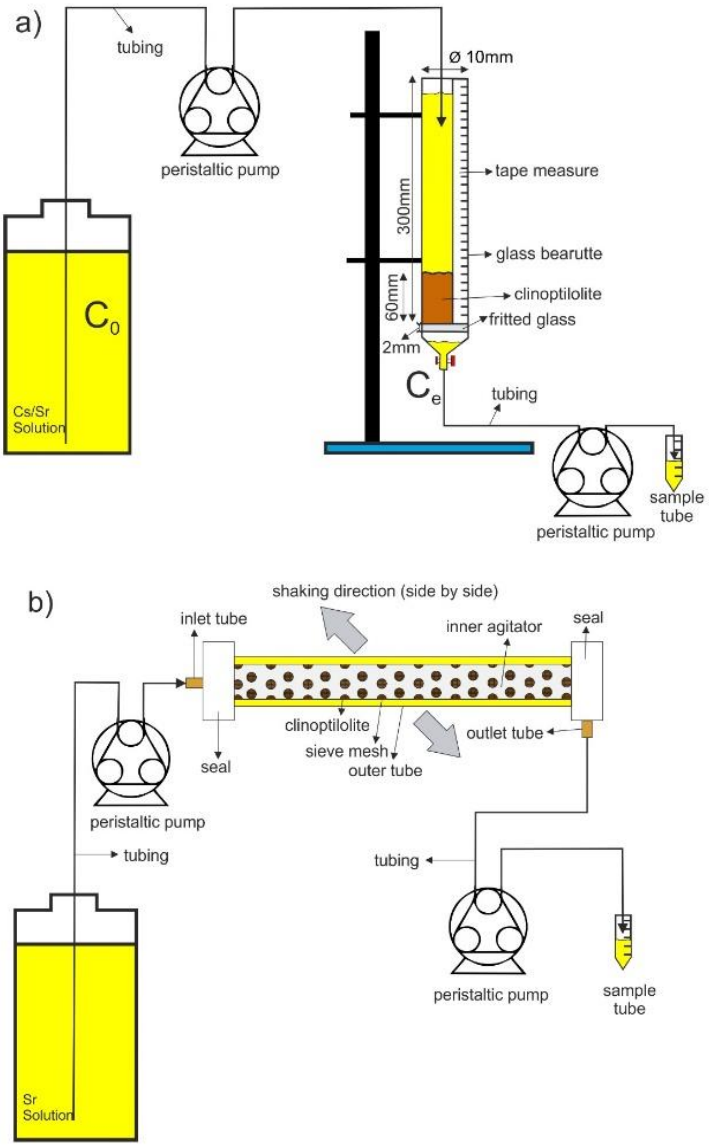

Figure 5.1: Schematic diagrams showing a) static vertical ion exchange column and b) agitated tubular reactor with horizontal ion exchange column (ATR).

The cesium and strontium were prepared by dissolving stock solutions of CsCl and $SrCl_2$ stock (1 M) with Milli-Q water at neutral pH (which tends to ~6.5 (32)) for nominal initial concentrations of 5 - 200 ppm, which is similar to the

concentration range used in previous research by the current authors (57, 59). The cesium and strontium solutions were pumped through the column for a minimum of 24 hours using two peristaltic pumps (Watson Marlow 323 series) to ensure both the inlet to the top of the column and the outlet were set at identical rates. Aliquots from the outlet were sampled every hour regularly within working hours, until the outlet concentration equalled the initial ion concentration. All samples were filtered through 0.3 µm filters (to ensure no fine particles were present) and analysed using an Atomic Absorption Spectrophotometer (AAS) 240fs (Varian/Agilent Technologies). For the initial cesium studies, a cesium lamp with wavelength and optimum working range of 459.3 nm and 5 – 4000 ppm was used, while for the main strontium studies, a strontium AAS lamp was used with wavelength of 460.7 nm and an optimum working range of 0.02 – 10 ppm (280).

5.3.3 Agitated Tubular Reactor (ATR) studies

To understand whether static ion exchange processes could be intensified using shear enhancement, a pilot-scale agitated tubular reactor (ATR) was modified, utilising a *Coflore* ATR (AM Technology, UK) where a schematic of the device is illustrated in Fig. 5.1b.

The ATR consists of an inner perforated agitator that sits within an outer reactor tube, which is subject to fast lateral movement (1 – 6 Hz) causing significant radial shear for low plug flows. The design is similar to that described by other authors in recent publications (67, 225). For testing purposes, a separated outer Perspex reactor tube of 25.4 mm inner diameter, 3 mm thickness and 392 mm length were utilised, with an inner perforated stainless steel agitator tube of 13.7 mm inner diameter and 0.6 mm thickness. For ion exchange studies, the inner agitator was covered with ±152 µm sieve mesh, and pre-sieved clinoptilolite filled into the agitator to various lengths (25 and 34 cm). The sieve mesh cover was small enough so that all the ion exchange resin was retained in the agitator as a plug, while the mesh perforations allowed liquid diffusion into the resin, with the aim of enhancing efficiency through the high lateral shear from agitation. For the flow experiments, the agitation frequency was set to 5 Hz (with corresponding amplitude of 12.5 mm) where a detailed schematic of the agitator arrangement is shown in Fig. 5.2.

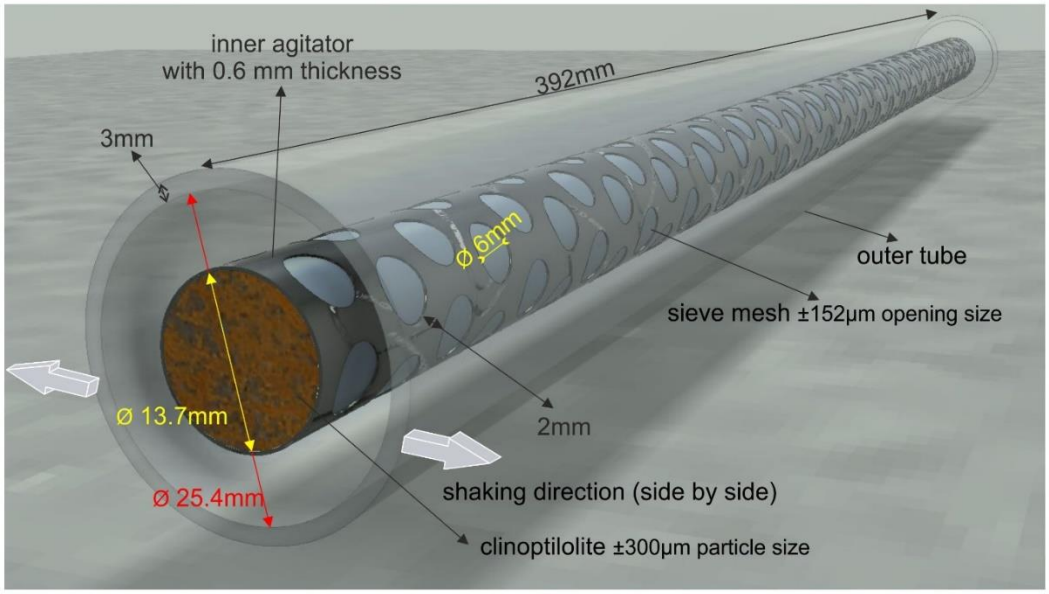

Figure 5.2: Rendered image highlighting motion of the inner agitator and outer tube of the ATR.

For the reactor studies, strontium solutions of 100 ppm concentration were pumped for a minimum of 24 hours through the ATR, again using identical peristaltic pumps (Watson Marlow 323 series) at the reactor inlet and outlet. Flow rates were set to give an equivalent residence time of 15 minutes for liquid contacting the ion exchange plug (based on the calculated average streamwise velocity of fluid in the liquid annulus around the plug). Therefore, the actual bulk flow rate varied depending length of the ion exchange plug and the ratio between the plug volume and total reactor volume. The supernatant was then collected at regular intervals, where samples were filtered by 0.3 µm filter and analysed using AAS to determine the strontium uptake and breakthrough curves, with the same parameters as previously described.

5.3.4 Kinetics breakthrough model analysis

The To determine the breakthrough behaviour during static column ion exchange and ATR experiments, the Thomas and Modified Dose Response (MDR) models were fitted to the kinetic adsorption data (219, 220, 286). The Thomas model is determined by the specific adsorption rate during ion exchange (K_{TH}) and the flowrate of the effluent injected through the column (Q) (219, 286). Meanwhile, the MDR model has been shown in some studies to improve breakthrough correlations, by altering the rate fitting parameter (a) to be a simpler (but non-physical) defined constant, dependent on the linear regression's gradient function (220). In both cases, the breakthrough models help determine

not only the kinetics, but critically give an estimate for the final equilibrium adsorption amount (q_e).

The Thomas model is determined in Section 2.5.1, Equations 2.16 – 2.17. Meanwhile, the Modified Dose Response (MDR) model is given in Section 2.5.1, Equations 2.18 – 2.20.

5.4 Results and discussion

5.4.1 Static column studies

Initially, the clinoptilolite's performance in removing cesium and strontium was compared, with the assumption from previous studies that the zeolite would be considerably more effective at removing cesium (1, 18, 20, 21, 24, 28, 31, 32, 34, 36, 37, 246). A high 200 ppm solution of the metal ions was chosen to reflect a worst-case scenario in terms of potential effluent concentrations, although, most nuclear treatment operations generally consider much lower levels (1, 32, 37, 121). Very low ion concentration effluents were also not considered in detail, owing to the long time periods required to reach breakthrough (which was not experimentally feasible). Indeed, an initial trial with 5 ppm cesium was completed and is shown within the Appendix C (Fig. C3). Due to the time constraints, the breakthrough was still not achieved after 4500 bed volumes (BV). This trend follows from the other results for low concentrations of cesium removal by nuclear grade clinoptilolite, as shown by *Dyer et al*. (32), where breakthrough started to occur after 10000 bed volumes.

The static column comparison for 200 ppm Cs^+ and Sr^{2+} at a 30 minute residence time is presented in Fig. 5.3, in terms of the ratio of the column outlet to inlet concentrations (C_e/C_o) versus the number of effective bed volumes (BV) of liquid effluent processed. Also given are the MDR and Thomas model correlations, with the linearised fits used to determine the optimised parameters shown in the Appendix C (Fig. C4). Fitted model parameters are given in Table 5.1.

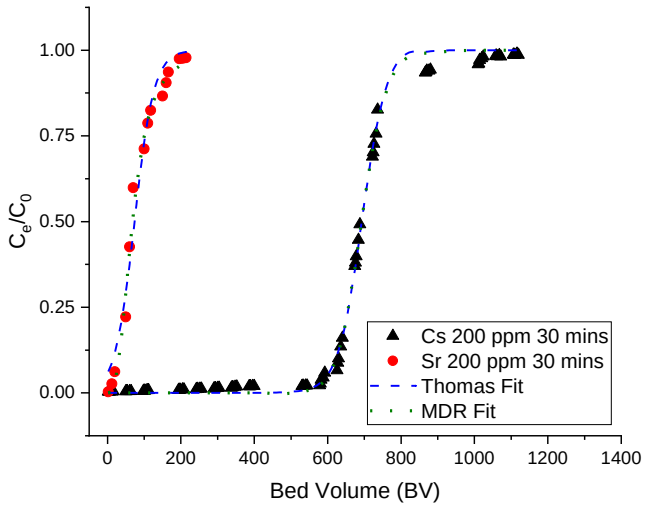

Figure 5.3: Static column breakthrough curve data for cesium and strontium at 200 ppm concentration, along with Thomas and Modified Dose Response (MDR) model fits.

It is clear based on Fig. 5.3, that clinoptilolite is able to remove significantly more cesium than strontium, with approximately a factor of 8 - 10 more column volumes being processed until exhaustion of the ion exchange (C_e/C_0 = 1). However, both species show expected breakthrough behaviour kinetics. In general, the breakthrough criterion is considered the condition where the equilibrium concentration at specific time (C_e) starts elevating dramatically over time (60), and is caused by the rapid reduction in adsorption once the ion exchange sites of the adsorbent are close to becoming fully occupied (60, 287). Once the on exchange is fully occupied, no more adsorption can take, which is considered as the exhaustion point (60). In this study, a breakthrough level 50% (C_e/C_0 = 0.5) was taken as a comparative point to help understanding the breakthrough kinetics.

Using the estimated breakthrough level of 50% as a comparison, the clinoptilolite was able to process around 700 bed volumes with cesium and only 70 bed volumes with strontium, which is broadly consistent with previous batch testing of the same clinoptilolite. The difference in performance from cesium and strontium is considered because of the general low energy state of adsorption for large monovalent ions in clinoptilolite ion exchange sites, where the ion valency effect is significant (20, 173, 216). Also, as discussed by Woods and Gunter (25), the affinity of adsorbent toward the ions is dependent on their hydrated ionic radii, where the hydrated radii for cesium and strontium is 3.29 and 4.12 Å, respectively

(25, 122). Generally, hydrated radii are inversely proportional to the dehydrated ion size, due to the better distribution of the charges (288, 289). Smaller hydrated ionic radii may diffuse more freely in or and out of adsorbent channels during the adsorption process (18, 25, 34, 123), where additionally in zeolite-cation exchange, the process happens in association with the bound water molecules. Dehydration of the bound was occurs prior to adsorption, which is more energetically favourable for smaller hydrated radii (25, 288).

Table 5.1: Fitted Thomas and Modified Dose Response (MDR) model parameters for 6 cm depth static column breakthrough tests with Cs^+ and Sr^{2+}.

Experimental Parameters			Thomas Model			MDR Model	
Diameter (cm)	**C_0 (ppm)**	**Q (mL/min)**	**K_{TH} (mL/mg.min)**	**q_e (mg/g)**	**R^2**	**q_e (mg/g)**	**R^2**
Cs^+ (30 min residence time)							
1	200	0.157	0.002	171.90	0.912	170.44	0.941
Sr^{2+} (30 min residence time)							
1	200	0.157	0.004	15.31	0.981	16.67	0.948
1	100	0.157	0.012	48.10	0.978	47.96	0.985
Sr^{2+} (15 min residence time)							
1	100	0.314	0.016	13.97	0.925	13.15	0.962
2	100	1.257	0.014	17.83	0.954	16.51	0.968

It is also evident from Fig. 5.3, that both the MDR and Thomas model were similar in their goodness of fit to the breakthrough data, although MDR model gave slightly higher R^2 values (see Table 5.1). The fitted equilibrium adsorption capacity (q_e) values were also correspondingly similar between both models, where importantly, the q_e for cesium are considerably higher than for strontium (at 171.90 or 170.44 mg/g for cesium against 15.31 or 16.67 mg/g for strontium, using the Thomas and MDR models respectively). There is also a direct comparison between the q_e values and number of bed volumes processed to breakthrough, which is expected to be a linear correlation following previous research (32, 57, 59, 206, 214).

It is interesting to compare the fitted q_e values from this kinetic data with adsorption capacity values from equilibrium batch experiments for clinoptilolite,

which have been previously described in Chapter 3, Sub Section 3.4.3. In fact, the q_e values estimated in the column tests are actually slightly greater than found directly for the same clinoptilolite pre-activated with NaCl in batch tests (which gave a maximum adsorption capacity value, Q_c = 140.53 mg/g). The slight discrepancy between column and batch capacities is most likely due to the additional uncertainties with q_e estimates from the column breakthrough model fits, although, the good correlation between the Thomas and MDR models gives confidence in the determined values.

Additionally, as it is also known that the clinoptilolite contains some ionic impurities, it suggests that the long elution times in the column experiments may have self-activated the zeolite as the fluid exchanged, exposing additional ion exchange sites. It is noted that normal potable tap water was used in these experiments, which would contain concentrations of various ions that may activate the clinoptilolite over time, such as sodium and calcium ions. While these ions will not affect the adsorption of strontium (owing to strontium's higher adsorption energy) they may exchange and elute secondary impurities from the zeolite. Thus, over the long time periods of the column tests, it is hypothesised that naturally present ions in the water are acting similar to the concentrated salt activation undertaken in Chapter 2a. The relatively slow flowrates utilised in these tests (and thus long elution times) will also affect the quality of adsorption, in comparison to batch testing. For example, Cortés-Martínez *et al* showed lower adsorption in column ion exchange compared to batch experiments, due to a higher flowrate (lower residence time) than our work (29). However, proving the concept of self-activation during column experiments, is a topic of important future research, where it is suggested that specific surface area, mean pore diameter and EDX analysis is completed on eluted samples. Nevertheless, the fact that column adsorption capacity is close to, or indeed, above maximum adsorption capacity estimates indicates that the experimental conditions (specifically the 30 minutes residence time) leads to high adsorption efficiency in the column.

It is also evident that the strontium exchange performs very differently. Here, previous batch tests (Chapter 3) with NaCl pre-activated clinoptilolite (of the same type) gave a maximum adsorption capacity of Q_c = 47.5 mg/g, almost three times the q_e value found from the breakthrough data fitted to the MDR model (and even more than from the Thomas model). The reason for the large difference in the case of strontium, is mostly likely due to its adsorption kinetics, where it has previously been found that the Pseudo Second Order (PSO) rate constant for strontium adsorption on activated clinoptilolite was less than half that as for

cesium. Thus, in these concentration conditions, it appears that the 30 minute column residence time is not sufficient for high material uptake efficiency.

Given the significant difference between cesium and strontium uptake, investigations were focused on modifying column conditions to better understand the system limitations for strontium removal. Presented in Fig. 5.4 is static column breakthrough data for strontium contamination, highlighting the effect of concentration, residence time and column scale-up. Here, the concentration of strontium was reduced to 100 ppm for column residence times of 30 mins and 15 mins. Additionally, a trial using a residence time of 15 minutes was repeated in the larger 2 cm diameter column (increasing the liquid flow rate, *Q*, from 0.314 to 1.257 mL/min for the same contact time). Again, resulting Thomas and MDR breakthrough model fits are also shown in Fig. 5.4, with linear forms used for parameter estimation shown in the Appendix C, Fig. C5. Resulting model parameters and R^2 fit values are also given in Table 5.1.

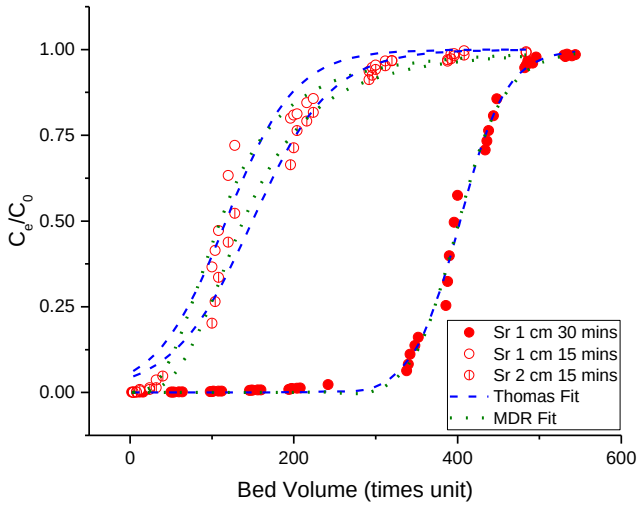

Figure 5.4: Static column breakthrough curve data for cesium and strontium at 100 ppm concentration, along with Thomas and Modified Dose Response (MDR) model fits.

It would be expected from previous research that reducing the strontium concentration would expand the breakthrough curve (57, 59). Indeed, it is evident from Fig. 5.4 that reducing strontium concentration from 200 ppm to 100 ppm, led to a considerably enhanced column performance, where the 50% breakthrough occurred around 400 bed volumes for the 100 ppm solution (as opposed to 70 bed volumes for 200 ppm, in Fig. 5.3). An increase in breakthrough time occurs due to the lower number of ions per unit volume at 100 ppm, leading to a greater

number of bed volumes being processed until the material becomes exhausted. However, the performance difference is greater than would be equated simply from the lower number of ions. In fact, the material efficiency of the clinoptilolite is also much improved at the lower 100 ppm concentration, with q_e = 48.1 mg/g (From the MDR model, Table 5.1) which is around three times higher than q_e of 200 ppm and consistent with maximum expected adsorption capacities from batch studies .

The reason for the greater material efficiency for the lower 100 ppm strontium solution is assumed to be due to the faster adsorption kinetics. Previous kinetic studies on strontium uptake using clinoptilolite in batch systems, suggested the pseudo second order rate constant reduced by almost two orders of magnitude, as concentration increased from 5 to 300 ppm. The reason for the faster adsorption kinetics at lower concentrations is the reduced statistical competition between ions for exchange sites. The faster kinetics coupled with the lower total amount of ions that must be removed in the 100 ppm system results in the large differences in overall column performance.

Figs. 5.4 also shows the change in column performance for a residence time of 15 minutes in comparison to 30 minutes for same 100 ppm of strontium concentration. By reducing the residence time, the breakthrough curve is shifted to lower bed volumes, where the 50% breakthrough point (C_e/C_0 = 0.5) is decreased to around 100 bed volumes. Testing column residence time limits is industrially important, as obviously, reducing residence times will also increase the effluent flowrate of solution (and increase process capacity) while at the same time it will lower the contact time between the adsorbent and contaminants (59, 60, 206). In this case, the contact time is far too small at 15 minutes for efficient material performance. In fact, it is observed from Table 5.1 that the q_e for 15 minutes residence time is only around 13 - 14 mg/g (taking an average between Thomas and MDR models) and thus critically smaller than the value for 30 minutes at 100 ppm.

The effect of scale-up is also examined in Fig. 5.4, with data for 100 ppm strontium and 15 minute residence time for a double, 2 cm, diameter column (with the adsorbent depth kept at 6 cm). The performance for the larger column was similar, although for the 2 cm column, the 50% breakthrough level and fitted q_e values did increase slightly to around 128 bed volumes and ~17 mg/g (average of Thomas and MDR values, see Table 5.1) respectively. This result is similar to McCabe *et al* (215), who used specific resins to remove cesium and technetium

from radioactive effluent waste in column ion exchange of different sizes, where the results showed that the breakthrough kinetics were not changed significantly. The slight reduction in performance from the smaller 1 cm diameter column may be attributed to enhanced wall effects, most likely influencing local flow tortuosity near the wall surface in relation to the bulk porous flow. It is noted also that similar performance was evidenced for 2 cm column tests where the volume of ion exchange was conserved rather than the height (given in Figure 5.5) highlighting good consistency in scale-up parameterisation. In general for the scale-up tests, the MDR model (Appendix C Fig.C6a) was found to give a better fit to the collected breakthrough data compared to Thomas model (Appendix C Fig.C6b) (from R^2 values in Table 5.1) which is similar to other works (206, 221, 222), although differences between the models were minor.

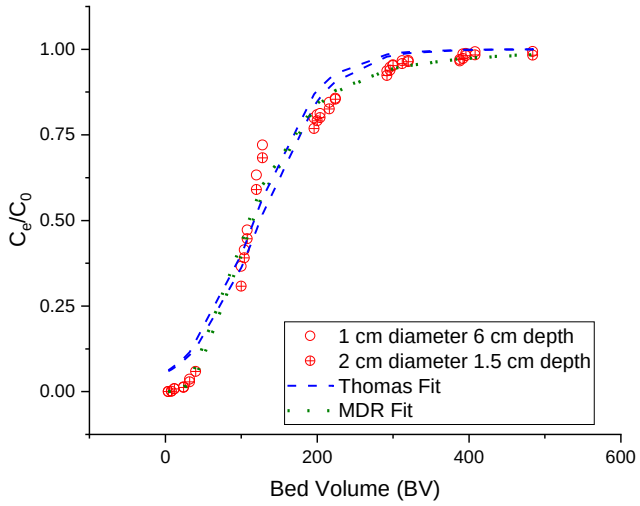

Figure 5.5: Experimental breakthrough data as well as Thomas and MDR fitting models for strontium 100 ppm concentration for two systems with identical residence times (15 mins) and the same adsorbent volume, with increasing column diameter

5.4.2 Ion exchange performance using an agitated tubular reactor (ATR)

Breakthrough kinetic curves for the clinoptilolite incorporated within the agitator bar of the agitated tubular reactor (ATR) are presented in Fig. 5.5. Results are given for two comparative column lengths, 25 and 34 cm (noting the full reactor length is 35 cm) along with resultant Thomas and MDR model fits, for 100 ppm strontium and a 15 minute active column residence time. In these experiments time is reemphasised the residence is that of the active ion

exchange column not the total reactor tube. Some datapoints for the 25 cm trial at intermediate times were omitted, due to some sampling issues that occurred (however, data up to a breakthrough level of 70% and > 90% were gained). Linearised data for model fitting are presented within the Appendix C (Fig. C7), where determined fit parameters are given in Table 5.2.

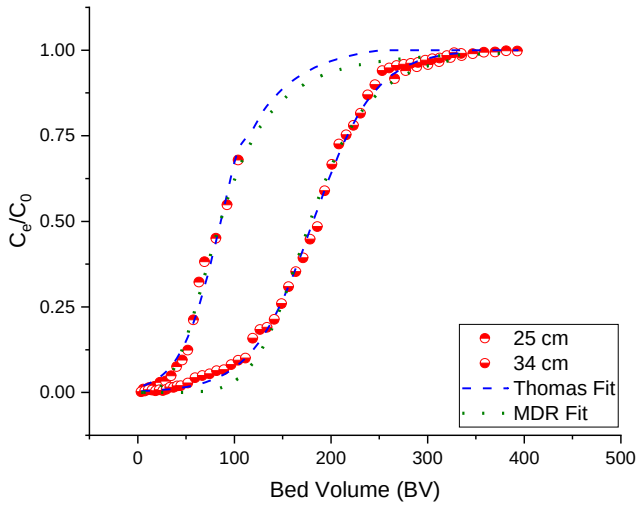

Figure 5.6: Agitated Tubular Reactor (ATR) breakthrough data, along with Thomas and Modified Dose Response (MDR) model fits, for strontium at 100 ppm concentration and residence times of 15 mins for two different bed lengths (25 cm and 34 cm).

Table 5.2: Fitted Thomas and Modified Dose Response (MDR) model parameters for agitated tubular reactor (ATR) breakthrough tests. Sr^{2+} concentration was set at 100 ppm concentration and trials maintained a 15 minutes residence time along the active column length.

Experimental Parameters		Thomas Model			MDR Model	
Bed depth (cm)	**Q (mL/min)**	**KTH (mL/mg.min)**	**q_e (mg/g)**	**R^2**	**q_e (mg/g)**	**R^2**
25	7.102	0.094	10.24	0.993	10.20	0.957
34	6.217	0.039	21.68	0.987	21.32	0.939

From Fig. 5.5, it is clear that the 34 cm length column outperforms the 25 cm column significantly (again noting that the residence time was 15 minutes through both lengths). The 25 cm adsorbent gives a 50% breakthrough level (C_e/C_0 = 0.5) of ~90 bed volumes, which is around half that of the 34 cm length at 180 bed volumes. Correspondingly, the q_e of the 25 cm was determined as

~10.2 mg/g, which is also around half that of the 34 cm bed at ~21.5 mg/g (average of Thomas and MDR model values from Table 5.2). The greater performance of the longer column is largely attributed to the larger column to reactor ratio for the 34 cm length. Unlike in the static ion exchange columns, the ATR operates with the active ion exchange (held within the agitator) completely submerged in the larger reactor tube, which was initially filled with the strontium solution at the beginning of the extraction. Therefore, for relatively small column lengths (low column to tube ratio) there is a large number of solution metal ions initially held in the tube, which are washed out in the initial start-up phase of the reactor. We believe the initial strontium ions in solution begin to adsorb onto the clinoptilolite in this initial start-up, reducing the efficacy of the column. To highlight this effect by changing the column to tube ratio, additional experiments were conducted with a 12 cm column length (see Appendix C, Fig. C8) which performed very poorly, where the 50% breakthrough level occurred after less than 25 bed volumes.

The performance of the ATR is compared to the static columns in Fig. 5.6, for 100 ppm strontium at a residence time of 15 minutes. Presented are the determined q_e values from the MDR model, for both 1 and 2 cm diameter (*Ø*) columns, in addition to the 25 and 34 cm active column length ATR (*a*) and the 50% breakthrough level (*b*). The figures also give the liquid flowrate (*Q*) through each system. It is noted that for the ATR experiments, the bulk flow rate is actually slightly lower for the longer 34 cm column in comparison to the 25 cm length (despite the same 15 minute active residence time) due to the reduction in overall tube volume with the longer active column.

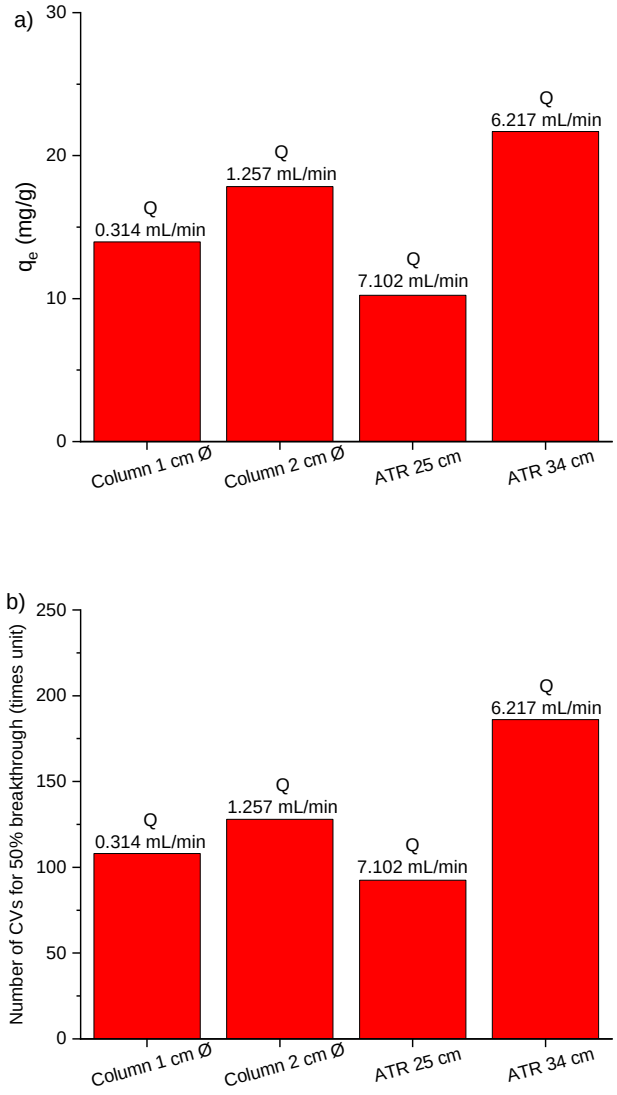

Figure 5.7: a) The maximum adsorption capacity (q_e) and b) number of column volumes (CVs) for 50% breakthrough (C_e/C_0 = 0.5) for both 1 cm and 2 cm diameter (Ø) static columns, and the agitated tubular reactor (ATR) for two different column lengths. All data for strontium at 100 ppm concentration and a 15 minutes residence time.

It is evident from Fig. 5.6 that the 34 cm ATR column system considerably outperforms both static column systems. The q_e value is around 30% greater than the 2 cm static column (and around 35% greater than the 1 cm diameter column) while the 50% breakthrough level is increased to around 40% greater than the 2 cm column. This increase in performance is assumed to be due to the lateral shear of the reactor causing enhanced mixing between the fluid and the column, increasing adsorption kinetics from the purely diffusion limited rate attainable in the static columns. Similar enhancements in mass transfer have been evidenced

in high centrifuge rotating bed reactors (64, 65); however, the ATR has an advantage that column residence times can be easily independently controlled, giving additional operational flexibility and control for this type of intensified system.

The increase in performance is even more considerable, when the differences to the process flowrate (Q) are analysed. As the 1 cm diameter column has a much smaller volume, the flowrate (at 0.314 mL/min) cannot be correlated directly to the ATR. Nevertheless, the larger 2 cm column is of the same order of size, where the mass of the static column is around half that of the 34 cm length ATR, while process flow rate is only ~1/6 of that of the ATR (1.257 mL/min against 6.217 mL/min respectively). Therefore, for a comparative column volume, the ATR would achieve almost three times the volume of treated liquid for a given time (because of its lower tube to column ratio). When this increase in process liquid capacity is considered along with the enhanced material performance from the lateral mixing, an industrial scale ATR system would require a significantly smaller footprint than traditional static columns, a key focus of process intensification (224).

5.5 Summary

This study compared the performance of static column ion exchange with a process intensified agitated tubular reactor (ATR) for the separation of cesium and strontium ions from nuclear effluents, using natural-grade clinoptilolite. In column ion exchange studies, it was found that cesium had ~10× greater removal efficiency than strontium, where the 50% breakthrough level (C_e/C_0 = 0.5) occurred after 700 bed volumes for cesium compared to 70 bed volumes for strontium, with 200 ppm solutions. Column performance envelopes were further evaluated using strontium systems, where the 50% breakthrough level was increased to 400 bed volumes, when concentration was reduced to 100 ppm. In comparison, minimising the residence time from 30 to 15 minutes with 100 ppm strontium, reduced the 50% breakthrough level down to ~100 bed volumes. Scale-up parameterisation was also considered, where doubling the column diameter to 2 cm resulted in a marginal relative increase in performance, associated with wall effects from the smaller 1 cm diameter system. Breakthrough kinetic data of all systems was fitted with the Thomas and Modified Dose Response (MDR) models, allowing calculation of adsorption capacities (q_e). Values were directly correlated to previous batch adsorption experiments on the

same systems , where it was highlighted that for 30 minute residence time conditions, the 100 ppm strontium and 200 ppm cesium systems were operating at close to the maximum adsorption capacity of the material, indicating optimum column operation.

For the comparison with the intensified ATR, two effective column lengths were considered (25 and 34 cm) where the inner agitator bar of the reactor was filled with clinoptilolite, using a sieve mesh to retain the resin. The 34 cm length system was found to materially outperform the static columns by ~30% (in terms of both q_e and breakthrough values) due to enhanced mixing and adsorption kinetics from the lateral shear imparted in the ATR. Critically also, the ATR was able to operate at much greater relative flow rates of 2-3× rates possible from the static columns (in relation the mass of the ion exchange) due to the smaller column to tube volume ratio. Industrially, such performance increases would result in a significant reduction to the overall size and number of required ion exchange columns, where it is noted that up to 10 column tubes can be run in parallel on the pilot-scale ATR. Therefore, the ATR could be incorporated into mobile, modular treatment units for nuclear effluent treatment with flexible operating capacity, especially for use in cases of radiation groundwater leaks or other hazard reduction activities.

Chapter 6 Conclusions and future research outlook

The use of natural clinoptilolite on different cesium and strontium removal techniques are studied in this project. The use of low-grade natural clinoptilolite which is usually used as food grade not for nuclear waste treatment is used in batch adsorption technique along with the pre-activation and milling for adsorption capacity improvement. It has been also examined to study the ions competition effect such as in simulated sea water. The use of fine particle of natural clinoptilolite is applied for flotation study. The flotation study includes the best surfactant selection in order to obtain the most optimum condition for both cesium contaminated clinoptilolite recovery and water reduction ratio. The use of low-grade natural clinoptilolite is also used in column ion exchange and agitated tubular reactor (ATR) techniques. Comprehensive investigations have been carried out to understand the breakthrough from different concentration of ions, residence time, column ion exchange diameter, and the application of ATR for removing the strontium as for rapid separation process. The following conclusions and future research outlook are drawn from these research works.

6.1 Conclusions

The novelty of Chapter 3 is the use of relatively low-grade clinoptilolite for removing cesium and strontium ions from nuclear effluent. The low-grade clinoptilolite could be an alternative solution of supply issues of nuclear-grade ores for current and future treatment operations worldwide, because the current clinoptilolite for nuclear effluent treatment is considered to be obtained from a single deposit in California, which has good selectivity for ^{137}Cs and ^{90}Sr, and contains a low level of impurities (32, 37-39). Another novelty is the effect of pre-activation which shows good adsorption improvement for non-nuclear application (40). The milling is also introduced to investigate the particle size effect in terms of enlarge the surface area in order to improve the adsorption performance. Another novelty is to study the effect of ions competition in simulated seawater solutions, which has been an issue during the accident of cooling system at Fukushima few years ago, for example (151-153).

The relatively low-grade clinoptilolite was characterised using STEM-EDX and XRD, where regions of high potassium ion contamination and iron based

impurities which potassium and iron have been shown by other research (18, 23, 31) could affect the clinoptilolite performance. From XRD, it showed that pre-activation both acid and salt currently does not change the structure of clinoptilolite significantly, but only affects the concentration of exchangeable ions which can increase the surface reactivity (40, 238). Changes to clinoptilolite zeta potentials with cesium and strontium adsorption indicated heterogeneous surface interactions occurring, driven both by ion exchange from interstitial sites and electrostatic surface attraction, although there was no evidence of separate two-site adsorption mechanisms.

Adsorption kinetics of natural and pre-activated materials in 5 ppm Cs^+ and Sr^{2+} salts were found to reach equilibrium around 360 mins (6h) which is similar to other research (18, 20, 30, 136, 145, 242, 243). The results were fitted using Pseudo-First Order (PFO) and Pseudo-Second Order (PSO) models which PSO is found to be the better fit due to higher average linear regression (R^2) ~ 0.99 in all cases (27, 30, 34, 131). While activation increased the initial adsorption rate of both cesium and strontium, the overall rate constant (k_2) was only enhanced in cesium systems, due to the general low affinity of the strontium. Equilibrium isotherms were observed that the uptake (q_e) of both ions is increased along with the final concentration (C_e) monotonically as expected for a monolayer coverage (18, 20, 30, 31, 59, 244). The effect of ion valency is significant, where the divalent strontium will be at a higher free energy state than the monovalent cesium which causes better adsorption performance on cesium (20, 173, 216) The pre-activation was shown better adsorption because the initial activation with small monovalent salts such sodium (or acid groups), which are weakly bound compared to other alkali and earth metals, exchange with larger ions including both cesium and strontium are highly energetically favourable (40, 111, 112). The results were then compared with Langmuir and Freundlich monolayer models, with the former providing closer fits. The Langmuir adsorption capacity (Q_c) for cesium was increased by over 100% in sodium activated clinoptilolite (from ~67 to 140 mg/g), while values for strontium were considerably smaller with a lower enhancement with activation of ~50% (from ~35 to ~52 mg/g).

Additionally, the effect of milling was observed to give a similar increase in performance to activation for cesium removal, with a strong linear dependency between adsorbed amount and overall specific surface area, where a combination of these two techniques will likely to lead to a much greater ion exchange capacity (19). The influence of contaminants on strontium removal in milled fractions was notably more significant, which reduced relative adsorption

in comparison to associated surface area increases on un-activated samples. The influence of ion competition on adsorption was also investigated, using solution mixtures of Na^+, Ca^{2+} and K^+, to represent seawater type solutions. The distribution coefficients (k_d) of both cesium and strontium were significantly reduced, with the magnitude of reduction directly proportional to the concentration of competing ions (from power-law fits) while pre-activation actually led to a more critical drop-off in uptake. Given the relatively low affinity of Na^+ and Ca^{2+} to clinoptilolite (37), it is assumed the major reason for the reduced performance is ion competition from the K^+ ions (18, 119). As potassium is assumed to have a higher affinity than strontium (37), its influence on strontium adsorption in seawater is comparatively greater (with Sr^{2+} distribution coefficients for activated clinoptilolite reducing by two orders of magnitude, in comparison to one order for Cs^+).

Collectively, these results highlight that pre-activation and milling could be used to considerably extend the range of natural clinoptilolite ores suitable for nuclear treatment processing of relatively freshwater effluents, but for high saline waters, modern synthetic products will still be required.

In Chapter 4, to date, unfortunately there has been no comprehensive study about the use of flotation to separate radioactive ion contaminated clinoptilolite. Therefore, some novelties were investigated and examined such as the potential surfactant collectors' adsorption in order to remobilize and remove contaminated radioisotopes; the effect of ion contamination which can reduce recovery during flotation removal; and the optimum parameters between the recovery and good dewatering ratio. The flotation is used as an alternative to gravitational separation or the use of large resins in elution columns.

The adsorption kinetics and equilibrium were investigated in order to observe the performance of fine clinoptilolite particle size while removing cesium. The kinetics adsorption showed faster kinetics (k_2 equalled 0.516 g/mg.min) which is higher than natural clinoptilolite values generally found in previous research (e.g. 0.0015 (30) and 0.163 g/mg.min in Chapter 3) and also higher than salt and acid activated clinoptilolite (e.g. 0.383 and 0.472 g/mg.min). This study is similar to other research where the adsorption was best modelled using a PSO model (30). It was observed that fine clinoptilolite contributed high capacities (q_c = 158.261 mg/g) when compared to much previous literature on non-modified clinoptilolite (18, 20, 24, 30, 31, 105) .

The co-adsorption of EHDa-Br and CPC surfactants onto both clean and 5 ppm Cs^+ contaminated clinoptilolite was then measured, using surface tension measurements modelled with a Langmuir isotherm, where the CMC for both surfactants was found experimentally to be similar, at ~0.85 mM which is close to values reported in literature (EHDA-Br = 0.8 mM and CPC = 0.84 mM (156)) and R^2 values for the Langmuir fits were > 0.97 both surfactants. Distribution coefficients (K_d) as high as 10,000 mL/g were evident with moderate concentrations of surfactant (below those leading to bilayer formation) where CPC outperformed EHDa-Br on Cs-contaminated samples. Measurements of particle size confirmed that adsorption of surfactant monolayers did not lead to significant flocculation of the particles, suggesting good stability for flotation separation. Importantly also, less than 8% of pre-adsorbed cesium was removed through subsequent adsorption of surfactant, highlighting that co-adsorption was energetically favourable, which is critical for flotation to be accepted as a feasible recovery technique.

In flotation tests, increasing surfactant concentration from both surfactants continually improved the recovery of 5 ppm Cs^+ contaminated clinoptilolite, while conversely impacting on performance by reducing the water reduction ratio (assumed to be due to higher levels of liquid entrainment). Moreover, the incorporation of MIBC frother significantly enhanced recovery further, for volume additions up to 30 – 50 µL. Overall, it was found that CPC surfactant at an 0.5 mM initial concentration and 50 µL MIBC gave optimum conditions for both recovery (at ~90%) while maintaining an adequate water reduction ratio (~4) leading to significant dewatering and consolidation of the zeolite in the froth phase. The effect of varying initial cesium concentration contaminated on clinoptilolite was also studied, where a clear reduction in recovery was observed for levels > 80 ppm (although this concentration is well above those relevant for most nuclear applications (20)). Overall, this investigation showed that by using cationic surfactants, flotation is a viable and industrially scalable technique for the separation of fine clinoptilolite that are used for the removal of cesium ions in nuclear applications. Additionally, it may also have far reaching applications to improve the material efficiency of many types of zeolites relevant to the clean-up of industrial effluents, from sectors such as mining, textiles and consumer fine chemicals.

Last, in Chapter 5, the use of natural-grade clinoptilolite, which is considered to have some impurities based on Figs. 3.3 and 3.4., have been studied for static column ion exchange and process intensified (PI) called agitated

tubular reactor (ATR). This clinoptiolilote has been used for cesium and strontium separation which similar to the nuclear waste industrial process. During column ion exchange studies, it was found that clinoptilolite had better performance on cesium removal compared to strontium removal, which almost 10 times higher removal efficiency than strontium at same concentration. In addition, by reducing the concentration of strontium from 200 ppm down to 100 ppm, the 50% breakthrough level (C_e/C_0 = 0.5) was occured at 400 bed volumes or almost 6 times higher when at 200 ppm concentration. In contrast, reduction of 50% breakthrough level was found when the residence time was reduced from 30 minutes down to 15 minutes at 100 ppm concentration, where the 50% breakthrough level was occurred at 100 bed volumes. The increasing of inner diameter up to 2 cm diameter, which relates to scale up experiment, did not produce significant increment of the 50% breakthrough level. All breakthrough kinetics data were fitted with Thomas and Modified Dose Response (MDR) models where MDR model showed better fit to the systems.

Meanwhile, during ATR experiment, the inner agitator bar of the reactor was filled by the clinoptilolite with different length (25 and 34 cm). The 34 cm length system was found to be the best performance compared to 25 cm and static columns ion exchange by ~30% (in terms of both q_e and breakthrough values).

Overall, a natural-grade clinoptilolite can be used for an alternative adsorbent in the static column ion exchange and ATR processes which the results are shown better than the use of natural-grade clinoptilolite in batch process. In addition, the ATR shows potential alternative separation technique which can remove large quantity of strontium from the effluent in few minutes only.

6.2 Future research outlook

There are some opportunities that can be conducted in the future from Chapter 3. Even though the results show potential alternative, It is noted that the ions competition study used was in simulated seawater, however the use of real seawater is interested to further study. The seawater itself contain complex metals' ion are taking place and affecting the reduction of cesium and strontium, which shown by Wajima when zeolite was treated in seawater (33). In addition, Yee *et al* observed that their nano chabazite could perform better cesium adsorption in high saline seawater (83), therefore reducing the clinoptilolite particle size down to nano size could be the alternative study for it. As far, the author has limitation up to micron size only. Alternatively, combination between pre-activation and milling of clinoptilolite during cesium and strontium adsorption potentially to be a good research framework which includes similar set up in Chapter 3. Because Amanipour and Faghihian showed that combination between milling and pre-activation as a composite could improve cesium and strontium removal in freshwater (31).

From Chapter 4, it is observed that cesium contaminated on fine particle clinoptilolite shows better flotation quality and good water reduction ratio. However, in order to find the best parameter, the optimum particle size of clinoptilolite is also essential to study which considers the cost and time effectiveness while producing the fine particle. As the rupture of the bubble-particle aggregates from buoyancy driven differences could be higher as the particle size is larger (165, 192, 198, 204). Also, higher particle size could reduce the froth stability during flotation (203). In addition, the study of mix metal ions (incorporates with strontium) contaminated on adsorbent such as clinoptilolite is interested to study, which so far the study has limitation in metal ions in solution without the adsorbent (51, 75, 182, 290-292). It is also noted that the optimum parameters possibility changes in order to accommodate the maximum recovery from both ions (cesium and strontium) and less water reduction ratio, therefore similar procedures which have been done in Chapter 4 could be used as guidance.

Some future works have potential to be studied extensively from Chapter 5. Even though, the study showed good performance, however, in order to enhance the performance for both static column ion exchange and ATR processes, some experiments could be conducted in several ways. First, by using pre activation treatment, which has been shown in Chapter 3 that pre activation

could improve the adsorption performance significantly on both cesium and strontium ions. Therefore, the pre-activated clinoptilolite by NaCl and HCl could be an alternative study for cesium and strontium removals on static column ion exchange and ATR systems. Second, by using multiple columns ion exchange. The use of multiple columns could improve the breakthrough performance which has been shown in some literatures (65, 205-207, 209, 210, 293). Third, by modifying the size of inner agitator tube in order to find the optimum surface area and specific density of adsorbent for ATR system.

Reference

1. Ojovan, M.I. and Lee, W.E. *An Introduction to Nuclear Waste Immobilisation.* second ed. ed. Oxford: Elsevier, 2014.
2. Wilson, P.D. The nuclear fuel cycle from ore to wastes. 1996.
3. IAEA. *Classification of Radioactive Waste.* Vienna: INTERNATIONAL ATOMIC ENERGY AGENCY, 2009.
4. Budnitz, R.J. Strontium-90 and strontium-89: a review of measurement techniques in environmental media. *Lawrence Berkeley Laboratory.* 1974.
5. Nagasaki, S. and Nakayama, S. *Radioactive Waste Engineering and Management.* Springer, 2015.
6. Bayliss, C. and Langley, K. *Nuclear decommissioning, waste management, and environmental site remediation.* Butterworth-Heinemann, 2003.
7. Makgae, M.E. Radioactive waste management plan for the PBMR (Pty) Ltd fuel plant. *Nuclear Engineering and Design.* 2009, **239**(10), pp.2196-2200.
8. IAEA. *Standardization of Radioactive Waste Categories.* Vienna: INTERNATIONAL ATOMIC ENERGY AGENCY, 1970.
9. IAEA, V. *Management of problematic waste and material generated during the decommissioning of nuclear facilities.* Technical reports series, 2006.
10. IAEA. *Radiation Protection and Safety of Radiation Sources: International Basic Safety Standards.* Vienna: INTERNATIONAL ATOMIC ENERGY AGENCY, 2011.
11. IAEA. *Radioactive Particles in the Environment: Sources, Particle Characterization and Analytical Techniques.* Vienna: INTERNATIONAL ATOMIC ENERGY AGENCY, 2011.
12. OECD/NEA. *Radioactive Waste Management and Constructing Memory for Future Generations.* OECD Publishing.
13. OECD. *Radioactive Waste in Perspective.* OECD Publishing.
14. OECD/NEA. *The Regulatory Control of Radioactive Waste Management.* OECD Publishing.
15. Olatunji, M.A., Khandaker, M.U., Mahmud, H.N.M.E. and Amin, Y.M. Influence of adsorption parameters on cesium uptake from aqueous solutions- a brief review. *RSC Advances.* 2015, **5**(88), pp.71658-71683.
16. IMechE. *Radioactive Waste Management 2000: Challenges, Solutions and Opportunities.* 2001.
17. Raj, K., Prasad, K. and Bansal, N. Radioactive waste management practices in India. *Nuclear Engineering and Design.* 2006, **236**(7), pp.914-930.
18. Smičiklas, I., Dimović, S. and Plećaš, I. Removal of Cs1+, Sr2+ and Co2+ from aqueous solutions by adsorption on natural clinoptilolite. *Applied Clay Science.* 2007, **35**(1-2), pp.139-144.
19. Coruh, S. Immobilization of copper flotation waste using red mud and clinoptilolite. *Waste Manag Res.* 2008, **26**(5), pp.409-418.

20. Borai, E.H., Harjula, R., Malinen, L. and Paajanen, A. Efficient removal of cesium from low-level radioactive liquid waste using natural and impregnated zeolite minerals. *Journal of Hazardous materials.* 2009, **172**(1), pp.416-422.
21. Abusafa, A. and Yücel, H. Removal of 137 Cs from aqueous solutions using different cationic forms of a natural zeolite: clinoptilolite. *Separation and Purification Technology.* 2002, **28**(2), pp.103-116.
22. Guangren, Q., Yuxiang, L., Facheng, Y. and Rongming, S. Improvement of metakaolin on radioactive Sr and Cs immobilization of alkali-activated slag matrix. *Journal of Hazardous materials.* 2002, **92**(3), pp.289-300.
23. Mimura, H. and Akiba, K. Adsorption Behavior of Cesium and Strontium on Synthetic Zeolite P. *Journal of Nuclear Science and Technology.* 1993, **30**(5), pp.436-443.
24. Faghihian, H., Marageh, M.G. and Kazemian, H. The use of clinoptilolite and its sodium form for removal of radioactive cesium, and strontium from nuclear wastewater and Pb 2+, Ni 2+, Cd 2+, Ba 2+ from municipal wastewater. *Applied Radiation and Isotopes.* 1999, **50**(4), pp.655-660.
25. Woods, R.-M. and Gunter, M.E. Na-and Cs-exchange in a clinoptilolite-rich rock: Analysis of the outgoing cations in solution. *American Mineralogist.* 2001, **86**(4), pp.424-430.
26. Gül, Ö. *Exchanges of Strontium on Clinoptilolite Zeolite*. thesis, METU, 2003.
27. Shahwan, T., Akar, D. and Eroglu, A.E. Physicochemical characterization of the retardation of aqueous Cs+ ions by natural kaolinite and clinoptilolite minerals. *Journal of Colloid and Interface Science.* 2005, **285**(1), pp.9-17.
28. Rajec, P. and Domianová, K. Cesium exchange reaction on natural and modified clinoptilolite zeolites. *Journal of Radioanalytical and Nuclear Chemistry.* 2007, **275**(3), pp.503-508.
29. Cortés-Martínez, R., Olguín, M. and Solache-Ríos, M. Cesium sorption by clinoptilolite-rich tuffs in batch and fixed-bed systems. *Desalination.* 2010, **258**(1), pp.164-170.
30. De Haro-Del Rio, D.A., Al-Jubouri, S., Kontogiannis, O., Papadatos-Gigantes, D., Ajayi, O., Li, C. and Holmes, S.M. The removal of caesium ions using supported clinoptilolite. *Journal of Hazardous materials.* 2015, **289**, pp.1-8.
31. Amanipour, S. and Faghihian, H. Potassium hexacyanoferrate–clinoptilolite adsorbent for removal of Cs+ and Sr2+ from aqueous solutions. *International Journal of Environmental Studies.* 2017, **74**(1), pp.86-104.
32. Dyer, A., Hriljac, J., Evans, N., Stokes, I., Rand, P., Kellet, S., Harjula, R., Moller, T., Maher, Z. and Heatlie-Branson, R. The use of columns of the zeolite clinoptilolite in the remediation of aqueous nuclear waste streams. *Journal of Radioanalytical and Nuclear Chemistry.* 2018, pp.1-19.
33. Wajima, T. Ion exchange properties of Japanese natural zeolites in seawater. *Analytical Sciences.* 2013, **29**(1), pp.139-141.
34. Ames, L.L., Jr. Effect of base cation on the cesium kinetics of clinoptilolite. *American Mineralogist.* 1962, **47**(11-12), pp.1310-1316.

35. Kuenzel, C., Cisneros, J., Neville, T., Vandeperre, L., Simons, S., Bensted, J. and Cheeseman, C. Encapsulation of Cs/Sr contaminated clinoptilolite in geopolymers produced from metakaolin. *Journal of Nuclear Materials.* 2015, **466**, pp.94-99.
36. Rajec, P., Macášek, F., Feder, M., Misaelides, P. and Šamajová, E. Sorption of caesium and strontium on clinoptilolite-and mordenite-containing sedimentary rocks. *Journal of Radioanalytical and Nuclear Chemistry.* 1998, **229**(1-2), pp.49-55.
37. Dyer, A. Use of zeolites in the treatment of nuclear waste. *Analytical Proceedings.* 1993, **30**(4), pp.190-191.
38. Handley-Sidhu, S., Mullan, T.K., Grail, Q., Albadarneh, M., Ohnuki, T. and Macaskie, L.E. Influence of pH, competing ions, and salinity on the sorption of strontium and cobalt onto biogenic hydroxyapatite. *Sci Rep.* 2016, **6**, p.23361.
39. Dyer, A. and Emms, T.I. Cation exchange in high silica zeolites. *Journal of Materials Chemistry.* 2005, **15**(47), pp.5012-5021.
40. Motsa, M.M., Mamba, B.B., Thwala, J.M. and Msagati, T.A. Preparation, characterization, and application of polypropylene-clinoptilolite composites for the selective adsorption of lead from aqueous media. *Journal of Colloid and Interface Science.* 2011, **359**(1), pp.210-219.
41. Salbu, B., Bjørnstad, H., Svaren, I., Prosser, S., Bulman, R., Harvey, B. and Lovett, M. Size distribution of radionuclides in nuclear fuel reprocessing liquids after mixing with seawater. *Science of the Total Environment.* 1993, **130**, pp.51-63.
42. Cabezon, L., Caballero, M., Cela, R. and Perez-Bustamante, J. Simultaneous separation of copper, cadmium and cobalt from sea-water by co-flotation with octadecylamine and ferric hydroxide as collectors. *Talanta.* 1984, **31**(8), pp.597-602.
43. Rogers, H., Bowers, J. and Gates-Anderson, D. An isotope dilution–precipitation process for removing radioactive cesium from wastewater. *Journal of Hazardous materials.* 2012, **243**, pp.124-129.
44. Kim, K.-W., Shon, W.-J., Oh, M.-K., Yang, D., Foster, R.I. and Lee, K.-Y. Evaluation of dynamic behavior of coagulation-flocculation using hydrous ferric oxide for removal of radioactive nuclides in wastewater. *Nuclear Engineering and Technology.* 2019, **51**(3), pp.738-745.
45. Teh, C.Y., Budiman, P.M., Shak, K.P.Y. and Wu, T.Y. Recent advancement of coagulation–flocculation and its application in wastewater treatment. *Industrial & Engineering Chemistry Research.* 2016, **55**(16), pp.4363-4389.
46. Deliyanni, E.A., Kyzas, G.Z. and Matis, K.A. Various flotation techniques for metal ions removal. *Journal of Molecular Liquids.* 2017, **225**, pp.260-264.
47. Peleka, E.N., Gallios, G.P. and Matis, K.A. A perspective on flotation: a review. *Journal of Chemical Technology & Biotechnology.* 2018, **93**(3), pp.615-623.
48. Ortiz-Oliveros, H.B., Flores-Espinosa, R.M., Jiménez-Domínguez, H., Jiménez-Moleón, M.C. and Cruz-González, D. Dissolved air flotation for treating wastewater of the nuclear industry: preliminary results. *Journal of Radioanalytical and Nuclear Chemistry.* 2012, **292**(3), pp.957-965.

49. Aziz, M. and Beheir, S.G. Removal of 60Co and 134Cs from radioactive process waste water by flotation. *Journal of Radioanalytical and Nuclear Chemistry.* 1995, **191**(1), pp.53-66.
50. Shakir, K., Benyamin, K. and Aziz, M. Separation of Co (II) from dilute aqueous solutions by precipitate and adsorbing colloid flotation. *Journal of Radioanalytical and Nuclear Chemistry.* 1993, **172**(2), pp.329-339.
51. Charewicz, W.A., Grabowska, J. and Bartsch, R.A. Flotation of Co(II), Sr(II), and Cs(I) cations with proton-ionizable lariat ethers. *Separation Science and Technology.* 2001, **36**(7), pp.1479-1494.
52. Ortiz-Oliveros, H.B. and Flores-Espinosa, R.M. Simultaneous removal of oil, total Co and 60Co from radioactive liquid waste by dissolved air flotation. *International Journal of Environmental Science and Technology.* 2019, **16**(7), pp.3679-3686.
53. Micheau, C., Schneider, A., Girard, L. and Bauduin, P. Evaluation of ion separation coefficients by foam flotation using a carboxylate surfactant. *Colloids and Surfaces A: Physicochemical and Engineering Aspects.* 2015, **470**, pp.52-59.
54. Shakir, K., Sohsah, M. and Soliman, M. Removal of cesium from aqueous solutions and radioactive waste simulants by coprecipitate flotation. *Separation and Purification Technology.* 2007, **54**(3), pp.373-381.
55. Zhang, H., Kim, Y.K., Hunter, T.N., Brown, A.P., Lee, J.W. and Harbottle, D. Organically modified clay with potassium copper hexacyanoferrate for enhanced Cs+ adsorption capacity and selective recovery by flotation. *Journal of Materials Chemistry A.* 2017, **5**(29), pp.15130-15143.
56. Zhang, H., Tangparitkul, S., Hendry, B., Harper, J., Kim, Y.K., Hunter, T.N., Lee, J.W. and Harbottle, D. Selective separation of cesium contaminated clays from pristine clays by flotation. *Chemical Engineering Journal.* 2019, **355**, pp.797-804.
57. Ararem, A., Bouras, O. and Bouzidi, A. Batch and continuous fixed-bed column adsorption of Cs+ and Sr2+ onto montmorillonite–iron oxide composite: Comparative and competitive study. *Journal of Radioanalytical and Nuclear Chemistry.* 2013, **298**(1), pp.537-545.
58. Brooks, K. *Cesium ion exchange using actual waste: Column size considerations.* Pacific Northwest National Lab., Richland, WA (United States), 1996.
59. El-Kamash, A. Evaluation of zeolite A for the sorptive removal of Cs+ and Sr 2+ ions from aqueous solutions using batch and fixed bed column operations. *Journal of Hazardous materials.* 2008, **151**(2), pp.432-445.
60. Patel, H. Fixed-bed column adsorption study: a comprehensive review. *Applied Water Science.* 2019, **9**(3), p.45.
61. Visscher, F., van der Schaaf, J., Nijhuis, T.A. and Schouten, J.C. Rotating reactors – A review. *Chemical Engineering Research and Design.* 2013, **91**(10), pp.1923-1940.
62. Lodha, H., Jachuck, R. and Suppiah Singaram, S. Intensified Biodiesel Production Using a Rotating Tube Reactor. *Energy & Fuels.* 2012, **26**(11), pp.7037-7040.
63. Modak, J.B., Bhowal, A. and Datta, S. Experimental study and mathematical modeling of breakthrough curve in rotating packed bed.

Chemical Engineering and Processing: Process Intensification. 2016, **99**, pp.19-24.
64. Wu, Y., Chang, C.-C., Guan, C.-Y., Chang, C.-C., Li, J.-W., Chang, C.-Y. and Yu, C.-P. Enhanced removal of ammonium from the aqueous solution using a high-gravity rotating packed bed loaded with clinoptilolite. *Separation and Purification Technology.* 2019, **221**, pp.378-384.
65. Ng, Y.-S., Tan, Y.-T., Chua, A.S.M., Hashim, M.A. and Sen Gupta, B. Removal of nickel from water using rotating packed bed contactor: Parametric studies and mode of operations. *Journal of Water Process Engineering.* 2020, **36**, p.101286.
66. Jones, E., McClean, K., Housden, S., Gasparini, G. and Archer, I. Biocatalytic oxidase: Batch to continuous. *Chemical Engineering Research and Design.* 2012, **90**(6), pp.726-731.
67. He, Y., Bayly, A.E., Hassanpour, A., Fairweather, M. and Muller, F. Flow behaviour of an agitated tubular reactor using a novel dynamic mesh based CFD model. *Chemical Engineering Science.* 2020, **212**, p.115333.
68. He, Y., Bayly, A.E., Hassanpour, A., Muller, F., Wu, K. and Yang, D. A GPU-based coupled SPH-DEM method for particle-fluid flow with free surfaces. *Powder Technology.* 2018, **338**, pp.548-562.
69. NDA. *Managing waste.* [Online]. 2015. [Accessed 29/04/2017]. Available from: https://www.gov.uk/government/collections/managing-waste
70. Stefanova, I. and Gradev, G. Development of a technology and a pilot plant for treatment of small volumes of liquid radioactive waste. *Treatment Technologies for Low and Intermediate Level Waste from Nuclear Applications. Final report IAEA-TECDOC.* 1997, **929**, pp.163-178.
71. Flüeler, T. *Decision making for complex socio-technical systems: Robustness from lessons learned in long-term radioactive waste governance.* Springer Science & Business Media, 2005.
72. Streffer, C., Gethmann, C.F., Kamp, G., Kröger, W., Rehbinder, E. and Renn, O. *Radioactive waste: technical and normative aspects of its disposal.* Springer Science & Business Media, 2011.
73. Cecille, M.L., Casarci, M. and Pietrelli, L. *New separation chemistry techniques for radioactive waste and other specific applications.* Springer Science & Business Media, 2012.
74. El-Kamash, A., El-Dakroury, A. and Aly, H. Leaching kinetics of 137 Cs and 60 Co radionuclides fixed in cement and cement-based materials. *Cement and Concrete Research.* 2002, **32**(11), pp.1797-1803.
75. Maciejewski, P., Walkowiak, W. and Robak, W. Selective removal of Cs-137, Sr-90, Ba-133, Co-60 and Pb-210 radioisotopes with proton-ionizable lariat ethers in the ion flotation process. *radioisotopes.* 2005, **2**, p.R1.
76. Efremenkov, V. Radioactive waste management at nuclear power plants. *IAEA Bulletin.* 1989, **31**(4), pp.37-42.
77. Wu, H., Wang, W., Huang, Y., Han, G., Yang, S., Su, S., Sana, H., Peng, W., Cao, Y. and Liu, J. Comprehensive evaluation on a prospective precipitation-flotation process for metal-ions removal from wastewater simulants. *Journal of Hazardous materials.* 2019, **371**, pp.592-602.

78. Soliman, M.A., Rashad, G.M. and Mahmoud, M.R. Fast and efficient cesium removal from simulated radioactive liquid waste by an isotope dilution–precipitate flotation process. *Chemical Engineering Journal.* 2015, **275**, pp.342-350.
79. Shakir, K., Ghoneimy, H.F., Beheir, S.G. and Refaat, M. Flotation of Cesium Coprecipitated with Nickel Hexacyanoferrate(II) from Aqueous Solutions and Radioactive Waste Simulants. *Separation Science and Technology.* 2007, **42**(6), pp.1341-1365.
80. Bengiat, R., Bogoslavsky, B., Mandler, D. and Almog, J. Selective Binding and Precipitation of Cesium Ions from Aqueous Solutions: A Size-Driven Supramolecular Reaction. *Chemistry – A European Journal.* 2018, **24**(13), pp.3161-3164.
81. Harjula, R. and Lehto, J. Effect of sodium and potassium ions on cesium absorption from nuclear power plant waste solutions on synthetic zeolites. *Nuclear and chemical waste management.* 1986, **6**(2), pp.133-137.
82. Chorover, J., Choi, S., Amistadi, M.K., Karthikeyan, K., Crosson, G. and Mueller, K.T. Linking cesium and strontium uptake to kaolinite weathering in simulated tank waste leachate. *Environmental Science & Technology.* 2003, **37**(10), pp.2200-2208.
83. Lee, K.-Y., Kim, K.-W., Park, M., Kim, J., Oh, M., Lee, E.-H., Chung, D.-Y. and Moon, J.-K. Novel application of nanozeolite for radioactive cesium removal from high-salt wastewater. *Water Research.* 2016, **95**, pp.134-141.
84. Awual, M.R., Suzuki, S., Taguchi, T., Shiwaku, H., Okamoto, Y. and Yaita, T. Radioactive cesium removal from nuclear wastewater by novel inorganic and conjugate adsorbents. *Chemical Engineering Journal.* 2014, **242**, pp.127-135.
85. Awual, M.R., Yaita, T., Taguchi, T., Shiwaku, H., Suzuki, S. and Okamoto, Y. Selective cesium removal from radioactive liquid waste by crown ether immobilized new class conjugate adsorbent. *Journal of Hazardous materials.* 2014, **278**, pp.227-235.
86. Wang, J. and Zhuang, S. Removal of cesium ions from aqueous solutions using various separation technologies. *Reviews in Environmental Science and Bio/Technology.* 2019, **18**(2), pp.231-269.
87. Ding, D., Zhang, Z., Chen, R. and Cai, T. Selective removal of cesium by ammonium molybdophosphate – polyacrylonitrile bead and membrane. *Journal of Hazardous materials.* 2017, **324**, pp.753-761.
88. Fantz, U., Friedl, R. and Fröschle, M. Controllable evaporation of cesium from a dispenser oven. *Review of Scientific Instruments.* 2012, **83**(12), p.123305.
89. Fantz, U., Gutser, R. and Wimmer, C. Fundamental experiments on evaporation of cesium in ion sources. *Review of Scientific Instruments.* 2010, **81**(2), p.02B102.
90. Deer, W., Howie, R., Wise, W. and Zussman, J. Rock-forming minerals, 4B. *Framework silicates: Silica minerals, feldspathoids and the zeolites.* 2004.

91. Koyama, K. and Takeuchi, Y. Clinoptilolite: the distribution of potassium atoms and its role in thermal stability. *Zeitschrift für Kristallographie-Crystalline Materials.* 1977, **145**(1-6), pp.216-239.
92. Wise, W., WJ, N. and Kokinos, M. Clinoptilolite and ferrierite from Agoura, California. *American Mineralogist.* 1969, **54**(5-6), pp.887-&.
93. Ming, D.W. and Dixon, J.B. Clinoptilolite in south Texas soils. *Soil Science Society of America Journal.* 1986, **50**(6), pp.1618-1622.
94. Braithwaite, R. Geological and mineralogical characterization of zeolites in lacustrine tuffs, Ngakuru, Taupo Volcanic Zone, New Zealand. *Clays and Clay Minerals.* 2003, **51**(6), pp.589-598.
95. Polatoğlu, İ. *Chemical behaviour of clinoptilolite rich natural zeolite in aqueous medium*. thesis, Citeseer, 2005.
96. Kulprathipanja, S. *Zeolites in industrial separation and catalysis.* John Wiley & Sons, 2010.
97. Favvas, E.P., Tsanaktsidis, C.G., Sapalidis, A.A., Tzilantonis, G.T., Papageorgiou, S.K. and Mitropoulos, A.C. Clinoptilolite, a natural zeolite material: Structural characterization and performance evaluation on its dehydration properties of hydrocarbon-based fuels. *Microporous and Mesoporous Materials.* 2016, **225**, pp.385-391.
98. Shadrikov, A. and Petukhov, A. Natural zeolite-clinoptilolite characteristics determination and modification. 2014.
99. Kraljević Pavelić, S., Simović Medica, J., Gumbarević, D., Filošević, A., Pržulj, N. and Pavelić, K. Critical Review on Zeolite Clinoptilolite Safety and Medical Applications in vivo. *Frontiers in pharmacology.* 2018, **9**, pp.1350-1350.
100. Huang, Y., Wang, W., Feng, Q. and Dong, F. Preparation of magnetic clinoptilolite/CoFe2O4 composites for removal of Sr2+ from aqueous solutions: kinetic, equilibrium, and thermodynamic studies. *Journal of Saudi Chemical Society.* 2013.
101. Li, Y., Bai, P., Yan, Y., Yan, W., Shi, W. and Xu, R. Removal of Zn2+, Pb2+, Cd2+, and Cu2+ from aqueous solution by synthetic clinoptilolite. *Microporous and Mesoporous Materials.* 2019, **273**, pp.203-211.
102. Kocasoy, G. and Şahin, V. Heavy metal removal from industrial wastewater by clinoptilolite. *Journal of Environmental Science and Health Part A.* 2007, **42**(14), pp.2139-2146.
103. Günay, A., Arslankaya, E. and Tosun, I. Lead removal from aqueous solution by natural and pretreated clinoptilolite: adsorption equilibrium and kinetics. *Journal of Hazardous materials.* 2007, **146**(1-2), pp.362-371.
104. Bektaş, N. and Kara, S. Removal of lead from aqueous solutions by natural clinoptilolite: equilibrium and kinetic studies. *Separation and Purification Technology.* 2004, **39**(3), pp.189-200.
105. Petrus, R. and Warchoł, J.K. Heavy metal removal by clinoptilolite. An equilibrium study in multi-component systems. *Water Research.* 2005, **39**(5), pp.819-830.
106. Petrus, R. and Warchoł, J. Ion exchange equilibria between clinoptilolite and aqueous solutions of Na+/Cu 2+, Na+/Cd 2+ and Na+/Pb 2+. *Microporous and Mesoporous Materials.* 2003, **61**(1), pp.137-146.

107. Camacho, L.M., Parra, R.R. and Deng, S. Arsenic removal from groundwater by MnO 2-modified natural clinoptilolite zeolite: effects of pH and initial feed concentration. *Journal of Hazardous materials.* 2011, **189**(1), pp.286-293.
108. Mamba, B., Nyembe, D. and Mulaba-Bafubiandi, A. The effect of conditioning with NaCl, KCl and HCl on the performance of natural clinoptilolite's removal efficiency of Cu2+ and Co2+ from Co/Cu synthetic solutions. *Water SA.* 2010, **36**(4), pp.0-0.
109. Charkhi, A., Kazemian, H. and Kazemeini, M. Optimized experimental design for natural clinoptilolite zeolite ball milling to produce nano powders. *Powder Technology.* 2010, **203**(2), pp.389-396.
110. Mansouri, N., Rikhtegar, N., Panahi, H.A., Atabi, F. and Shahraki, B.K. Porosity, Characterization and structural properties of natural zeolite-clinoptilolite-as a sorbent. *Environment Protection Engineering.* 2013, **39**(1).
111. Inglezakis, V.J. The concept of “capacity” in zeolite ion-exchange systems. *Journal of Colloid and Interface Science.* 2005, **281**(1), pp.68-79.
112. Wang, S. and Peng, Y. Natural zeolites as effective adsorbents in water and wastewater treatment. *Chemical Engineering Journal.* 2010, **156**(1), pp.11-24.
113. Yosefi, L., Haghighi, M., Allahyari, S. and Ashkriz, S. The beneficial use of HCl-activated natural zeolite in ultrasound assisted synthesis of Cu/clinoptilolite–CeO2 nanocatalyst used for catalytic oxidation of diluted toluene in air at low temperature. *Journal of Chemical Technology and Biotechnology.* 2015, **90**(4), pp.765-774.
114. Wang, X. and Nguyen, A.V. Characterisation of electrokinetic properties of clinoptilolite before and after activation by sulphuric acid for treating CSG water. *Microporous and Mesoporous Materials.* 2016, **220**, pp.175-182.
115. Dyer, A. An introduction to zeolite molecular sieves. 1988.
116. Sobolev, I.A., Dmitriev, S.A., Lifanov, F.A., Varlakov, A.P. and A., K.E. Results of Testing The Pilot Plant For Cementation of Radioactive Waste. In: *WM'99 CONFERENCE*, *February 28 - March 4, 1999*, *Arizona*. WM Symposia, Inc, 1999, pp.59-63.
117. Lihareva, N., Petrov, O., Tzvetanova, Y., Kadiyski, M. and Nikashina, V.A. Evaluation of the possible use of a Bulgarian clinoptilolite for removing strontium from water media. *Clay Minerals.* 2015, **50**(1), pp.55-64.
118. Akar, D. *Physicochemical characterization of the sorption behavior of Cs+ and Sr2+ Ions on natural kaolinite and cliptilolite minerals*. Master thesis, İzmir Institute of Technology, 2005.
119. Ma, B., Oh, S., Shin, W.S. and Choi, S.-J. Removal of Co2+, Sr2+ and Cs+ from aqueous solution by phosphate-modified montmorillonite (PMM). *Desalination.* 2011, **276**(1-3), pp.336-346.
120. Hwang, K.S., Park, C.W., Lee, K.-W., Park, S.-J. and Yang, H.-M. Highly efficient removal of radioactive cesium by sodium-copper hexacyanoferrate-modified magnetic nanoparticles. *Colloids and*

Surfaces A: Physicochemical and Engineering Aspects. 2017, **516**, pp.375-382.
121. NDA. *Ion Exchange Material (Clinoptilolite) and Sand.* Cumbria: Nuclear Decommissioning Authority, 2013.
122. Nightingale Jr, E. Phenomenological theory of ion solvation. Effective radii of hydrated ions. *The Journal of Physical Chemistry.* 1959, **63**(9), pp.1381-1387.
123. Ames Jr, L. *Characterization of a strontium-selective zeolite.* General Electric Co. Hanford Atomic Products Operation, Richland, Wash., 1961.
124. Inglezakis, V.J. and Zorpas, A.A. Heat of adsorption, adsorption energy and activation energy in adsorption and ion exchange systems. *Desalination and Water Treatment.* 2012, **39**(1-3), pp.149-157.
125. Rhodes, M.J. *Introduction to particle technology.* John Wiley & Sons, 2008.
126. Faghihian, H., Iravani, M. and Moayed, M. Application of PAN-NaY Composite for CS+ and SR2+ Adsorption: Kinetic and Thermodynamic Studies. *Environmental Progress & Sustainable Energy.* 2015, **34**(4), pp.999-1008.
127. Rani, R.D. and Sasidhar, P. Sorption of cesium on clay colloids: kinetic and thermodynamic studies. *Aquatic geochemistry.* 2012, **18**(4), pp.281-296.
128. El-Batouti, M., Sadek, O.M. and Assaad, F.F. Kinetics and thermodynamics studies of copper exchange on Na–montmorillonite clay mineral. *Journal of Colloid and Interface Science.* 2003, **259**(2), pp.223-227.
129. El-Batouti, M., Zaghloul, A.A. and Hanna, M.T. A Kinetic Study of the Copper Exchange Reaction on a Sodium-Montmorillonite Clay Mineral in Acetonitrile and Dimethylformamide. *Journal of Colloid and Interface Science.* 1996, **180**(1), pp.106-110.
130. Ben-Tal, N., Honig, B., Bagdassarian, C.K. and Ben-Shaul, A. Association Entropy in Adsorption Processes. *Biophysical Journal.* 2000, **79**(3), pp.1180-1187.
131. Azizian, S. Kinetic models of sorption: a theoretical analysis. *Journal of Colloid and Interface Science.* 2004, **276**(1), pp.47-52.
132. Jaskūnas, A., Subačius, B. and Šlinkšienė, R. Adsorption of potassium ions on natural zeolite: kinetic and equilibrium studies. *chemija.* 2015, **26**(2), pp.69-78.
133. Guo, X., Li, X. and Park, H.-S. Ammonium and potassium removal for anaerobically digested wastewater using natural clinoptilolite followed by membrane pretreatment. *Journal of Hazardous materials.* 2008, **151**(1), pp.125-133.
134. Jha, V.K. and Hayashi, S. Modification on natural clinoptilolite zeolite for its NH 4+ retention capacity. *Journal of Hazardous materials.* 2009, **169**(1), pp.29-35.
135. Jorgensen, S., Libor, O., Graber, K.L. and Barkacs, K. Ammonia removal by use of clinoptilolite. *Water Research.* 1976, **10**(3), pp.213-224.
136. Rodríguez-Iznaga, I., Petranovskii, V. and Rodríguez-Fuentes, G. Ion-exchange of amino-and aqua-complexes of nickel and cobalt in natural

clinoptilolite. *Journal of Environmental Chemical Engineering.* 2014, **2**(3), pp.1221-1227.
137. Xu, W., Li, L.Y. and Grace, J.R. Dealumination of clinoptilolite and its effect on zinc removal from acid rock drainage. *Chemosphere.* 2014, **111**, pp.427-433.
138. Arifi, A. and Hanafi, H. Adsorption of cesium, thallium, strontium and cobalt radionuclides using activated carbon. *Asian Journal of Chemistry.* 2011, **23**(1), p.111.
139. Mimura, H. and Kanno, T. Distribution and fixation of cesium and strontium in zeolite A and chabazite. *Journal of Nuclear Science and Technology.* 1985, **22**(4), pp.284-291.
140. Singh, O.V. and Tandon, S. Studies on the adsorption of cesium and strontium radionuclides on hydrated manganese oxide. *The International journal of applied radiation and isotopes.* 1977, **28**(8), pp.701-704.
141. Cornell, R. Adsorption of cesium on minerals: a review. *Journal of Radioanalytical and Nuclear Chemistry.* 1993, **171**(2), pp.483-500.
142. El-Kamash, A., El-Naggar, M. and El-Dessouky, M. Immobilization of cesium and strontium radionuclides in zeolite-cement blends. *Journal of Hazardous materials.* 2006, **136**(2), pp.310-316.
143. Zhang, H., Zhao, X., Wei, J. and Li, F. Removal of cesium from low-level radioactive wastewaters using magnetic potassium titanium hexacyanoferrate. *Chemical Engineering Journal.* 2015, **275**, pp.262-270.
144. Lagergren, S. *Zur theorie der sogenannten absorption gelöster stoffe.* PA Norstedt & söner, 1898.
145. Yuh-Shan, H. Citation review of Lagergren kinetic rate equation on adsorption reactions. *Scientometrics.* 2004, **59**(1), pp.171-177.
146. Ho, Y.-S. and McKay, G. Pseudo-second order model for sorption processes. *Process Biochemistry.* 1999, **34**(5), pp.451-465.
147. Ho, Y.-S. Review of second-order models for adsorption systems. *Journal of Hazardous materials.* 2006, **136**(3), pp.681-689.
148. Shahwan, T. Sorption kinetics: Obtaining a pseudo-second order rate equation based on a mass balance approach. *Journal of Environmental Chemical Engineering.* 2014, **2**(2), pp.1001-1006.
149. Hassan, N.M., Nash, C.A., Hardy, B.J. and Marra, J.C. Evaluating the residence time for cesium removal from simulated Hanford tank wastes using SuperLig® 644 resin. *Journal of Radioanalytical and Nuclear Chemistry.* 2003, **258**(3), pp.487-495.
150. Wahlberg, J. and Fishman, M.J. *Adsorption of cesium on clay minerals.* US Government Printing Office, 1962.
151. Chino, M., Nakayama, H., Nagai, H., Terada, H., Katata, G. and Yamazawa, H. Preliminary estimation of release amounts of 131I and 137Cs accidentally discharged from the Fukushima Daiichi nuclear power plant into the atmosphere. *Journal of Nuclear Science and Technology.* 2011, **48**(7), pp.1129-1134.
152. Kato, H., Onda, Y. and Teramage, M. Depth distribution of 137 Cs, 134 Cs, and 131 I in soil profile after Fukushima Dai-ichi Nuclear Power Plant accident. *Journal of environmental radioactivity.* 2012, **111**, pp.59-64.

153. Ueda, S., Hasegawa, H., Kakiuchi, H., Akata, N., Ohtsuka, Y. and Hisamatsu, S.i. Fluvial discharges of radiocaesium from watersheds contaminated by the Fukushima Dai-ichi Nuclear Power Plant accident, Japan. *Journal of environmental radioactivity.* 2013, **118**, pp.96-104.
154. Mavros, P. and Matis, K.A. *Innovations in flotation technology.* Dordrecht: Springer Netherlands, 2013.
155. Zhang, M., Lu, X., Zhou, Q., Xie, L. and Shen, C. Polyaluminum chloride-functionalized colloidal gas aphrons for flotation separation of nanoparticles from water. *Journal of Hazardous materials.* 2019, **362**, pp.196-205.
156. Atkin, R., Craig, V., Wanless, E.J. and Biggs, S. Mechanism of cationic surfactant adsorption at the solid–aqueous interface. *Advances in Colloid and Interface Science.* 2003, **103**(3), pp.219-304.
157. Rao, S.R. *Surface Chemistry of Froth Flotation: Volume 1: Fundamentals.* Springer Science & Business Media, 2013.
158. Chang, L., Cao, Y., Fan, G., Li, C. and Peng, W. A review of the applications of ion floatation: wastewater treatment, mineral beneficiation and hydrometallurgy. *RSC Advances.* 2019, **9**(35), pp.20226-20239.
159. Mohammed, A.A., Ebrahim, S.E. and Alwared, A.I. Flotation and sorptive-flotation methods for removal of lead ions from wastewater using SDS as surfactant and barley husk as biosorbent. *Journal of Chemistry.* 2013, **2013**.
160. Mahmoud, M.R., Lazaridis, N.K. and Matis, K.A. Study of flotation conditions for cadmium (II) removal from aqueous solutions. *Process Safety and Environmental Protection.* 2015, **94**, pp.203-211.
161. Fu, F. and Wang, Q. Removal of heavy metal ions from wastewaters: A review. *Journal of Environmental Management.* 2011, **92**(3), pp.407-418.
162. Huang, Y., Takaoka, M., Takeda, N. and Oshita, K. Polychlorinated biphenyls removal from weathered municipal solid waste incineration fly ash by collector-assisted column flotation. *Journal of Hazardous materials.* 2003, **100**(1), pp.259-270.
163. Polat, H. and Erdogan, D. Heavy metal removal from waste waters by ion flotation. *Journal of Hazardous materials.* 2007, **148**(1), pp.267-273.
164. Le, T.N., Phan, C.M., Nguyen, A.V. and Ang, H.M. An unusual synergistic adsorption of MIBC and CTAB mixtures at the air–water interface. *Minerals Engineering.* 2012, **39**, pp.255-261.
165. Hunter, T.N., Pugh, R.J., Franks, G.V. and Jameson, G.J. The role of particles in stabilising foams and emulsions. *Advances in Colloid and Interface Science.* 2008, **137**(2), pp.57-81.
166. Rahman, R.M., Ata, S. and Jameson, G.J. The effect of flotation variables on the recovery of different particle size fractions in the froth and the pulp. *International Journal of Mineral Processing.* 2012, **106**, pp.70-77.
167. Zamboulis, D., Pataroudi, S., Zouboulis, A. and Matis, K. The application of sorptive flotation for the removal of metal ions. *Desalination.* 2004, **162**, pp.159-168.
168. Fainerman, V.B., Miller, R., Wüstneck, R. and Makievski, A.V. Adsorption isotherm and surface tension equation for a surfactant with changing

partial molar area. 1. Ideal Surface Layer. *The Journal of Physical Chemistry.* 1996, **100**(18), pp.7669-7675.
169. Farrokhpay, S. The significance of froth stability in mineral flotation—A review. *Advances in Colloid and Interface Science.* 2011, **166**(1-2), pp.1-7.
170. Doyle, F.M. Ion flotation—its potential for hydrometallurgical operations. *International Journal of Mineral Processing.* 2003, **72**(1), pp.387-399.
171. Rao, S.R. Flotation Surfactants. In: *Surface Chemistry of Froth Flotation: Volume 1: Fundamentals*. Boston, MA: Springer US, 2004, pp.385-478.
172. Zouboulis, A., Peleka, E., Zamboulis, D. and Matis, K. Application of Flotation for the Separation of Metal-Loaded Resins. *Separation Science and Technology.* 2005, **40**(4), pp.861-876.
173. Ersoy, B. and Çelik, M.S. Electrokinetic properties of clinoptilolite with mono-and multivalent electrolytes. *Microporous and Mesoporous Materials.* 2002, **55**(3), pp.305-312.
174. Song, W., Shi, T., Yang, D., Ye, J., Zhou, Y. and Feng, Y. Pretreatment effects on the sorption of Cr(VI) onto surfactant-modified zeolite: Mechanism analysis. *Journal of Environmental Management.* 2015, **162**, pp.96-101.
175. Li, Z. and Bowman, R.S. Counterion effects on the sorption of cationic surfactant and chromate on natural clinoptilolite. *Environmental Science & Technology.* 1997, **31**(8), pp.2407-2412.
176. Grieves, R.B. Foam Separations for Industrial Wastes: Process Selection. *Journal (Water Pollution Control Federation).* 1970, **42**(8), pp.R336-R344.
177. Grieves, R.B. Foam separations: A review. *The Chemical Engineering Journal.* 1975, **9**(2), pp.93-106.
178. Matis, K.A., Zouboulis, A.I., Gallios, G.P., Erwe, T. and Blöcher, C. Application of flotation for the separation of metal-loaded zeolites. *Chemosphere.* 2004, **55**(1), pp.65-72.
179. NCBI. *PubChem Database.* [Online]. [Accessed Aug. 30, 2019]. Available from: https://pubchem.ncbi.nlm.nih.gov/compound/
180. McDonald, C. and Taheri, S. Ion flotation of cadmium using ethylhexadecyldimethylammonium bromide. *Microchemical Journal.* 1979, **24**(4), pp.553-559.
181. Moore, P. and Phillips, C.R. An Equilibrium Study of Reactions Involving a Cationic Surfactant and Various Counterions: Prediction of Ion Selectivity. *Separation Science.* 1974, **9**(4), pp.325-336.
182. Hoseinian, F.S., Irannajad, M. and Nooshabadi, A.J. Ion flotation for removal of Ni(II) and Zn(II) ions from wastewaters. *International Journal of Mineral Processing.* 2015, **143**, pp.131-137.
183. Walcarius, A., Lamdaouar, A.M., El Kacemi, K., Marouf, B. and Bessiere, J. Recovery of lead-loaded zeolite particles by flotation. *Langmuir.* 2001, **17**(7), pp.2258-2264.
184. Nguyen, A.V., Schulze, H.J. and Ralston, J. Elementary steps in particle—bubble attachment. *International Journal of Mineral Processing.* 1997, **51**(1), pp.183-195.

185. Nguyen, A.V., Ralston, J. and Schulze, H.J. On modelling of bubble–particle attachment probability in flotation. *International Journal of Mineral Processing.* 1998, **53**(4), pp.225-249.
186. Nguyen Van, A. On the sliding time in flotation. *International Journal of Mineral Processing.* 1993, **37**(1), pp.1-25.
187. Verrelli, D.I., Koh, P.T.L. and Nguyen, A.V. Particle–bubble interaction and attachment in flotation. *Chemical Engineering Science.* 2011, **66**(23), pp.5910-5921.
188. Wang, G., Nguyen, A.V., Mitra, S., Joshi, J.B., Jameson, G.J. and Evans, G.M. A review of the mechanisms and models of bubble-particle detachment in froth flotation. *Separation and Purification Technology.* 2016, **170**, pp.155-172.
189. Sven-Nilsson, I. Einfluß der Berührungszeit zwischen Mineral und Luftblase bei der Flotation. *Kolloid-Zeitschrift.* 1934, **69**(2), pp.230-232.
190. Xing, Y., Gui, X., Pan, L., Pinchasik, B.-E., Cao, Y., Liu, J., Kappl, M. and Butt, H.-J. Recent experimental advances for understanding bubble-particle attachment in flotation. *Advances in Colloid and Interface Science.* 2017, **246**, pp.105-132.
191. Albijanic, B., Ozdemir, O., Hampton, M.A., Nguyen, P.T., Nguyen, A.V. and Bradshaw, D. Fundamental aspects of bubble–particle attachment mechanism in flotation separation. *Minerals Engineering.* 2014, **65**, pp.187-195.
192. Klimpel, R.R. and Hansen, R.D. The interaction of flotation chemistry and size reduction in the recovery of a porphyry copper ore. *International Journal of Mineral Processing.* 1988, **22**(1), pp.169-181.
193. Klimpel, R.R. and Isherwood, S. Some industrial implications of changing frother chemical structure. *International Journal of Mineral Processing.* 1991, **33**(1), pp.369-381.
194. Wang, J., Li, G., Hu, S., Zhao, L. and Cao, Y. Influence of gas flow rate and surfactant concentration on SDBS foam properties. *Energy Sources, Part A: Recovery, Utilization, and Environmental Effects.* 2019, **41**(16), pp.2039-2049.
195. Darton, R.C. and Sun, K.H. The effect of surfactant on foam and froth properties. *Chemical Engineering Research and Design.* 1999, **77**(6), pp.535-542.
196. Mahmoud, M.R., Soliman, M.A. and Rashad, G.M. Performance appraisal of foam separation technology for removal of Co(II)-EDTA complexes intercalated into in-situ formed Mg-Al layered double hydroxide from radioactive liquid waste. *Chemical Engineering Journal.* 2017, **326**, pp.781-793.
197. Ata, S. Phenomena in the froth phase of flotation — A review. *International Journal of Mineral Processing.* 2012, **102-103**, pp.1-12.
198. George, P., Nguyen, A.V. and Jameson, G.J. Assessment of true flotation and entrainment in the flotation of submicron particles by fine bubbles. *Minerals Engineering.* 2004, **17**(7), pp.847-853.
199. Stevenson, P., Mantle, M.D., Sederman, A.J. and Gladden, L.F. Quantitative measurements of liquid holdup and drainage in foam using NMRI. *AIChE Journal.* 2007, **53**(2), pp.290-296.

200. Siddiqui, F.A. and Franses, E.I. Surface tension and adsorption synergism for solutions of binary surfactants. *Industrial & Engineering Chemistry Research.* 1996, **35**(9), pp.3223-3232.
201. Phan, C.M., Nguyen, C.V., Yusa, S.-i. and Yamada, N.L. Synergistic adsorption of MIBC/CTAB mixture at the air/water interface and applicability of Gibbs adsorption equation. *Langmuir.* 2014, **30**(20), pp.5790-5796.
202. Tan, S.N., Pugh, R.J., Fornasiero, D., Sedev, R. and Ralston, J. Foaming of polypropylene glycols and glycol/MIBC mixtures. *Minerals Engineering.* 2005, **18**(2), pp.179-188.
203. Norori-McCormac, A., Brito-Parada, P., Hadler, K., Cole, K. and Cilliers, J. The effect of particle size distribution on froth stability in flotation. *Separation and Purification Technology.* 2017, **184**, pp.240-247.
204. Woodburn, E.T., King, R.P. and Colborn, R.P. The effect of particle size distribution on the performance of a phosphate flotation process. *Metallurgical and Materials Transactions B.* 1971, **2**(11), pp.3163-3174.
205. Metwally, S.S., El-Sherief, E.A. and Mekhamer, H.S. Fixed-bed column for the removal of cesium, strontium, and lead ions from aqueous solutions using brick kiln waste. *Separation Science and Technology.* 2020, **55**(4), pp.635-647.
206. Foster, R.I., Amphlett, J.T.M., Kim, K.-W., Kerry, T., Lee, K.-Y. and Sharrad, C.A. SOHIO Process Legacy Waste Treatment: Uranium Recovery Using Ion Exchange. *Journal of Industrial and Engineering Chemistry.* 2019.
207. Araneda, C., Basualto, C., Sapag, J., C.Tapia, Cotorás, D. and Valenzuela, F. Uptake of copper (II) ions from acidic aqueous solutions using a continuous column packed with microcapsules containing a β-hydroxyoximic compound. *Chemical Engineering Research and Design.* 2011, **89**(12), pp.2761-2769.
208. Han, R., Wang, Y., Yu, W., Zou, W., Shi, J. and Liu, H. Biosorption of methylene blue from aqueous solution by rice husk in a fixed-bed column. *Journal of Hazardous materials.* 2007, **141**(3), pp.713-718.
209. Kumar, U. and Bandyopadhyay, M. Fixed bed column study for Cd(II) removal from wastewater using treated rice husk. *Journal of Hazardous materials.* 2006, **129**(1), pp.253-259.
210. Luo, X., Deng, Z., Lin, X. and Zhang, C. Fixed-bed column study for Cu2+ removal from solution using expanding rice husk. *Journal of Hazardous materials.* 2011, **187**(1), pp.182-189.
211. Medvidović, N.V., Perić, J. and Trgo, M. Column performance in lead removal from aqueous solutions by fixed bed of natural zeolite–clinoptilolite. *Separation and Purification Technology.* 2006, **49**(3), pp.237-244.
212. Robshaw, T.J., Dawson, R., Bonser, K. and Ogden, M.D. Towards the implementation of an ion-exchange system for recovery of fluoride commodity chemicals. Kinetic and dynamic studies. *Chemical Engineering Journal.* 2019, **367**, pp.149-159.
213. Zhang, W., Dong, L., Yan, H., Li, H., Jiang, Z., Kan, X., Yang, H., Li, A. and Cheng, R. Removal of methylene blue from aqueous solutions by

straw based adsorbent in a fixed-bed column. *Chemical Engineering Journal.* 2011, **173**(2), pp.429-436.
214. Ararem, A., Bouzidi, A., Mohamedi, B. and Bouras, O. Modeling of fixed-bed adsorption of Cs+ and Sr2+ onto clay–iron oxide composite using artificial neural network and constant–pattern wave approach. *Journal of Radioanalytical and Nuclear Chemistry.* 2014, **301**(3), pp.881-887.
215. McCabe, D.J. Comprehensive Scale Testing of the Ion Exchange Removal of Cesium and Technetium from Hanford Tank Wastes. In: *WM'01 Conference*, *Arizona*. 2001.
216. Valisko, M., Boda, D. and Gillespie, D. Selective adsorption of ions with different diameter and valence at highly charged interfaces. *The Journal of Physical Chemistry C.* 2007, **111**(43), pp.15575-15585.
217. Chu, K.H. Fixed bed sorption: Setting the record straight on the Bohart–Adams and Thomas models. *Journal of Hazardous materials.* 2010, **177**(1), pp.1006-1012.
218. Han, R., Wang, Y., Zou, W., Wang, Y. and Shi, J. Comparison of linear and nonlinear analysis in estimating the Thomas model parameters for methylene blue adsorption onto natural zeolite in fixed-bed column. *Journal of Hazardous materials.* 2007, **145**(1), pp.331-335.
219. Thomas, H.C. Heterogeneous Ion Exchange in a Flowing System. *Journal of the American Chemical Society.* 1944, **66**(10), pp.1664-1666.
220. Yan, G., Viraraghavan, T. and Chen, M. A New Model for Heavy Metal Removal in a Biosorption Column. *Adsorption Science & Technology.* 2001, **19**(1), pp.25-43.
221. Sana, D. and Jalila, S. A comparative study of adsorption and regeneration with different agricultural wastes as adsorbents for the removal of methylene blue from aqueous solution. *Chinese Journal of Chemical Engineering.* 2017, **25**(9), pp.1282-1287.
222. Lee, C.-G., Kim, J.-H., Kang, J.-K., Kim, S.-B., Park, S.-J., Lee, S.-H. and Choi, J.-W. Comparative analysis of fixed-bed sorption models using phosphate breakthrough curves in slag filter media. *Desalination and Water Treatment.* 2015, **55**(7), pp.1795-1805.
223. Stankiewicz, A.I. and Moulijn, J.A. Process intensification: transforming chemical engineering. *Chemical Engineering Progress.* 2000, **96**(1), pp.22-34.
224. Wang, H., Mustaffar, A., Phan, A.N., Zivkovic, V., Reay, D., Law, R. and Boodhoo, K. A review of process intensification applied to solids handling. *Chemical Engineering and Processing: Process Intensification.* 2017, **118**, pp.78-107.
225. Derksen, J.J. Mixing in an agitated tubular reactor. *The Canadian Journal of Chemical Engineering.* 2019, **97**(2), pp.523-527.
226. Owens, S., Higgins-Bos, M., Bankhead, M. and Austin, J. Using chemical and process modelling to design, understand and improve an effluent treatment plant. *NNL Science.* 2015, **3**(3), pp.1-13.
227. Djukić, A., Jovanović, U., Tuvić, T., Andrić, V., Novaković, J.G., Ivanović, N. and Matović, L. The potential of ball-milled Serbian natural clay for removal of heavy metal contaminants from wastewaters: Simultaneous sorption of Ni, Cr, Cd and Pb ions. *Ceramics International.* 2013, **39**(6), pp.7173-7178.

228. Vhahangwele, M. and Mugera, G.W. The potential of ball-milled South African bentonite clay for attenuation of heavy metals from acidic wastewaters: Simultaneous sorption of Co2+, Cu2+, Ni2+, Pb2+, and Zn2+ ions. *Journal of Environmental Chemical Engineering.* 2015, **3**(4), pp.2416-2425.
229. Cheng, S., Syamsiro, M. and Yoshikawa, K. Effect of HCl Pretreatment on the Performance of Natural Zeolite in a two-stage Pyrolysis and Catalytic Reforming of Polypropylene and Polystyrene. In: *The 19th Research Debate*, *Kitakyushu*. 2016.
230. Wu, F.-C., Tseng, R.-L., Huang, S.-C. and Juang, R.-S. Characteristics of pseudo-second-order kinetic model for liquid-phase adsorption: A mini-review. *Chemical Engineering Journal.* 2009, **151**(1), pp.1-9.
231. Rafiqi, F.A. and Majid, K. Removal of copper from aqueous solution using polyaniline and polyaniline/ferricyanide composite. *Journal of Environmental Chemical Engineering.* 2015, **3**(4), pp.2492-2501.
232. Gupta, N. and Sen, R. Kinetic and equilibrium modelling of Cu (II) adsorption from aqueous solution by chemically modified Groundnut husk (Arachis hypogaea). *Journal of Environmental Chemical Engineering.* 2017, **5**(5), pp.4274-4281.
233. Cotruvo, J.A. *Water Desalination Processes and Associated Health and Environmental Issues.* [Online]. 2005. [Accessed 28 December 2017]. Available from: http://www.wcponline.com/2005/01/31/water-desalination-processes-associated-health-environmental-issues/
234. Maleki, S. and Karimi-Jashni, A. Effect of ball milling process on the structure of local clay and its adsorption performance for Ni (II) removal. *Applied Clay Science.* 2017, **137**, pp.213-224.
235. Kosanović, C., Subotić, B. and Čižmek, A. Thermal analysis of cation-exchanged zeolites before and after their amorphization by ball milling. *Thermochimica Acta.* 1996, **276**, pp.91-103.
236. Zielinski, P., Van Neste, A., Akolekar, D. and Kaliaguine, S. Effect of high-energy ball milling on the structural stability, surface and catalytic properties of small-, medium-and large-pore zeolites. *Microporous Materials.* 1995, **5**(3), pp.123-133.
237. Sprynskyy, M., Buszewski, B., Terzyk, A.P. and Namieśnik, J. Study of the selection mechanism of heavy metal (Pb2+, Cu2+, Ni2+, and Cd2+) adsorption on clinoptilolite. *Journal of Colloid and Interface Science.* 2006, **304**(1), pp.21-28.
238. Dziedzicka, A., Sulikowski, B. and Ruggiero-Mikołajczyk, M. Catalytic and physicochemical properties of modified natural clinoptilolite. *Catalysis Today.* 2016, **259**, pp.50-58.
239. Korkuna, O., Leboda, R., Skubiszewska-Zie, J., Vrublevs'ka, T., Gun'ko, V. and Ryczkowski, J. Structural and physicochemical properties of natural zeolites: clinoptilolite and mordenite. *Microporous and Mesoporous Materials.* 2006, **87**(3), pp.243-254.
240. Erdoğan, B., Sakızcı, M. and Yörükoğulları, E. Characterization and ethylene adsorption of natural and modified clinoptilolites. *Applied Surface Science.* 2008, **254**(8), pp.2450-2457.

241. Marco, J.F., Gracia, M., Gancedo, J.R., González-Carreño, T., Arcoya, A. and Seoane, X.L. On the state of iron in a clinoptilolite. *Hyperfine Interactions.* 1995, **95**(1), pp.53-70.
242. Kim, Y., Kim, Y.K., Kim, S., Harbottle, D. and Lee, J.W. Nanostructured potassium copper hexacyanoferrate-cellulose hydrogel for selective and rapid cesium adsorption. *Chemical Engineering Journal.* 2017, **313**, pp.1042-1050.
243. Kim, Y.K., Kim, Y., Kim, S., Harbottle, D. and Lee, J.W. Solvent-assisted synthesis of potassium copper hexacyanoferrate embedded 3D-interconnected porous hydrogel for highly selective and rapid cesium ion removal. *Journal of Environmental Chemical Engineering.* 2017, **5**(1), pp.975-986.
244. Munthali, M., Johan, E., Aono, H. and Matsue, N. Cs+ and Sr2+ adsorption selectivity of zeolites in relation to radioactive decontamination. *Journal of Asian Ceramic Societies.* 2015, **3**(3), pp.245-250.
245. Başçetin, E. and Atun, G.l. Adsorptive removal of strontium by binary mineral mixtures of montmorillonite and zeolite. *Journal of Chemical & Engineering Data.* 2009, **55**(2), pp.783-788.
246. Endo, M., Yoshikawa, E., Muramatsu, N., Takizawa, N., Kawai, T., Unuma, H., Sasaki, A., Masano, A., Takeyama, Y. and Kahara, T. The removal of cesium ion with natural Itaya zeolite and the ion exchange characteristics. *Journal of Chemical Technology & Biotechnology.* 2013, **88**(9), pp.1597-1602.
247. Leyva-Ramos, R., Aguilar-Armenta, G., Gonzalez-Gutierrez, L.V., Guerrero-Coronado, R.M. and Mendoza-Barron, J. Ammonia exchange on clinoptilolite from mineral deposits located in Mexico. *Journal of Chemical Technology and Biotechnology.* 2004, **79**(6), pp.651-657.
248. Moharir, A., Kunzru, D. and Saraf, D. Effect of adsorbent particle size distribution on breakthrough curves for molecular sieve columns. *Chemical Engineering Science.* 1980, **35**(8), pp.1795-1801.
249. Kaushal, D., Sato, K., Toyota, T., Funatsu, K. and Tomita, Y. Effect of particle size distribution on pressure drop and concentration profile in pipeline flow of highly concentrated slurry. *International Journal of Multiphase Flow.* 2005, **31**(7), pp.809-823.
250. Mikoda, B., Gruszecka-Kosowska, A. and Klimek, A. Copper flotation waste from KGHM as potential sorbent for heavy metal removal from aqueous solutions. *Human and Ecological Risk Assessment: An International Journal.* 2017, **23**(7), pp.1610-1628.
251. S, G., Giannakopoulou, F., Gasparatos, D. and Massas, I. Potassium Solution Concentration Effect on Cs Sorption in An Acid Soil. In: *Protection and Restoration of the Environment XI*, *Greece*. Greece, 2012, pp.740-747.
252. Mimura, H., Ishihara, Y. and Akiba, K. Adsorption behavior of americium on zeolites. *Journal of Nuclear Science and Technology.* 1991, **28**(2), pp.144-151.
253. Rashad, G.M., Mahmoud, M.R. and Soliman, M.A. Combination of coprecipitation and foam separation processes for rapid recovery and

preconcentration of cesium radionuclides from water systems. *Process Safety and Environmental Protection.* 2019, **130**, pp.163-173.
254. Hu, N., Shu, T., Wu, Z., Liu, G., Li, Z., Zhao, Y., Yin, H. and Huang, D. BS12-assisted flotation for the intensification of SNPs separation from CMP wastewater using a novel flotation column. *Journal of Hazardous materials.* 2018, **344**, pp.788-796.
255. Karimi, H., Ghaedi, M., Shokrollahi, A., Rajabi, H.R., Soylak, M. and Karami, B. Development of a selective and sensitive flotation method for determination of trace amounts of cobalt, nickel, copper and iron in environmental samples. *Journal of Hazardous materials.* 2008, **151**(1), pp.26-32.
256. Dhenain, A., Mercier, G., Blais, J.-F. and Chartier, M. Combined column and cell flotation process for the treatment of PAH contaminated hazardous wastes produced by an aluminium production plant. *Journal of Hazardous materials.* 2009, **165**(1), pp.394-407.
257. Han, B., Altansukh, B., Haga, K., Stevanović, Z., Jonović, R., Avramović, L., Urosević, D., Takasaki, Y., Masuda, N., Ishiyama, D. and Shibayama, A. Development of copper recovery process from flotation tailings by a combined method of high–pressure leaching–solvent extraction. *Journal of Hazardous materials.* 2018, **352**, pp.192-203.
258. James, E., Tangparitkul, S., Brooker, A., Amador, C., Graydon, A., Vaccaro, M., Cayre, O.J., Hunter, T.N. and Harbottle, D. Accelerated spreading of inviscid droplets prompted by the yielding of strongly elastic interfacial films. *Colloids and Surfaces A: Physicochemical and Engineering Aspects.* 2018, **554**, pp.326-333.
259. Stanimirova, R., Marinova, K., Tcholakova, S., Denkov, N., Stoyanov, S. and Pelan, E. Surface rheology of saponin adsorption layers. *Langmuir.* 2011, **27**(20), pp.12486-12498.
260. Hodges, C.S. and Tangparitkul, S.M. Comment on “Patterns in Drying Drops Dictated by Curvature-Driven Particle Transport”. *Langmuir.* 2019, **35**(30), pp.9988-9990.
261. Binks, B.P. Particles as surfactants—similarities and differences. *Current Opinion in Colloid & Interface Science.* 2002, **7**(1), pp.21-41.
262. Liu, Y. New insights into pseudo-second-order kinetic equation for adsorption. *Colloids and Surfaces A: Physicochemical and Engineering Aspects.* 2008, **320**(1), pp.275-278.
263. Hunter, T.N., Wanless, E.J. and Jameson, G.J. Effect of esterically bonded agents on the monolayer structure and foamability of nano-silica. *Colloids and Surfaces A: Physicochemical and Engineering Aspects.* 2009, **334**(1), pp.181-190.
264. Belton, G.R. Langmuir adsorption, the Gibbs adsorption isotherm, and interfacial kinetics in liquid metal systems. *Metallurgical and Materials Transactions B.* 1976, **7**(1), pp.35-42.
265. Lunkenheimer, K., Lind, A. and Jost, M. Surface tension of surfactant solutions. *The Journal of Physical Chemistry B.* 2003, **107**(31), pp.7527-7531.
266. Phan, C.M., Le, T.N., Nguyen, C.V. and Yusa, S.-i. Modeling Adsorption of Cationic Surfactants at Air/Water Interface without Using the Gibbs Equation. *Langmuir.* 2013, **29**(15), pp.4743-4749.

267. Ozeki, S., Tsunoda, M.-a. and Ikeda, S. Surface tension of aqueous solutions of dodecyldimethylammonium chloride, and its adsorption on aqueous surfaces. *Journal of Colloid and Interface Science.* 1978, **64**(1), pp.28-35.
268. Abbas, A.H., Moslemizadeh, A., Wan Sulaiman, W.R., Jaafar, M.Z. and Agi, A. An insight into a di-chain surfactant adsorption onto sandstone minerals under different salinity-temperature conditions: Chemical EOR applications. *Chemical Engineering Research and Design.* 2020, **153**, pp.657-665.
269. Olesen, K.B., Fogang, L.T., Palm-Henriksen, G., Alyafei, N. and Sølling, T.I. How a range of metal ions influence the interfacial tension of n-decane/carboxylic acid/water systems: The impact of concentration, molecular- and electronic structure. *Journal of Petroleum Science and Engineering.* 2019, **182**, p.106307.
270. Gao, Y., Du, J. and Gu, T. Hemimicelle formation of cationic surfactants at the silica gel–water interface. *Journal of the Chemical Society, Faraday Transactions 1: Physical Chemistry in Condensed Phases.* 1987, **83**(8), pp.2671-2679.
271. El-Shall, H., Abdel-Khalek, N. and Svoronos, S. Collector–frother interaction in column flotation of Florida phosphate. *International Journal of Mineral Processing.* 2000, **58**(1-4), pp.187-199.
272. Elliott, L.N., Bourne, R.A., Hassanpour, A., Edwards, J.L., Sutcliffe, S. and Hunter, T.N. Salt enhanced solvent relaxation and particle surface area determination via rapid spin-lattice NMR. *Powder Technology.* 2018, **333**, pp.458-467.
273. Johnson, M., Peakall, J., Fairweather, M., Biggs, S., Harbottle, D. and Hunter, T.N. Characterization of Multiple Hindered Settling Regimes in Aggregated Mineral Suspensions. *Industrial & Engineering Chemistry Research.* 2016, **55**(37), pp.9983-9993.
274. Bournival, G., Ata, S. and Jameson, G.J. Bubble and froth stabilizing agents in froth flotation. *Mineral Processing and Extractive Metallurgy Review.* 2017, **38**(6), pp.366-387.
275. Bournival, G., Pugh, R.J. and Ata, S. Examination of NaCl and MIBC as bubble coalescence inhibitor in relation to froth flotation. *Minerals Engineering.* 2012, **25**(1), pp.47-53.
276. Tian, M., Gao, Z., Sun, W., Han, H., Sun, L. and Hu, Y. Activation role of lead ions in benzohydroxamic acid flotation of oxide minerals: New perspective and new practice. *Journal of Colloid and Interface Science.* 2018, **529**, pp.150-160.
277. Feng, D. and Aldrich, C. Effect of particle size on flotation performance of complex sulphide ores. *Minerals Engineering.* 1999, **12**(7), pp.721-731.
278. Pérez-Garibay, R., Ramírez-Aguilera, N., Bouchard, J. and Rubio, J. Froth flotation of sphalerite: Collector concentration, gas dispersion and particle size effects. *Minerals Engineering.* 2014, **57**, pp.72-78.
279. Drzymala, J., Bednarek-Gąbka, P. and Kowalczuk, P.B. Simplified empirical and phenomenological evaluation of relation between particle size and kinetics of flotation. *Powder Technology.* 2020, **366**, pp.112-118.

280. Prajitno, M.Y., Harbottle, D., Hondow, N., Zhang, H. and Hunter, T.N. The effect of pre-activation and milling on improving natural clinoptilolite for ion exchange of cesium and strontium. *Journal of Environmental Chemical Engineering.* 2020, **8**(1), p.102991.
281. Prajitno, M.Y., Tangparitkul, S., Zhang, H., Harbottle, D. and Hunter, T.N. The effect of cationic surfactants on improving natural clinoptilolite for the flotation of cesium. *Journal of Hazardous materials.* 2021, **402**, p.123567.
282. Ortiz-Oliveros, H.B. and Flores-Espinosa, R.M. Design of a mobile dissolved air flotation system with high rate for the treatment of liquid radioactive waste. *Process Safety and Environmental Protection.* 2020, **144**, pp.23-31.
283. Nagar, A. and Pradeep, T. Clean Water through Nanotechnology: Needs, Gaps, and Fulfillment. *ACS Nano.* 2020, **14**(6), pp.6420-6435.
284. Kheshti, Z., Ghajar, K.A., Moreno-Atanasio, R., Neville, F. and Ghasemi, S. Investigating the high gradient magnetic separator function for highly efficient adsorption of lead salt onto magnetic mesoporous silica microspheres and adsorbent recycling. *Chemical Engineering and Processing - Process Intensification.* 2020, **148**, p.107770.
285. Kim, J.-H., Kim, S.-M., Yoon, I.-H. and Kim, I. Application of polyethylenimine-coated magnetic nanocomposites for the selective separation of Cs-enriched clay particles from radioactive soil. *RSC Advances.* 2020, **10**(37), pp.21822-21829.
286. Thomas, H.C. CHROMATOGRAPHY: A PROBLEM IN KINETICS. *Annals of the New York Academy of Sciences.* 1948, **49**(2), pp.161-182.
287. Xu, Z., Cai, J.-g. and Pan, B.-c. Mathematically modeling fixed-bed adsorption in aqueous systems. *Journal of Zhejiang University SCIENCE A.* 2013, **14**(3), pp.155-176.
288. Mihaly-Cozmuta, L., Mihaly-Cozmuta, A., Peter, A., Nicula, C., Tutu, H., Silipas, D. and Indrea, E. Adsorption of heavy metal cations by Na-clinoptilolite: Equilibrium and selectivity studies. *Journal of Environmental Management.* 2014, **137**, pp.69-80.
289. Tansel, B., Sager, J., Rector, T., Garland, J., Strayer, R.F., Levine, L., Roberts, M., Hummerick, M. and Bauer, J. Significance of hydrated radius and hydration shells on ionic permeability during nanofiltration in dead end and cross flow modes. *Separation and Purification Technology.* 2006, **51**(1), pp.40-47.
290. Maciejewski, P. and Walkowiak, W. SELECTIVE REMOVAL OF CESIUM (I), STRONTIUM (II) and BARIUM (H) CATIONS WITH PROTON IONIZABLE LARIAT ETHERS IN THE ION FLOTATION PROCESS. *Fizykochemiczne Problemy Mineralurgii/Physicochemical Problems of Mineral Processing.* 2004, (38), pp.139-146.
291. Sobianowska-Turek, A., Ulewicz, M. and Sobianowska, K. ION FLOTATION AND SOLVENT SUBLATION OF ZINC (II) AND MANGANESE (II) IN THE PRESENCE OF PROTON-IONIZABLE LARIAT ETHERS. *PHYSICOCHEMICAL PROBLEMS OF MINERAL PROCESSING.* 2016, **52**(2), pp.1048-1060.

292. Ulewicz, M., Walkowiak, W. and Bartsch, R.A. Ion flotation of zinc(II) and cadmium(II) with proton-ionizable lariat ethers—Effect of cavity size. *Separation and Purification Technology.* 2006, **48**(3), pp.264-269.
293. Senthilkumar, R., Vijayaraghavan, K., Thilakavathi, M., Iyer, P.V.R. and Velan, M. Seaweeds for the remediation of wastewaters contaminated with zinc(II) ions. *Journal of Hazardous materials.* 2006, **136**(3), pp.791-799.

Appendix A

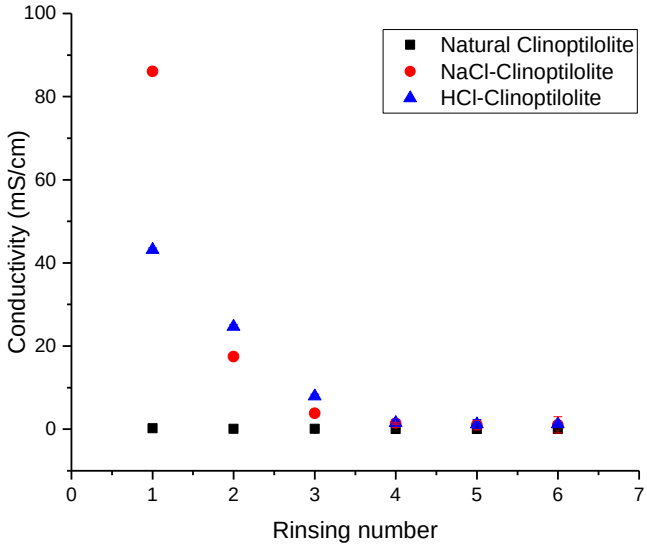

Figure A1: Conductivity of natural and activated clinoptilolite after several rinsing processes.

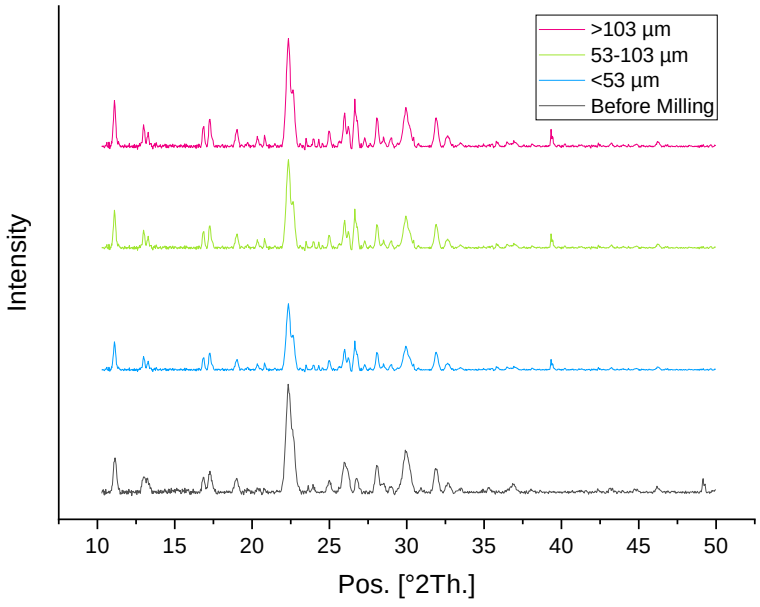

Figure A2: The XRD results of clinoptilolite fractions between before and after milling

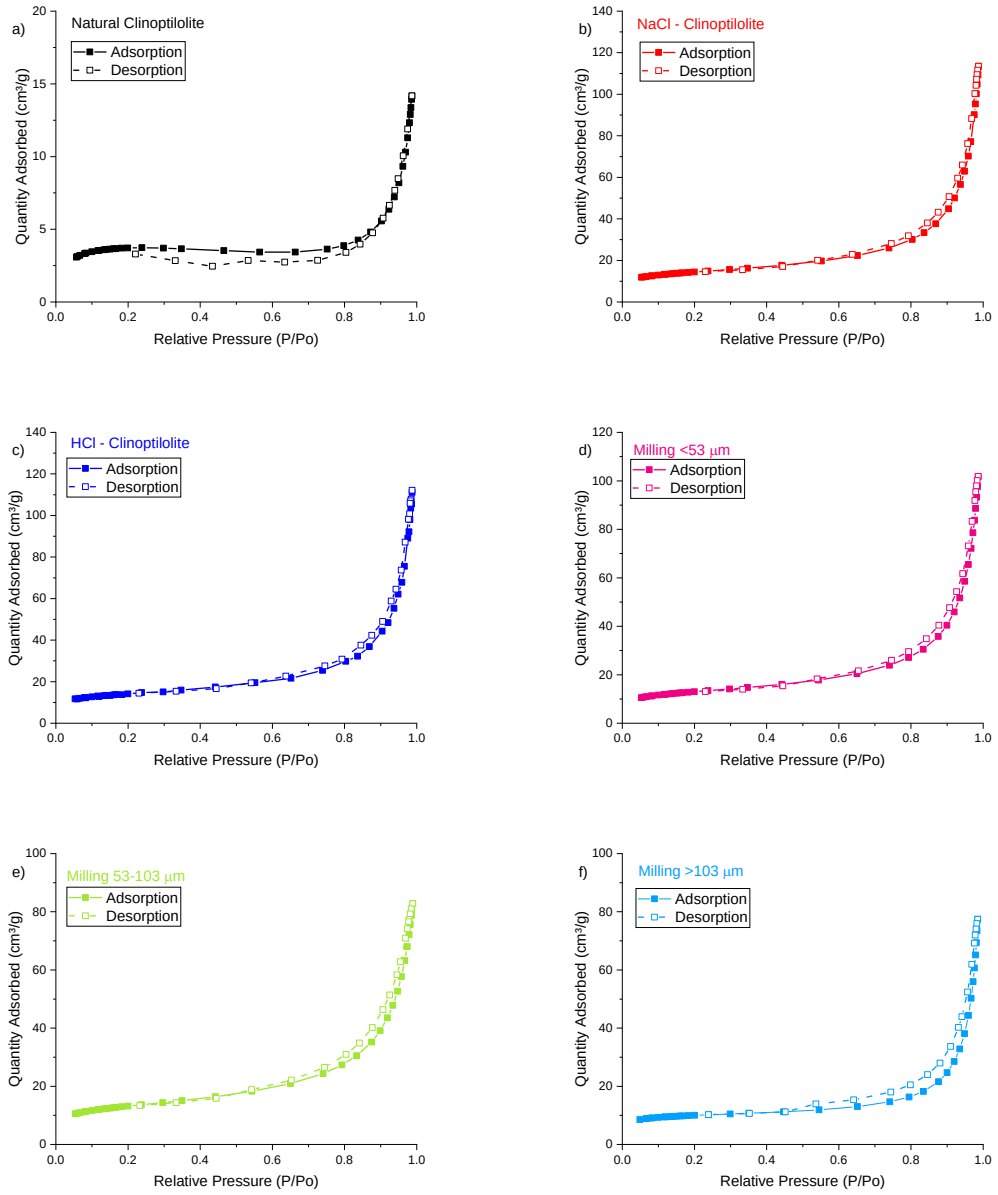

Figure A3: The adsorption/desorption isotherms of BET on: a) natural clinoptilolite; b) NaCl-clinoptilolite; c) HCl-clinoptilolite; d) Sieve <53 µm clinoptilolite; e) Sieve 53-103 µm clinoptilolite; and f) Sieve >103 µm clinoptilolite

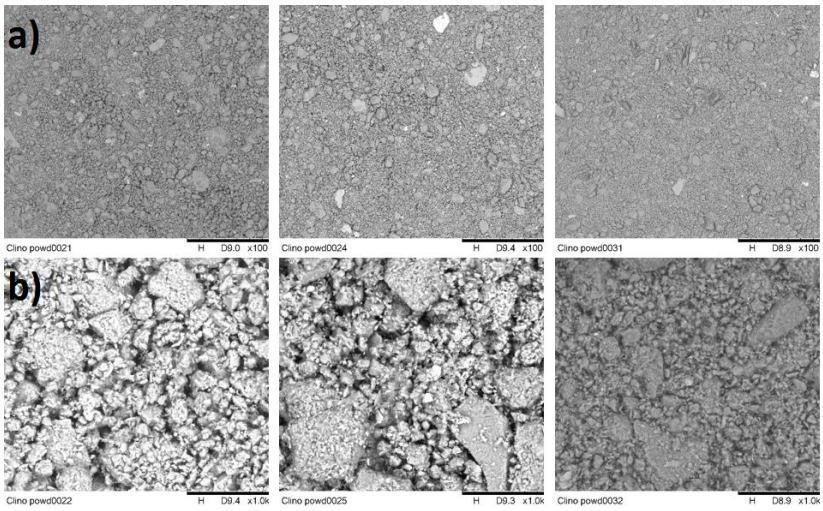

Figure A4: The morphology of natural and activated clinoptilolite (from left to right: natural clinoptilolite, NaCl-clinoptilolite and HCl-clinoptilolite) with different magnification scales of a) 100 and b) 1000.

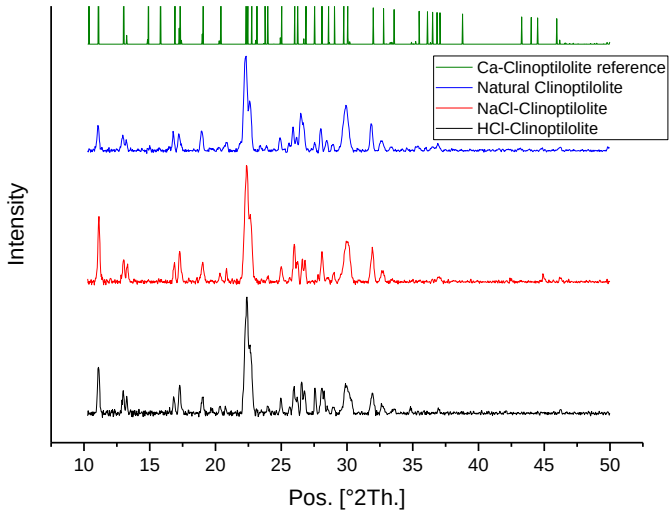

Figure A5: XRD of natural as well as salt (NaC) and acid (HCl) activated clinoptilolite with reference profile.

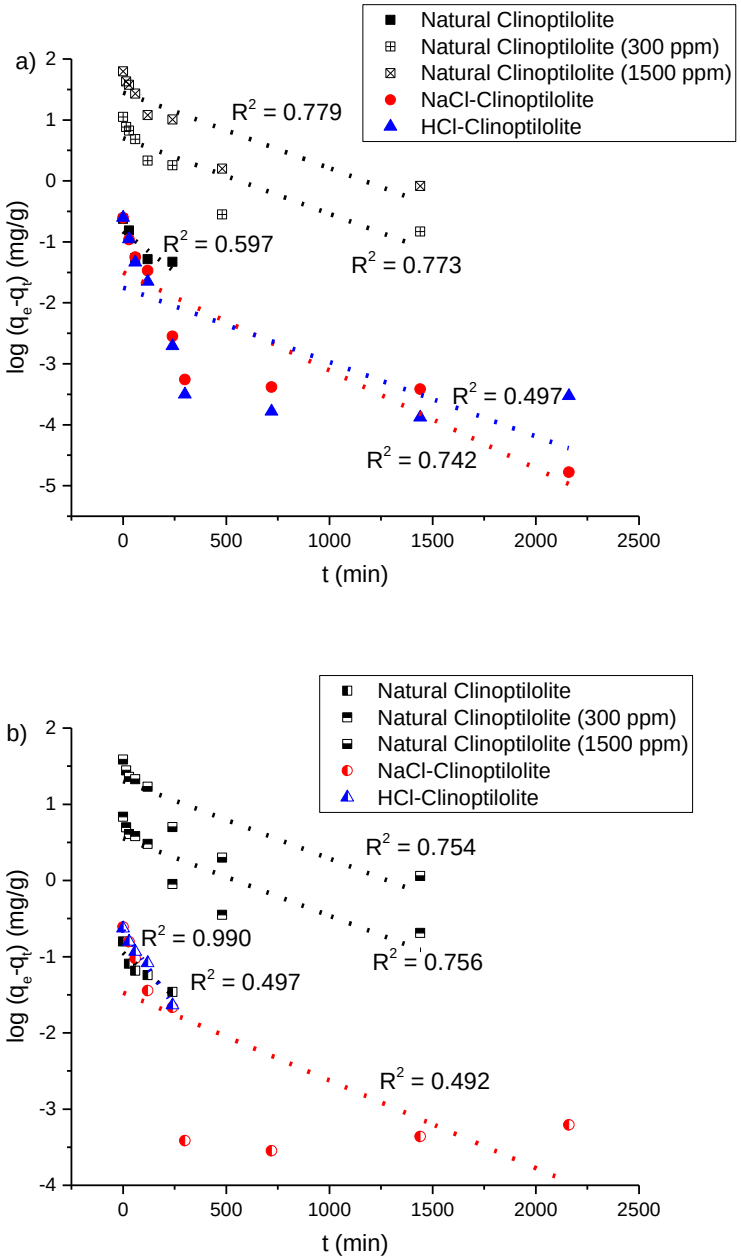

Figure A6: Pseudo-first order fitting of a) Cs^{+} and b) Sr^{2+} from adsorption kinetics tests. The dashed lines represent linear fits.

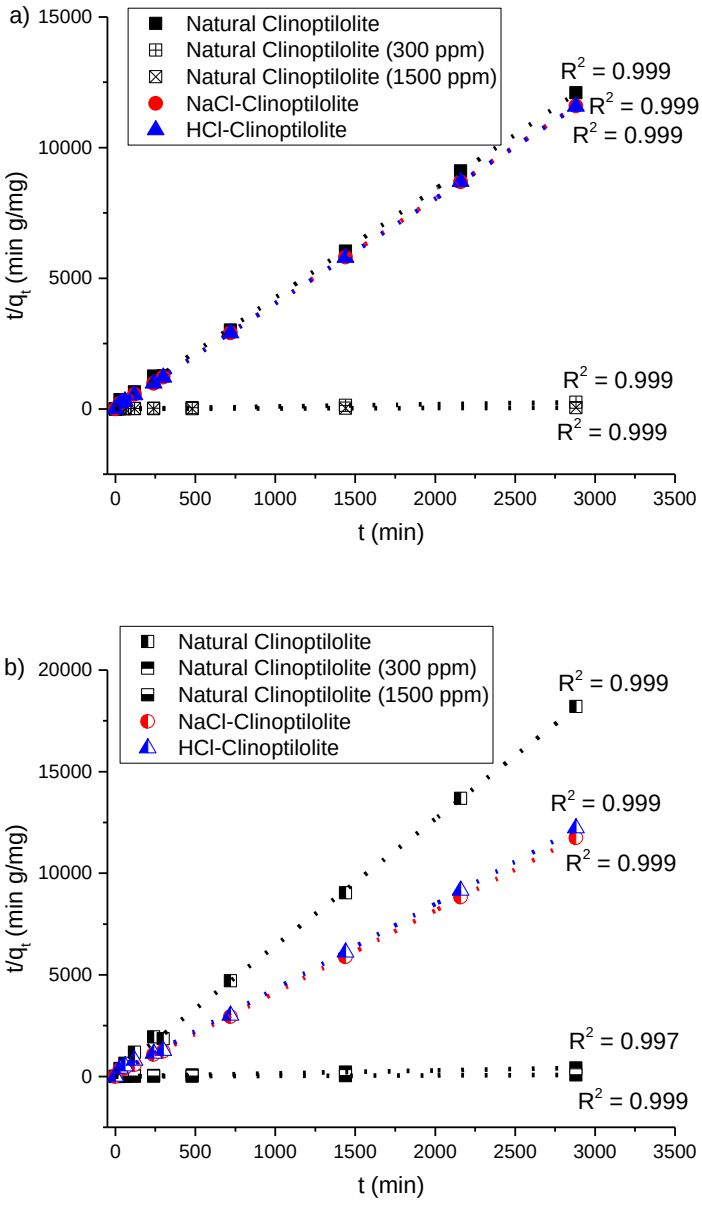

Figure A7: Pseudo-second order fitting of a) Cs^{+} and b) Sr^{2+} from adsorption kinetics tests. The dashed lines represent linear fits

Table A1: Activation Energy (ΔG) (J/mol) at 20 °C solution.

Material	Cs^+	Sr^{2+}
Natural clinoptilolite	12.088	14.681
NaCl activated clinoptilolite	8.965	9.456
HCl activated clinoptilolite	8.529	11.709

Table A2: Pseudo-second order rate constants (k_2), initial adsorption rates (h) and adsorbed solute amounts at equilibrium (q_e) from dynamic uptake tests of 5 ppm Cs^+ solution.

k_2 (g/mg.min)	h (mg/g.min)	$q_{e,cal}$ (mg/g)	$q_{e,exp}$ (mg/g)
0.516	0.032	0.251	0.245

Table A3: Langmuir and Freundlich isotherm fit parameters for equilibrium Cs^+.

Langmuir isotherm fit parameters		
q_c (mg/g)	*b (dm^3/g)*	*R^2*
158.261	0.019	0.995
Freundlich isotherm fit parameters		
K_f (mg/g)	*n*	*R^2*
0.764	2.001	0.955

Activation energies calculated using the Langmuir constant related to energy of adsorption, as described in Eq. A1 below.

$$\Delta G = -RT \ln b \qquad \text{(Eq. A1)}$$

Where ΔG denotes activation energy (J/mol), R is Gas constant (8.3144598 J/mol.K), T is the temperature (K) and *b* (dm^3/g) is the Langmuir constant related to the energy of adsorption.

Appendix B

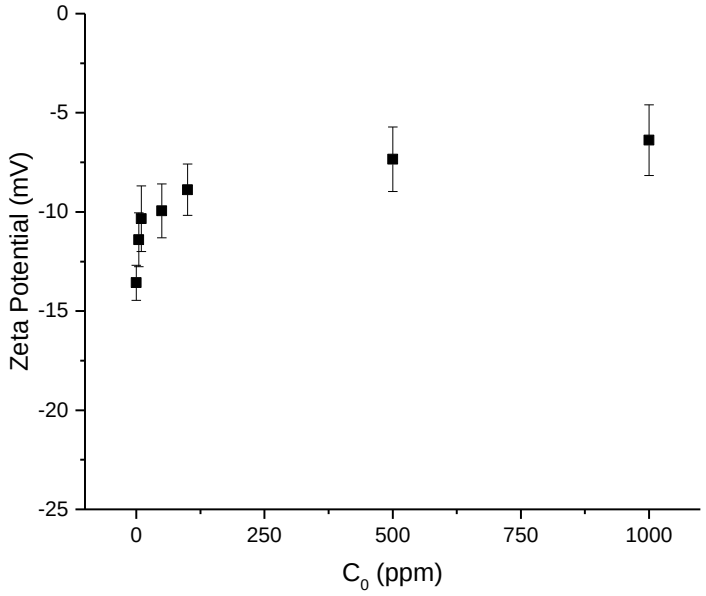

Figure B1: Zeta potential of natural clinoptilolite at neutral pH with different concentrations of Cs^+ ions. Error bars represent ± 1 Standard deviation.

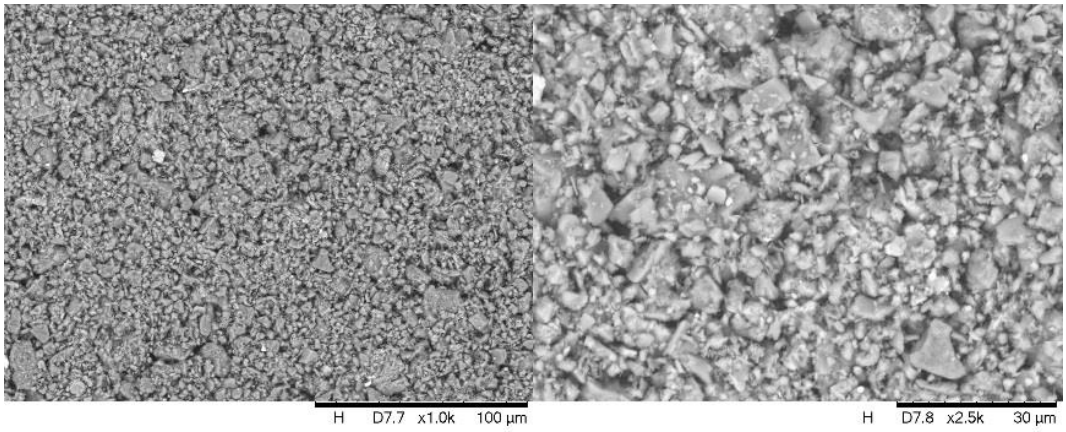

Figure B2: Scanning electron microscopy (SEM) of clinoptilolite powder at two magnification scales.

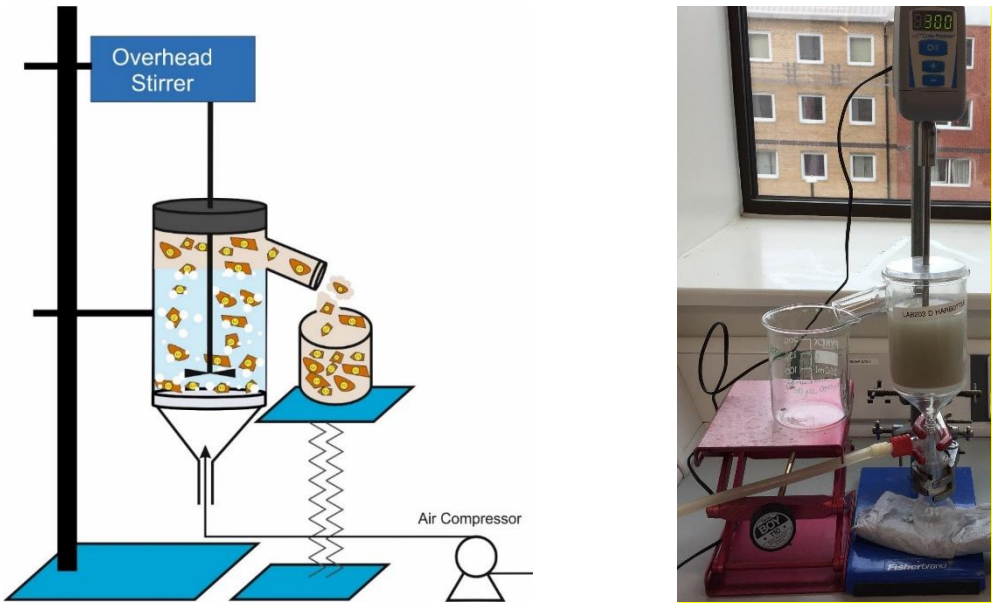

Figure B3: Schematic design (left) and real pictures (right) of the flotation and collection cell

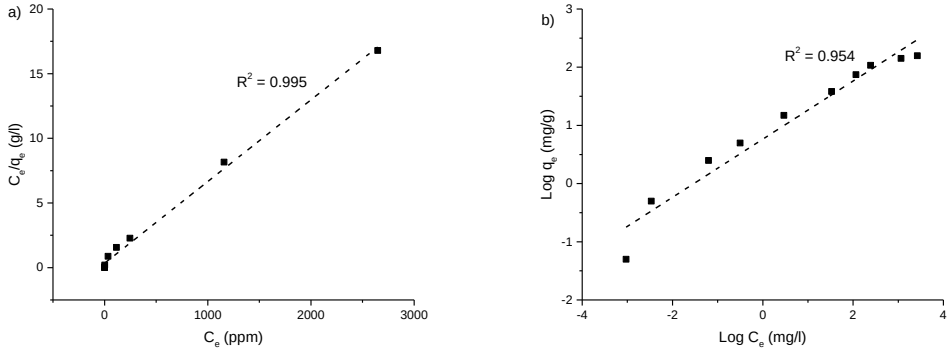

Figure B4: a) Langmuir and b) Freundlich isotherms of equilibrium Cs^+ adsorption. Dashed lines represent linear fits.

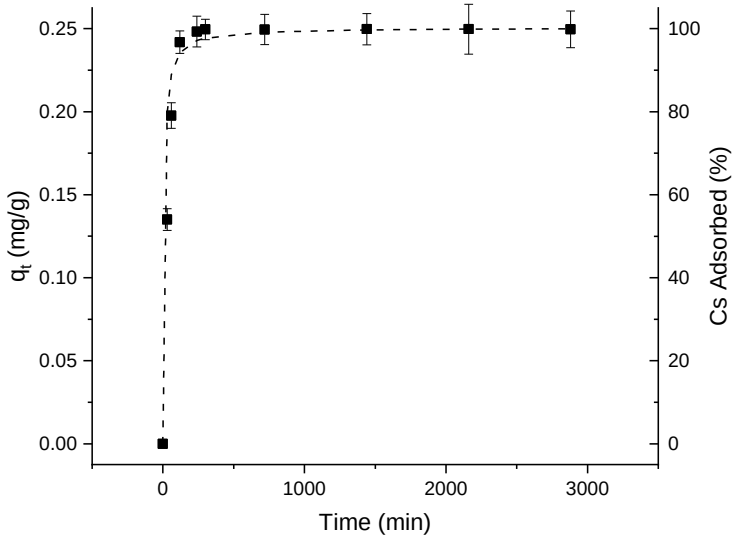

Figure B5: The adsorption kinetics of Cs^+ at an initial concentration of 5 ppm, shown in terms of q_t (mg/g) (left hand side axis, LHS) and adsorbed percent (right hand side axis, RHS). Dashed line represents the pseudo second order (PSO) rate fit. Error bars represent ± 1 Standard deviation.

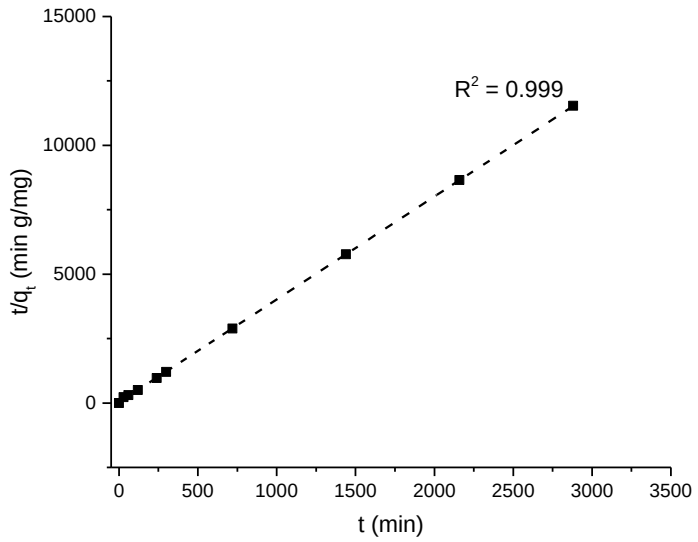

Figure B6: Pseudo-second-order fitting of Cs^+ from 5 ppm adsorption kinetics tests. The dashed lines represent linear fits.

Table B1: Langmuir and Freundlich isotherm fit parameters for equilibrium Cs^+.

Langmuir isotherm fit parameters		
q_c (mg/g)	*b (dm^3/g)*	*R^2*
158.261	0.019	0.995
Freundlich isotherm fit parameters		
K_f (mg/g)	*n*	*R^2*
0.764	2.001	0.955

Table B2: Pseudo-second order rate constants (k_2), initial adsorption rates (h) and adsorbed solute amounts at equilibrium (q_e) from dynamic uptake tests of 5 ppm Cs^+ solution.

k_2 (g/mg.min)	***h (mg/g.min)***	***$q_{e,cal}$ (mg/g)***	***$q_{e,exp}$ (mg/g)***
0.516	0.032	0.251	0.245

The percent adsorption of cationic surfactants was determined using Equation B1, where, C_o is initial surfactant concentration (mM) and C_e is the remaining surfactant concentration left on the supernatant (mM).

$$\% = \frac{(C_0 - C_e)}{C_0} \times 100\% \qquad \text{(Eq. B1)}$$

Meanwhile, the percent clinoptilolite recovery was determined using Equation B2, where, m_o is initial mass of contaminated clinoptilolite (g) and m_e is the mass of recovered contaminated clinoptilolite (g).

$$\% = \frac{(m_0 - m_e)}{m_0} \times 100\% \qquad \text{(Eq. B2)}$$

Appendix C

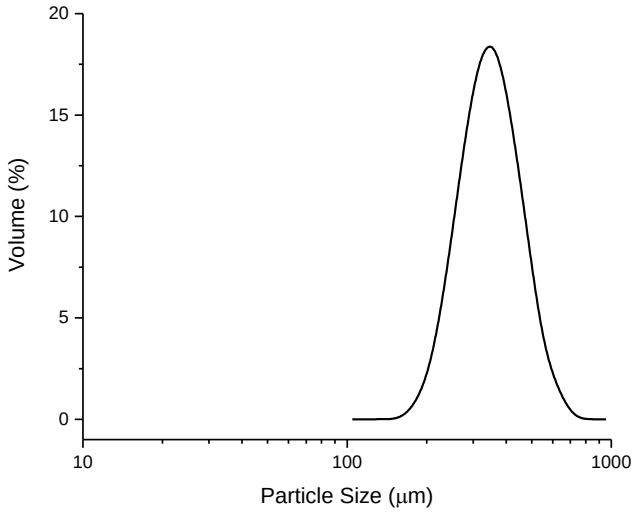

Figure C1: Particle size distribution of clinoptilolite after sieving

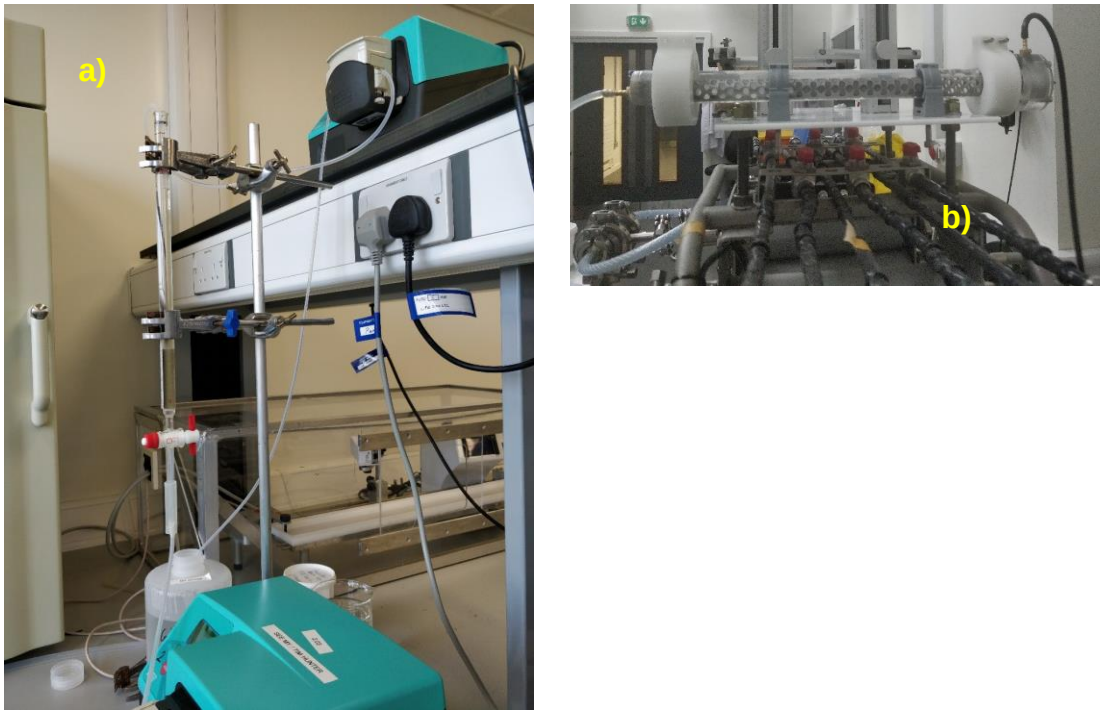

Figure C2: The real picture of experimental setup for a) column ion exchange and b) agitated tubular reactor (ATR)

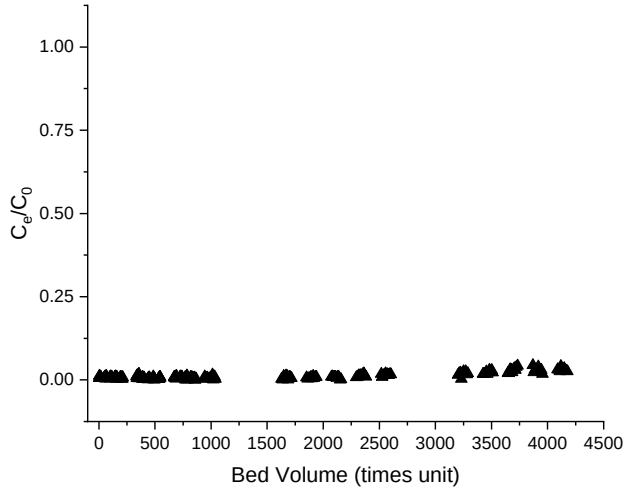

Figure C3: The breakthrough of cesium at 5 ppm initial concentration.

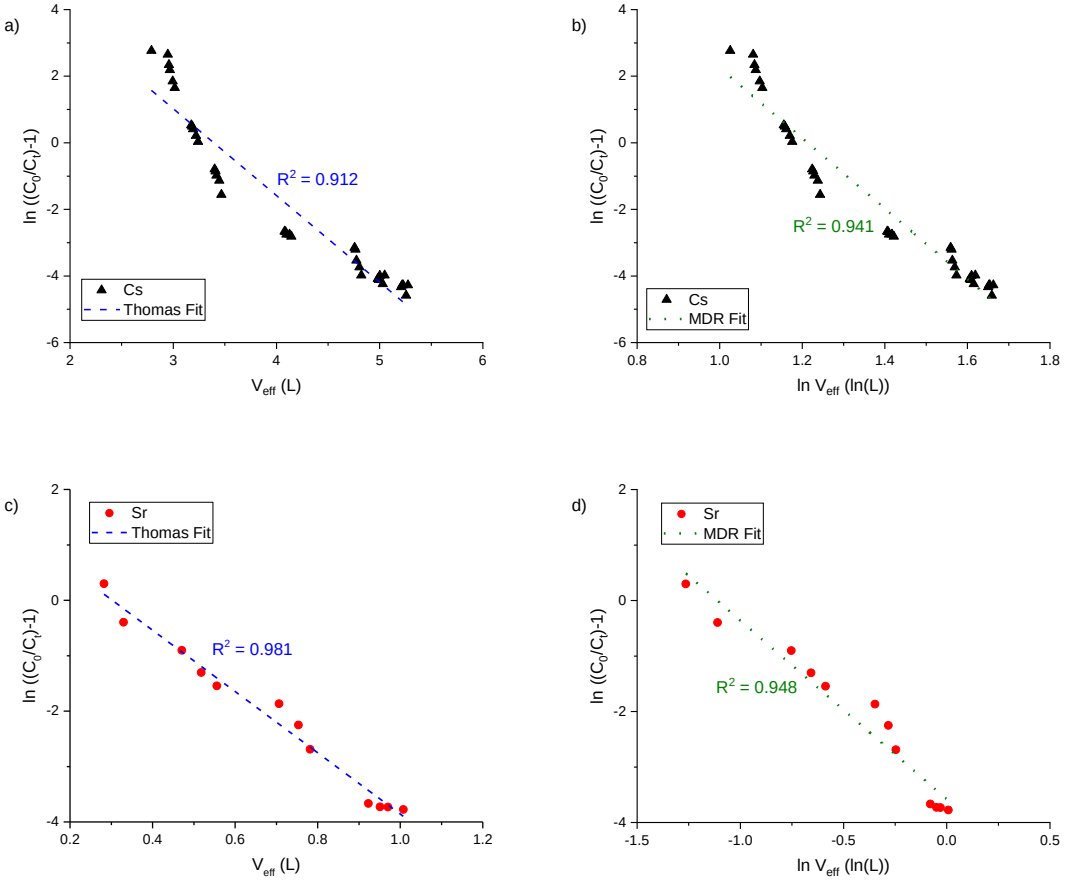

Figure C4: The linearised column breakthrough fits for cesium and strontium solutions at 200 ppm. Shown is a) Thomas model for cesium; b) MDR model for cesium; c) Thomas model for strontium and d) MDR model for strontium. The dashed lines represent linear fits.

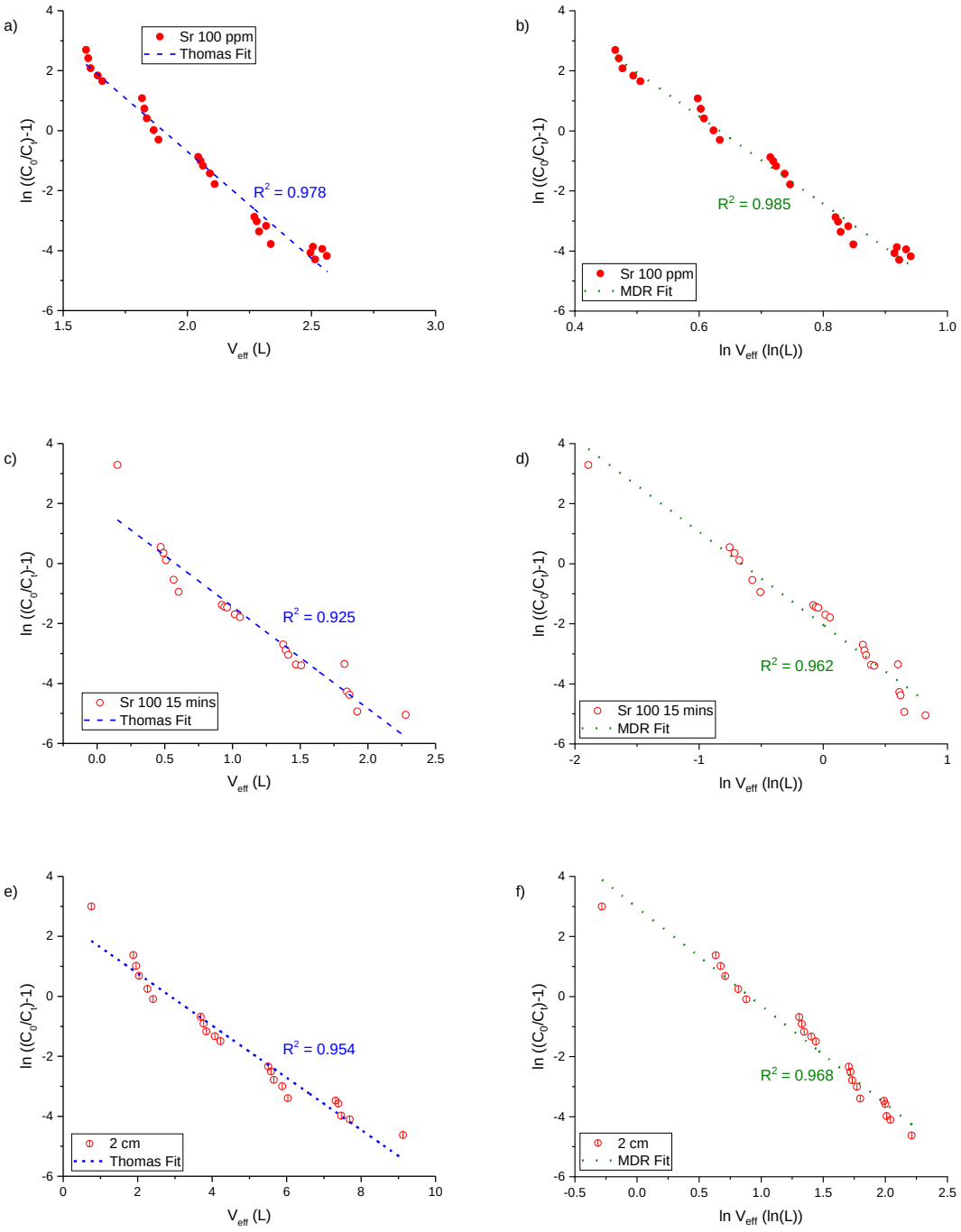

Figure C5: The linearised column breakthrough fitting for strontium at 100 ppm. Shown is a) Thomas model for 30 mins residence time; b) MDR model for 30 mins residence time; c) Thomas model for 15 mins residence time; d) MDR model for 15 mins residence time; e) Thomas model for 15 mins residence time at 2 cm column ion exchange diameter and f) MDR model for 15 mins residence time at 2 cm column ion exchange diameter. The dashed lines represent linear fits.

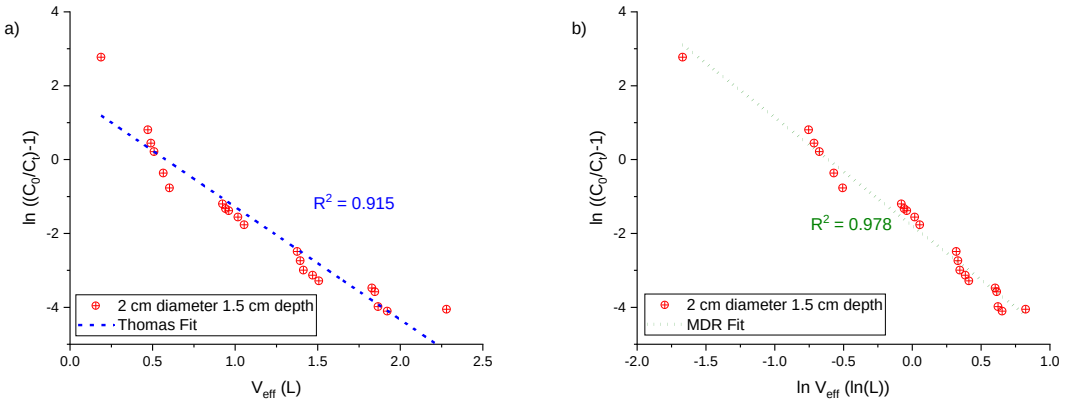

Figure C6: a) The linearised fitting of Thomas model for 1.5 cm adsorbent height at 2 cm diameter of column ion exchange; and b) The linearised fitting of MDR model for 1.5 cm adsorbent height at 2 cm diameter of column ion exchange. The dashed lines in a) and b) represent linear fits

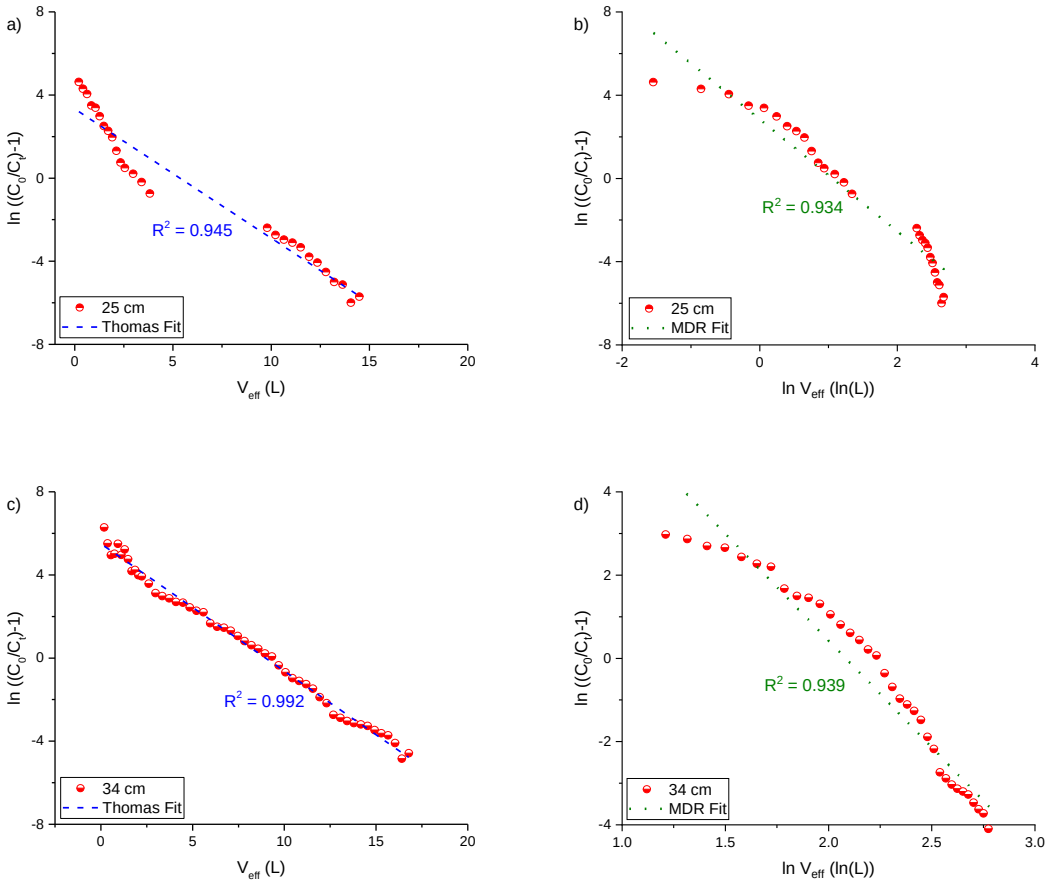

Figure C7: The linearised breakthrough fitting data from the agitated tubular reactor ATR. Shown is a) Thomas model with 25 cm of adsorbent bed length; b) MDR model with 25 cm of adsorbent bed length; c) Thomas model with 34 cm of adsorbent bed length; and d) MDR model in 34 cm of adsorbent bed length. The dashed lines represent linear fits.

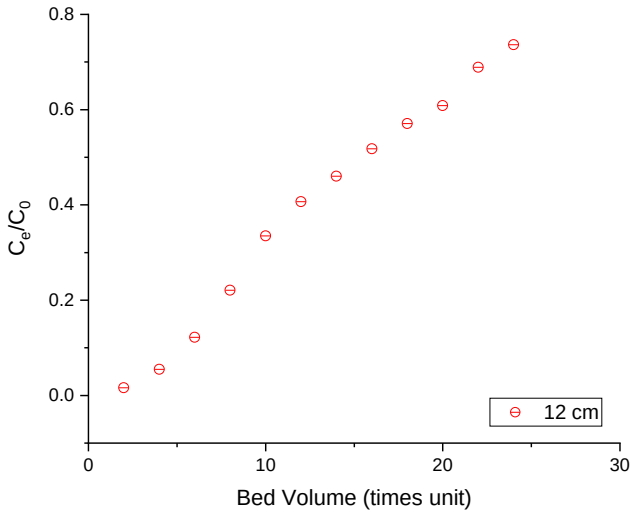

Figure C8: Preliminary breakthrough data from the agitated tubular reactor (ATR) with a 12 cm column length (for a 100 ppm strontium liquid concentration). Note, trial was aborted after Ce/Co reached ~0.75, due to poor performance.